University of Glasgow and Strathclyde

Department of Naval Architecture and Marine Engineering

Application of Smart Materials

for

Vibration Reduction in Ships

By

SERKAN TURKMEN

A thesis submitted for the degree of

Doctor of Philosophy

December 2013

University of Glasgow and Strathclyde

Department of Naval Architecture and Marine Engineering

Application of Smart Materials for Vibration Reduction in Ships

By

SERKAN TURKMEN

A thesis submitted for the degree of

Doctor of Philosophy

December 2013

Acknowledgements

This thesis was a rowing race in a single scull boat. There was no competitor to beat but finishing the race was a great challenge and passing the finish line was the best prize. A boat and oars were not enough to complete the race with success. A coach, team mates, and of course a good support are always needed when you are pedalling on the endless river of knowledge. I would like to acknowledge people who help me to win this unique race.

I am very thankful to my supervisor Prof. Osman Turan. He gave me the opportunity to study in Strathclyde University and supported me greatly knowledge and funding wise. Without his scientific aspect and constant coaching my PhD would have been impossible to complete. Furthermore he is not only a good coach but a great chef as well. I will never forget our lunch meetings in his garden.

I am also very thankful to my second supervisor Prof. Atilla Incecik. His experience and critical questions helped me develop my PhD.

I would like to thank my parents Ilkay & Ali Türkmen. I am very lucky person as they were with me at any time of my life. They have been always very patient and supportive. This is not only my thesis but also their. Teşekkürler anne ve baba ...

A big thank to a special lady, Miss Eva Malessa, who helped me with proof reading. Although she is more interested in Marimekko she listened patiently to me talking about my PhD. It would have been impossible to finish this study without her support.

During the PhD period I had invaluable support from my PhD mates who shared their knowledge and friendship without expecting anything in return. I am deeply thankful to Petrus Zoet (Pepijn), Olgun G Hizir, Dr Dimitri Mylonas, Dr Mahdi Khorasanchi, Dr Giuseppe Mortola, Çağan Diyaroğlu and Dr Nabile Hifi.

I am also thankful to my friends and colleagues who always had an ear, a smile and herbal tea for me: Tineke Bosma, Emek Kurt, Dr Iraklis Lazakis, Charlotte Banks, Yiğit Kemal, Eduardo Blanco Davis (Eddie), Gonzalo Azqueta Gavaldon, Elisabeth Wilson (Lis), Abayomi Amosu, Dr Sulaiman B El-Ladan, Dr Hassan Khalid, Dr Hao Cui, Dr Camille Azzi, Dr Hany Elosta, Dr Hauwa Raji, Dr Rod Sampson, Dr Kwang Cheol Seo, Batuhan Aktaş, George Politis, Dr Bekir Şener, Dr. Erkin Altunsaray.

I want to thank Mrs Thelma Will for making my academic life easier by helping me with administrative duties and Mrs Fiona MacKie, Mrs Carolyn McLellan and Mr David Percival who were all very kind and willing to help me all the time.

My overseas supporters deserver acknowledgements as well. Cok değerli hocalarım, sizlerin desteği olmadan bu doktora asla gercekleşemezdi: Dr Ismail Bayer, Prof. Nurten Vardar , Prof. Ahmet Dursun Alkan, Prof. Mesut Guner, Prof Barbaros Okan, Prof. Emin Korkut, Dr Şebnem Helvacıoğlu ve Prof. Muhittin Soylemez.

In the end my special thanks goes to Prof Mehmet Atlar. He encouraged me to pursue my academic career and followed it very closely.

I am grateful for the funding I received for this study. This study was sponsored by Lloyd Register, British Overseas Research Students Awards Scheme (ORSAS) and the University of Strathclyde.

Contents

Nomenclature

Sym	Definition	Unit
δ	Variation operator	
ε	The permittivity (IEEE std)	F/m or C/(m·V)
ε_o	Permittivity of vacuum (8.854E-12)	Farad/meter
ϕ	Voltage, electrical potential	V/m
ω	Frequency	rad/s
Ω	Surface, area	m^2
ρ	The mass density	kg/m^3
P	Surface charge density	C/m^2
C_p	Capacitance	Farad
E	Electric field	V/m
F_P	Point force	N
F_V	Body force	N
F_Ω	Surface force	N
C	Mechanical stiffness (IEEE std)	N/m^2
[C]	Structural damping matrix	
d	Piezoelectric strain constants	C/N
D	Electric displacement field	C/m^2
H	Total potential energy or electric enthalpy	Joules
K	Kinetic energy	Joules
L	Inductance	Henry
[M]	Mass matrix	kg
P	Power	Watts
Q	Total electrical charge	V/m^2

R	Electrical resistance	Ohm
S	Strain (IEEE std)	m/m
t_1,t_2	Time	s
σ	Stress (IEEE std)	N/m^2
{u}	Displacement field vector	m
{u}	Velocity field vector	m/s
W	Total virtual work	Joules
Z	Impedance	ohm

Superscripts

T	Values taken at constant stress (T=0)
s	Values taken at constant strain (S = 0)
E	Values taken at constant electric field (E=0)
T	Transpose of a matrix (Italic)

Subscripts

i,*j*	Strain or stress applied in the j-axis and the normal direction of the electrode is i-axis.

Abbreviations

CFD	Computational Fluid Dynamics
SEA	Statistical Energy Analysis
FEA	Finite Element Analysis
FEM	Finite Element Method
SMs	Smart Materials
TL	Transmission Loss Factor
CLF	Coupling Loss Factor

List of Tables

List of Figures

Abstract

Smart Materials have been investigated for decades and widely used in the automotive and aeronautics industries to measure and control noise and vibration. This study covered ship structure vibration and Smart Materials were employed for the purpose of ship vibration attenuation. One specific Smart Material, piezoelectric material, was the focus of the study.

Although previous research has been conducted on vibration mitigation employing piezoelectric shunt systems, this study identified the need for specific applications regarding ship vibration mitigation. Passive piezoelectric shunt damping systems for ships were described and investigated in this study.

Computational methods were used to investigate structural vibration of a cantilever beam, a Liquid Natural Gas (LNG) carrier and a bulb keel. The Finite Element Method (FEM) was used to calculate the vibration and vibration treatment with the passive piezoelectric shunt damping system.

The numerical results of the passive piezoelectric shunt system bonded to the cantilever beam were compared to experimental results obtained from a previous study. The FEM delivered results, which showed a high degree of similarity in comparison to the experimental results. Both experimental and numerical studies validate the theory that piezoelectric material, connected to an electrical circuit, can be successfully used to achieve vibration reduction. Significant vibration attenuation was found in the numerical simulation of the LNG vessel. The simulation of the bulb keel also provided promising outcome regarding substantial vibration reduction by means of piezoelectric shunt system.

1.Introduction

1.1 Motivation of the Study

Two important comfort reducing factors on-board of ships for both the crew and the passengers are noise and vibration. They cause discomfort and many occupational problems regarding safety and health such as hearing loss are, therefore, making crew members reluctant to work. Noise and vibration produced by ships are not only problematic for humans, but also for their surrounding environment. Many animals like birds, fish, sea turtles and marine mammals (cetaceans) migrate on a regular basis, on time scales ranging periodically. They can get distracted and diverge from their specific migration routes. Further, it may become harder for some animals to find mates, because noise can block, distort, change or interfere with the animals' communication.

National and international authorities require the marine industry to run their ships and floating structures in habitability, comfort vibration and noise limits. All issued codes, directives or regulations concerning acceptable noise levels on ships intend to improve measurement techniques, accurate noise prediction programs and hull structure dynamic performance to overcome the noise and vibration problem.

It is difficult to change ships noise and vibration level, once they are produced. Therefore scientists investigate methods to overcome this problem in pre-manufacturing stage, using state-of-the-art technology. One method is the use of Smart Materials as passive or active dampers. They can be used as sensor and actuator in intelligent structures and as elements of active noise-vibration damping systems. Although the promising potential of smart materials has been investigated for decades, their marine applications are not often found apart from the use in small electronic devices.

It is necessary to investigate smart materials' noise and vibration applications theoretically with the help of modern simulation techniques to check the feasibility, location and amount of smart materials which tend to be very expensive. Further, trial-and-error approaches have the tendency to be also costly, as well as inefficient and time-consuming (Bertram 2011). Computational methods used in this study intend to solve governing equations with the approved boundary conditions numerically and semi-numerically (e.g. finite element method, statistical energy analysis).

1.2 Criteria and Guidelines for Ship Noise and Vibration

There are international and national authorities such as IMO, EC, and ISO which enforce noise and vibration criteria. The regulations give safe noise and vibration level for different types of ships and operation areas. It is necessary to be aware of these criteria to apply suitable and economic treatment to prevent noise and vibration high level. Therefore, having an acoustical plan during the early stage of ship design or maintaining periods has become crucial. This issue has caused an increasing demand of research in this specific field.

The International Maritime Organization "IMO" has set the noise level criteria. The IMO Resolution A.468(XII) (IMO,1981) is the code on noise levels on board of ships. The criteria included in this resolution are proposed to provide:

- Protection from hearing loss
- Safe working conditions (considering the need for speech communication, and hearing audible alarms)
- Comfort in rest
- Recovery from effects of exposure to high noise levels

Resolution A.468 (XII) has being superseded by The Safety of Life at Sea (SOLAS) which is an international maritime safety agreement. The SOLAS regulation II-1/3-12 requires new ships to be constructed in a way that reduces on-board noise and personnel to be protected from noise, in accordance with the revised code on noise levels of ships. However, the regulation II-1/3-12 has been updated to set out mandatory maximum noise level limits for machinery spaces, control rooms, workshops, accommodation and other spaces on-board of ships. The Code will come into effect when the new regulation enters into force on 1 July 2014 (IMO 2012).

The European Union (2003) has approved a treaty on two directives on noise and vibration in the working environment: The Human Vibration Directive 2002/44/EC defines the minimum requirements for the health and safety of workers exposed to vibration. The Noise at Work Directive 2003/10/EC focuses on the minimum health and safety requirements regarding the exposure of workers to the risks arising from physical agents (such as noise). The directives quantify the noise impact in the short, medium and long term of major sources. ISO 2922:2000 sets the regulation of the noise level of vessels on inland waterways and harbours (ISO 2000).

The directive 2006/87/EC names technical requirements for inland waterway vessels. This directive is to control noise limit in dB (A-weighted) levels. Article 8.10 states the requirements for noise emitted by vessels:

- The noise produced by a vessel under way, and in particular the engine air intake and exhaust noises, shall be damped by using appropriate means.
- The noise generated by a vessel under way shall not exceed 75 dB (A-weighted) at a lateral distance of 25 m from the ship's side.
- Apart from transhipment (loading and unloading) operations the noise generated by a stationary vessel shall not exceed 65 dB (A-weighted) at a lateral distance of 25 m from the ship's side.

ISO 3746.2010 is a similar standard to 2006/87/EC. It determines sound power levels around a static source such as a moored ship (ISO 2010).

ISO 6954:2000 (previously ISO 6954:1984) is a criterion of assessment for ship structure-borne vibration. The criterion was based on evaluation of human exposure to whole-body vibration with respect to the comfort or annoyance of the persons on-board. An overall weighted root mean square (r.m.s.) velocity is used in habitability and comfort measurements to ISO 6954:2000 in a frequency range from 1Hz to 80 Hz. The r.m.s. value is related to the energy content and is used in measurements of vibration. Fast Fourier Transform (FFT) is used to record vibration responses in the three translational directions of a ship (longitudinal, transversal and vertical). Measurements are carried out at least at two locations on each deck.

1.3 Ship Noise and Vibration

Ships are installed with many types of machinery, causing different noise and vibration levels. Most commercial vessels are built of steel, which is a lightly damped material. There are two main types of ships' noise and vibration sources: structure borne and fluid borne, given in Figure 1-1.

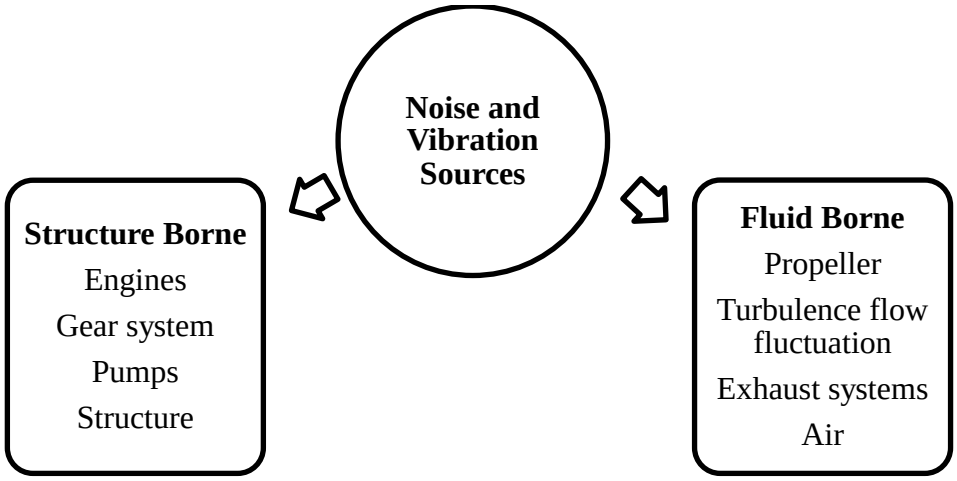

Figure 1-1: Main noise and vibration sources

These sources cause propagation of vibration energy to adjoining structures and surrounding fluids (air and water). Figure 1-2 illustrates the noise radiation from a commercial ship.

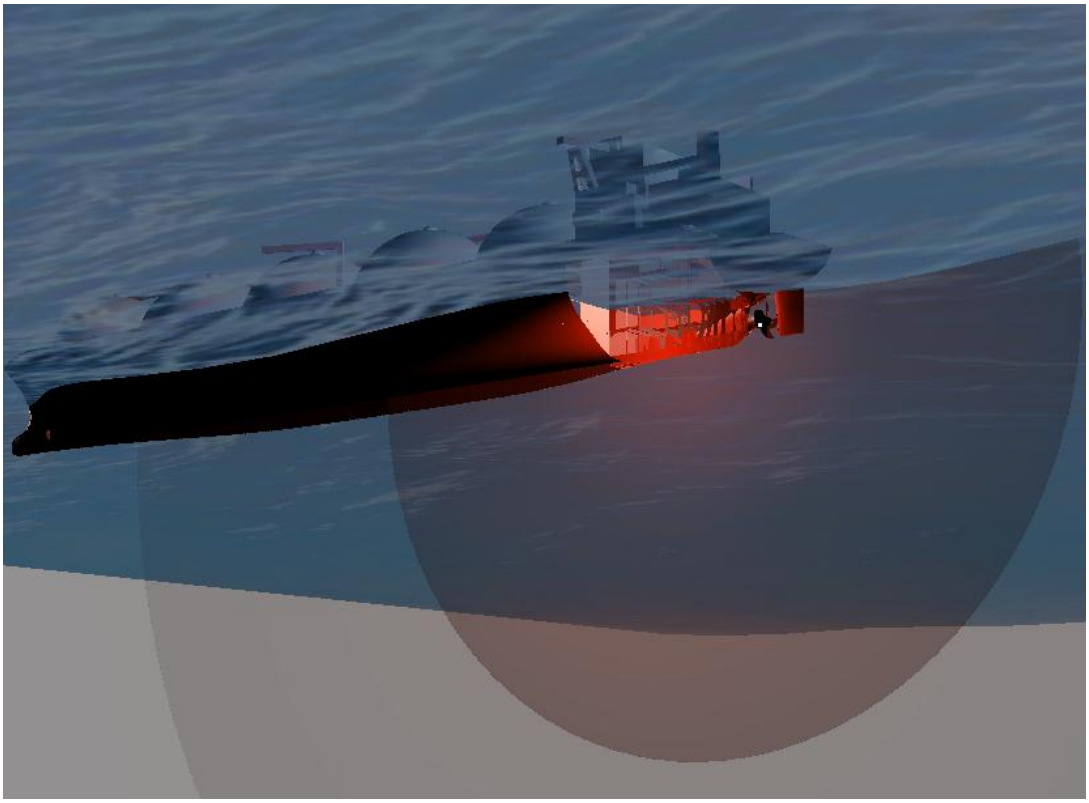

Figure 1-2: Demonstration of noise radiation

1.4 Noise and Vibration control

Any motion that repeats itself after an interval of time is called vibration or oscillation (Rao and Yap 1995). The vibration in machines and structures results in oscillatory motion that propagates in surrounding domain (air, water etc.). This motion is known as noise (or sound). Noise can also be produced by the oscillatory

motion of the fluid itself, for example turbulent mixing of a jet with the atmosphere, in which no vibrating structure is involved (Norton and Karczub 2003).

There are several options, which can be utilized to mitigate the vibration and noise.

- Optimization of structural design in terms of vibration
- Adequate and resilient isolation
- Localized additions such as brackets, stiffeners etc.
- Application of damping devices such as viscoelastic material (silicone rubber, butyl rubber etc.)
- Feedback systems such as actuators and transducers

The common point of these options is the oscillation energy (kinetic energy) dissipated by external applications or the system, which can naturally damp the oscillation itself. The dissipated energy becomes potential energy or kinetic energy for the external system. Therefore, noise and vibration mitigation techniques can be grouped by means of energy control systems:

- Passive Control: No external energy is applied to the vibrating system and no intelligent system is used to control and mitigated noise and vibration. Visco-elastic layers are used as dampers.
- Semi-passive control: No energy is given into the vibrating system, but the system is connected to energy conversion materials such as piezoelectric materials and magnetic transducers. A resistive shunt circuit is connected to the system, therefore vibration energy is diverged to an electrical circuit.
- Active control: An intelligent feedback loop control device is included. The device includes sensors, gain controller, amplifier, and actuator.

Active damping systems are difficult to apply for complex large structures such as ships, because the system needs always external power supply and a qualified technician to control and maintain it. The environment surrounding the active damping system should be well insulated to prevent possible damage due to humidity etc.

Passive damping mitigates directly vibration by dissipating kinetic energy of vibration. Passive damping systems are cheaper than active ones. However the passive systems have disadvantages such as increasing weight and poor performance in the low-frequency range.

Semi-passive systems, such as the piezoelectric shunt circuit, can be considered an alternative to active control techniques. Semi-passive systems neither require an external power supply nor a feedback control system. By attaching a piezoelectric material to a resonant mechanical structure and shunting the material with electrical impedance, kinetic energy from the resonant structure can be dissipated. Thus, vibration control is possible when a piezoelectric plate is used on the structure.

1.5 Smart materials

Smart materials (SMs) are defined as materials that are able to adapt to either a changing external or a changing internal environment. These environments can be stress, temperature, pH, moisture damage, failure as well as electric and magnetic fields. Mainly, there are four unique features of SMs:

1. Capability of property change
2. Capability for energy exchange
3. Discrete size or location
4. Reversibility

Commonly, smart materials are used as actuators and sensors. Thus, it is possible to change system characteristics (stiffness or damping) as well as system response (strain or shape). There are different smart materials. This study focuses on piezoelectric material, as it is widely used e.g. in automotive and aerospace industries to measure and actively control noise and vibration control. In Figure 1-3, piezoelectric materials were used as an actuator to reduce flow induced noise and vibration of jet engine stator (Crocker, 2007).

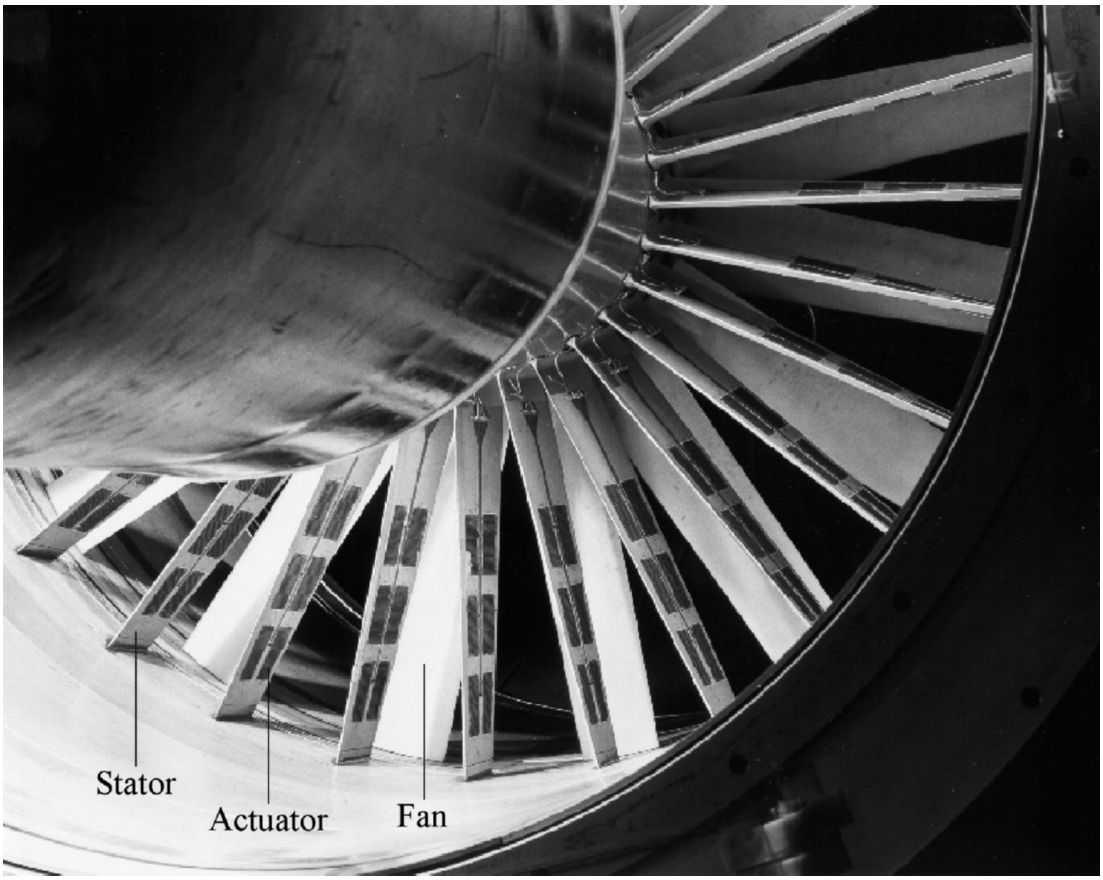

Figure 1-3: Active noise and vibration control for jet engine fan

1.6 Layout of the Study

This thesis is organized into eight chapters. Chapter 1 gives the Motivation for the study performed. The major noise and vibration sources in ships are identified. Existing solution systems are given and smart materials are briefly introduced as an alternative solution to reduce ship noise and vibration. Following the presentation of Aims and Objectives in Chapter 2, a Literature Review is given in Chapter 3. Important regulations, previous research and smart material (in particular piezoelectric material) applications regarding (ship) noise and vibration, are described. Chapter 4 gives the Methodology. Elementary concepts of vibration mitigation with piezoelectric material for numerical simulation are introduced. Statistical Energy Analysis (SEA) and Finite Element Method (FEM) are briefly reviewed. Chapter 5 focuses on the Theory of passive piezoelectric shunt damping systems. The foundations of piezoelectricity and electromechanical coupling are reviewed. Further, the governing equations of motion of the FEM for piezoelectric material are introduced. Electrical circuit parameters for the FEM are also given. Chapter 6 presents a numerical study carried out for the purpose of Validation. The simulated Application of a piezoelectric shunt damping system for a ship and a ship's appendage is given in Chapter 7. Chapter 8 draws discussion and future works from the study and makes recommendations for further study. The overall conclusions are given in Chapter 9.

Supplementary information relevant to this study is provided in the appendices. Appendix A provides detailed information on Statistical Energy Analysis. Appendix B presents thermodynamic consideration and Gibbs free energy function. Appendix C gives ANSYS® APDL codes, which are used to model the beam in chapter 6. Appendix D presents the elements used for FEM in ANSYS^{R}. The piezoelectric constants are shown in Appendix E. Root mean square is shown in table form in Appendix F. The complete list of piezoelectric coupling constants is given in Appendix G. The detailed results of the LNG application are shown in Appendix H. The basics of finite element analysis are introduced in Appendix I. The processes of a numerical calculation in ANSYS are given in Appendix J. The alternative forms of the piezoelectric constitutive equations are introduced in Appendix K.

1.7 The Summary of the Chapter

In this chapter, the phenomenon of ship noise and vibration was explained. The main national and international noise and vibration criteria regarding ships were given to support the motivation of this study. General noise and vibration mitigation methods were briefly given. The smart material concept was presented and the use of piezoelectric materials was highlighted. Finally, the structure of the thesis was introduced in a logical manner.

2.Aims and Objectives

2.1 Aims

The overall aim of this study is to investigate the feasibility of using smart materials to attenuate the vibration and noise on board ships and develop suitable prediction/assessment techniques. The scope of the study will cover:

1. Prediction of ship vibration level
2. Mitigation of ship vibration level

2.2 Objectives

In order to achieve the overall aim of the thesis following specific objectives will be addressed in this research study.

- Review of Noise of vibration damping techniques including smart materials and their potential as noise and vibration damping.
- Investigation of working principals of Smart materials and feasibility of smart materials for mitigating the ship noise and vibration
- Development of most suitable mathematical and numerical modelling for Smart materials and their implementation on mitigating the vibration onboard ships.
- Validation of the developed approach for modelling the smart materials
- Application of smart materials on ships through a parametric study to investigate the effectiveness of the smart materials to reduce the vibration on board ships
- Recommendations on the use of Smart Materials with regard to noise and vibration damping for the broader marine community.

3.Critical Review

3.1 Chapter Introduction

|

In Chapter 3, critical review, based on the open literature, is given. The chapter starts with a review of nature of ship's structural responses (3.2) followed by discussion of means to isolate noise and ship vibration (3.3). The chapter then presents the notion of damping of vibration (3.4) and smart material applications for mitigating noise and vibration (in subchapter 3.5). Finally the review of modelling techniques of noise and vibration are discussed in 3.6.

3.2 Nature of Ship's Structural Reponses

Identification of the fundamental natural modes of a ship in the early design state is very critical in order to avoid possible problems such as deformation, structural failure, and interference of equipment, human and environmental factors.

As ships are complex structures they have a number of modes of vibration in the vertical, horizontal and torsional directions. Before giving a detailed structural model of any ship it is common to express a ship hull-girder vibration by representing the ship as a beam structure. Figure 3-1 presents the basic global mode shapes of a ship. *V* stands for vertical vibration, *T* stands for tortional vibration and node stands for a location of zero or minimum deflection. The node numbers are proportional to modal order (natural frequency).

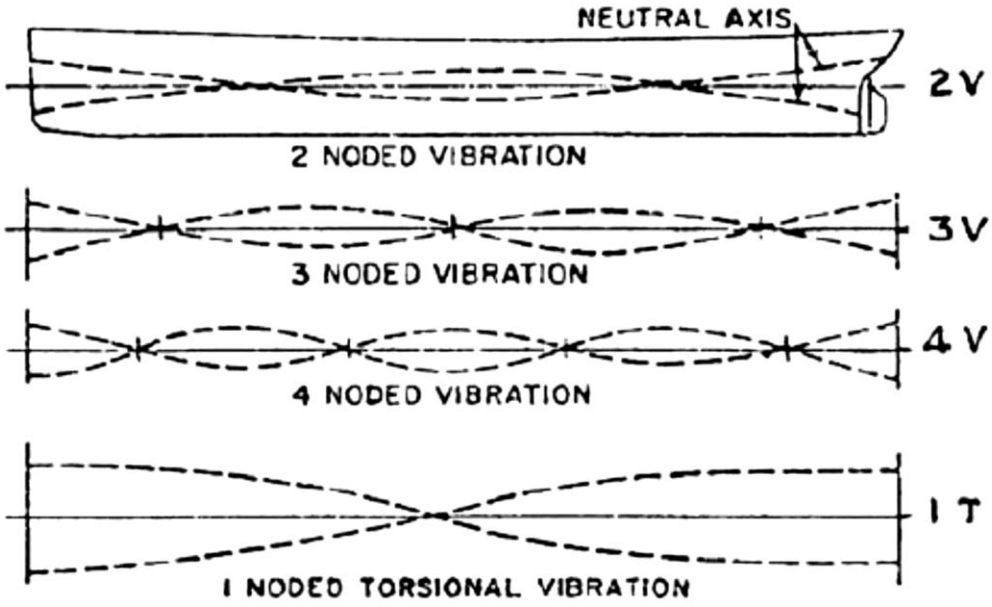

Figure 3-1: Modes of hull girder vibration (Vorus 2010)

Johannessen and Skaar (1980) collected data from sea-going ships and estimated the natural frequencies of the first four vertical bending modes of general cargo ships and of the first five vertical bending modes of tankers. They employed the ship displacement to define the hull girder natural frequencies for the chosen mode order (see Figure 3-2).

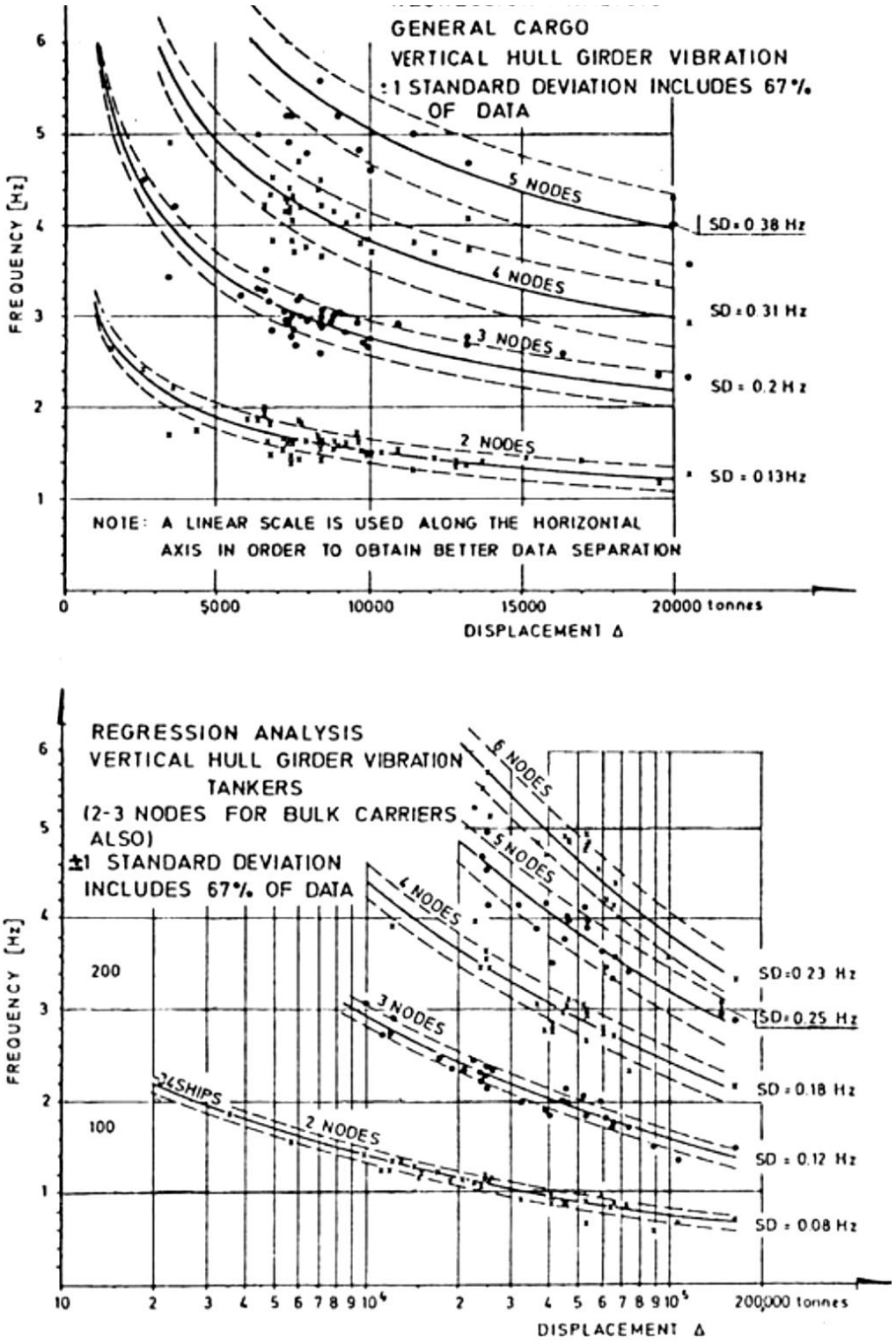

Figure 3-2: Natural frequencies of vertical hull vibration (Johannessen, Skaar 1980)

Nilsson and Tyvand (1981) presented the general noise spectrum of cavitating ship propellers. Figure 3-3 shows the noise spectrum level which has four regions:

1. Low-frequency that contains blade frequency ω_0 and its harmonics. The mean-power level increases as ω^4.
2. Mid-frequency that starts at bubble frequency ω_b. The mean power level increases as $\omega^{-5/2}$.
3. Intermediate-frequency is the transition region ω_t from II to IV.
4. The high-frequency region starts at bubble frequency ω_c and the mean power level decreases as ω^{-2}.

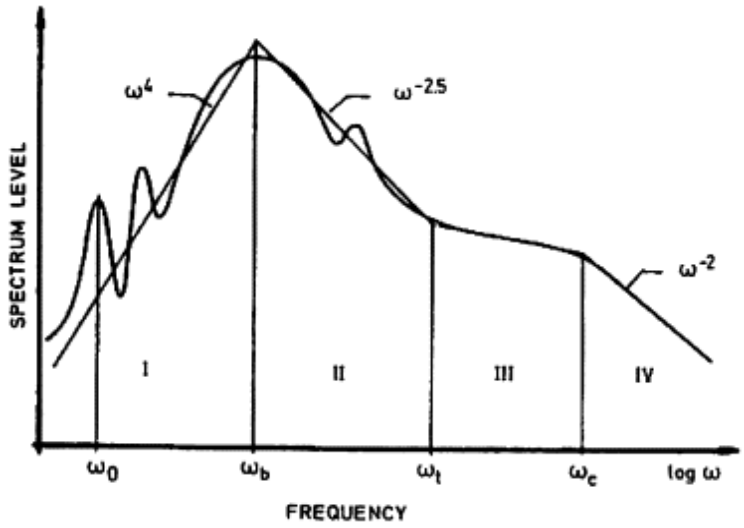

Figure 3-3: General noise spectrum of a cavitating propeller (Nilsson and Tyvand 1981)

Nilsson and Tyvand (1981) explained the fluctuations of the sheet cavitation volumes in region I and II. The pressure fluctuations seem very smooth at the high frequency noise in region IV. In this region, oscillations due to cavity collapse or shock wave generation would be expected to be observed.

Asmussen and Mumm (2001) presented fundamental natural modes for different type of ships, which were simulated with finite element models (FEM). Their study explained the relation between the ships and the natural frequencies. Figure 3-4 shows the global mode shapes and natural frequencies of the ship.

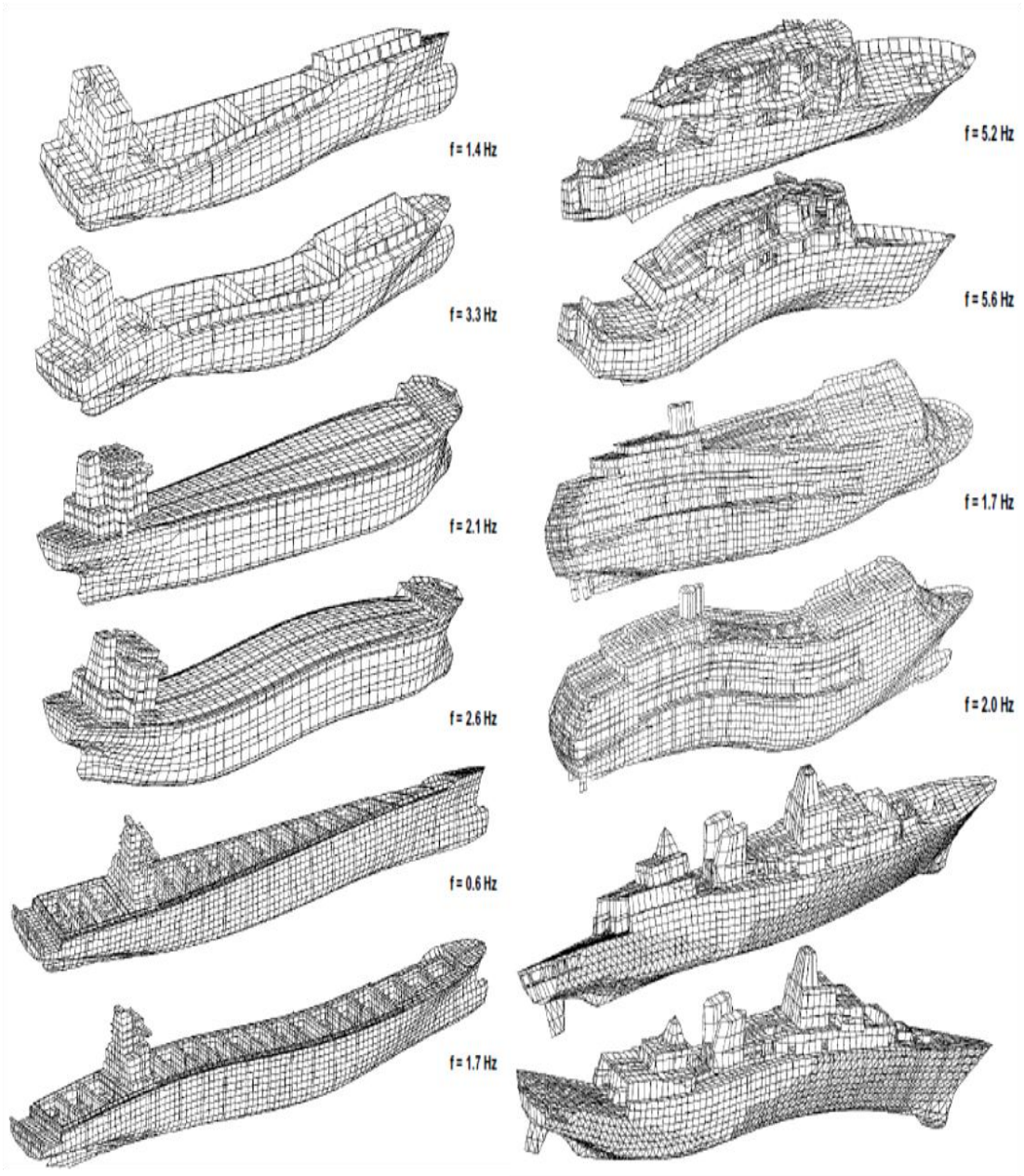

Figure 3-4: Natural torsional and vertical bending modes of various ship types (Asmussen and Mumm. 2001)

Asmussen and Mumm (2001) also introduced natural frequencies of typical ship members in a wide band.

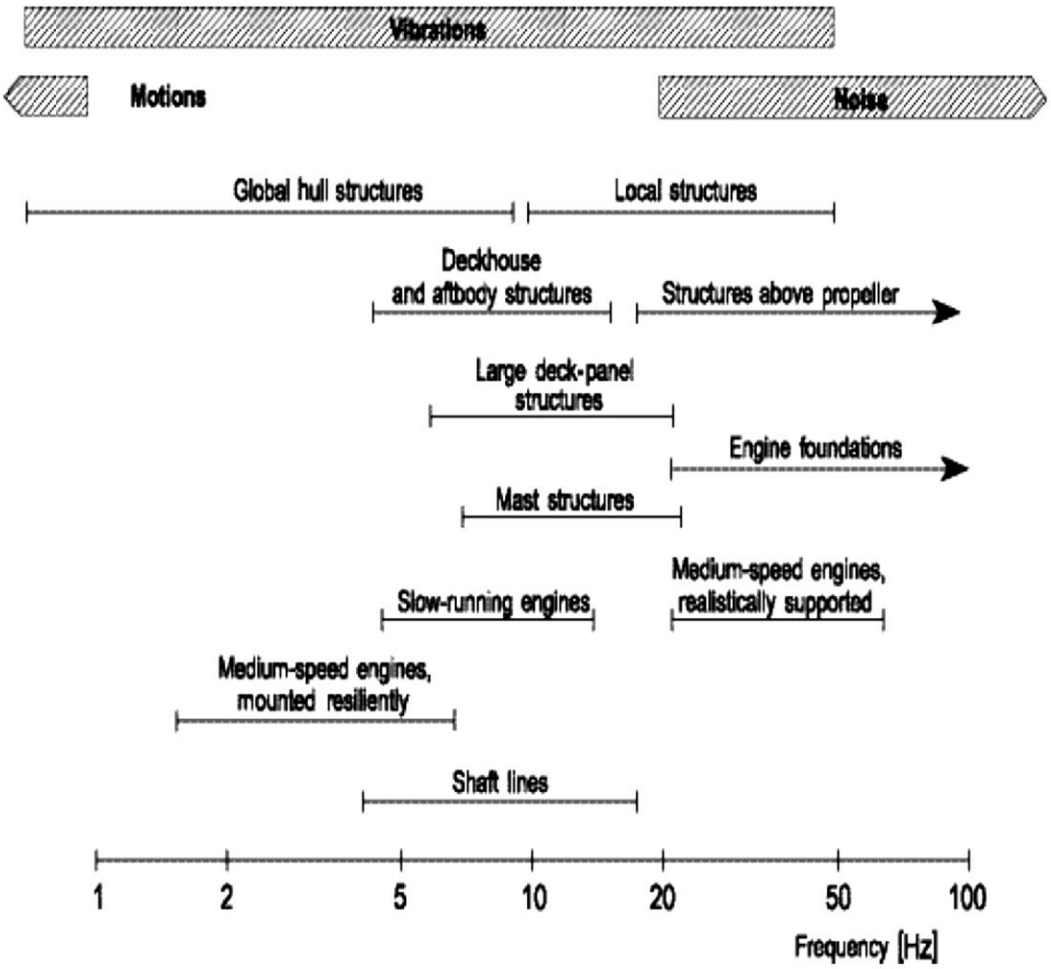

Figure 3-5: Natural frequency ranges in shipbuilding applications (Asmussen and Mumm 2001)

Noise and vibration propagation can be described as an energy flow from a source to a receiver. Ships are equipped with several machinery systems and have appendages such as rudder(s), keel(s) and fin(s), which can cause vibration due to combustion, rotation and flutter flow. These systems are connected by many transmission paths such as ship structure (solid domain) and surrounding water and air (fluid domain). A noise and vibration radiation model is illustrated in Figure 3-6.

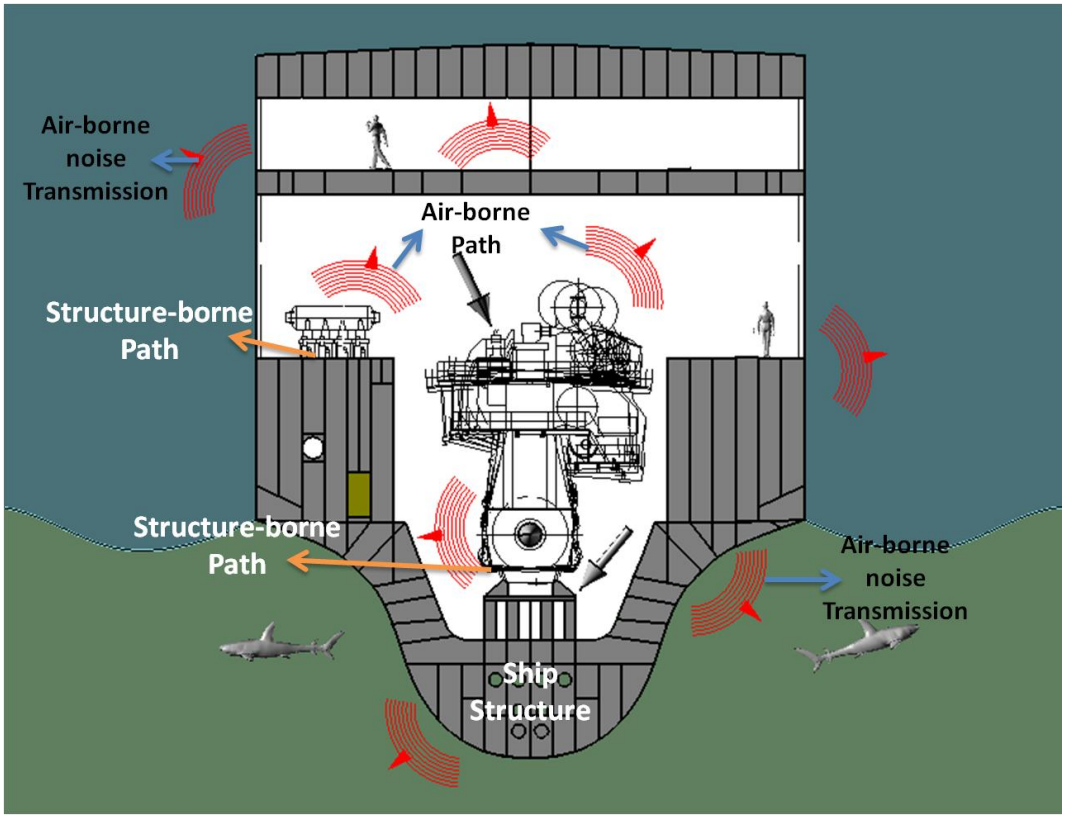

Figure 3-6: Noise and vibration radiation model

Koko et al (2002) illustrated the sources of noise within a ship's structure with its mounting system, as schematically depicted in Figure 3-7. The figure shows the various vibroacoustic paths through which the engine vibration is transmitted to the ship structure and eventually radiated into the surrounding mediums.

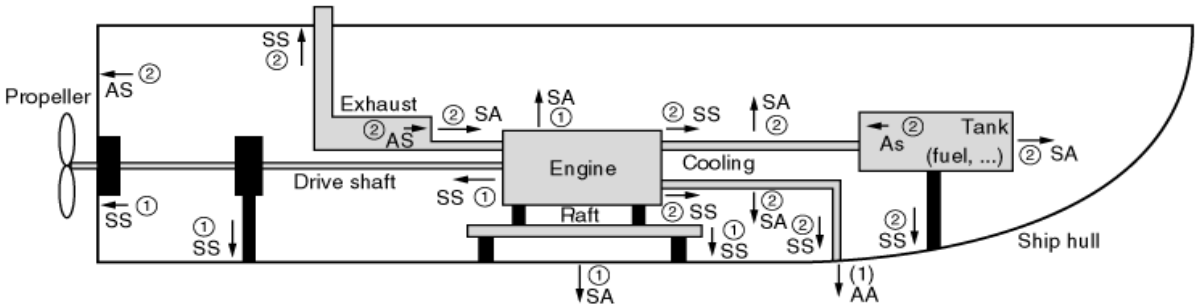

Figure 3-7: Typical marine diesel engine mounted on a ship hull (Koko et al. 2002)

In Figure 3-7, AA is acoustic to acoustic coupling, SS is structural to structural coupling, AS is acoustic to structural coupling, SA is structural to acoustic coupling. The relative importance of energy coupling for radiation into seawater is illustrated by number (1) for more important and (2) for less important.

3.3 Isolating Noise and Ship Vibration

Isolation is one of the ways to reduce or cancel the noise and vibration transmission between coupled systems by introducing discontinuities in order to decouple two points along the transmission path. The concept of the isolation can be explained with a mass-spring-damper model. Figure 3-8 shows the system of steady-state harmonic vibration for a single mass element. *M* is the mass, *K* is the stiffness, *C* is the damping, *x(t)* is the response frequency function, *f(t)* is the simple harmonic exiting force of amplitude *F* and *w* is the frequency of the oscillation.

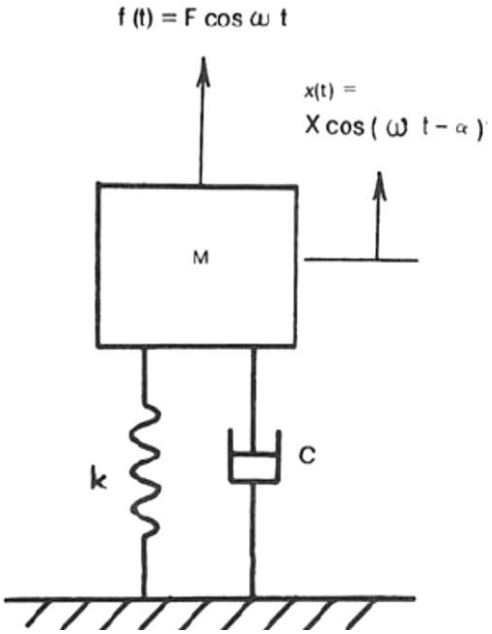

Figure 3-8: Steady-state harmonic vibration of one-mass system (Vorus 2010)

In Figure 3-9 the basic behaviour of the one-mass vibrating system is given (Vorus 2010). *w* is indicated as a excitation frequency and w_n is the natural frequency of a

system (engine foundation etc.). If w/w_n=1 exciting frequency is equal to the natural frequency of the system. This is so-called critical zone. Introducing flexibility (low stiffness) can shift the natural frequencies under to the zone lower than natural frequency.

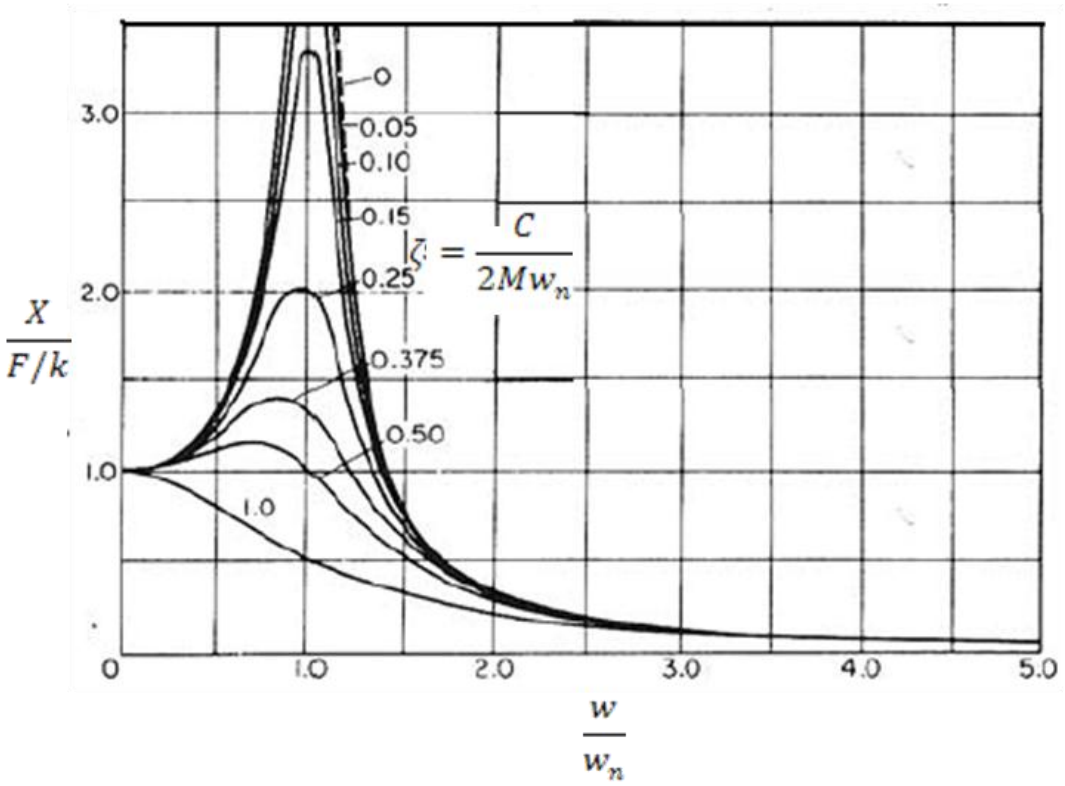

Figure 3-9: Vibration response characteristic, one-mass system

Discontinuity can be of two natures:

1. Geometric discontinuities: an element of almost the same material is inserted but with a much lower section area in order to have a lower rigidity (steel spring,)
2. Material discontinuities: a material with different elastic properties is interposed (machinery rubber mounting, floating floor)

Figure 3-10 shows the basic model of floating-floor construction. Plate 1 is simply supported and exited by a bending moment at x=0 and Plate 2 is supported by a continuous elastic interlayer (Nilson 1977).

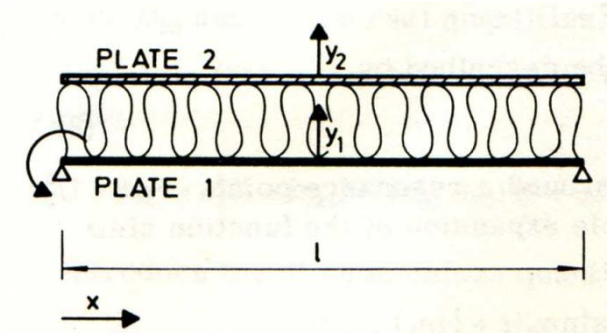

Figure 3-10: The model of floating floor (Nilson 1977)

3.4 Damping of Vibration

Damping is mitigating energy from vibrating structure and dissipating it into heat energy by repeated hysteretic cycles. Viscoelastic materials and rubber damping are introduced for their damping capabilities used as damper. Figure 3-11 shows the loading and unloading curve in the stress-strain plane creates an area (highlighted in grey) proportional to the dissipated energy per cycle.

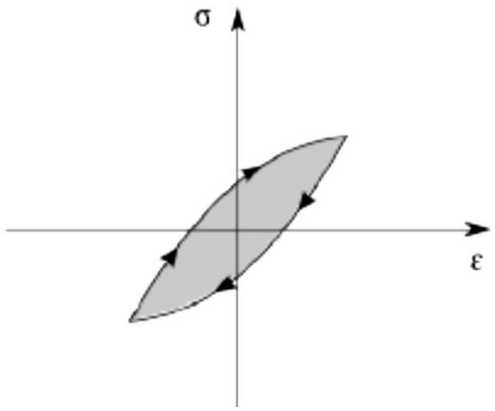

Figure 3-11: Example of hysteretic cycle of a viscoelastic material

The damping effect is proportional to the area size of the hysteretic cycle. Damping materials are particularly effective in areas where large deformations are present and, accordingly, large strains are imposed to the materials themselves.

Although the introduction of resilient mounting system as an isolating machinery support reduces vibration levels on the engine foundation vibration level on the

machinery itself may increase. In addition the machinery system has become more sensitive for excitation sources related to unbalance and misalignment (Silenv 4.2.2 D 4.7 2012).

Furthermore, temperature may be an important factor affecting the performance of damping materials. An appropriate damping material must be selected for the expected operating environment. Figure 3-12 shows that the total loss is a function of the temperature.

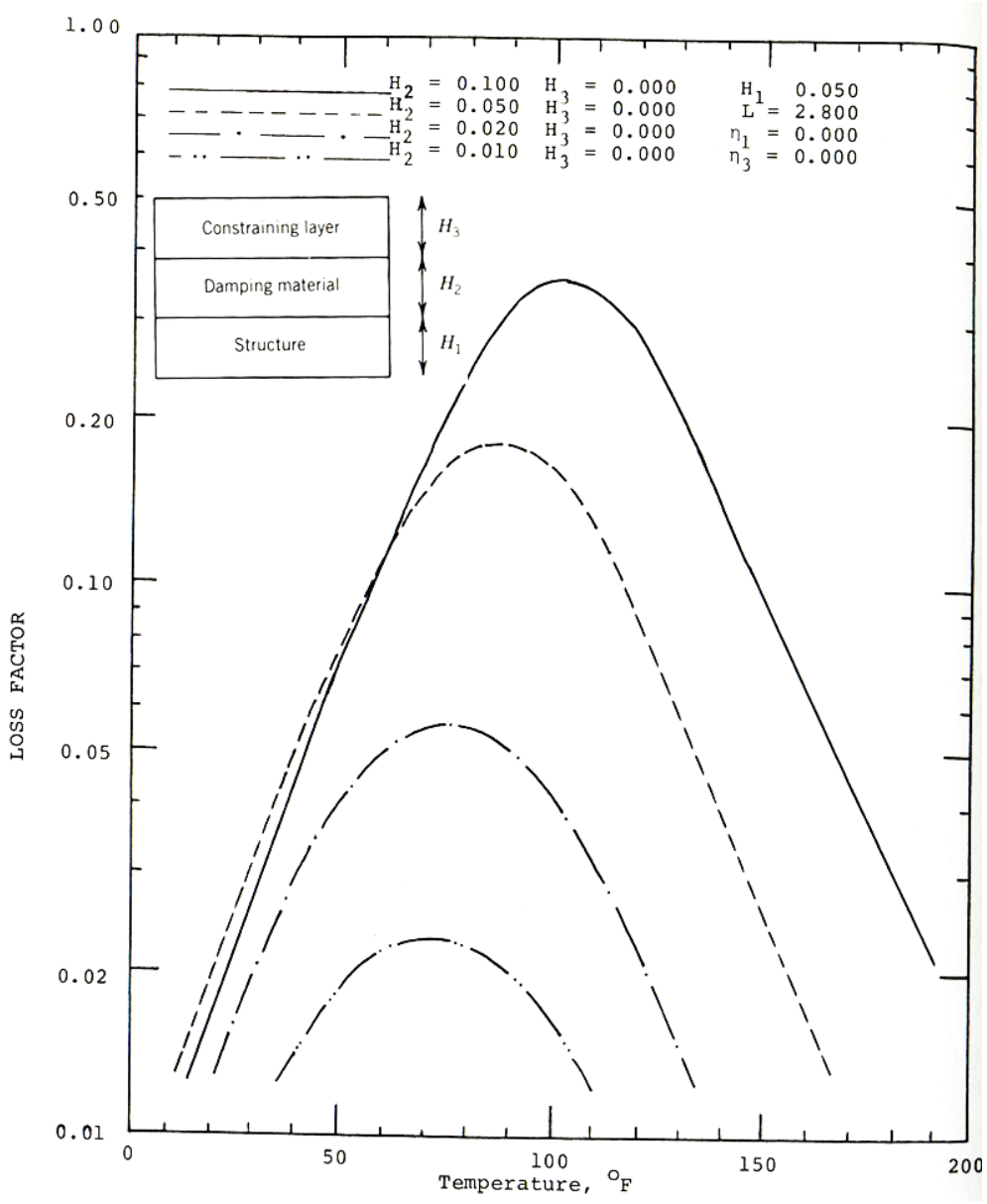

Figure 3-12: Variation of the damping performance of an unconstrained-layer treatment with temperature (Nashif et al. 1985)

3.5 Damping through Smart Materials

3.5.1 Smart Materials

Smart materials resemble biological structures or systems. A basic essential configuration of a biological system includes a control centre, sensors, actuators, a host structure and an energy source as can be seen in Figure 3-13.

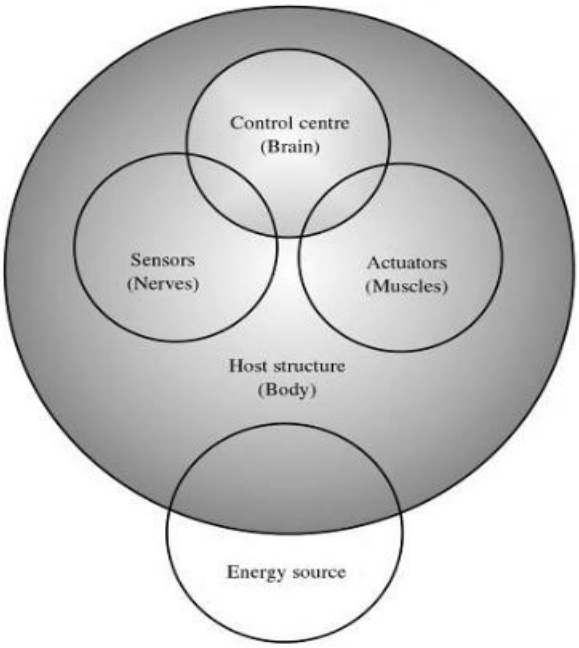

Figure 3-13 The basic essential configuration of a living system (Wadhawan 2007)

Gabbert and Tzou (2007) described applications of SMs with different terms such as smart structures, intelligent structures, adaptive structures, active structures, adaptronics, and structronics. SMs were defined as materials that can adapt to external loads or environmental changing. This is why SMs are very similar to what biological structures or systems are doing all the time.

There are a number of smart materials e.g. piezoelectric and electrostrictive materials, magnetostrictive materials, shape-memory alloys, optical fibers,

electrorheological and magnetoeheological fluids. Their common applications can be seen in microphones, loudspeakers, electrodynamic actuators, as well as hydraulic and pneumatic actuators (Schwartz 2002)

Gandhi and Thompson (1992) showed the historical development of material technology. Their study showed examples of the application of smart materials. Useful decision-making algorithms for material selection and comparison of smart materials were presented in terms of cost, technical maturity, linearity, working frequency range, and temperature.

Banks et al. (1996) introduced fundamental mechanisms of smart materials such as piezoelectric and electrostrictive elements, magnetostrictive transducers, electrorheological (ER) fluids, shape memory alloys, fiber optics. Their study highlighted also advantages and disadvantages of smart materials. Feedback control methodologies were discussed and theatrical applications were supported with experimental validations. They presented their application on self-excitation/self-sensing methods for detection, characterization of damage and active control of structural vibrations and structure-borne noise in smart material structures.

Koko et al. (2002) reviewed the application of active noise control (ANC) for noise and vibration of ship engines, machinery and appendages. They also recommended sensors and actuators for ship noise control requiring intelligent feedback systems which can be very complicated to operate and maintain as well as pricey.

Hurlebaus and Gaul (2006) reviewed smart material applications in dynamics technologies. Their applications were given as semi-passive concepts, energy harvesting, semi-active concepts, active vibration control, and active structural acoustic control fields.

3.5.2 Piezoelectric Materials

Crystal physics covers pyroelectricity, permittivity, piezoelectricity, elasticity, specific heat and thermal expansion. The interaction between electric field strength

and temperature is called pyroelectricity. Piezoelectricity can be explained as a relationship between electrical and mechanical systems. Piezoelectric materials (and pyroelectric materials) are made from ferroelectric crystals. They have been commonly labelled as smart material and applied as actuator and transducer.

The following literature survey about the research of piezoelectric materials is given in chronological order.

The piezoelectric effect was discovered in 1880 by the Curie brothers who studied the relationship between pyroelectric and crystal symmetry (Curie and Curie 1880). A material which has pyroelectric properties can generate electricity under heat, whereas piezoelectric materials can generate electricity under pressure. Knowing that the electrification is generated by mechanical pressure they investigated in what direction pressure should be applied. One of the early applications of piezoelectric material was made to detect submarines made in the early 20^{th} century. Paul Langevin used quart-steel sandwich transducers, which are hence called Langevin-type transducers in ultrasonic engineering. (Ikeda 1996).

Lawson (1942) investigated the dynamic characteristics of infinite piezoelectric plates. He located a piezoelectric crystal between two grounded electrodes and introduced a function to define resonance frequencies of free vibrating piezoelectric plates. His function has limitations as the boundary conditions are chosen for zero volt electrical potential.

The dynamic equations of piezoelectric materials were derived by Tiersten (1962) for the first time. He introduced linear piezoelectric constitutive equations for the thickness vibrations of an infinite anisotropic plate with installed electrodes on the top and the bottom surfaces. Tiersten satisfied the differential equations of linear elasticity for piezoelectric materials.

The properties of piezoelectric crystals and ceramics in the field of electroacoustic transducers were reviewed by Jaffe and Berlincourt (1965). The variables of linear piezoelectric constitutive equations are presented in an electroelastic matrix for Crystal Class 2MM (see Table 3-1). This matrix gives a formulation to understand

the relationship between electrical properties and mechanical properties. For example,

Independent variable E,T $S_1 = d_{31}E_3 + s_{11}T_1$ 3-1

Independent variable E,T $D_1 = e_{11}E_1 + d_{15}T_5$ 3-2

Table 3-1 Electroelastic Matrix for Crystal Class 2MM

	E_1	E_2	E_3	T_1	T_2	T_3	T_4	T_5	T_6
D_1	e_{11}							d_{15}	
D_2		e_{22}					d_{24}		
D_3			e_{33}	d_{31}	d_{32}	d_{33}			
S_1			d_{31}	s_{11}	s_{12}	s_{13}			
S_2			d_{32}	s_{12}	s_{22}	s_{23}			
S_3			d_{33}	s_{13}	s_{23}	s_{33}			
S_4		d_{24}					s_{44}		
S_5	d_{15}							s_{55}	
S_6									s_{66}

where *T* is the stress and *S* is the strain, *E* is the electric field, *D* is the displacement, The piezoelectric compliances are *d* (strain coefficients), *e* (stress coefficients), *s* is the elastic compliances.

Dökmeci (1974) studied piezoelectric materials for low and high frequency vibration. He introduced the theory of crystal finite surfaces and used a variational theorem derived from Hamilton's principle in the three-dimensional theory of linear piezoelectricity.

Haun et al. (1987) conducted experimental studies on the properties of piezoelectric materials. They used high-temperature x-ray diffraction to determine the piezoelectric constants *d* (meter per volt) and *g* (meter per Newton). The output is given in Figure 3-14 and Figure 3-15. Those constants were used in the elastic Gibbs free-energy expansion and the equations are explained in Appendix B.

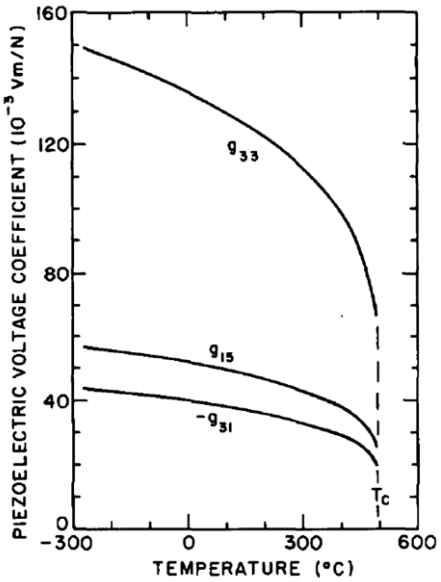

Figure 3-14: Piezoelectric voltage coefficients (g_{ij}) plotted vs. temperature (Haun et al. 1987)

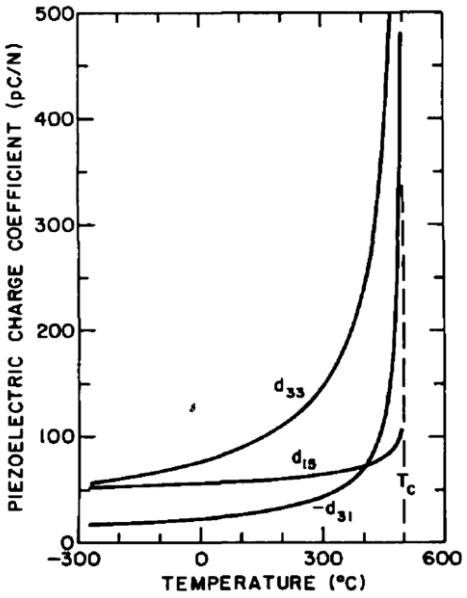

Figure 3-15: Piezoelectric charge coefficients (d_{ij}) plotted vs. temperature (Haun et al. 1987)

Ray et al. (1993) presented the exact solutions for static analysis of a simply supported rectangular plate-type intelligent structure. The structure is composed of a laminated substrate of graphite/epoxy composite coupled with distributed sensor and actuator layers of biaxially polarized piezoelectric polymer (PVDF).

Tzou (1993) investigated the electromechanical phenomenon of the coupling between the elastic and electric fields. He proposed a linear piezoelastic thin-shell vibration theory. The theory was based on the Hamilton's principle, the linear piezoelectric theory, and the Kirchhoff-Love hypothesis which neglects the effect of transverse shear deformations and rotator inertias.

Piezoelectric sensors and actuators were investigated by Hwang and Park (1993) using the finite element method. They modelled the mechanical-electrical interaction and developed an efficient finite element code for vibration control with piezoelectric material. They presented one of the early numerical applications of an active damping system as the system had a feedback controller.

Zhou and Tiersten (1994) applied voltage on the top and bottom surfaces of a piezoelectric material laminated onto a composite plate. Externally applied voltage forced the composite plate into cylindrical bending. The shearing stress along the interface between the top surface of piezoelectric material and the top surface of the composite plane was obtained by using an elastic solution. Plate theory and three-dimensional elasticity were used to validate results of the linear elastic solutions.

Harris and Priesol (2002) presented the piezoelectric material types and their usage in measurement, testing, design, and control fields. The applications of piezoelectric materials were given for different working conditions and application areas. Some of the most known piezoelectric materials are introduced below:

1. PZT (lead zirconate titanate) is the most common piezoelectric material. PZT is a polarized ceramic used in accelerometers, sonars etc. This material

is low in cost, high in sensitivity and durable in the temperature range from -100°C to +288°C.

2. Quartz is a single-crystal material used in accelerometers, watches etc. It has a substantially lower sensitivity than polarized ceramics, but its characteristics are very stable with time and temperature; further it has high resistivity.
3. Lithium niobate and tourmaline are single-crystal materials used in accelerometers at high temperatures (up to 649°C and 760°C).
4. Polarized polyvinylidene fluoride (PVDF) is an engineering plastic similar to Teflon. It is used as a sensing element in accelerometers and active damping systems. PVDF materials are highly pyroelectric, as a result they are also used as thermal sensing devices. PVDF is an economical material, however, it is less stable with time and temperature changes than ceramics or single-crystal materials.

Fernandes and Pouget (2003) created a new analytical approach to evaluate static and dynamic performance of piezoelectric bimorph structure. They refined the elastic displacement and electrical potential to develop the approach. Two different arrangements were investigated as series and parallel bimorphs. The results were compared to results from the Love-Kirchhoff theory and the finite element method.

3.5.3 Piezoelectric Shunt Damping Systems

Piezoelectric materials have typically been used for sensor and actuator applications, because of their strain-dependent charge output. This ability led to the invention of many devices such as accelerometers, sonars, microphones, load cells, etc. All of these applications can be called sensors as they sense the dynamic or static loads. Forward (1979) suggested a passive damping system and an active vibration controlling system by using piezoelectric materials. His pioneering concept was explained experimentally. He used small piezoelectric transducers bonded on the glass frame. Dynamic structural responses were reduced by inductive shunting.

The earliest mathematical model of passive piezoelectric shunt damping system was introduced by Hagood and von Flotow (1991). They configured this new damping method with a piezoelectric material which was bonded on a base structure and a simple passive electrical circuit was shunted with piezoelectric material (see Figure 3-16). The electrical circuit had also different configurations. Each configuration had different electrical components such as resistor, inductor and/or capacitor. Hagood and von Flotow established derivation and analytical foundation for analysis of a general system with shunted piezoelectric material. They also classified two shunting circuits: the resistor circuit and the resistor-inductor circuit. Their experimental study was carried out with a cantilever beam structure and a good agreement found between the equivalent circuit approach and the real model. Hagood and von Flotow defined the material loss factor as high as 42% in longitudinal loading case for common resistor shunted piezoelectric. For this reason, piezo-shunt damping systems can be seen as an alternative to viscoelastic materials in structural damping applications.

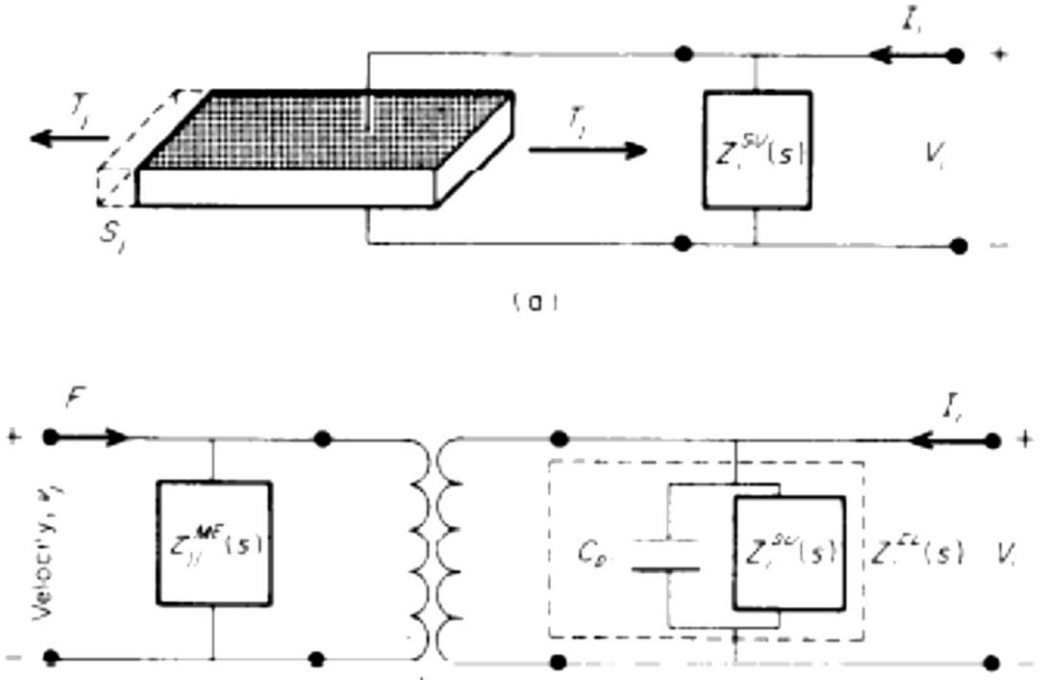

Figure 3-16: Simple physical model of a uniaxial shunted piezoelectric and its equivalent electrical network (Hagood and von Flotow (1991)

In the passive piezoelectric shunt damping approach, the electrical output of the piezoelectric material is used for damping purposes rather than sensing (Anton and Sodano 2007). This approach is regarded as simple, low-cost, light-weight, and easy-to-implement (Fein 2008).

Holkamp (1994) investigated the performance of passive piezoelectric damping devices for a vibration beam. Successfully, he achieved peak reductions of responses as 19 dB and 12 dB in the second and third bending modes respectively.

Piezo-shunt damping systems were reviewed by Lesieutre (1998). He explained four basic types of piezo-shunt systems causing a characteristically different electrical-dynamics behaviour. Configurations of the different shunt circuits were given as inductive, resistive, capacitive, switched.

Steffen and Inman (1999) studied active vibration control systems and passive shunt damping systems with piezoelectric materials. Instead of comparing the techniques, a general methodology was presented for optimal design of piezoelectric materials for mitigating vibration over a frequency band. Their study also provided information regarding the attenuation or reduction of the vibration.

Park (2003) studied simple beam vibration damping with a piezoelectric material shunted circuit (resistor-inductor circuit). He analysed the circuit components in series and in parallel setups which are shown in Figure 3-17.

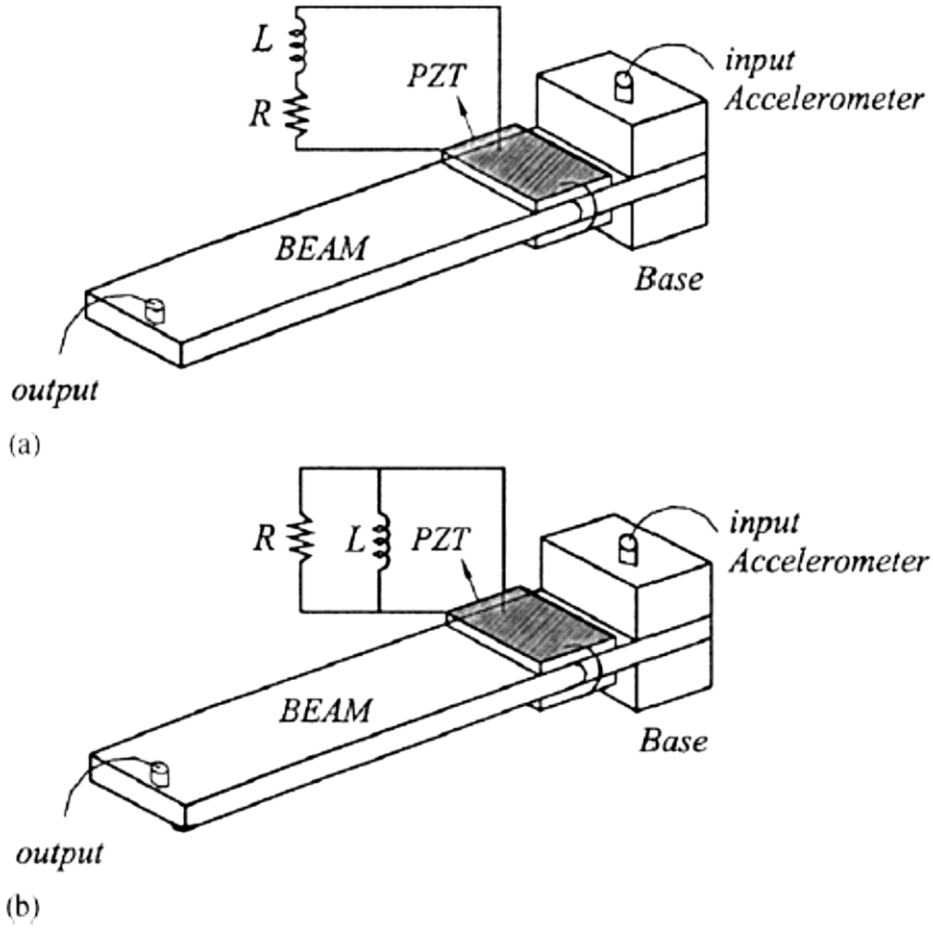

Figure 3-17: Schematic drawings of experimental setup for: (a) a series R-L and (b) R-L shunt circuit (Park 2003)

Park (2003) further developed a piezo/beam system combined with a series and a parallel resistor-negative capacitor branch circuit. The system had a piezoelectric damper connected to a series and a parallel resistor-negative capacitor branch circuit shown in Figure 3-18. His theoretical analysis showed this damping system could significantly reduce the multiple-mode vibration amplitudes over the whole structural frequency range. Park (2003) also applied a synthetic inductor. That helps to reduce the size of the inductor and provides various inductance.

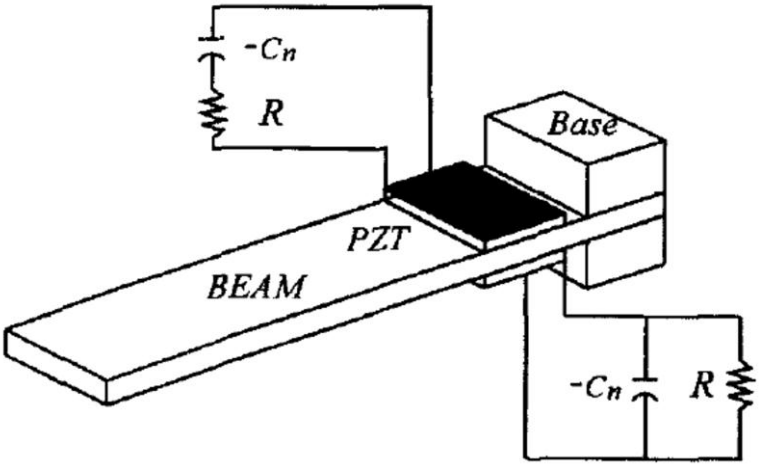

Figure 3-18: A schematic drawing of the shunted piezo/beam system (Park 2003)

Wang (2004) investigated the effect of different finite element modelling such as a different number of finite sub-layers, two dimensions and three dimensions. This was done in order to establish more accurate and efficient piezoelectric models. In Wang's study a frequency shifting was shown when open and close circuit boundary conditions were applied. Meitzler et al. (1988) reported the frequency differences between two boundary conditions, which were defined as the generalized electromechanical coupling constant (K_{ij}). The coupling constant defines a piezoelectric material's first order electrical-to-mechanical energy conversion efficiency. K_{ij} is a measure of efficiency, but not the actual efficiency.

Park and Baz (2005) presented theoretical and experimental techniques for simple and effective passive vibration dampers with negative capacitive shunting. A pair of interdigital electrode piezoceramics was used to mitigate multimode vibration of a simple beam. Park and Baz used a hybrid passive damping system to mitigate the multiple vibration modes of beams. This damping system contained multi layers (constraining layer, piezoelectric material, viscoelastic layer), which were bonded on to a base beam element and a resonant shunt circuit was bonded to piezoelectric material. As a consequence this unconventional damping system has a wide frequency range damping capacity.

All those passive piezoelectric shunt damping systems were applied to simple geometries such as beam elements and cylinder bodies. This can be problematic if this damping system is applied to complex geometries (like ships), which have a number of structural members. Barker et al. (2005) presented a finite element model solution for piezoelectric elements attached to a host structure to reduce the vibration of the system. They further made parametrical investigations of piezoelectric shunt damping. Those parameters included piezoelectric patch thickness and impedance of the passive electrical network.

Nguyen and Pietrko (2006) used the finite element method to simulate actuator-beam-sensor vibrating systems. A commercial software (ANSYS^{R}) was employed for the numerical model. A resistance-inductor circuit was chosen as an electrical component to be connected to piezoelectric material in order to mitigate vibration. They optimized tuned values for the resistor and inductor of the shunt circuits at the resonant frequencies. This numerical application successfully calculated the dynamics of the system and simulated vibration reduction was achieved.

Anton and Sodano (2007) reviewed vibration energy harvesting. They highlighted the important parameters, operation condition, and configuration of piezoelectric material with examples from literature.

Fein (2008) studied piezo-resistive damping systems and developed a two dimensional analytical model. He improved the basic concept of a damping system for one-dimensional structures and developed the more general two-dimensional model.

Min et al. (2010) investigated the effectiveness of a piezoelectric shunt circuit damping system for the turbo-machinery rotor blades vibration control, specifically for a condition with centrifugal rotation. A FEM of piezoelectric shunted circuit was used for carrying out harmonic analysis. This analysis was used to simulate vibration damping of rotating blades.

Khaligh et al. (2010) investigated harvesting kinetic energy of small scale devices. The devices had functionalities such as wearable electronic devices, mobile electronics and self-powered wireless network nodes. Their study summarized the

technical ratings (output power, size, mass, usage frequency) of the existent piezoelectric generators.

Kim et al. (2011) studied passive and active piezoelectric shunt damping systems for a single degree of vibration structure. Resistance-Inductor parallel circuits were analysed by using the impedance-mobility approach for passive damping.

Han et al. (2012) used an approach called “synchronized switching damping on negative capacitor and inductor” (SSDNCI). It is an adaptive shunt damping circuit which consists of a switched inductance-resistance network (SSDI) and is connected in parallel to a negative capacitance for improved damping performance.

3.6 Review of Modelling Technique

Lyon et al. (1959) developed the Statistical Energy Analysis (SEA) method to predict dynamic performance of thin space-craft or aircraft structures. The target structures have complex geometry and they are excited by sources such as jet noise, turbulent boundary layer, etc. SEA is a successful tool to predict structural responses (as average vibration amplitudes) and sound pressure in space vehicles, airplanes, buildings, large machines and ships in a high frequency band. The SEA energy balance equations result in a set of linear equations that can be used to calculate loss factors, coupling loss factors or net energy flows and incoming powers (Lyon and DeJong 1995). In SEA, the entire structure is divided into coupled, simple subsystems to be analysed. Figure 3-19 illustrates a simplified model of a ship.

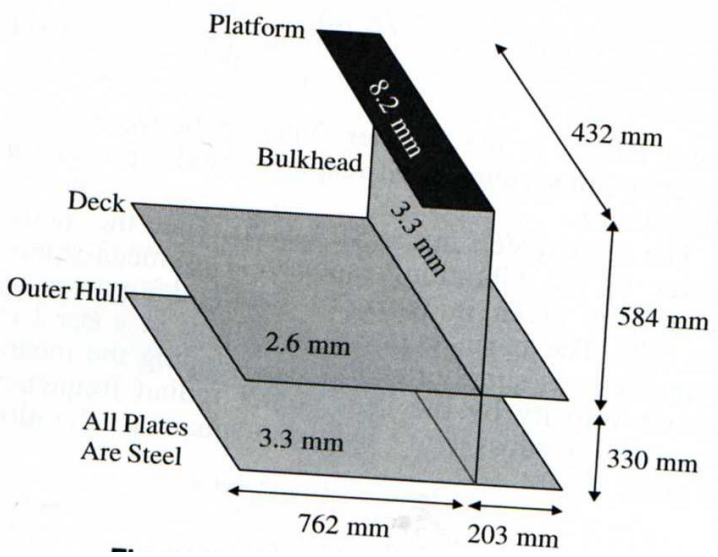

Figure 3-19: Simplified ship structure (Crocker, 2007)

Sawley (1969), Jensen (1976), Kihlman and Plunt (1976) applied the approach to predict a ship's noise level. Their noise level predictions showed a good accuracy with measurements. However, the predictions were not accurate in the low frequency level. Although the SEA approach predicts noise levels successfully in the high frequency range, it still needs parameters such as coupling loss factors (CLF) and noise level of sources. These parameters should be estimated or measured to complete numerical setting up before any calculation. Therefore, a number of studies have been estimating CLF (Fahy 1982; Gibbs and Tattersall 1987; Craik and Smith 2000). De Langhe (1996) introduced different approaches to predict noise and vibration. Mainly, he compared the statistical method and deterministic methods (e.g. finite element method, boundary element method). His study can be seen as an useful guideline for different prediction techniques of structural dynamics.

The Finite Element Method (FEM) has been widely used to simulate and solve a structural problem of ship since early seventies. Genalis (1972) explained the technique briefly as five sequence steps:

1. Discretization of the structure. A collection of simply connected domains, called finite elements, represents the true structure.
2. Discretization of the field variable. It is assumed that the finite elements are a form of a continuous variation of forces and/or displacements.

3. Local and global stiffness. Each element has (local) stiffness. As the overall structure is composed of many elements and these elements are connected at their adjacent points (nodes), superposition of the local stiffness matrices will lead to the global matrix . The global matrix relates the nodal forces and displacements of the assembled structure in its coordinate system which is transformed from local coordinated to global coordinates.
4. Solution for the displacements. Unknown variables in the global matrix will be obtained by some methods (Gaussian elimination, matrix decomposition, partial pivoting etc.)
5. Stress computation. The obtained displacements are used to calculate the stresses based on the strain field derived from the assumed displacement pattern. Averaging techniques may be employed to interpret the results at this step.

Genalis (1972) applied the FEM to a multihull ship (ASR-21) structural analysis. The ship structure was presented as finite elements shown in Figure 3-20. He interpreted the FEM in terms of definition of the structural modelling, the boundary conditions and accuracy of findings as well as required computational power needed to solve the problem.

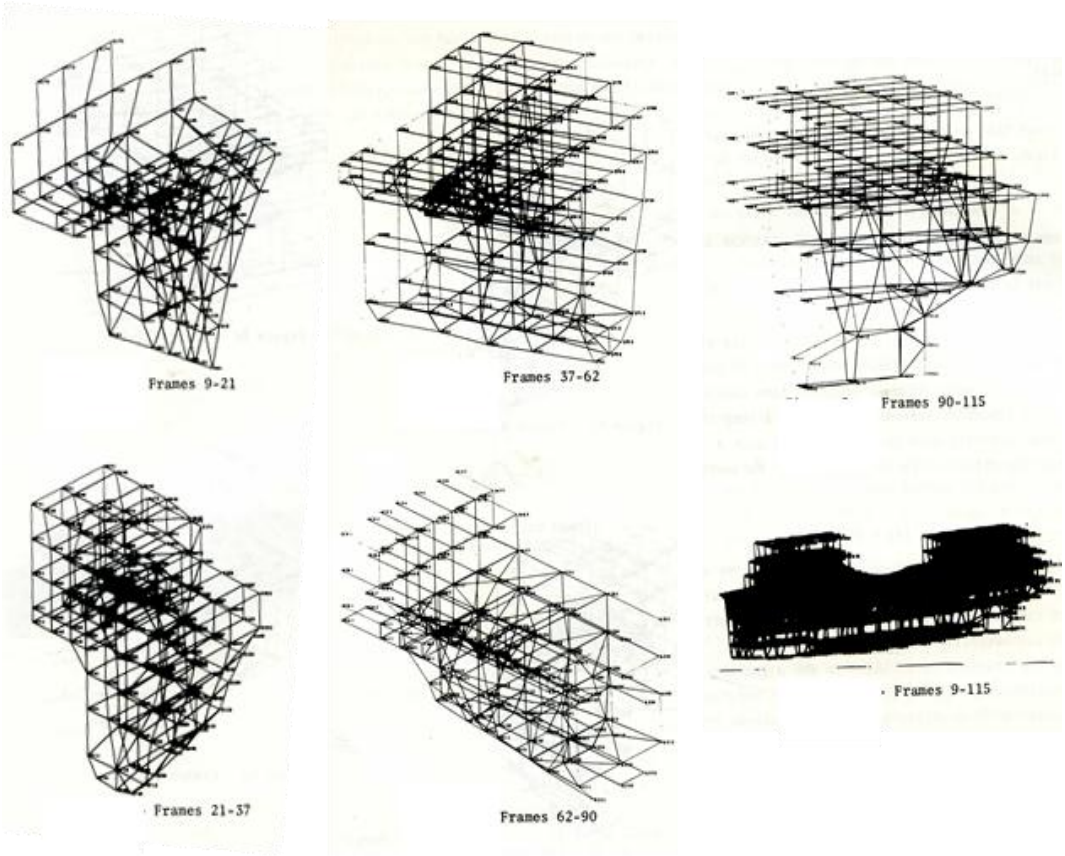

Figure 3-20: The FEM model of the half catamaran vessel (Genalis 1972)

Ross (1976) collected ship noise data simultaneously and carried out research on prediction of noise level. In his statistical study, the source spectrum level of ships was estimated as a function of ship speed and displacement. The estimations were based on a number of measurements, shown in Figure 3-21.

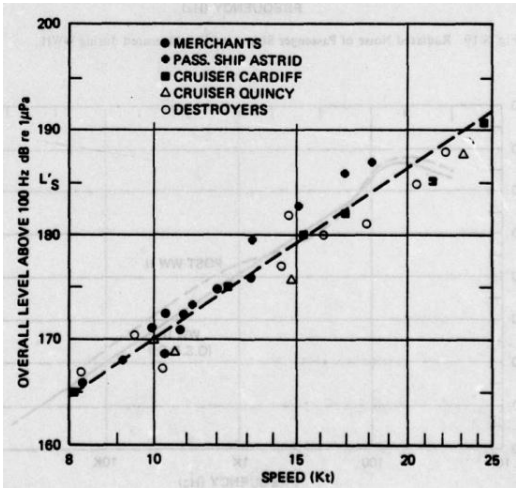

Figure 3-21: Speed dependence of overall radiated level of surface ships, as measured during The Second World War (Ross 1976)

The functions were given as following:

$$L_s = 112 + 50log\frac{U_a}{10knots} + 15logDT \quad 3\text{-}3$$

and

$$L_s = 134 + 60log\frac{U_a}{10knots} + 9logDT \quad 3\text{-}4$$

where U_a is ship speed in knots and DT is the displacement tonnage. Ross' prediction method has, however, limitations regarding the maximum weight of ships (30000 tons) and the speed range. Moreover, the results were given in terms of the overall noise level above 100 Hz. This means that the noise level cannot be investigated in a wide frequency band.

Nilsson (1978, 1980) has proposed a noise prediction program, so-called waveguide methods, for early design stage to estimate noise level in a ship. His method is describing the structure-borne noise propagation. This method is similar to the SEA method (Lyon and DeJong 1995). The propeller excited hull plate vibration and full scale measurements of a ship for different operation conditions were carried out.

Nilsson made noise level predictions using a simple plate model in a tanktop construction or in an engine foundation. However, uncertainties occurred for the predicted noise level in the low frequency band.

Nilsson (1976, 1978, 1981) developed another method for extending his previous noise prediction model. This model predicted the structure-born noise damping in the junctions of plate panels and stiffeners of a ship structure. He highlighted that finite element modelling was needed to estimate dynamic responses of the hull.

Brown (1999) provided a definition of hull plate acceleration. Further, he developed an approach to predict the noise level of cavitating propellers. This approach was based on the acoustic intensity, the number of blades and the diameter of the propeller, tip speed and the absolute head above vapour pressure. Brown suggested that the level of cavitation noise can be reduced by the application of swept-forward leading edge outlines and more rounded blade section leading edge profiles. His study can be used as a propeller analysis tool for early design state as well as defining boundary condition for a structural analysis. Brown's approach described area of sheet cavitation on the propeller blade and provided valuable information for the cavitation development at the near field of a propeller. This approach can be improved when the volume of the cavity is taken into account, because travelling cavitation bubbles, from near field to far field, are collapsing after reaching the maximum volume. This situation causes noise in the high frequency range. The noise level can be estimated based on the volume of the bubble (Ceccio and Brennen 1991).

3.7 The Summary of the Chapter

In Chapter 3 Previous studies investigating noise and vibration in ships and smart material applications for noise and vibration controlling techniques were presented and discussed. Emphasis was put on piezoelectric materials and vibration damping with passive piezoelectric shunt electrical circuits. The critical review given in this

chapter intended to highlight the main findings of past research. The investigation of damping ship structural vibration with piezoelectric materials and passive electrical circuits has become the main focus of this study.

4.Methodology

4.1 Chapter Introduction

In Chapter 4 the methodology is given to satisfy aims and objectives of this study. The concept of passive piezoelectric shunt damping is analysed in subchapter 4.2. Then the Finite Element Analysis and Statistical Energy Analysis used to calculate noise and vibration in this study are briefly explained in subchapter 4.3. Finally the case studies employed to fulfilled aim and objectives are introduced in subchapter4.4.

4.2 Methodology of Piezoelectric Shunt Damping

A piezoelectric shunt damping system is a passive vibration damping system including piezoelectric material and an external electric circuit (Hagood and von Flotow 1991; Hollkamp 1994; Lesieutre 1998; Park 2003; Park and Baz 2005; Han et al. 2013). A vibrating structure is comprised of bonded piezoelectric material in conjunction with an electrical network to mitigate the vibration energy.

Piezo-shunt damping systems can be of different types, depending on the configuration of the electrical component of the circuit. Configurations of four different shunt circuits are listed below (Lesieutre 1998):

1. Inductive: An inductive-shunt circuit is a resonant (damped) absorber and is similar to a mechanical vibration absorber. An inductive shunt causes a resonant LC circuit (see Figure 4-1).

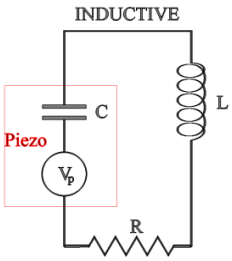

Figure 4-1: Inductive-shunt circuit (Lesieutre 1998)

2. Resistive: A resistance shunt circuit is a frequency dependent damping and is converting vibration energy to joule heating. This results in structural damping (Figure 4-2).

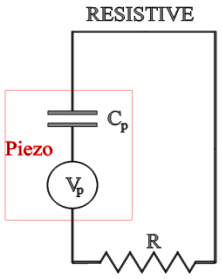

Figure 4-2: Resistive-shunt circuit (Lesieutre 1998)

3. Capacitive: A capacitive-shunt circuit is a frequency depended stiffness and alters the stiffness of the piezoelectric material. Mechanical vibration can slowly be mitigated with this approach (Figure 4-3).

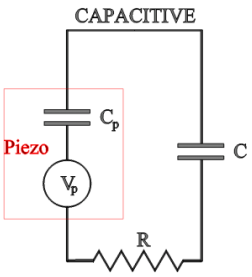

Figure 4-3: Capacitive-shunt circuit (Lesieutre 1998)

4. Switched: A switched-shunt system is controlling energy transfer and has the capability to vary rapidly in response to the instantaneous conditions of a

structure/shunt system. Vibration energy can be converted with a switched-shunts system (Figure 4-4).

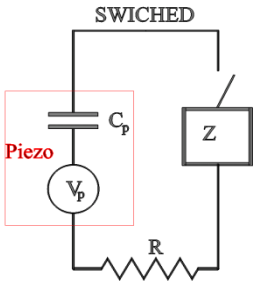

Figure 4-4: Switched-shunt circuit (Lesieutre 1998)

The most effective passive piezoelectric vibration control configuration is the Resistor-Inductor (R-L) shunt control. Energy is dissipated by joule heating through a connected resistor (R). The inductor (L) is used for tuning the electrical natural frequency.

This damping system can also be explained with the analogy between structural elements and electrical elements. Resistor, inductor and voltage are considered as spring, mass and alternating force.

A chosen circuit is connected to a piezoelectric material, located on a host structure. A piezoelectric inductive-resistive shunt circuit is shown in Figure 4-5.

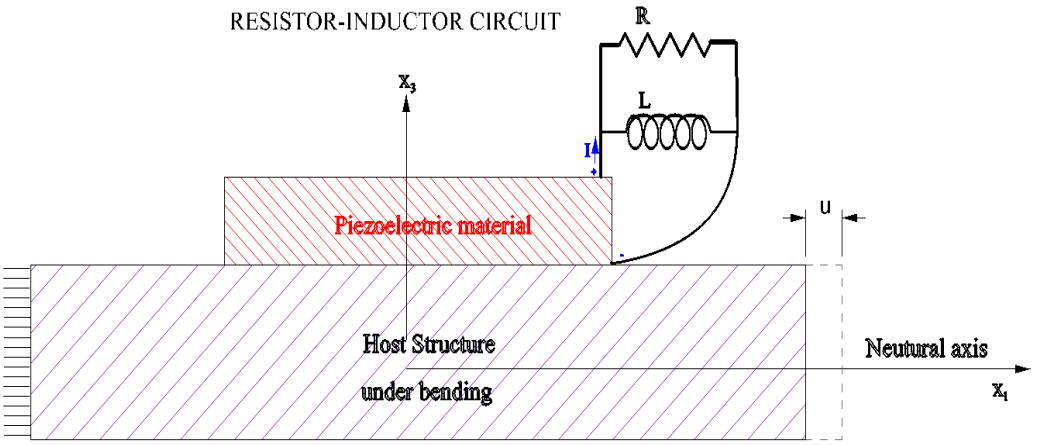

Figure 4-5 : Demonstration of a piezoelectric shunt circuit vibration damping system

4.3 Methods to simulate noise and vibration

Generally vibrating systems are complex and, therefore, taking into account all details of these systems for mathematical analysis can be quite challenging. Thus, the most important features should be concentrated on. Crucial features include input (geometry, material, excitations) and output (responses) factors.

There are several existing methods to simulate noise and vibration, for example the Statistical Energy Analysis (SEA) for middle and high frequency noise-vibration estimation of ships and the Finite Element Method (FEM) for low frequency structural analysis of ships.

4.3.1 Statistical Energy Analysis

SEA was developed in 1959 by Lyon, Smith and Maidinik to predict the mean square velocities of thin space-craft or aircraft structures, excited by sources (such as jet noise, turbulent boundary layer, etc.), which are random in nature and contain wide frequency bands. The responses of complex systems are estimated by using power flows. The technique focuses on the analysis of energy levels in resonant modes of coupled subsystems (Richard H. Lyon 1995). The detailed explanation of SEA is given in Appendix A.

4.3.2 The Finite Element Analysis

The FEM is a numerical method, which has been used since the late 1960's, for continuous systems in engineering. Very early applications of the method were to solve complex structural problems occurring in the aerospace industry. The method is used to estimate the governing partial differential equation, when exact solutions are not available.

The structure is divided into a number of small elements (usually rectangular or triangular). Each element has nodes or joints and structural responses are continuous at the nodes, where the elements are joined. In other words, a node is a point on the structure representing the boundary between two elements and corresponds to the coordinate or point on the structure. In FEM the nodes are used to capture the global motions of the structure. The basics of FEM are given in Appendix I.

4.4 Applications of the Proposed Model

A cantilever beam structure is used to validate the method (FEM), which is adapted for passive piezoelectric damping system. Then LNG vessel and a sailing yacht keel are introduced to achieve the aim of the research in a logical manner. The geometrical parameters of the piezoelectric materials and electrical components of the shunt circuit will be modified systematically. The location and the amount of the piezoelectric materials are also investigated to find effective damping and reduction of vibration.

4.5 The Summary of the Chapter

In Chapter 4 the mechanism of the passive piezoelectric shunt damping system was introduced. A resistor-inductor shunt circuit was chosen for application purposes of this study. The choice was made based on findings of previous research regarding the vibration reduction efficiency of RL circuits. A brief introduction was also given for the noise and vibration simulation tools SEA and FEM. Although SEA can be successfully applied to many different structures of aerospace and marine vehicles, the extensive use of stiffened plating in these structures can cause complication for the usage of SEA. In these cases, it is necessary to use other numerical approaches such as FEM. In the end, the applications of the study are introduced.

5.Theory

5.1 Chapter Introduction

In Chapter 5 the theory of the passive shunted piezoelectric damping concept is given. In subchapter 5.2 piezoelectric and electromechanical phenomena are introduced. In subchapter 5.3 the foundations of electromechanical coupling are presented. The constitutive linear piezoelectric equations are given in subchapter 5.4. Subchapter 5.5 presents the variational principles, used to create the governing equation of motion for piezoelectric material. This is done by substituting constitutive equations into the total energy formulation. As governing equations of motion are partial differential equations, the FEM method is employed to calculate these equations. In order to be able to use FEM the equations of motion must be given in the form of the electroelastic matrix (in subchapter 5.5). The electrical parameters (capacitor, resistor and inductor) are expressed in the nodal form in subchapter 5.6. A theoretical approach based on the study of Park (2003) is presented in subchapter 5.7. Subchapter 5.8 shows the definition of the capacitance of piezoelectric materials.

5.2 Piezoelectric Materials

The linear interactions between electrical, mechanical and thermal variables are presented as a diagram in Figure 5-1 (Ikeda 1996). The constitutive relationships and coupling coefficients in a linearly coupled system are shown as well. This diagram helps to understand how mechanical, electrical and thermal properties are mediated by the different material constants (Ikeda 1996; Heywang et al. 2008).

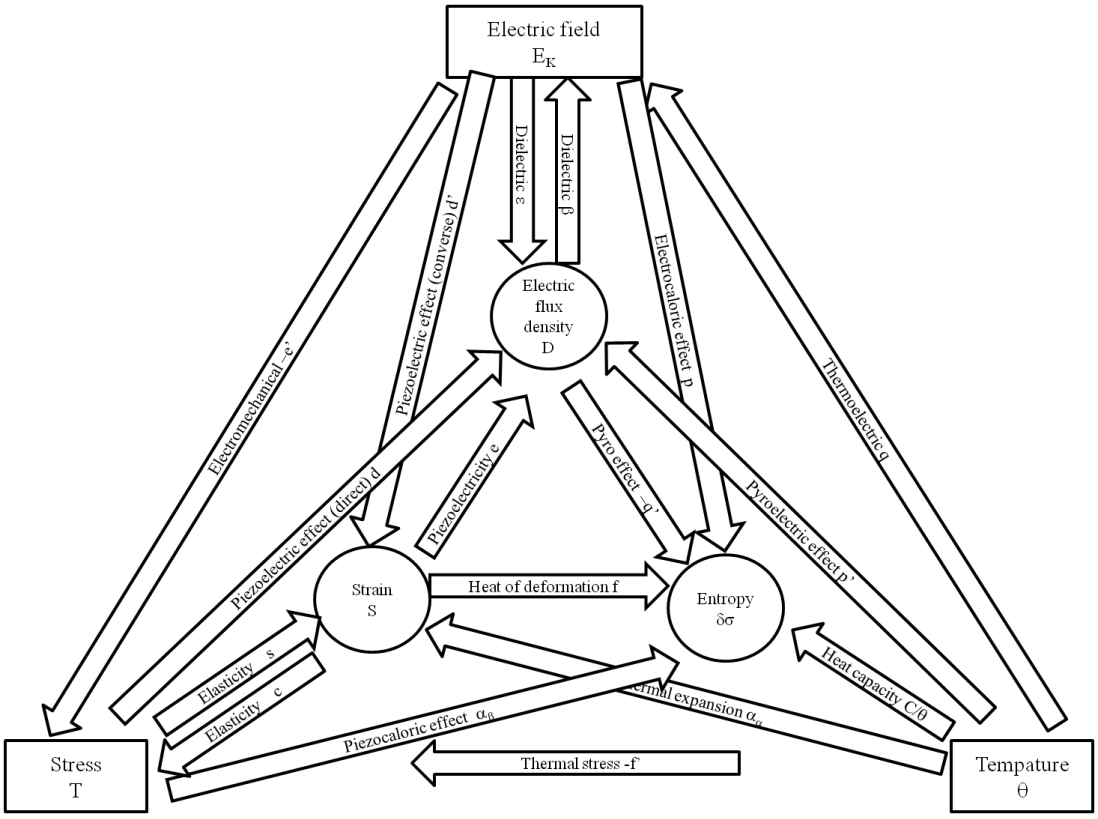

Figure 5-1: Interaction process between electrical, mechanical and thermal properties

The rectangles demonstrate the intensive variables (e.g. force) and the circles demonstrate the extensive variables (e.g. displacement). Thus, the piezoelectric material characteristics are the elastic, dielectric and piezoelectric tensor components (Heywang et al. 2008).

The basis crystal-physics formulation of a piezoelectric system is derived from thermodynamic considerations. To generate the equations of state, thermodynamic potentials are defined in Appendix B. The elastic Gibbs free-energy equations are used to determine the fundamental piezoelectric relations (Haun et al. 1987).

5.3 Electromechanical Coupling

A piezoelectric system can be isothermal or adiabatic. In most of the situations thermal-mechanical and thermal-electrical couplings are quite weak. Besides, the

electromechanical measurements are generally made under an alternating field or stress. Therefore, the observed piezoelectric constants are adiabatic. (Ikeda 1996).

One of the electromechanical phenomena is coupling between the elastic field and the electric field, introduced in subchapter 5.2. The coupling can be simplified when the temperature remains constant ($\Delta\theta=0$). Figure 5-2 shows the simplified version of the piezoelectric effect.

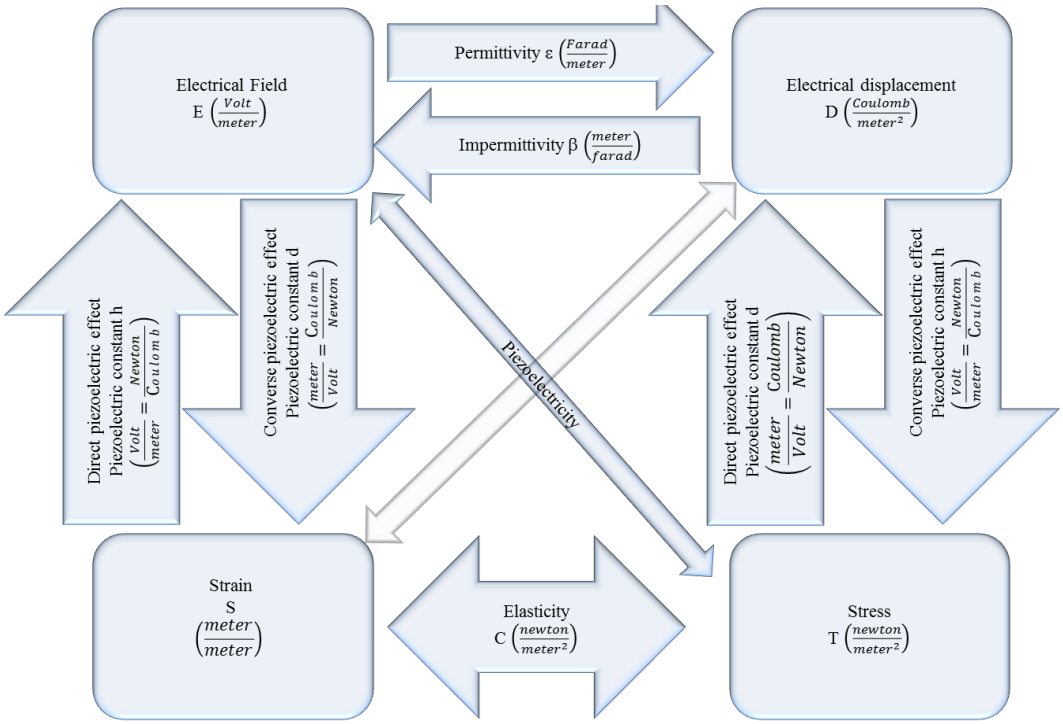

Figure 5-2: The piezoelectric effect

The classifications of fundamental electromechanical relations used for the entire piezoelectric constitutive equations (Heywang et al. 2008) are given in Appendix K.

Oscillating systems can be treated either as linear or non-linear. Most engineering and industrial type noise sources and the associated mechanical vibrations can be assumed to behave in a linear manner. Although the piezoelectric theory has nonlinear electroelastic equations, those equations are reduced to the linear piezoelectric theory. The small amplitude of an electroelastic body motion should be

considered under mechanical and electrical loads. (Mason 1950; Mindlin 1972; Dökmecí 1980; Meitzler, Tiersten et al. 1988).

The electromechanical coupling factor k describes the strength of the electromechanical response. The coupling factor may also be considered as an efficiency of conversion of either mechanical energy to electrical energy (Equation 5-1) or electrical energy to mechanical energy (Equation 5-2). Although the coupling factor is measured in percentage it is used as k^2. (Ikeda 1996; Heywang et al. 2008). The electromechanical coupling constants of piezoelectric materials are given in Appendix G.

$$k^2 = \frac{output\ electrical\ energy}{input\ mechanical\ energy} \qquad 5\text{-}1$$

$$k^2 = \frac{output\ mechanical\ energy}{input\ electrical\ energy} \qquad 5\text{-}2$$

There is a conversion cycle of mechanical to electric energy for thickness-stretch vibration. The steps of the cycle (a–d) are illustrated in Figure 5-3. The mechanical and electrical cycle are visualized in Figure 5-4.

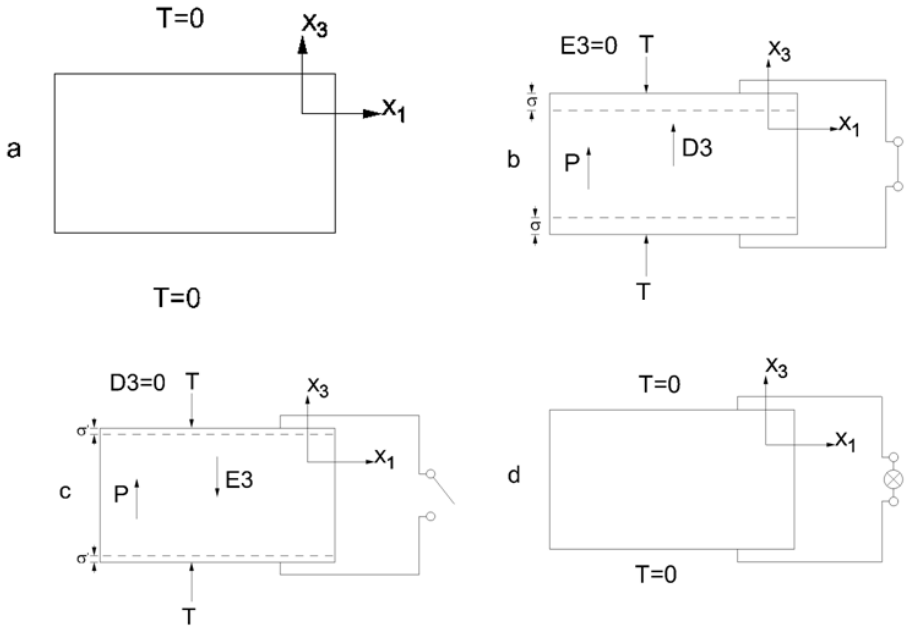

Figure 5-3: A conversion cycle of mechanical to electric energy

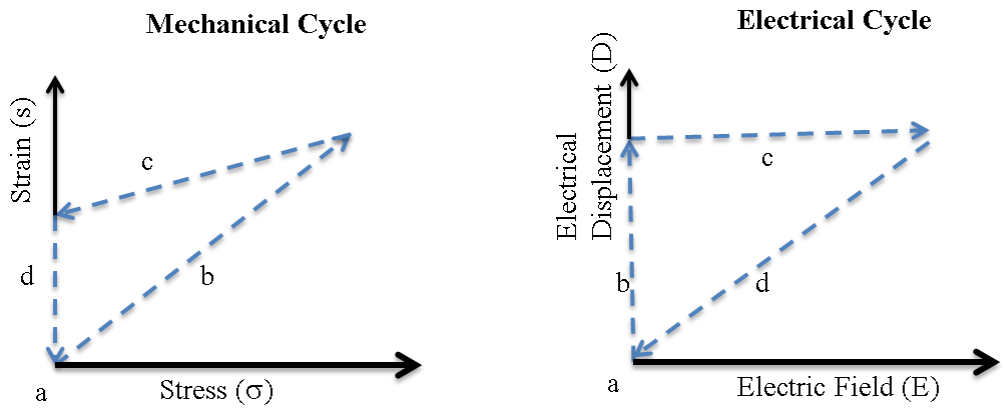

Figure 5-4: Strain(s)-stress (σ) diagram and dielectric displacement (or flux density, D)-electrical field (E) diagram

In practice, the electrical condition, which is important for defining the elastic constant of the electromechanical system, is specified by either constant-D or constant-E.

When stress σ is applied (step b) under short-circuit (E=0) condition, the strain is:

$$S = s^E \sigma_{max} \qquad 5\text{-}3$$

where s^E is elastic compliance which is the inverse of the Young's modulus (elasticity modulus). The extensional elastic compliance (s^E) arises and polarization (P) is included in the thickness direction (step b). The mechanical energy, input energy, applied to the piezoelectric material is:

$$W_{mech} = \frac{1}{2} s_{33}^E {\sigma_{max}}^2 \qquad 5\text{-}4$$

Then, the short-circuit is opened (step b). To realize the state D=0, the flux density should be eliminated by adding a new opposite flux density D'=-dT, this causes a new field:

$$E' = (\frac{1}{\varepsilon^T})D' \qquad 5\text{-}5$$

The electrical field across the material increases at the beginning of step c. Mechanical energy at this stage is:

$$W_{mech}{}' = \frac{1}{2} s_{33}^{D} T_{max}{}^{2} \quad 5\text{-}6$$

Stress is removed during step c. That creates a new strain, which is:

$$S' = dE' = -\left(\frac{d^2}{\varepsilon^T}\right)\sigma_{max} \quad 5\text{-}7$$

The new total strain becomes (open circuit + removing the pressure):

$$S = S + S' = \left(s^E - \left(\frac{d^2}{\varepsilon^T}\right)\right) T_{max} \quad 5\text{-}8$$

Finally, the transducer connects to external load (resistance, inductor etc.) and the stored electrical energy is transferred in step d. The electrical output energy is:

$$W_{elec} = W_{mech} - W_{mech}{}' = \frac{1}{2}(s_{33}^{E} - s_{33}^{D}) T_{max}{}^{2} \quad 5\text{-}9$$

The coupling factor $k_{33}{}^2$ can be calculated as:

$$k_{33}{}^{2} = \frac{W_{elec}}{W_{mech}} = \frac{s_{33}^{E} - s_{33}^{D}}{s_{33}^{E}} = \frac{d_{33}{}^{2}}{s_{33}^{E} \varepsilon_{33}^{T}} \quad 5\text{-}10$$

5.4 Linear Constitutive Equations of Piezoelectricity

The constitutive equations were developed for piezoelectric materials. The equations were based on the elastic Gibbs free-energy thermodynamic expansion, explained in detail in Appendix B.

Piezoelectricity equations were standardized in 1988 by the IEEE association (Meitzler, Tiersten et al. 1988). The linear piezoelectric relation of a piezoelectric continuum (at constant temperature) is given as:

Independent variable S,E $\quad \{\sigma_{ij}\} = [c_{ijkl}{}^{E}]\{S_{kl}\} - [e_{kij}]\{E_k\}$ 5-11

Independent variable S,E $\quad \{D_i\} = [e_{ikl}]\{S_{kl}\} + [\varepsilon_{ik}{}^{S}]\{E_k\}$ 5-12

The stress vector $\{\sigma_{ij}\}$ has two different types of effects: mechanical and electrical. Equation 5-11 denotes the converse piezoelectric effect and Equation 5-12 describes the direct piezoelectric effect. In the linear piezoelectric constitutive equations, the electrical field vector E is related to the electric potential field ϕ given as:

$$E_k = -\phi_{,k} \qquad 5\text{-}13$$

The strain tensor S_{ij} related to the mechanical displacement relations is:

$$S_{ij} = \frac{1}{2}(u_{i,j} + u_{j,i}) \qquad 5\text{-}14$$

where $u_{i,j}$ and $u_{j,i}$ are mechanical displacement gradient in the Cartesian coordinate system (*i=j=1,2,3*). An index, *j*, preceded by a comma denotes differentiation with respect to the space coordinate x_j, for example (Tiersten 1963):

$$u_{i,j} \equiv \frac{\partial u_i}{\partial x_j} \text{ and } u_{j,i} \equiv \frac{\partial u_j}{\partial x_i} \qquad 5\text{-}15$$

An alternative formula of the linear piezoelectric constitutive equations can be created, when different independent variables are chosen, such as:

Independent variable *T,E* $\quad S_{ij} = s_{ijkl}{}^{E}\sigma_{ij} + d_{kij}E_k$ 5-16

Independent variable *T,E* $\quad D_i = d_{ikl}\sigma_{ij} + \varepsilon_{ik}{}^{T}E_k$ 5-17

See Appendix K for all linear piezoelectric constitutive equations.

The linear piezoelectric constitutive equations can be written in a general expression form as:

$$\begin{bmatrix} D \\ S \end{bmatrix} = \begin{bmatrix} \varepsilon^T & d \\ d_t & s^E \end{bmatrix} \begin{bmatrix} E \\ \sigma \end{bmatrix} \qquad 5\text{-}18$$

The electrical displacement vector ***D*** (charge/area, C/m^2) is:

$$[D] = \begin{bmatrix} D_1 \\ D_2 \\ D_3 \end{bmatrix} \qquad 5\text{-}19$$

The vector of electrical field ***E*** (volt/meter) is:

$$[E] = \begin{bmatrix} E_1 \\ E_2 \\ E_3 \end{bmatrix} \quad \text{5-20}$$

The vector of material engineering strain ***S*** (meter/meter) is:

$$[S] = \begin{bmatrix} S_{11} \\ S_{22} \\ S_{33} \\ 2S_{23} \\ 2S_{13} \\ 2S_{123} \end{bmatrix} = \begin{bmatrix} S_1 \\ S_2 \\ S_3 \\ S_4 \\ S_5 \\ S_6 \end{bmatrix} \quad \text{5-21}$$

The vector of material stress σ (force/area) is:

$$[\sigma] = \begin{bmatrix} \sigma_{11} \\ \sigma_{22} \\ \sigma_{33} \\ \sigma_{23} \\ \sigma_{13} \\ \sigma_{12} \end{bmatrix} = \begin{bmatrix} \sigma_1 \\ \sigma_2 \\ \sigma_3 \\ \sigma_4 \\ \sigma_5 \\ \sigma_6 \end{bmatrix}$$

The piezoelectric constant *d* (C/N) measures either the ratio of generated strain to applied electrical field or the ratio of short circuit density to applied stress. The piezoelectric material properties depend on their actuation mode. The piezoelectric constant is used to choose the appropriate material properties for actuator applications. The piezoelectric constant *d* is given as*:*

$$[d] = \begin{bmatrix} 0 & 0 & 0 & 0 & d_{15} & 0 \\ 0 & 0 & 0 & d_{15} & 0 & 0 \\ d_{31} & d_{31} & d_{33} & 0 & 0 & 0 \end{bmatrix} \quad \text{5-22}$$

Piezoelectric materials, as actuators, can be divided into three groups in terms of their actuation mode (Ikeda 1996):

a) Thickness (axial) actuators (d_{33}-mode)
b) In-plane(Transversal) actuators (d_{31}-mode)
c) Shear (flexural) actuators (d_{15}-mode)

Figure 5-5 demonstrates the different piezoelectric actuator displacement modes.

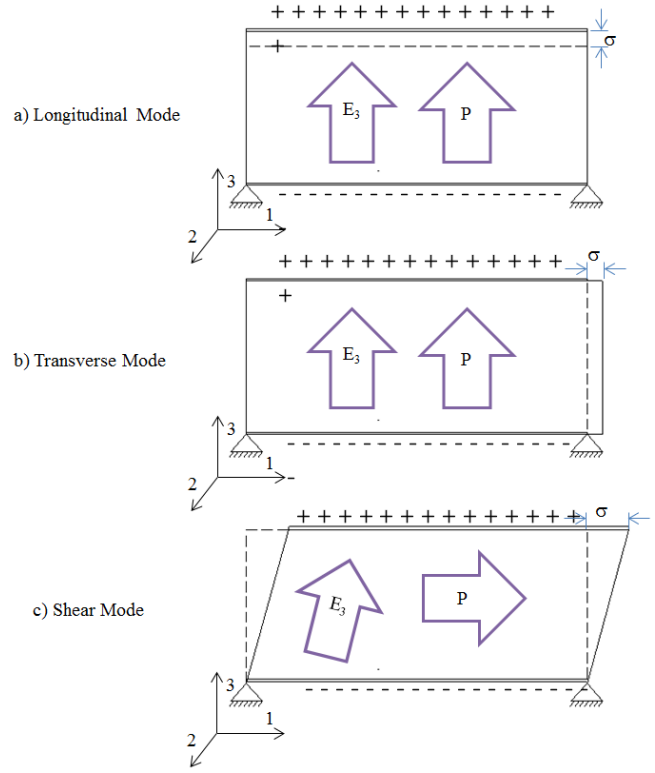

Figure 5-5: Piezoelectric actuator modes

The elastic compliance matrix [*s*] (m^2/N) relates to stress and strain, the permittivity or the dielectric constant matrix [ε] (F/m or C/m·V) relates to electrical displacement. Those matrixes are given below for the electrical field poled in the thickness (x_{33}) direction (Tzou and Tseng 1991):

$$[s] = \begin{bmatrix} s_{11} & s_{12} & s_{13} & 0 & 0 & 0 \\ s_{21} & s_{11} & s_{31} & 0 & 0 & 0 \\ s_{13} & s_{13} & s_{33} & 0 & 0 & 0 \\ 0 & 0 & 0 & s_{44} & 0 & 0 \\ 0 & 0 & 0 & 0 & s_{44} & 0 \\ 0 & 0 & 0 & 0 & 0 & s_{66}{}^{*} \end{bmatrix} \qquad 5\text{-}23$$

*$s_{66}=2(s_{11}-s_{12})$

$$[\varepsilon] = \begin{bmatrix} \varepsilon_{11} & 0 & 0 \\ 0 & \varepsilon_{11} & 0 \\ 0 & 0 & \varepsilon_{33} \end{bmatrix} \quad 5\text{-}24$$

Another piezoelectric constant g can also be used as the ratio of generating electrical charge for a given stress versa vice. It is used to choose the appropriate material properties for sensor applications. The piezoelectric constant g is given as:

$$[g] = [\varepsilon^T]^{-1}[d] \quad 5\text{-}25$$

5.5 Variational principles of Linear Piezoelectricity and the Finite Element Formulation

Variational principles are derived from the Hamilton's principle can be written as:

$$\delta \int_{t_1}^{t_2} (K - U + W)dt = 0 \quad 5\text{-}26$$

where K is the kinetic energy, U is the total potential energy, W is the virtual energy, δ denotes the variation, t_1 and t_2 are starting and finishing time.

The variation of total energy leads to the classical form of equation of motion. The governing equations of motion in variational form can be written as (Rao and Yap 1995) :

$$[M]\{\ddot{u}\} + [C]\{\dot{u}\} + [K]\{u\} = \{F\} \quad 5\text{-}27$$

where M is the mass matrix, C is the damping matrix, K is the mechanical stiffness matrix and F is the external force matrix.

Classic passive damping systems convert kinetic energy to potential energy. Potential energy has mechanical parameters such as strain and stiffness. However, both structural and electrical components must be involved in the structural analysis of piezoelectric materials. This is called electromechanical coupling, which brings electrical parameters into the total energy formulation. The potential energy

formulation must be reviewed and the equation of motion must be determined from the new energy formulation. Therefore, Hamilton's principle can be rewritten for theoretical derivations of the piezoelectric material governing equations of motion (Tzou 1993).

$$\delta \int_{t_1}^{t_2} (K - H + W) dt = 0 \qquad 5\text{-}28$$

where *K* is the kinetic energy and *H* is the electric enthalpy, including potential and electrical energy. Kinetic energy and electric enthalpy functions are called Lagrangian work $\mathcal{L}$. The kinetic energy K for volume Ω of the piezoelectric material is:

$$K = \frac{1}{2} \int_{\Omega} \dot{u}^T \rho \dot{u} \, d\Omega \qquad 5\text{-}29$$

where $\dot{u}$ is the velocity field vector and ρ is the mass density.

It is important to notice that the isothermal process, thermomechanical coupling and pyroelectric effects are neglected. The piezoelectric constitutive equations for the stress σ and the electric displacement *D* are derived from the electrical enthalpy function. The electrical enthalpy is used for the potential energy of the piezoelectric element, which includes mechanical strain and electrical potential energies. In this regard, *H* is used as an indicator:

$$H = \frac{1}{2} \int_{\Omega} \left(\sigma_{ij}^T S_{ij} - E_i^T D_i \right) d\Omega \qquad 5\text{-}30$$

where σ^T stands for the components of the stress tensor; E_i^T is the electrical field vector; D_i is the electric displacement or induction vector. The total electrical enthalpy, done by the external mechanical and electrical forces on the domain boundary $\partial\Omega$, is :

$$\delta H = \int_{\partial\Omega} T_i \delta u_i \, ds + \int_{\partial\Omega} \varrho \delta \phi \, ds \qquad 5\text{-}31$$

where T_i is the surface traction and ϱ is the surface charge density on the domain boundary $\partial\Omega$. u_i is the displacement and ϕ is the electrical potential.

$$T_i = \sigma_{ij} n_i \quad 5\text{-}32$$

$$\varrho = D_i n_i \quad 5\text{-}33$$

where n_i is the normal vector.

The linear piezoelectric enthalpy function is given as (Tzou 1993):

$$\mathrm{H}(\mathrm{S_{kl}}, \mathrm{E_i}) = \frac{1}{2}\{\mathrm{S_{ij}}\}^{\mathrm{T}}[\mathrm{c}]\{\mathrm{S_{ij}}\} - \{\mathrm{S_{ij}}\}^{\mathrm{T}}[\mathrm{e}]^{\mathrm{T}}\{\mathrm{E_j}\} - \frac{1}{2}\{\mathrm{E_j}\}^{\mathrm{T}}[\varepsilon]\{\mathrm{E_j}\} \quad 5\text{-}34$$

where $[c]$ is the elasticity coefficient matrix measured at a constant electric field, $[e]$ is the piezoelectric constant matrix, [ε] is the dielectric constant matrix measured at a constant strain. The virtual work W done by external mechanical and electrical loads is given as (Tzou 1993):

$$\delta W = \int_V \{\delta u\}^T \{F_V\} dV + \int_{\Omega s} \{\delta u\}^T \{F_\Omega\}\, d\Omega + \{\delta u\}^T \{F_P\} - \int_{\Omega\phi} \delta\phi \varrho d\Omega - \delta\phi Q \quad 5\text{-}35$$

where $\{F_V\}$,$\{F_\Omega\}$, and $\{F_P\}$ are the body, the surface, the point load vectors, respectively. Q is the total charge on the surfaces. Ωs is the external mechanical loading surface, and $\Omega\phi$ is the external electrical loading surface.

The governing equations of motion in variational form are given by taking into account the constitutive equations above and substituting the Lagrangian and virtual work into Hamilton's principle (Piefort 2001):

$$\begin{aligned} -\int_V [\rho[\delta\dot{u}]^T[\dot{u}] - \{\delta S\}^T[c^E]\{S\} + \{\delta S\}^T[e^E]^T\{E\} + \{\delta E\}^T[e^E]\{S\} \\ + \{\delta E\}^T[\varepsilon^S]\{E\} + \{\delta u\}^T\{F_V\}]dV + \int_{\Omega s} \{\delta u\}^T\{F_\Omega\} d\,\Omega \\ + \{\delta u\}^T\{F_P\} - \int_{\Omega\phi} \delta\phi\varrho d\Omega - \delta\phi Q = 0 \end{aligned} \quad 5\text{-}36$$

where the mechanical displacement u and electric potential field ϕ are unknown variables in the variational form of governing equations of motion.

Variational equations (5-28 and 5-36) with the constitutive relations (5-11 and 5-12) are the used for piezoelectric finite element formulations.

$$\begin{bmatrix} M_{uu} & 0 \\ 0 & 0 \end{bmatrix} \begin{Bmatrix} \ddot{u} \\ \ddot{\phi} \end{Bmatrix} + \begin{bmatrix} C & 0 \\ 0 & 0 \end{bmatrix} \begin{Bmatrix} \dot{u} \\ \dot{\phi} \end{Bmatrix} + \begin{bmatrix} K_{uu} & K_{u\phi} \\ K_{\phi u} & K_{\phi\phi} \end{bmatrix} \begin{Bmatrix} u \\ \phi \end{Bmatrix} = \begin{Bmatrix} F \\ Q \end{Bmatrix} \quad 5\text{-}37$$

where $[M]$ is the mass matrix, $[C]$ is the mechanical damping matrix, K_{uu} is the mechanical stiffness, $\{u\}$ is the nodal displacement vector, $\{F\}$ is the external force vector, $K_{u\phi}$ is the piezoelectric coupling matrix containing piezoelectric constants in either $[d]$ form (strain/electric field) or $[e]$ form (stress/electric field), $K_{\phi\phi}$ is the dielectric permittivity matrix, ϕ is the nodal electric voltage vector, $\{Q\}$ is the externally applied charge vector. (Tzou and Tseng 1991).

Natural frequencies and mode shapes can be obtained from the governing equations of motion, presented in Equation 5-37. In eigenvalue analysis (modal analysis), external loads are considered zero. Therefore, the undamped homogeneous system matrixes are given as:

$$[M]\{\ddot{u}\} + [K_{uu}]\{u\} + [K_{u\phi}]\{u\} = 0 \quad 5\text{-}38$$

$$[K_{\phi u}]\{u\} + [K_{\phi\phi}]\{\phi\} = 0 \quad 5\text{-}39$$

5.6 Finite Element Modelling of Passive Piezoelectric Shunt Vibration Damping Systems

FEM can be used to calculate mechanical displacement and electrical potential. The basic components of the electrical circuit, such as capacitor (C), resistor (R) and inductor (L), can be linked to the finite element model of piezoelectric material. The finite element equations for those electrical components were derived using the nodal analysis technique by Wang and Ostergaard (1999). The equation of motion of piezoelectric material is given in Equation 5-37. In the equation, the electrical dynamic of the system is given as the nodal charge balance matrix, in order to be

compatible with the system of piezoelectric finite element equations (Min, Duffy et al. 2010):

$$[K]\{V\} = \{Q\} \quad \text{5-40}$$

where $[K]$ is the capacitance stiffness matrix, $\{V\}$ is the vector of nodal voltages and $\{Q\}$ is the load vector of nodal charges.

In a harmonic analysis, the stiffness matrix for a Capacitor becomes:

$$C_p \begin{bmatrix} 1 & -1 \\ -1 & 1 \end{bmatrix} \begin{Bmatrix} V_1 \\ V_2 \end{Bmatrix} = \begin{Bmatrix} 0 \\ 0 \end{Bmatrix} \quad \text{5-41}$$

where C_p is the capacitance, V_1 and V_2 are the shunt voltage as degrees of freedom at the two nodes for each element.

The stiffness matrix for a Resistor becomes:

$$j\omega \left(-\frac{1}{\omega^2 R}\right) \begin{bmatrix} 1 & -1 \\ -1 & 1 \end{bmatrix} \begin{Bmatrix} V_1 \\ V_2 \end{Bmatrix} = \begin{Bmatrix} 0 \\ 0 \end{Bmatrix} \quad \text{5-42}$$

where j is the imaginary unit, ω is the angular speed and R is the resistance.

The stiffness matrix for an Inductor becomes:

$$\left(-\frac{1}{\omega^2 L}\right) \begin{bmatrix} 1 & -1 \\ -1 & 1 \end{bmatrix} \begin{Bmatrix} V_1 \\ V_2 \end{Bmatrix} = \begin{Bmatrix} 0 \\ 0 \end{Bmatrix} \quad \text{5-43}$$

where L is the inductance.

The tuning inductance L is calculated as a function of natural frequency of the piezo-beam structure:

$$L = \frac{1}{C_p w_s^2} \quad \text{5-44}$$

where C_p is the capacitance of the piezoelectric element and w_s is the ith angular frequency of piezoelectric material. The capacitance of a piezoelectric element is:

$$Cp = \frac{A\varepsilon_{33}^S}{t} \quad \text{5-45}$$

where A is the area of the cross section in the thickness axis, t is the thickness of the piezoelectric element and ε_{33}^S is the permittivity measured at constant strain.

5.7 A Theoretical Solution of Passive Piezoelectric Shunt Damper

A piezoelectric shunt damper includes an external electric shunt circuit and a piezoelectric material (Hagood and von Flotow 1991; Hollkamp 1994; Lesieutre 1998; Park 2003; Park and Baz 2005; Han, Neubauer et al. 2013).

In this subchapter, a theoretical approach is presented based on the study of Park (2003). A resistor-inductor circuit and piezoelectric actuator/sensor equations are used to derive an additional shunt damping matrix.

Actuator equation:

$$M\ddot{x} + C\dot{x} + Kx = f_{ext} + \theta V_{SH} \qquad 5\text{-}46$$

Sensor equation:

$$q = \theta^T x + C_p V_{SH} \qquad 5\text{-}47$$

where x is the displacement, M is the mass, C is the damping and K is the stiffness of the piezoelectric/beam system at a constant electric field. The stiffness contains the mechanical stiffness and the piezoelectric stiffness. C_p is the open circuit capacitance of piezoelectric material. θ is the electromechanical coupling matrix and q is the piezoelectric charge matrix. V_{SH} is the shunt voltage. Dynamic coupling causes the piezoelectric effect, which creates a current, demonstrated in Figure 5-6.

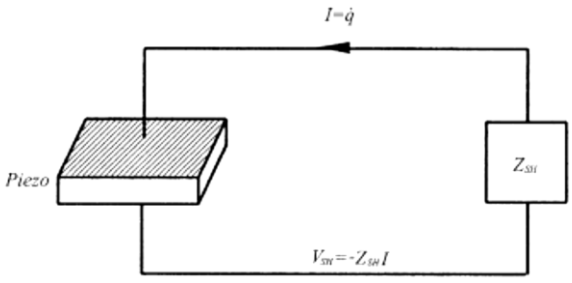

Figure 5-6: Feedback current into a piezoelectric material (Park 2003)

The voltage equation can be given as:

$$V_{SH} = -Z_{SH} I \tag{5-48}$$

where I is the current, Z_{SH} is the impedance of the circuit. The current is the first derivative of the charge and the equation of the current is:

$$I = \frac{dq}{dt} = \theta^T \dot{x} + C_p \dot{V_{SH}} = \theta^T s x + C_p s V_{SH} \tag{5-49}$$

where s is the Laplace parameter. The shunt voltage becomes:

$$V_{SH} = \frac{-Z_{SH} \theta^T s x}{1 + Z_{SH} C_p s} \tag{5-50}$$

Substituting the voltage equation into the actuator equation gives the governing equation of a shunted system. The new governing equation is added to the Laplace domain:

$$M s^2 x + \left(C + \frac{Z_{SH} \theta \theta^T}{1 + Z_{SH} C_p s} \right) s x + K x = f_{ext}(s) \tag{5-51}$$

To obtain the transfer function of the shunted system, the following parameters are used. The natural frequency of a mechanical system with the piezoelectric open circuit:

$$w_n = \sqrt{\frac{K + K_p^E}{M}} \tag{5-52}$$

A non-dimensional frequency:

$$\gamma = \frac{s}{w_n} \tag{5-53}$$

The generalized electromechanical coupling factor, K_{ij}:

$$K_{ij}^2 = \frac{\theta \theta^T}{C_p K} \tag{5-54}$$

A generalized electrical resonant impedance for R-L shunted piezoelectric material:

$$\hat{Z} = Z_{SH} C_p s \tag{5-55}$$

The damping stiffness ratio with the Laplace parameter is:

$$\frac{C}{K}s = 2\xi\gamma \tag{5-56}$$

The new governing equation can be rewritten as:

$$\left(\gamma^2 + 2\xi\gamma + 1 + K_{ij}^2 \frac{\hat{Z}}{1+\hat{Z}}\right)x = x_{st} \tag{5-57}$$

Finally, a non-dimensional form of the transfer function of the mechanical structure with shunted piezoelectric material is:

$$\frac{x}{x_{st}} = \frac{1+\hat{Z}}{(1+\hat{Z})(\gamma^2 + 2\xi\gamma + 1) + K_{31}^2\hat{Z}} \tag{5-58}$$

The transfer function can be described for a parallel resistor-inductor shunt circuit. First, the impedance of the R-L parallel circuit is expressed in Laplace form as:

$$Z_{SH}^{pa} = \frac{LRs}{Ls + R} \tag{5-59}$$

where *R* is the resistance and *L* is the inductance.

The generalized resonant impedance for a parallel RL shunt is:

$$\hat{Z} = Z_{SH}^{pa} C_p s = \frac{\gamma^2 r}{\gamma + r\delta^2} \tag{5-60}$$

where δ is the non-dimensional turning ratio for which the electrical resonant frequency w_e is tuned in the vicinity of a mechanical resonant frequency (Hagood and von Flotow 1991; Park 2003) :

$$\delta = \frac{w_e}{w_n} \tag{5-61}$$

$$w_e = \frac{1}{\sqrt{LC_p}} \tag{5-62}$$

The damping parameter *r* is:

$$r = RC_P w_n \tag{5-63}$$

Substituting $\hat{Z}$ into the transfer function produces the final form of the transfer function with a structural damping for a parallel RL shunted piezoelectric material and structure:

$$\frac{x}{x_{st}} = \frac{r\delta^2 + \gamma + \gamma^2 r}{(\delta^2 + r\gamma\delta^2 + \gamma^2)(\gamma^2 + 2\xi\gamma + 1) + K_{31}^2(\gamma^2 r)} \quad \text{5-64}$$

5.8 Definition of the Capacitance of Piezoelectric Materials

The piezoelectric material constants are generally measurements under an alternating field or stress (Ikeda 1996) . Compression, tension or bending forces develop stress on the structure. The piezoelectric effect is a change in the electrostatic charge generated across certain materials when mechanically stressed (Figure 5-7).

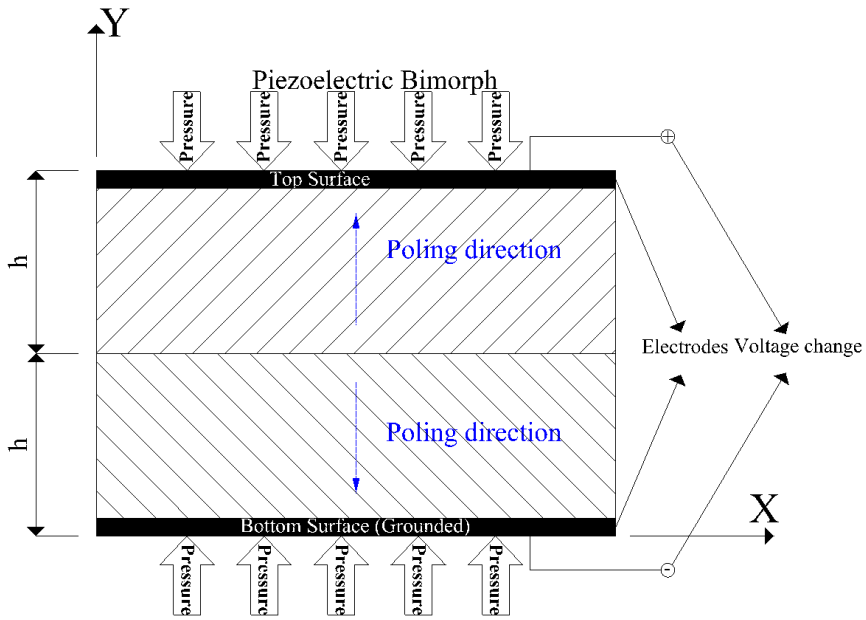

Figure 5-7: Electrical charge across the piezoelectric material

In Figure 5-8, the top and the bottom electrodes are shunted by an external capacitor. F_3 is the force on the major surfaces (the top and bottom). The top and bottom surface areas are A (each surface) and applied stress is T_3 ($F_3=T_3A$).

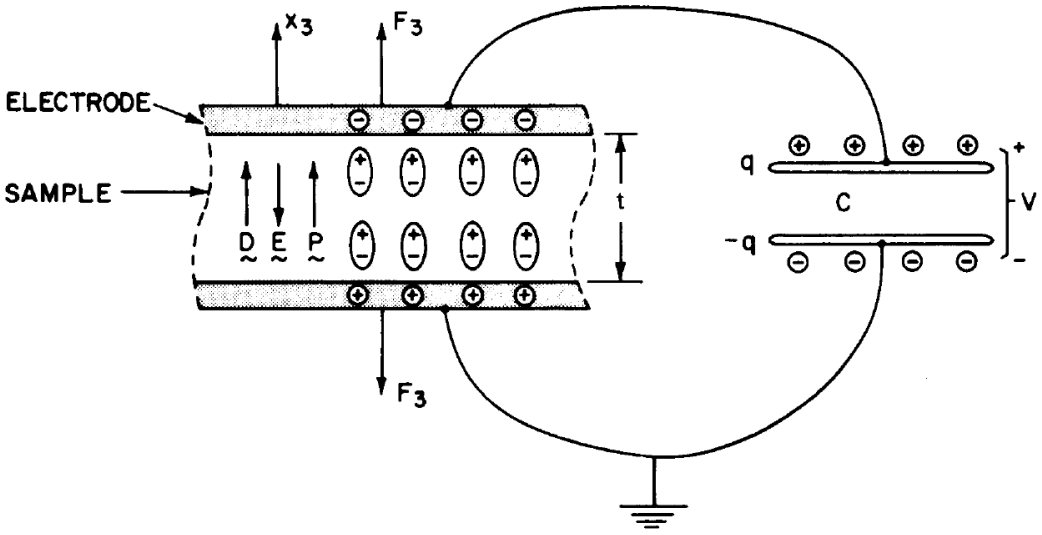

Figure 5-8: Signs of charges and fields for static test of sample with $d_{33}>0$ under tension (Meitzler, Tiersten 1988)

Generated charge (q) is a function of the piezoelectric strain constant (d) when force is applied:

$$q = dF \tag{5-65}$$

The output voltage is expressed as open-circuit voltage (V):

$$V = \frac{q}{C_p} \tag{5-66}$$

where q is the charge and C_p is the capacitance value of the external capacitor. This capacitance value equals the capacitance value of the piezoelectric material under constant pressure. The following equation calculates the capacitance value of the piezoelectric material:

$$c_p = \frac{\varepsilon_{33}\varepsilon_o A}{t} \tag{5-67}$$

where ε_o is the permittivity of free space (8.85 x 10^{-12} farad/meter), A is the surface area and t is the thickness of the piezoelectric patch. Equation 5-67 can be used to determine the value of permittivity (ε_{33}) for displacement and the electric field in thickness direction.

5.9 The Summary of the Chapter

In Chapter 5 the most known types of piezoelectric materials and the theory of piezoelectricity were explained. The constitutive relations and the energy conversion of piezoelectric materials were presented to be employed in the governing equation of motion. In order to develop the motion equation of the piezoelectric material the Hamilton's principle and the FEM were used.

Mechanical displacements and electrical potential were defined as unknown parameters as they depend on mechanical and electrical boundary conditions. To calculate these parameters the FEM and a theoretical solution, based on the study of Park (2003), were introduced for piezoelectric materials. The parameters of the shunted circuit were given in a nodal form to enable calculations with the FEM of piezoelectric material.

Although this study is about vibration and vibration damping, statics tests were needed to determine elastic, electric and piezoelectric properties. The method to calculate the capacitance of the piezoelectric material was mentioned at the end of this chapter, as this parameter will be used for all applications of the study.

6. Numerical Modelling of a Passive Piezoelectric Vibration Damping System

6.1 Chapter Introduction

In Chapter 6 a numerical study is carried out for a cantilever beam equipped with a pair of passive piezoelectric shunt damping systems to demonstrate vibration control capabilities. The obtained results of the numerical model are compared to previous experimental research carried out by Park (2003).

6.2 Numerical Modelling

In Park's (2003) application a simple aluminium cantilever beam with rectangular cross-section was studied. A pair of piezoelectric material (PZT 5-H) was bonded on the upper and the lower sides of the beam and RL shunt circuit was connected to the piezoelectric material, as illustrated in Figure 6-1. There was a 1mm gap between clamped side of the beam and the piezoelectric material. The geometrical parameters of the aluminium beam and piezoelectric material are given in Table 6-1.

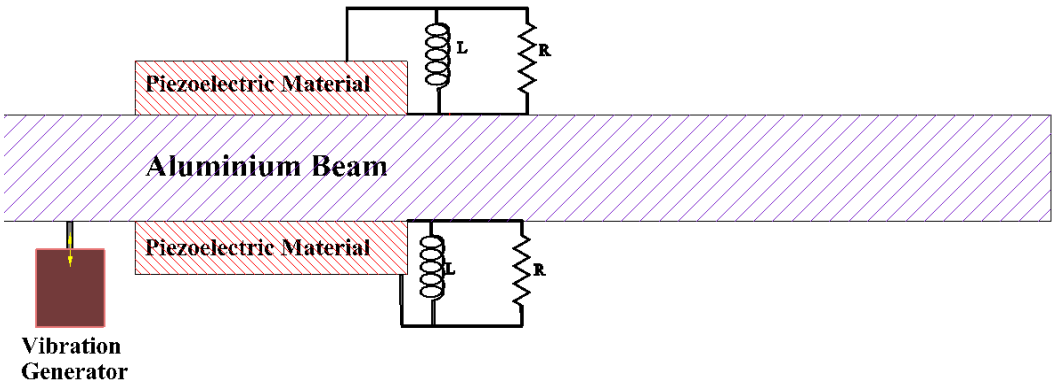

Figure 6-1: Canvilever beam passively controlled by a piezoelectric material

Table 6-1: Main dimensions of the aluminium beam and piezoelectric patch

	Aluminium	PZT-5H
Length m	0.2	4.50E-02
Wight m	0.0254	0.0254
Thickness m	8.00E-04	8.00E-04

The aluminium beam material properties are given as Young's modulus $71 \text{x} 10^9$ N/m^2, poisson ratio 0.33 and density 2700 kg/m^3. The natural damping of the aluminium beam is assumed as 0.02.

The piezoelectric material properties are given below for poling in the thickness direction.

Stiffness matrix *c*:

$$[c] = \begin{bmatrix} 12.6 & 8.0 & 8.41 & 0 & 0 & 0 \\ 7.95 & 12.6 & 8.41 & 0 & 0 & 0 \\ 8.41 & 8.5 & 11.7 & 0 & 0 & 0 \\ 0 & 0 & 0 & 2.3 & 0 & 0 \\ 0 & 0 & 0 & 0 & 2.3 & 0 \\ 0 & 0 & 0 & 0 & 0 & 2.325 \end{bmatrix} \text{x} 10^{10} \frac{\text{N}}{\text{m}^2}$$

Permittivity ε (permittivity of vacuum 8.854x10^{-12} F/m x relative permittivity):

$$[\varepsilon] = \begin{bmatrix} 1.505 & 0 & 0 \\ 0 & 1.505 & 0 \\ 0 & 0 & 1.302 \end{bmatrix} \text{x}10^{-8} \frac{C}{Vm}$$

Piezoelectric coupling coefficient *e* (electrical field/ stress):

$$[e] = \begin{bmatrix} 0 & 0 & 0 & 0 & 17 & 0 \\ 0 & 0 & 0 & 17 & 0 & 0 \\ -6.5 & -6.5 & 23.3 & 0 & 0 & 0 \end{bmatrix} \frac{C}{m^2}$$

Piezoelectric coupling coefficient *d* (electric field/strain):

$$[d] = \begin{bmatrix} 0 & 0 & -274 \\ 0 & 0 & -274 \\ 0 & 0 & 593 \\ 0 & 0 & 0 \\ 0 & 741 & 0 \\ 741 & 0 & 0 \end{bmatrix} \frac{C}{m^2}$$

The finite element method was used to determine natural frequencies and frequency response function.

6.2.1 The Modal Analysis

The electrical boundary condition is set for the modal analysis. Top and bottom electrodes of the piezoelectric patches are shorted (electrical potential is zero volt) to calculate mode shapes and mode numbers. Therefore, with this boundary condition only structural stiffness of the overall structure is taken into account (Steffen and Inman 1999). The frequencies and nature of the first eight modes of the beam are given in Figure 6-2.

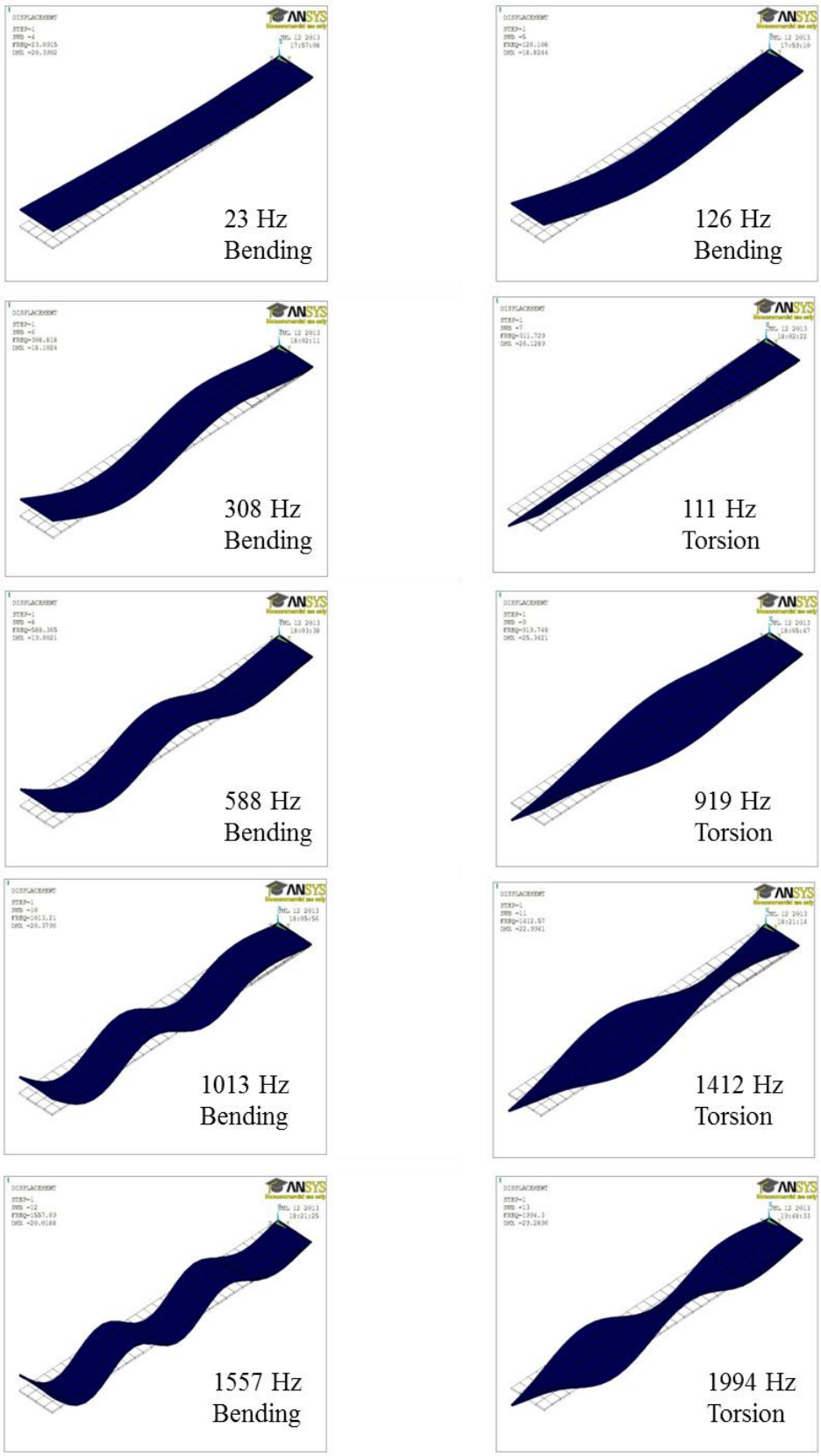

Figure 6-2: The frequencies and nature of the first 8 modes of the system

6.2.2 Vibration Damping

The beam was excited by a vibration generator and the piezoelectric materials were polarized due to the mechanic responses. The piezoelectric material's capacitor value is taken as 2.0E-7F (Park 2003). R-L electric circuit was used to control vibration for different modes (Figure 6-3). The second flexural frequency 126 Hz was chosen as fundamental frequency. Therefore, the circuit was tuned for the second mode vibration of the cantilever beam. Structural responses were calculated in harmonic analysis and compared to Park's (2003) experimental study.

Shunt resistance values were taken from Park's study and the tuning inductance L in the parallel R-L circuit was calculated by using Equation 5-45 from Chapter 5.

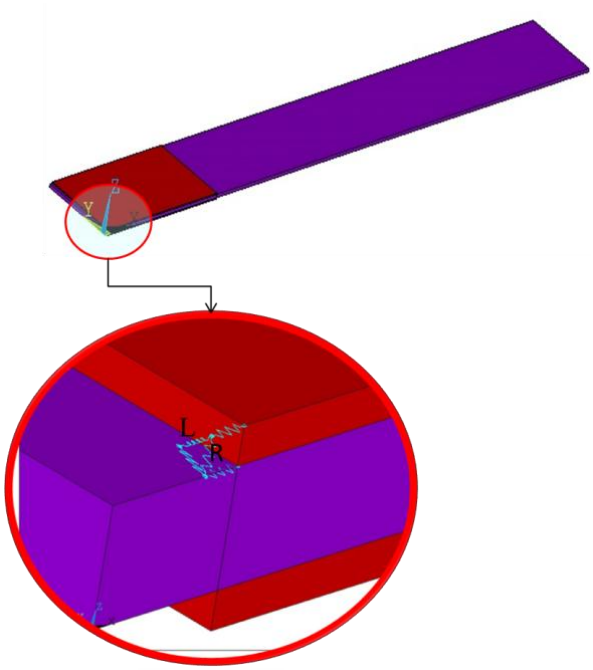

Figure 6-3: The numerical model for a parallel R-L shunt circuit

6.3 Results and Discussion

The resistance of the R-L circuit was increased to improve the vibration reduction of the parallel R-L shunt circuit. Numerical results are presented in Figure 6-4. As expected, a vibration reduction was achieved when the resistance of the electrical circuit was increased.

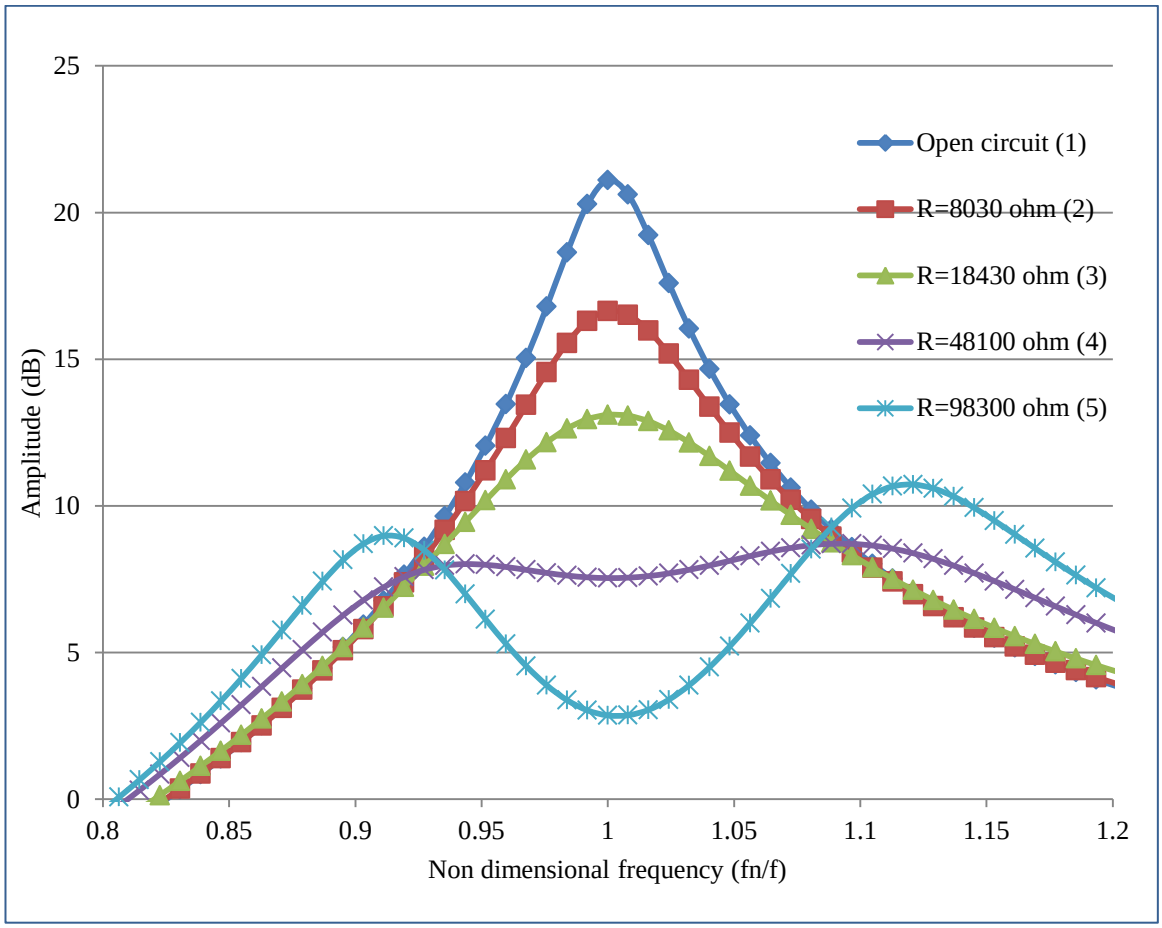

Figure 6-4:Non-dimensional frequency vs displacement for different resistance

The experimental study of Park (2003) was compared to the numerical results of the FEM of the beam. In Figure 6-5 Park's results and FEM results are superposed. The results of Park's experimental study are highlighted with numbered curves and the numerical results are given as marked curves.

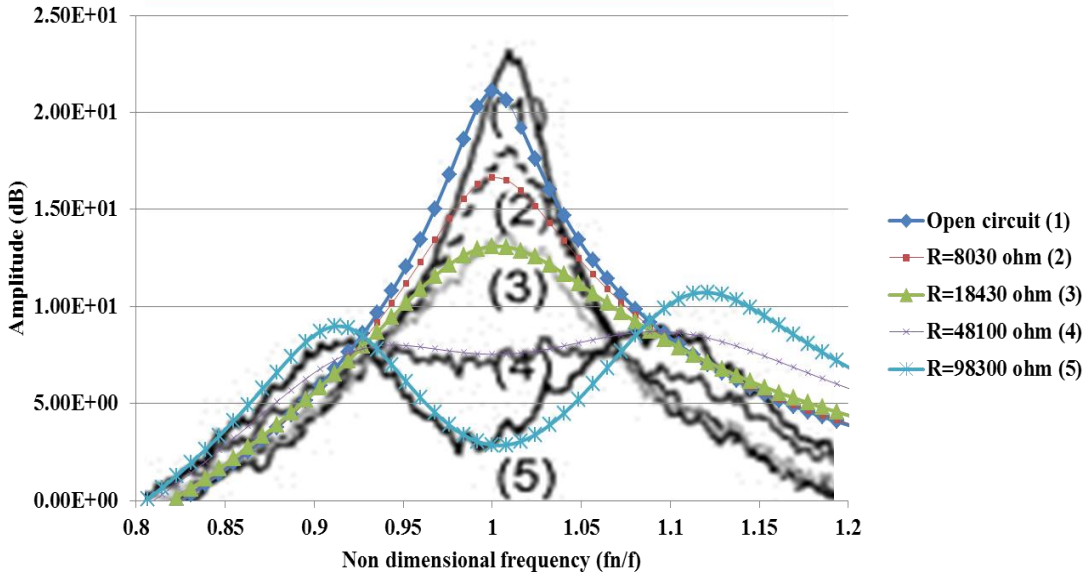

Figure 6-5: Park's results vs. FEM results

The numerical model results show a high degree of similarity compare to Park's experimental results. The error percentage is given in Table 6-2/

Table 6-2 The error between experimental and numerical transfer response

Tuned electrical circuit resistance	Error
Open Circuit	6.6%
8030 ohm	8.0%
18430 ohm	2.9%
48100 ohm	5.0%
98300 ohm	4.4%

Subsequently, the results are considered satisfactory even though there is a frequency shifting in numerical results. This may be due to possible experimental uncertainty. Minor changes on the boundary can cause frequency shifting as the size of the beam is small.

The mathematical model of the shunted piezoelectric-beam is uniform and continuous in Park's study. Consequently, the use of this model for complex

geometries, such as ships, is not entirely applicable. Firstly, a typical ship does not act rigidly and has a discrete number of members (Vorus 2010) Secondly, the properties of a piezoelectric material are anisotropic for a three-dimensional structure. The material properties (dielectric permittivity, the elastic coefficient) can be given by specifying either orthotropic or anisotropic properties (ANSYS 2011).

6.4 The Summary of the Chapter

In Chapter 6 the numerical results of the passive piezoelectric shunt circuit were compared to the experimental study of Park (2003) to validate the methodology of this study. Park's approach has shown to be very useful for the understanding of the fundamentals of the shunted piezoelectric vibration damping system. However, it seems that the behaviours of the complex system cannot be explicitly and directly identified in Park's theory.

Both experimental and numerical studies validate the theory that piezoelectric material, connected to an electrical circuit, can be successfully used to achieve vibration reduction. The electric circuit bonded to piezoelectric material needs to be configured to change the vibration level.

The numerical results obtained by FEM show a high degree of similarity in comparison to the experimental results. FEM has proven to be a functional and reliable tool for simulating both structural vibration and the passive piezoelectric shunt vibration dampers. Therefore, the application of shunted piezoelectric material on a ship and a ship appendage is calculated by FEM (in Chapter 7).

7.Application

7.1 Chapter Introduction

Chapter 7 presents the simulated performance of a piezoelectric shunt damping system for a ship (LNG vessel) and a ship's appendage (keel). For illustration purposes, a full-scale Liquid Natural Gas (LNG) vessel and a bulb keel of a racing boat are modelled (Figure 7-1 and Figure 7-2).

The finite element method (FEM) was chosen as the numerical calculation tool to calculate structural performance of the damping system. On-board vibration measurements, scaled model tests and validated numerical studies were used to set up the numerical models. In the following subchapter 7.2 the main application of the passive piezoelectric shunt damping system on the LNG carrier is given. The results of the numerical study concerning the LNG are presented and discussed at the end of subchapter 7.2. In subchapter 7.3, a further application of the damping system, this time located on the keel, is studied.

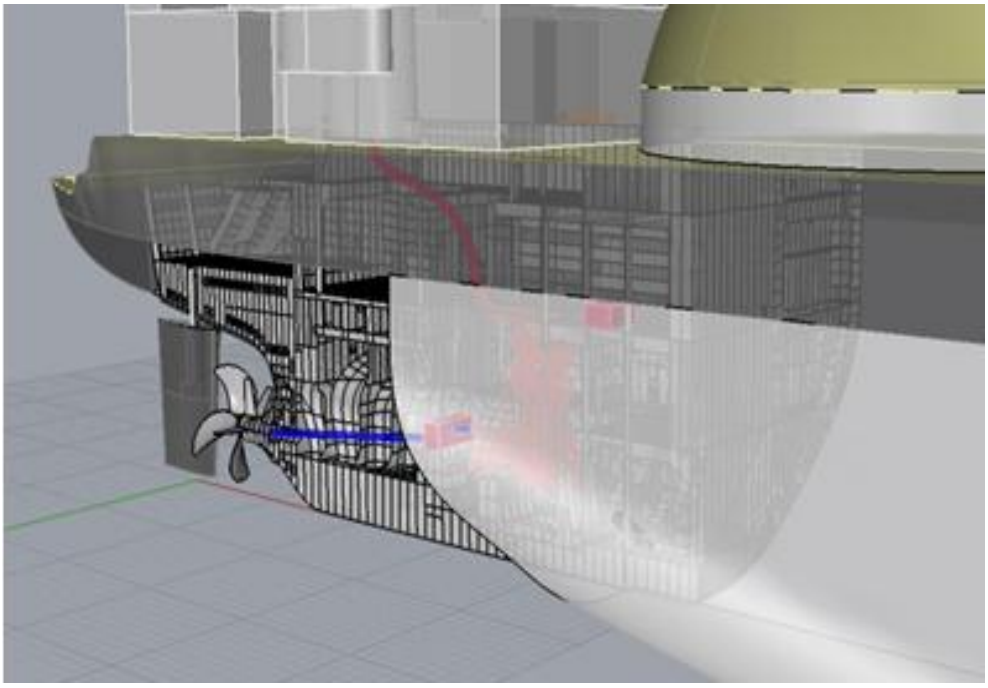

Figure 7-1: Three-dimensional model of the LNG vessel

Figure 7-2: Three-dimensional model of the sailing boat

7.2 Vibration Damping on a LNG Vessel with Passive Piezoelectric Shunt Resistance-Inductance Circuit

The vibration mitigation with the passive piezoelectric shunt Resistance-Inductance (RL) circuit approach is demonstrated in this subchapter. The main objective is to systematically estimate the performance of this damping system for ship vibration. Therefore, an existing 155,000m^3 LNG carrier was chosen for calculations in this study. The general arrangement of the vessel is shown in Figure 7-3.

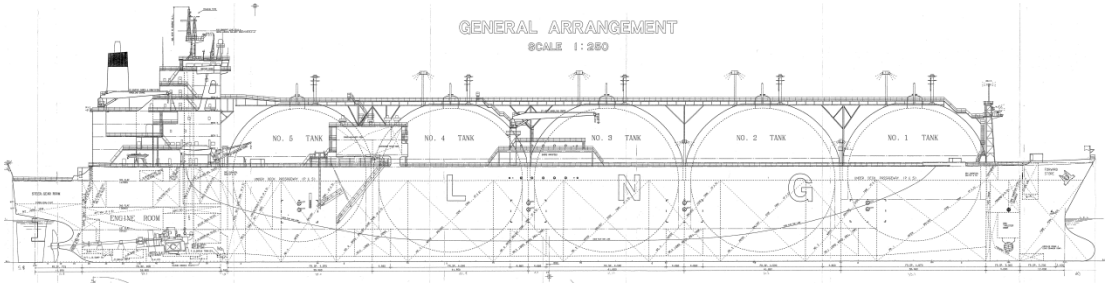

Figure 7-3: The general arrangement of the LNG vessel

7.2.1 The Geometry and the Numerical Model of the Vessel

The main dimensions and general properties of the vessel are given in Table 7-1.

Table 7-1: LNG vessel properties

Year of construction	2003
Class	LNG
WL max length	266.9 m
Max beam on WL	46 m
Displacement	84491 Ton
Max speed	19.84 kn
Draft during trials	Aft 9.37m, Fwrd 9.37m
Power	21569 kW
Max Propeller Revolution	81 rpm
Number of propeller blades	4
Pitch	Fixed
Steam turbines max power	21569 kW
Low and high pressure turbine	3966 rpm, 5800 rpm

A physical model and a numerical model of the ship were developed. The 3D modelling software Rhinoceros 4.0 was the tool used to generate hull and plate members of the vessel. The finite element model was created with the commercial

ANSYS^{R} software (Figure 7-4). ANSYS^{R} was also used for numerical modelling and calculations.

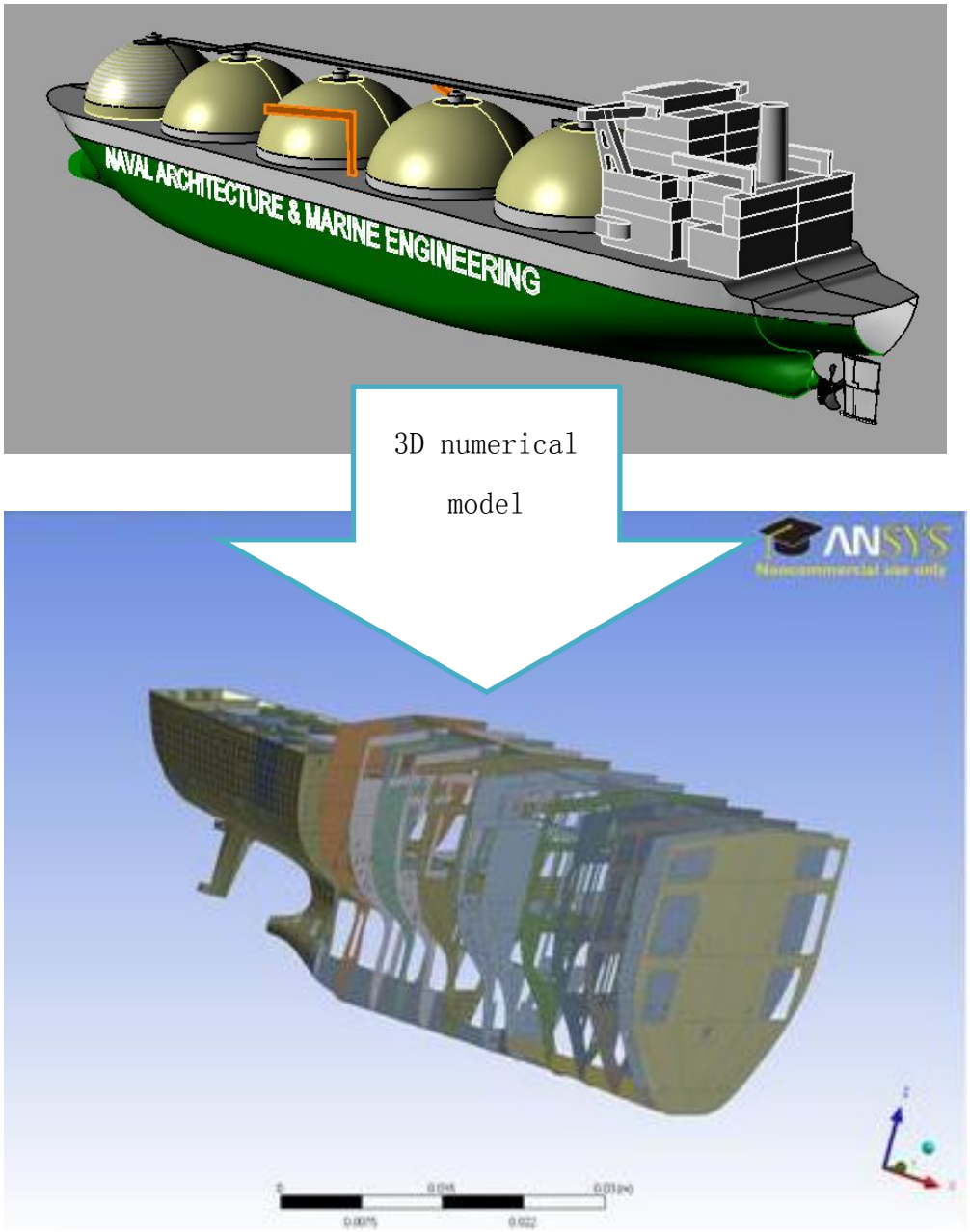

Figure 7-4: LNG vessel 3D FEM modelling

The numerical model of the ship differs from the real ship as every structural member (or sub-system) is produced as three-dimensional in any real system. The

simplification process was applied to reduce the number of elements in the numerical model of the vessel.

1. Girders and stiffeners were modelled as beam elements due to their uniform cross section of elastic modulus *E* and moment of inertia *I* in the length axes:

   $$\text{length} >> \ width\ and\ thickness \qquad 7\text{-}1$$

2. Plates were modelled as shell elements due to their uniform cross section of elastic modulus *E* and moment of inertia *I* about its thickness:

   $$width\ and\ length >> thickness \qquad 7\text{-}2$$

Those assumptions and simplifications helped to make modelling and calculation more time efficient. The entire structure was modelled with different types of elements from the element library of ANSYS. It is very important to choose the correct elements for this particular simulation. In this study, four types of elements were used in structural analysis:

1. SHELL181 elements for modelling hull, deck plating
2. BEAM188 elements for modelling stiffeners and girders
3. SOLID5 elements for piezoelectric materials
4. CIRCU94 elements for electric circuits

The SHELL181 was used to analyse a plate structure ranging from thin to thick. Each element has four nodes and calculation can be carried out for six degrees of freedom at each node.

The BEAM188 element has two nodes and was used to analyse the hull girders and stiffeners. The effect of the rotary inertia and shear deformation are included in this element.

The SOLID5 element was used in the analysis of the piezoelectric effect. Each element has eight nodes with six degrees of freedom. It also represents an electromechanical coupling, where the effect of the electrical and mechanical responses was taken into account. Therefore, piezoelectric materials were modelled using SOLID5.

The CIRCU94 element was used in the analysis of an electrical circuit shunted to piezoelectric material. The element has two or three nodes to define electrical components (resistor, inductor etc.) as well as two degrees of freedom. Detailed descriptions of elements are given in Appendix D. The structural members of the mooring deck are shown in Figure 7-5.

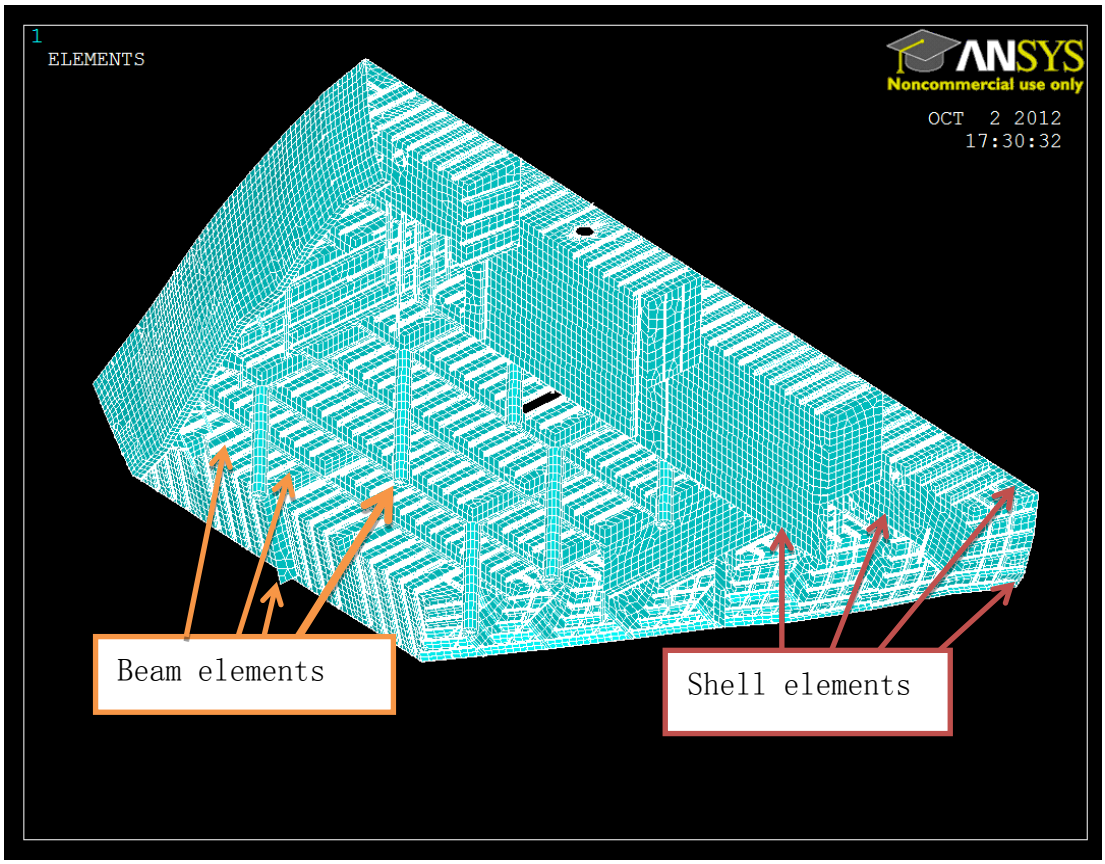

Figure 7-5: Structure members of LNG mooring deck

The propeller was modelled as a mass element having two nodes and was bonded to the stern tube. The nodes add up to the total mass of the propeller, 46 tons. The mass of the rudder has been modelled as two separate concentrated masses as well. The model consists of

- 7171 key points
- 12252 lines
- 5132 areas
- 69345 nodes

- 84100 elements

7.2.2 The Major Vibration Source of the Ship

Ship structures can be excited to vibrate mechanically due to onboard reciprocating engines, machinery and/or hydrodynamically due to their propeller(s). The LNG vessel is powered by steam turbines known to generate little alternating force. However, most ships are installed with diesel engines which have cylinders where the internal combustion occurs. During the combustion process, high pressurized gas causes pistons of the engine striking against the wall of the cylinder. High gas pressure forces and inertial forces excite the system to vibrate in the firing rate harmonics (Vorus 1988; Arveson and Vendittis 2000). This order is, generally, the dominant frequency of vibrating structure.

The on-board vibration measurements employed in the study identify the main vibration sources of the vessel. Vibration measurements were presented in Zoet et al. (2012). Figure 7-6 shows the locations, where measurements were taken in the engine room and Figure 7-7 presents the measurement results. Figure 7-8 shows the vibration measurement locations on the steering deck. The measured results are given in Figure 7-9.

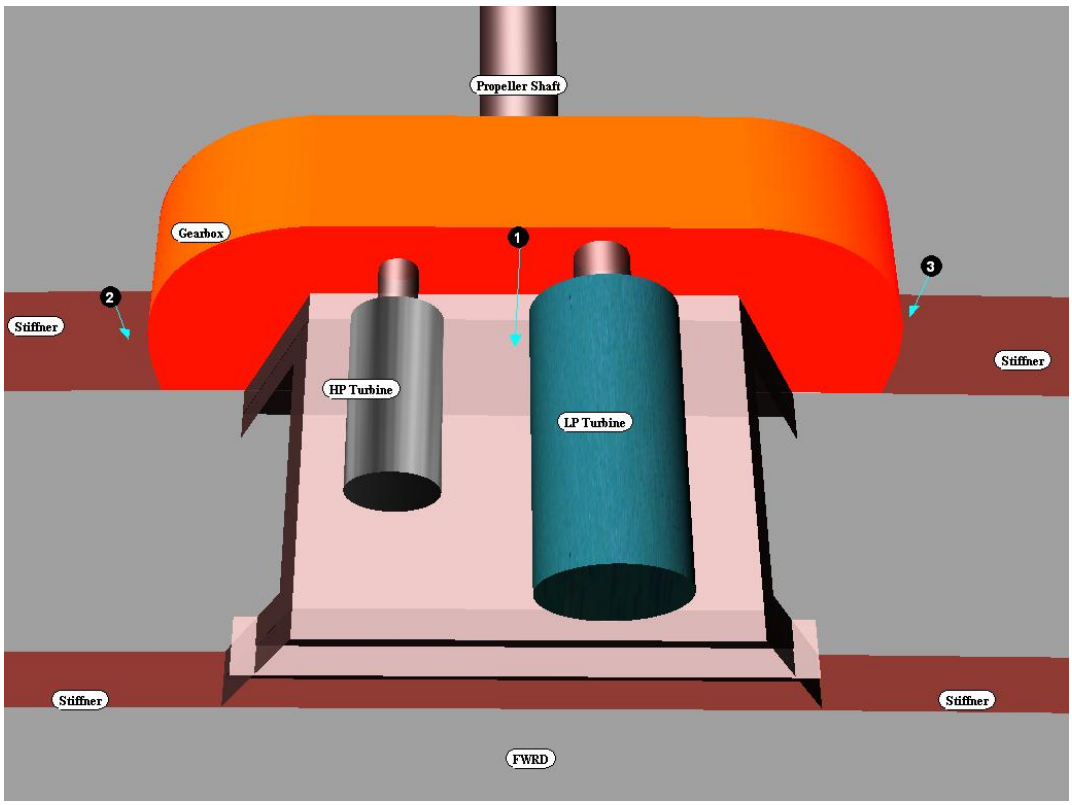

Figure 7-6: Measurement locations on the steam turbine foundation

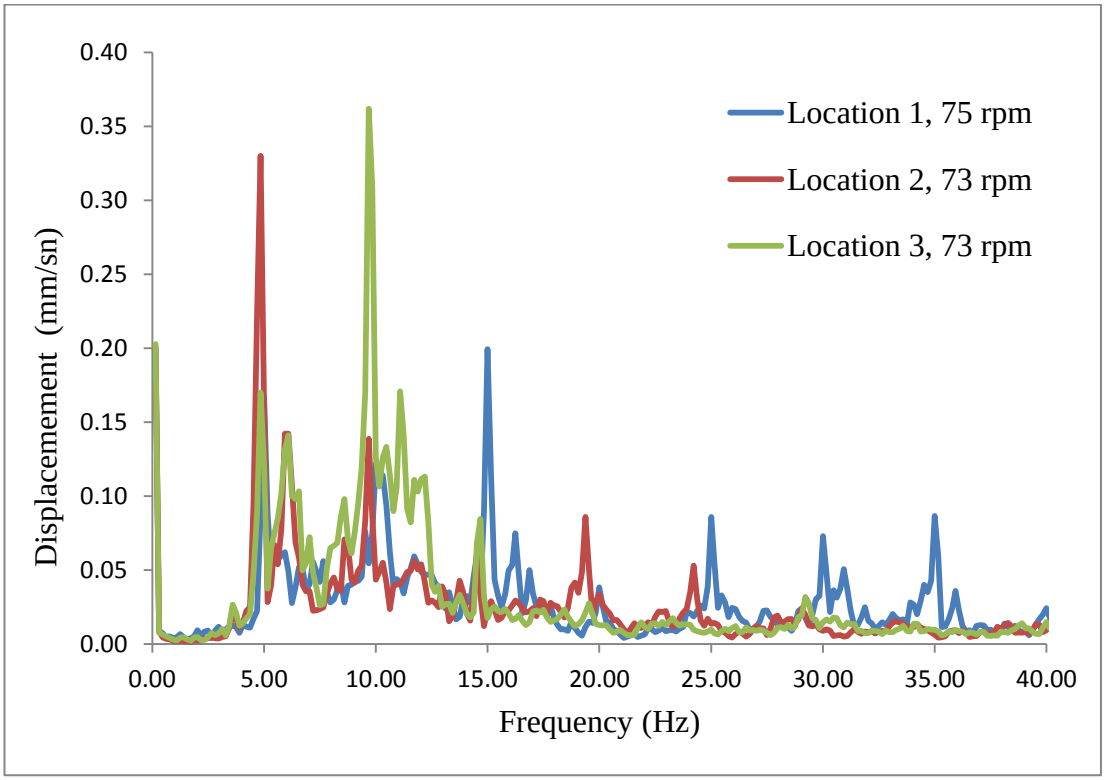

Figure 7-7 Measured spectra shape in the main engine room (Zoet 2012)

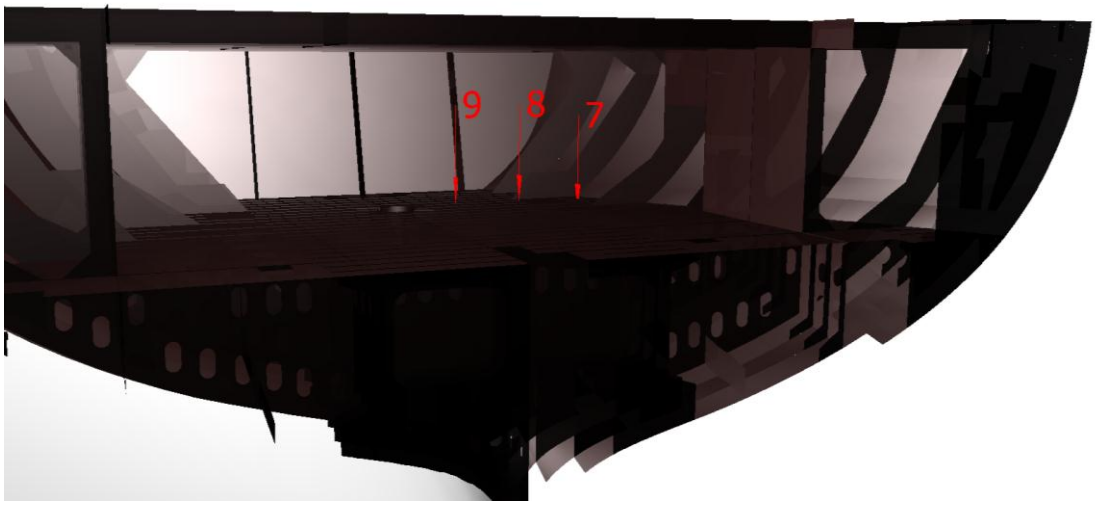

Figure 7-8: Vibration measurement locations on the steering deck

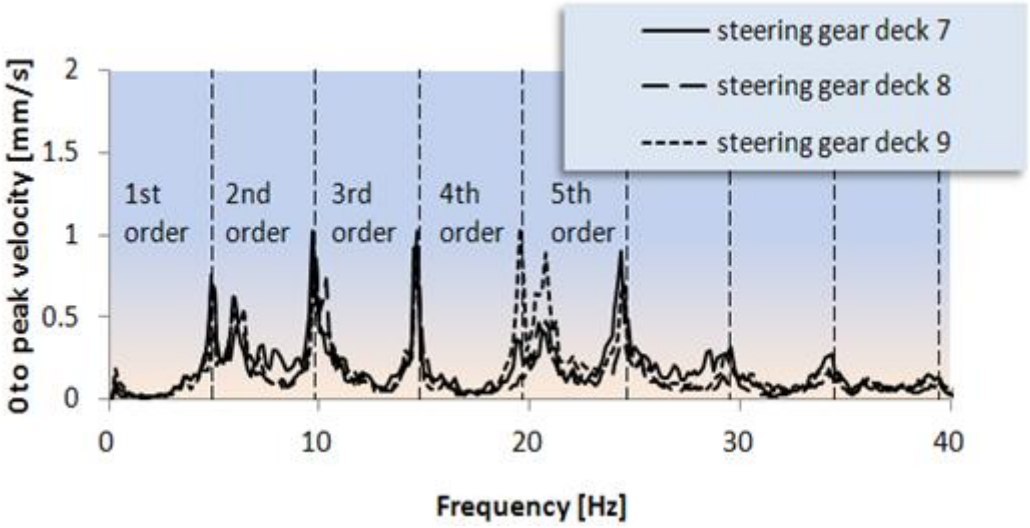

Figure 7-9: Measured spectra shape on the steering deck (Zoet et al. 2012)

The vibration measurement results in the main engine room showed that steam turbines play an insignificant role in the total ship vibration and structure borne noise. Therefore, the dominant excitation source in the vessel is the propeller. The propeller blades generate a signal at the blade passing frequency and its harmonics.

Vibration measurement on the steering deck also showed the peak points, which are the propeller blade passing frequency and its harmonics. The operation condition was 19knot and propeller revolution was around 75 rpm. A simple formulation was used to define harmonic components of the blade passing frequency:

$$f_B = \frac{nN}{60} \qquad 7\text{-}3$$

where f_B is the blade frequency (Hz), n is the angular speed (rpm), and N is the number of blades of the propeller.

The propeller induced alternating pressure pulse distribution over the hull used in this model has been derived from simulation results calculated by a computational fluid dynamic software and published by Zoet et al. (2012). The excitation pressures have been translated into excitation forces. These pressures have been converted using MATLAB into force (per node) in y and z direction taking into consideration the mesh of the finite element model of the vessel produced by Zoet et al. (2012). The propeller excitation force distribution on the aft part of the LNG is shown in Figure 7-10.

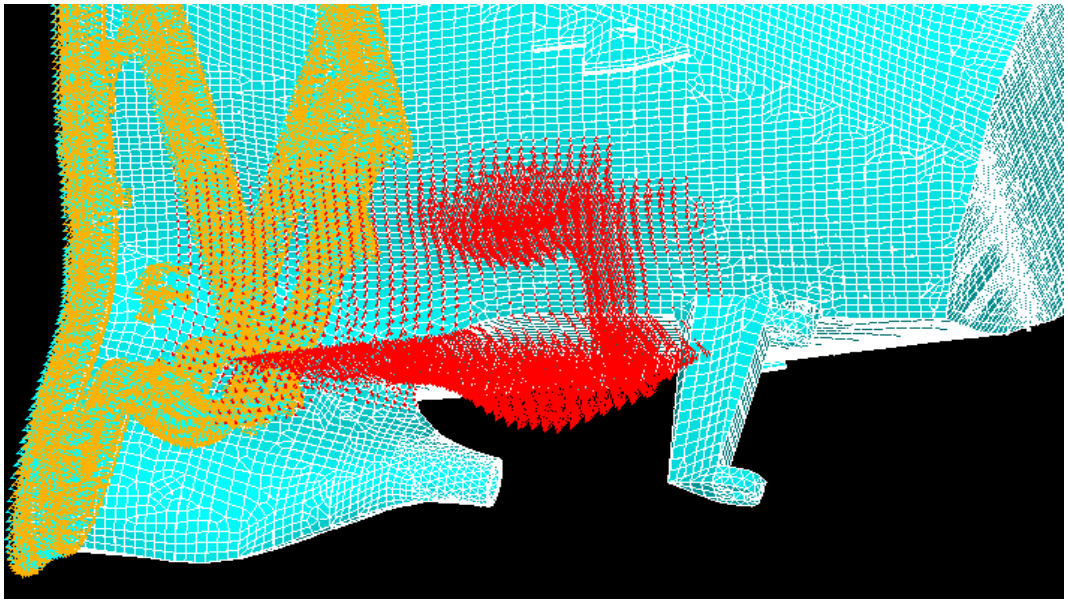

Figure 7-10: The propeller excitation force distribution on the aft ship

The applied total pressure for the first three blade passing harmonics plotted in the FE model is shown in Table 7-2 .

Table 7-2: The applied total pressure for the first three blade passing harmonics

Frequency	Total pressure
1x blade freq (5.2 Hz). (kPa)	3.3138
2x blade freq. (10,4 Hz) (kPa)	1.8093
3x blade freq (15.6 Hz). (kPa)	0.3831

7.2.3 Harmonic Analysis of the LNG

A resistor-inductor piezoelectric vibration shunt is designed to control vibration for a single mode harmonic. The functionality of piezoelectric materials and electrical circuit depends on working frequency and magnitude of deflections. Flexible piezoelectric materials are attractive for vibration energy harvesting applications, because of their ability to withstand large amounts of strain. Larger strains provide more mechanical energy available for conversion into electrical energy (Anton and Sodano 2007). Thus, the choice of the location of piezoelectric material was made based on the biggest deformation obtained from the bare steel ship structural dynamics analysis results. The highest deformation is actually the highest strain.

The concentration was put on the stern part of the vessel, because this part is near to the propeller excitation forces. As the ship structure is steel the numerical model was generated with the steel element's properties. The element data is given in Table 7-3.

Table 7-3: Steel element's properties

Density of Steel	7850 kg/m^3
Young's modulus	2.1x10^{11}N/m^2
Poisson's ratio	0.3
Material damping ratio	0.01

A harmonic response analysis was used to determine the response of the structure over a frequency range from 1 Hz to 40 Hz. This frequency range is covering up to 6^{th} harmonic of the blade passing frequency.

The finite element models of vessel were calculated for different boundary conditions. Main aim was to compare different boundary conditions to choose the most accurate numerical model of the vessel which represents the full scale. Therefore, the numerical model was constrained all degrees of freedom at frame 21 and 25 (Figure 7-11).

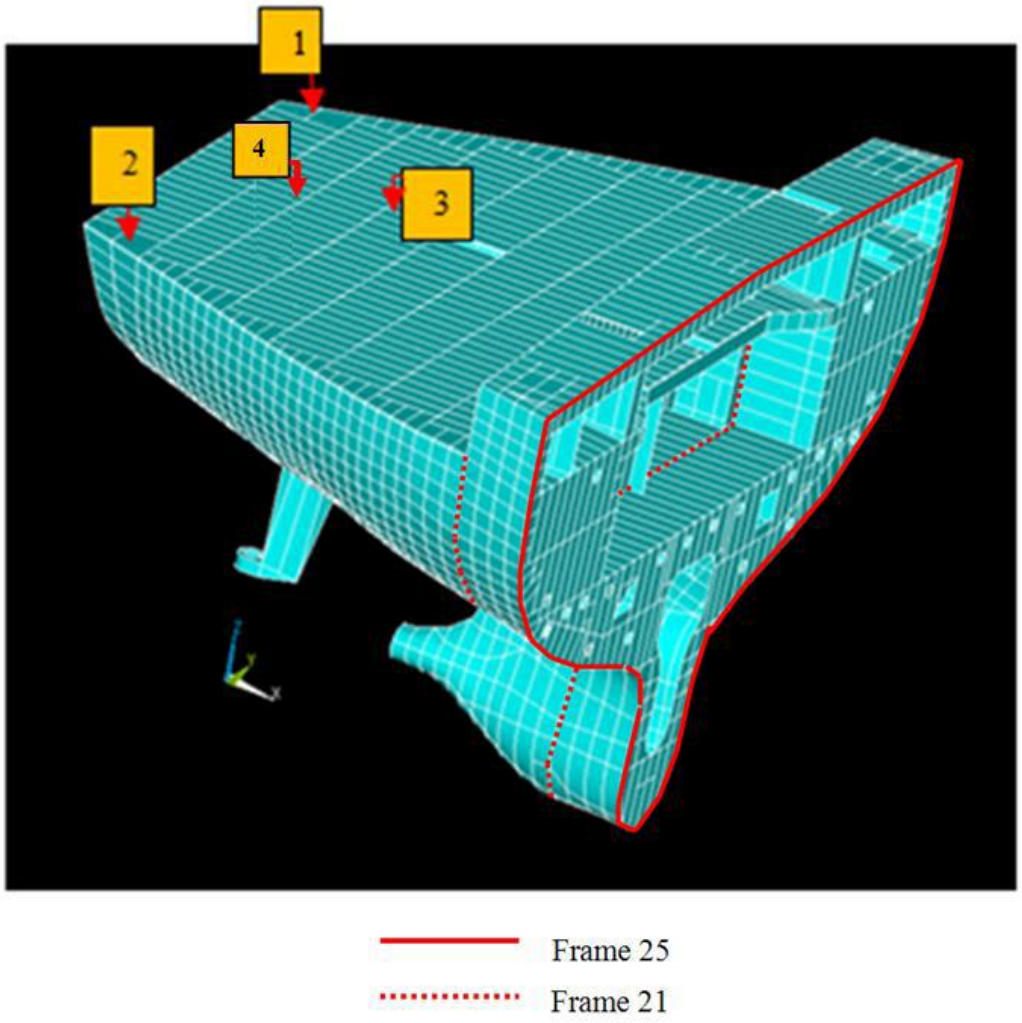

Figure 7-11: Different boundaries of the FEM of the vessel

Figure 7-12 and Figure 7-13 show the frequency response curves are roughly the same for the location 3 and 4 on the mooring deck. Furthermore, peak points are coincided with the propeller blade frequencies which are dominating the structural vibration. It can be also observe from the Figures that that the response below 20 Hz becomes more sensitive to the definition of boundary conditions. The model constrained at frame 25 was chosen for further investigations.

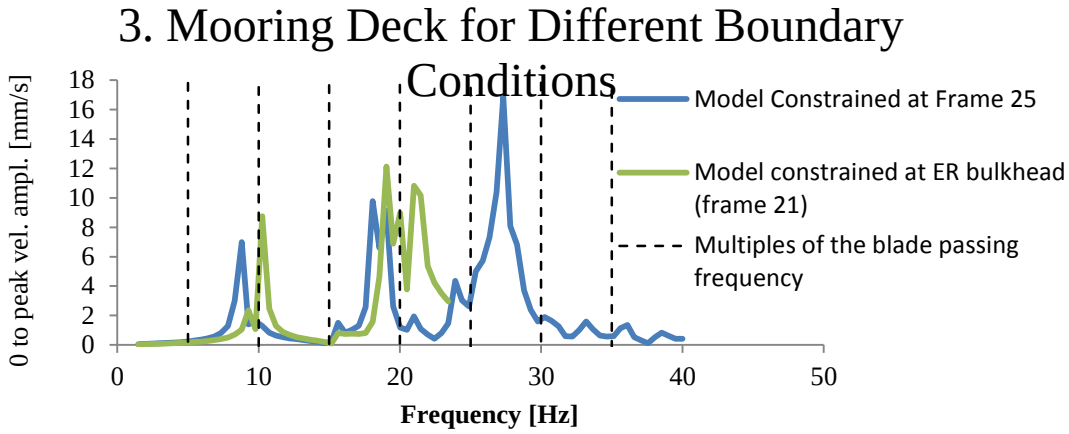

Figure 7-12: Frequency response graphs at 3th location

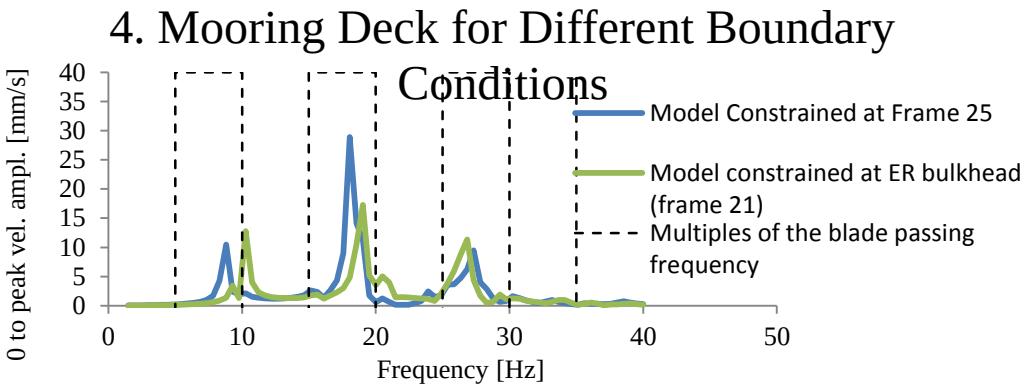

Figure 7-13: Frequency response graphs at 4th location

In the post-processes, the dynamic behaviour of the LNG's aft part was also examined to find the highest deformation on the structure. The deformed shape is given in Figure 7-14.

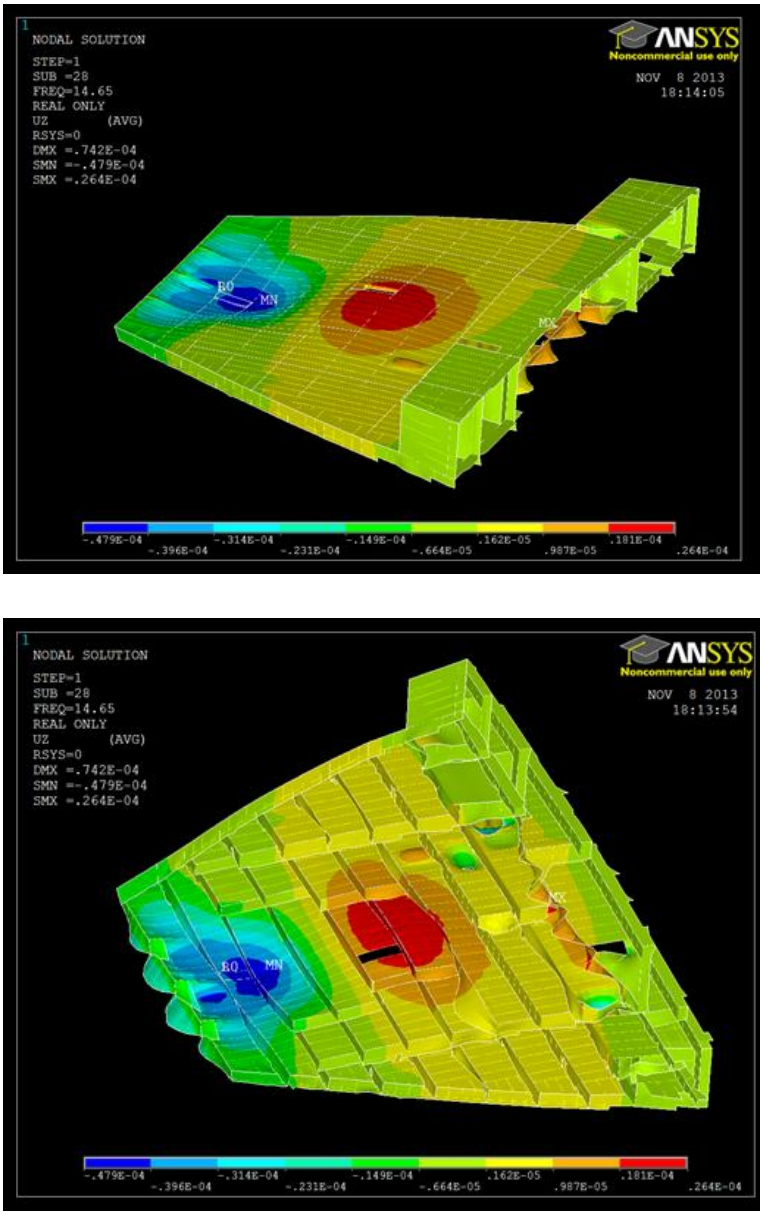

Figure 7-14 Deformed structure of LNG mooring deck at 14.615 Hz (2nd mode)

As it can clearly be seen in Figure 7-14, the high deformation was in the aft centre of the mooring deck. There was also some deformation in the central area. According to this calculation it was decided where to locate the piezoelectric patch(es).

7.2.4 Damping with Single Mode Resistor-Inductor Shunted Electrical Circuits

Piezoelectric materials have size and flexibility limitations. The size limitation problem can be solved by connecting and/or laminating the materials to each other. The flexibility problem was overcome with the piezoelectric Macro Fiber Composite (MFC) (Sodano et al. 2004). This material's properties were used for the numerical applications. PZT-5A material used in the MFC has a coupling coefficient (K_{33}) of about 0.69. The MFC's coupling coefficient value is one of the highest of all piezoelectric materials (see Appendix G).

Distributed piezoelectric materials can be either embedded or surface bonded with an elastic base structure (Tzou 1993). The piezoelectric patch is bonded on the mooring deck structure. The thickness of the piezoelectric patch is given as 0.3mm, 30mm and 90mm. The areas (length x width) of piezoelectric patches were chosen as:

1. Piezoelectric patch 1 which is 2.145x0.85m^2,
2. Piezoelectric patch 1+2 which is 4.290x0.85m^2
3. Piezoelectric patch 1+2+3+4 which is 4.290x1.7m^2

Each piezoelectric patch is bonded to another. Thus, they are acting as only one solid part. The areas are shown in Figure 7-15.

The dynamics performance of the structure of the mooring deck was calculated. The numerical model contains a number of elements due to the complexity of the entire structure. This causes a big size output data, which makes the analysis very time consuming. Therefore, some of the points on the structure, called nodes, were highlighted to evaluate the results. In Figure 7-15, the numbers represent the location of these nodes. The distances between the nodes are 2.90m longitudinal and 2.27m horizontal.

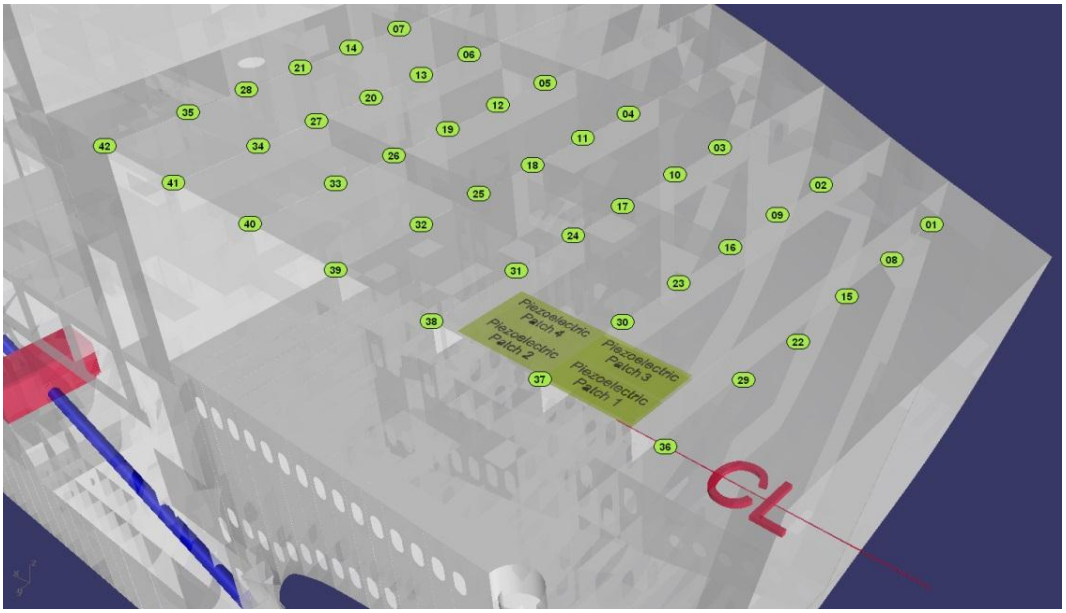

Figure 7-15: The location of piezoelectric patches and result readings

A parallel resistor-inductor (RL) electrical circuit was connected to the piezoelectric structure bonded on the ship deck (Figure 7-16). Both electrical and geometrical parameters were changed to maximize the dissipated vibration energy.

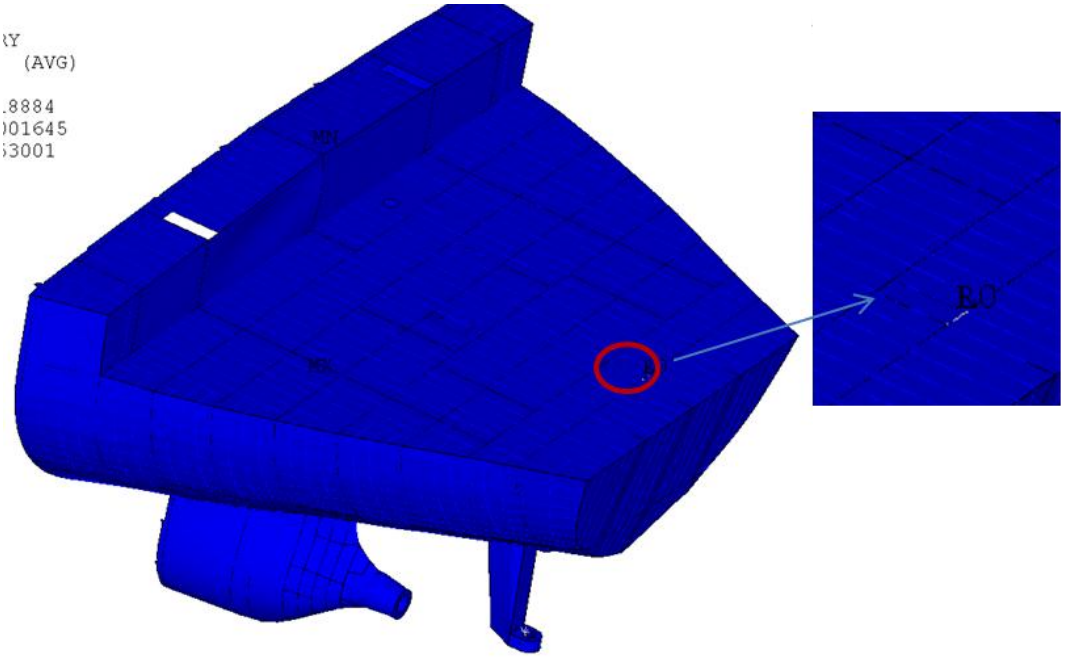

Figure 7-16: The RL circuit shunted on the FEM model

The shunt circuit was tuned for 4th blade passing frequency (20 Hz). This frequency is a critic frequency as it is in the range of the structure's resonant frequencies. However the equation 5-44 was modified by the Author for effective vibration reduction at this frequency. Equation 5-44 was successfully applied for the simple beam structure but no effective damping was achieved for the LNG application. Therefore a new tuning inductance *L* was calculated according to:

$$L = \frac{1}{C_p\,(w_n - \frac{w_n}{10})^2} \qquad \textbf{7-4}$$

This may be a particular case for the LNG carrier aft deck structure. It might be related to complexity of the ship structure.

7.2.5 Modelling of Passive Piezoelectric Shunt Damping on a LNG vessel and Results

A series of harmonic analysis was carried out to calculate the response of the stern part of the vessel when a passive piezoelectric shunt damping system was added to the mooring deck surface. The results were examined at the different locations to obtain a graph of response quantity (displacements) versus frequency. Peak points of responses were identified from graphs. The complete results are given in Appendix H. The structural responses are also included and are presented in a frequency range from 1 to 40 Hz (see Appendix H).

The quantity of vibration reduction is given as attenuation (in decibels) using the following definition:

$$A_{dB} = 20log\frac{u_{peak}}{u_{shunt}} \qquad 7\text{-}5$$

The output data for chosen nodes and the thickness of the piezoelectric material is 30mm. The results are given in Table 7-4, Table 7-5, Table 7-6 and Table 7-7.

Table 7-4: The effect of different resistance on attenuation vibration at Node23

Frequency (Hz)	R=10,000,000 Ω	R=1,000,000 Ω
19.038	-1.77	-1.66
20.5	-1.76	-1.73
23.425	-0.08	-0.11
26.838	-2.22	-2.20

Table 7-5: The effect of different resistance on attenuation vibration at Node29

Frequency (Hz)	R=10,000,000 Ω	R=1,000,000 Ω
19.038	-3.21	-3.09
20.5	-0.38	-0.38
23.913	-0.01	-0.02
26.838	-2.22	-2.20

Table 7-6: The effect of different resistance on attenuation vibration at Node37

Frequency (Hz)	R=10,000,000 Ω	R=1,000,000 Ω
19.038	-2.7	-2.5
23.913	-0.2	-0.2
26.838	-1.9	-1.9

Table 7-7: The effect of different resistance on attenuation vibration at Node38

Frequency (Hz)	R=10,000,000 Ω	R=1,000,000 Ω
19.038	-1.7	-1.6
26.838	-0.5	-0.5

It is apparent that reduction occours when passive piezoelectric shunt damping is applied. The shunted resistant is also effective for mitigation. The peak displacements were reduced around 2 dB for the chosen nodes.

Further simulations were run to investigate the improvement of vibration damping. The results are given for the specific nodes:

1. Attenuation versus thickness of the piezoelectric structure (Figure 7-17, Figure 7-19, Figure 7-21 and Figure 7-23)
2. Attenuation versus the number of piezoelectric patches (Figure 7-18, Figure 7-20, Figure 7-22 and Figure 7-24)

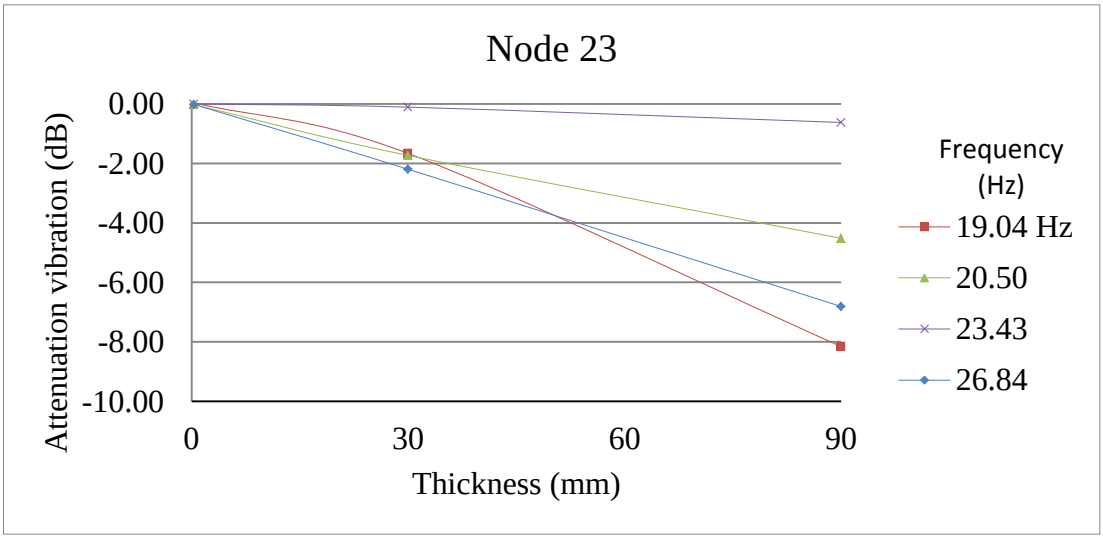

Figure 7-17: Attenuation vs. Thickness of the piezoelectric patch at Node 23

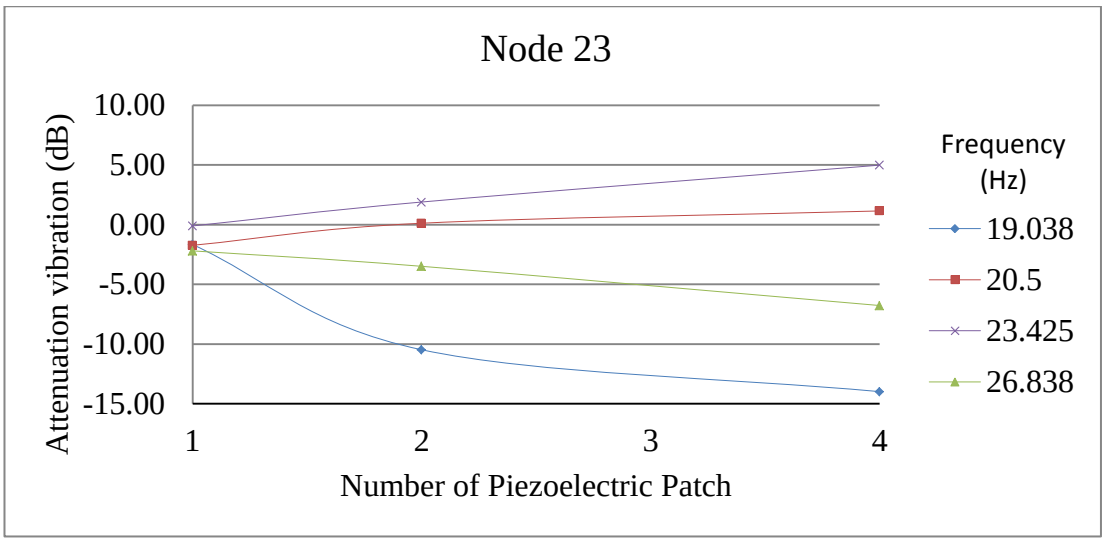

Figure 7-18: Attenuation vs. the Number of the piezoelectric patch of the structure at Node 23

The vibration level is slightly increasing at Node 23, when the number of piezoelectric material is increasing. The resason is that the natural frequency is shifting in the 20–23 Hz frequency range (see Appendix H, Figure 2). At this frequency range the given results were not read from the peak points. To be comparable the results are, nevertheless, presented.

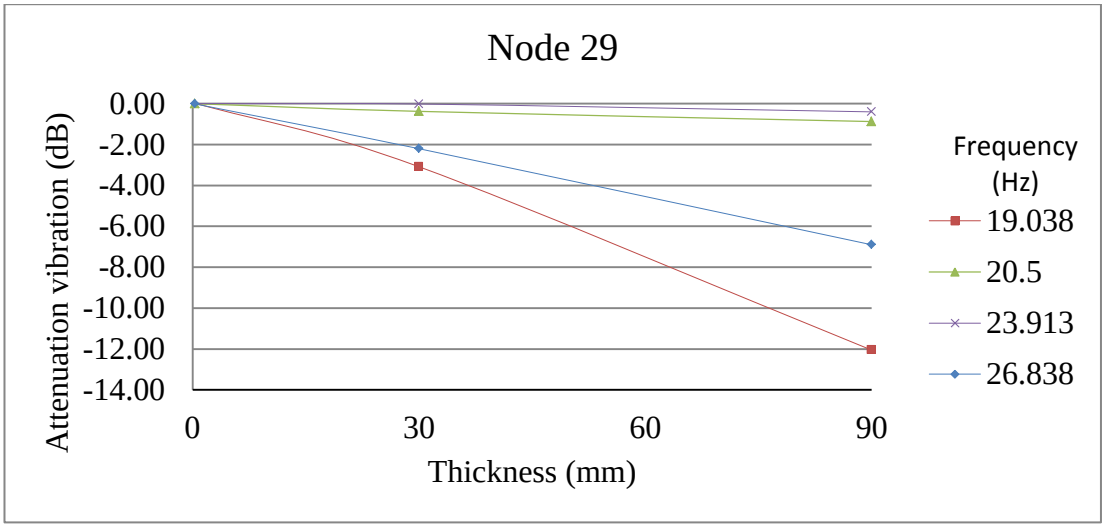

Figure 7-19: Attenuation vs. Thickness of the piezoelectric patch at Node 29

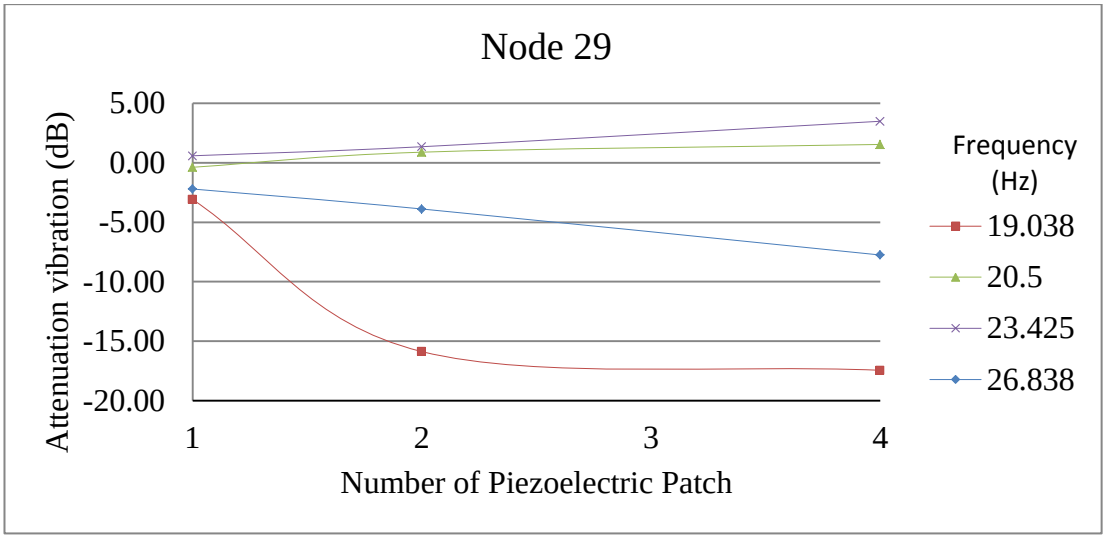

Figure 7-20: Attenuation vs. the Number of the piezoelectric patch of the structure at Node 29

Increasing the number of piezoelectric patchs does not seem to successfully mitigating vibration at Node 29. This might be due to the fact that the piezoelectric effect is less efficient as the mooring deck structure has members which increase the stiffness in this area.

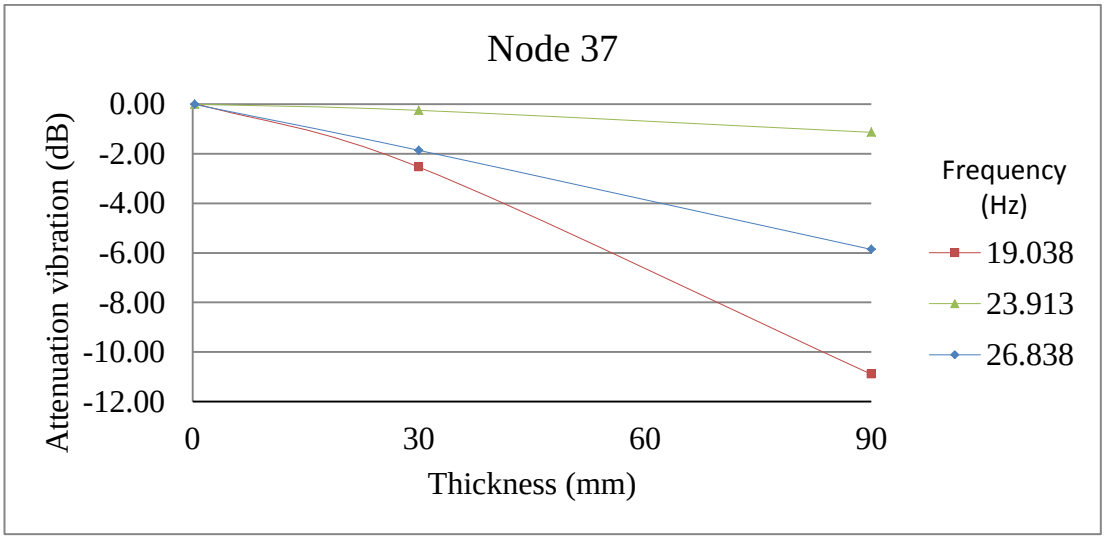

Figure 7-21: Attenuation vs. Thickness of the piezoelectric patch at Node 37

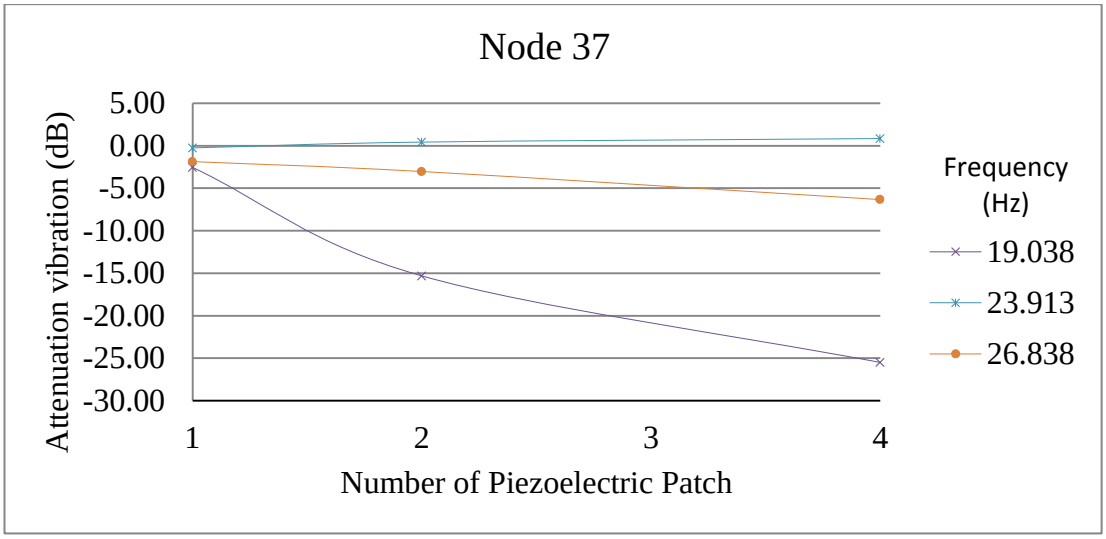

Figure 7-22: Attenuation vs. the Number of the piezoelectric patch of the structure at Node 37

The highest mitigation was observed at Node 37, the point attached to the piezoelectric patch. The vibration was damped around 25dB (the 4th harmonic of blade passing frequency).

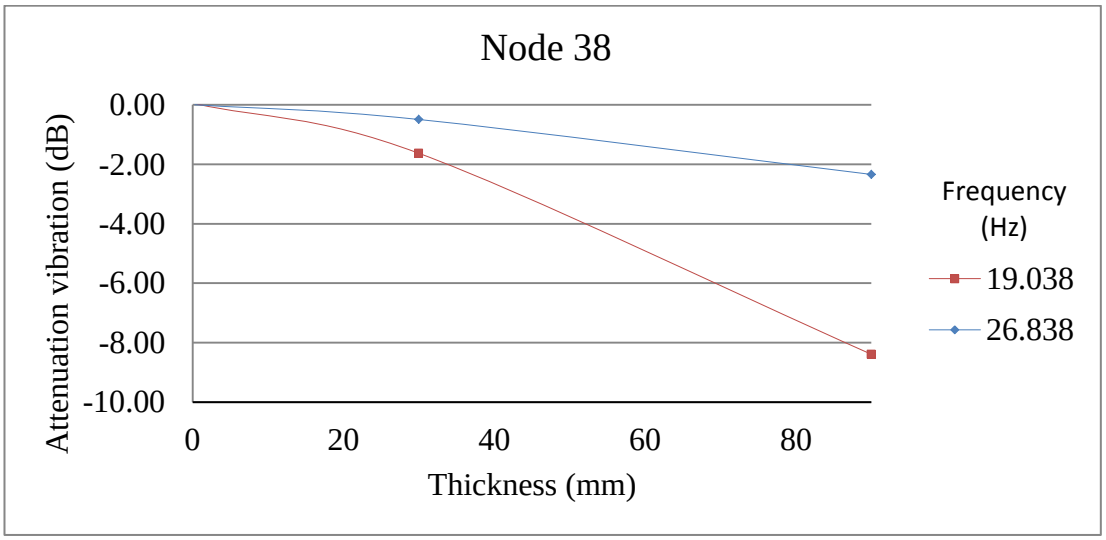

Figure 7-23 Attenuation vs. Thickness of the piezoelectric patch at Node 38

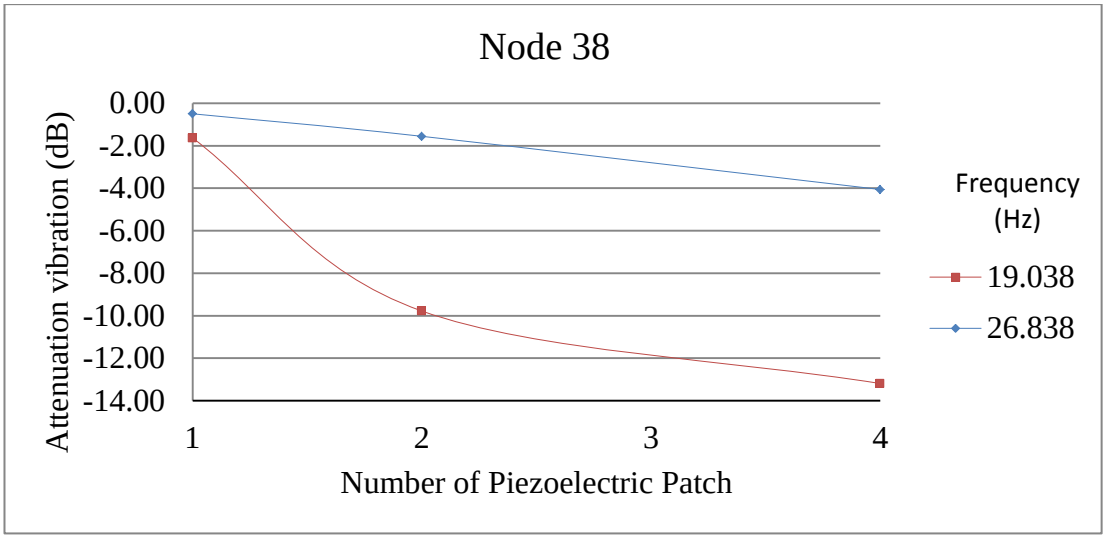

Figure 7-24: Attenuation vs. the Number of the piezoelectric patch of the structure at Node 38

Attenuation at Node 38 is similar to Node 23. However, the structure is not giving a peak point in the frequency range 20–23Hz.

7.2.6 Rearrangement of Piezoelectric Patches and Results

A new piezoelectric material localization involving four separate patches was also investigated. The four patches have a 2.86m longitudinal and 0.85 m horizontal gap between each other, shown in Figure 7-25. The results of the rearrangement were compared with previous results (see Table 7 8–Table 7 11).

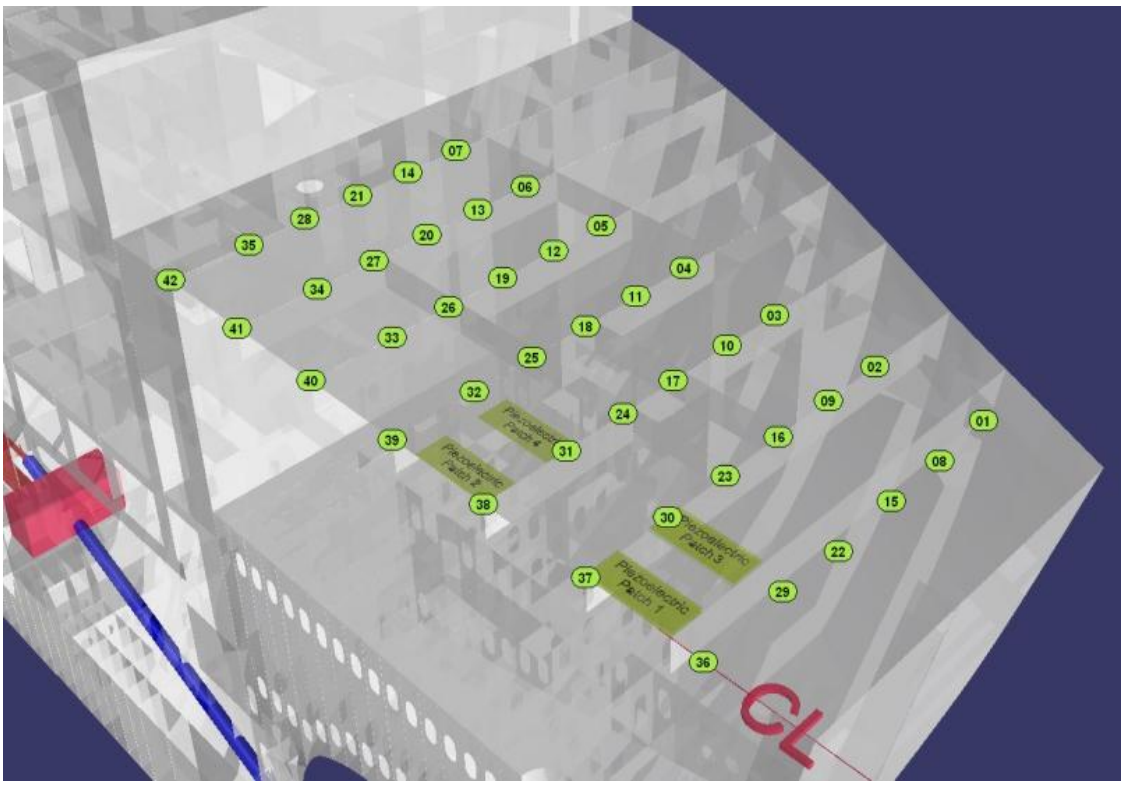

Figure 7-25: The new localization of the four piezoelectric patches

Table 7-8: Attenuation (dB) at Node 23 for the combined piezoelectric patches vs. the separated piezoelectric patches

Frequency (Hz)	t=30mm 4 PZT Patch	t=30mm 4 separated PZT Patch
19.038	-14.98	-15.43
26.838	-2.97	-6.94

Table 7-9: Attenuation (dB) at Node 29 for the combined piezoelectric patches vs. the separated piezoelectric patches

Frequency	t=30mm 4 PZT Patch	t=30mm 4 separated PZT Patch
19.038	-17.44	-15.15
26.838	-7.75	-18.71

Table 7-10: Attenuation (dB) at Node 37 for the combined piezoelectric patches vs. the separated piezoelectric patches

Frequency	t=30mm 4 PZT Patch	t=30mm 4 separated PZT Patch
19.038	-25.5	-22.9
26.838	-6.3	-14.2

Table 7-11: Attenuation (dB) at Node 38 for the combined piezoelectric patches vs. the separated piezoelectric patches

Frequency	t=30mm 4 PZT Patch	t=30mm 4 separated PZT Patch
19.038	-13.2	-9.7
26.838	-4.1	-17.6

The density of piezoelectric patches per deck area is important. The results provide a clear picture how the localization of the patches can affect vibration mitigation. The combined piezoelectric patches are more effective at 19.038 Hz as the mode shape is

developing longitudinally. The separated patches are more effective at 26.838 Hz as the mode shape is developing in the lateral direction, where two out of four patches were located.

7.2.7 Discussion

Vibration reduction was detected when different electrical boundaries and sizes of piezoelectric materials were applied. The thickness of the piezoelectric material was kept reasonably small compared to the thickness of the deck structure. Therefore, the key parameters were electrical values of both the piezoelectric patch and the electrical circuit. This altered the dynamics behaviour of the structure. The numerical results showed significant vibration attenuation in the frequency range of approximately 18–26 Hz.

The new damping system had, nevertheless, a negative effect in the very low frequency range. The amplitude of the vibration was increased around the 8Hz resonance frequency. This finding was expected as the system was tuned for a single mode which was around 4^{th} harmonics of the ship structure. Therefore, the damping system was fail for multi-mode frequency damping. This was expected from the study of (Hagood and von Flotow 1991).

A successful piezoelectric effect can be detected where higher responses are developing. Piezoelectric materials show good efficiency of converting mechanic energy into electric energy when the material experiences high strain. Figure 7-26 shows electrical potential energy of different piezoelectric patch sizes and combinations.

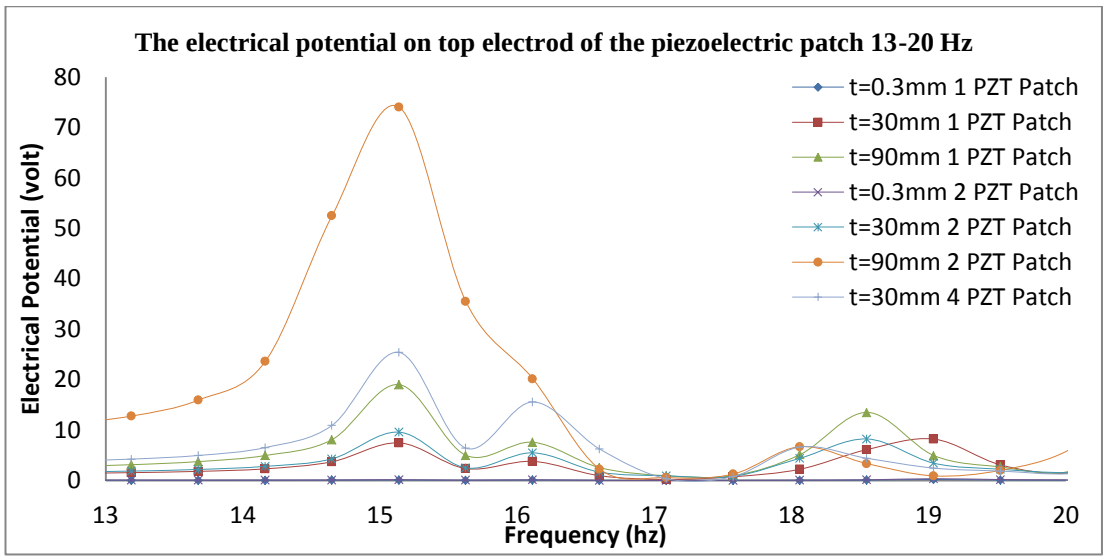

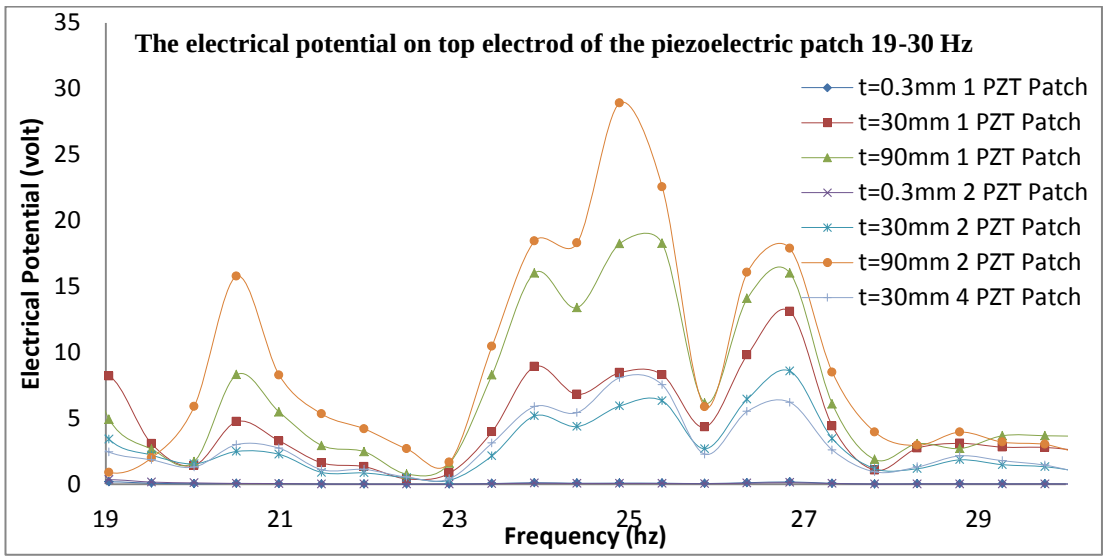

Figure 7-26: The electrical potential (in volt) on the top electrode of the piezoelectric patch

High amplitude of structural responses is giving high amplitude of electrical energy as can seen in Figure 7-26. This energy is stored in the material as electrical potential if no circuit is shunted (Min et al. 2010). This is why piezoelectric materials act like capacitors.

7.3 Vibration Damping on a Keel Structure with Passive Piezoelectric Shunt RL Circuit

The passive piezoelectric shunt damping system is used to reduce dynamic responses of the flow-induced vibration on a yacht keel. Two numerical approaches were used: computational fluid dynamics (CFD) to calculate the excitation forces and finite element analysis (FEM) to find structural and electrical responses. A fast Fourier transform (FFT) analysis was carried out to find vortex shedding frequency (as a dominant frequency) over the keel. Detailed CFD results were published in Mylonas et al. (2013).

7.3.1 Flow-Induced Vibration of Keel

An America's Cup Keel developed by Werner et al. (2006) under the version 5 of the IACC rules was studied for experimental and numerical calculations, in which a scaled model of the keel bulb was used (Werner et al. 2006; Werner et al. 2007). The same scaled model was investigated in this study for the purpose of structural calculations.

Different keel bulb configurations, for example with winglets in different locations on the bulb and without winglets, were used in Werner et al. (2007). In this study's application no winglet configuration of the keel was chosen and the main dimensions of the keel are shown in Figure 7-27.

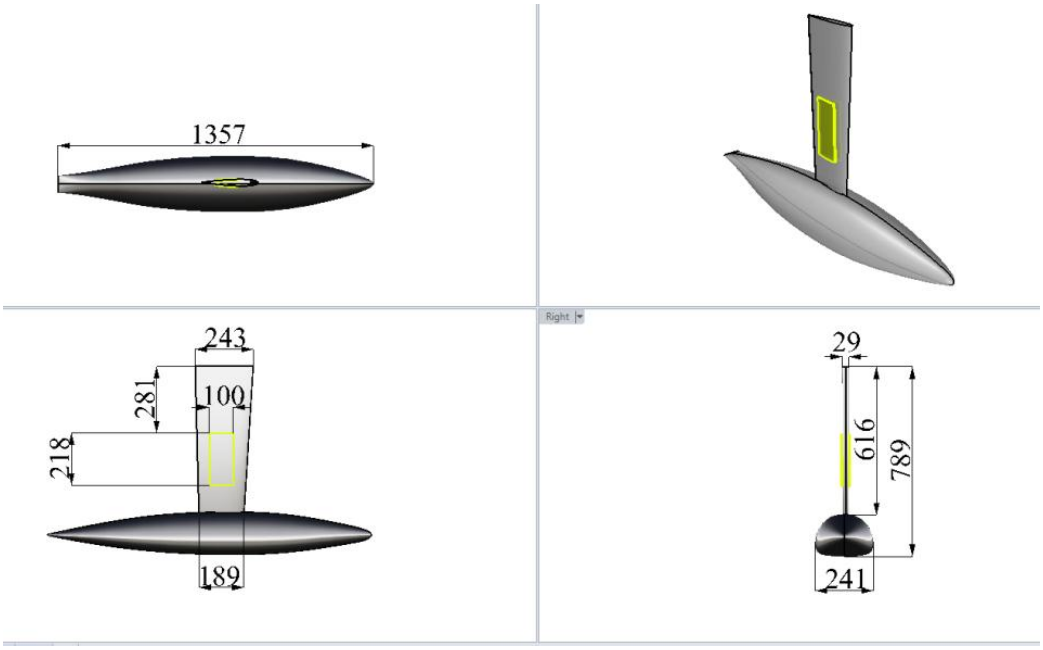

Figure 7-27: Main dimensions (mm) of the keel bulb

The sailing boat's structure was not used for calculation, only for demonstrational purposes. The output data were collected from the location points called middle node and tip node as can be seen in Figure 7-28.

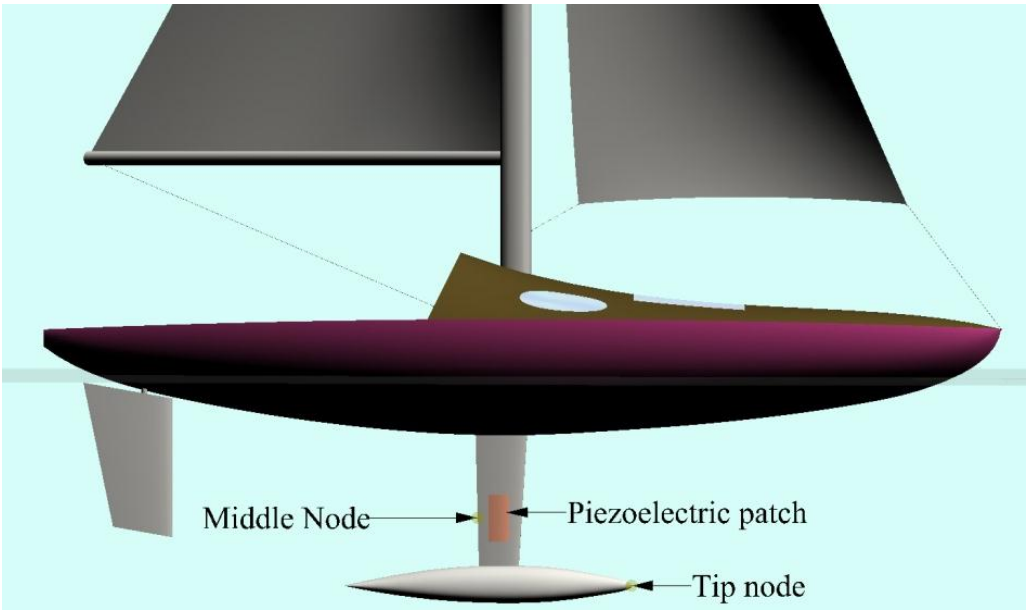

Figure 7-28: A sailing boat's structure and the keel bulb

The commercial CFD package STAR-CCM+ was used to calculate the pressure and velocity distribution on the structure (Figure 7-29). The study of Mylonas et al. (2013), in which they presented the forces acting on the keel model, showed a good accuracy between their own CFD results and the experimental results of Werner et al. (2006).

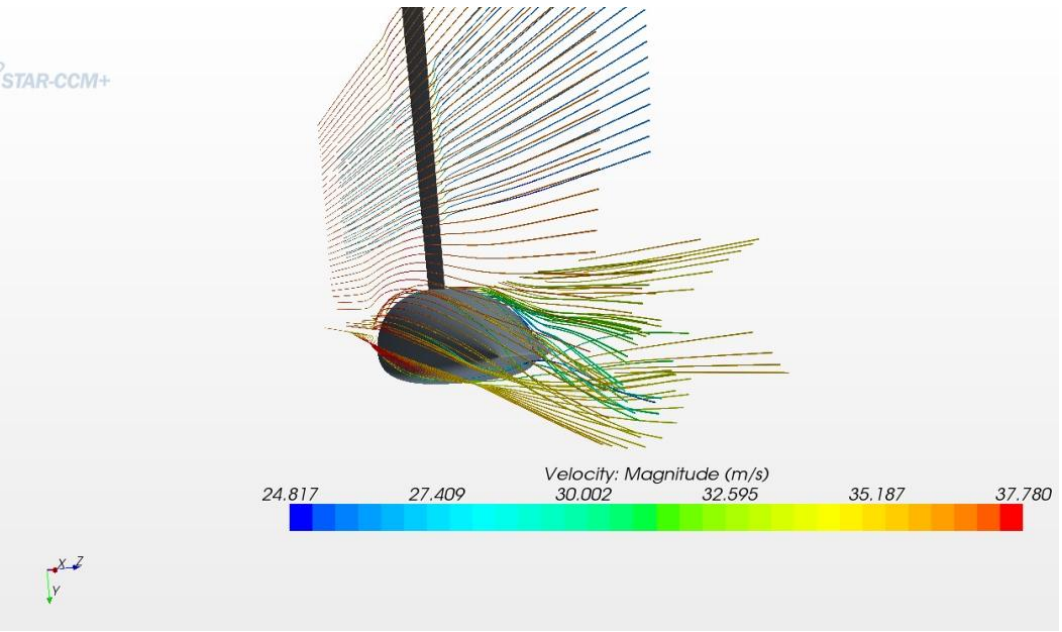

Figure 7-29: Stream lines around the keel bulb

Pressure fluctuations on the surface occur as vortices are shed from the body and they can excite the structure to vibrate and generate acoustic sound (Blevins 1990). The frequency of excitation forces is equal to the vortex shedding frequency, which depends on the shape and size of the body, the velocity of the flow, the surface roughness and the turbulence of the flow. The relation between vortex shedding frequency (f_s) and flow speed (U) is identified by the Strouhal number (St).

$$St = \frac{f_s c}{U} \qquad 7\text{-}6$$

where c is a characteristic length.

A spectral analysis was performed on the results to find the vortex-shedding frequency. The quantity pressure on the keel surface used for the calculation of the sound pressure level is defined by

$$Lp = 20 \log_{10} \frac{P_{rms}}{P_{ref}} \qquad 7\text{-}7$$

where p_{ref} is a reference pressure of 20 µPa. Figure 7-30 shows Sound Pressure Level.

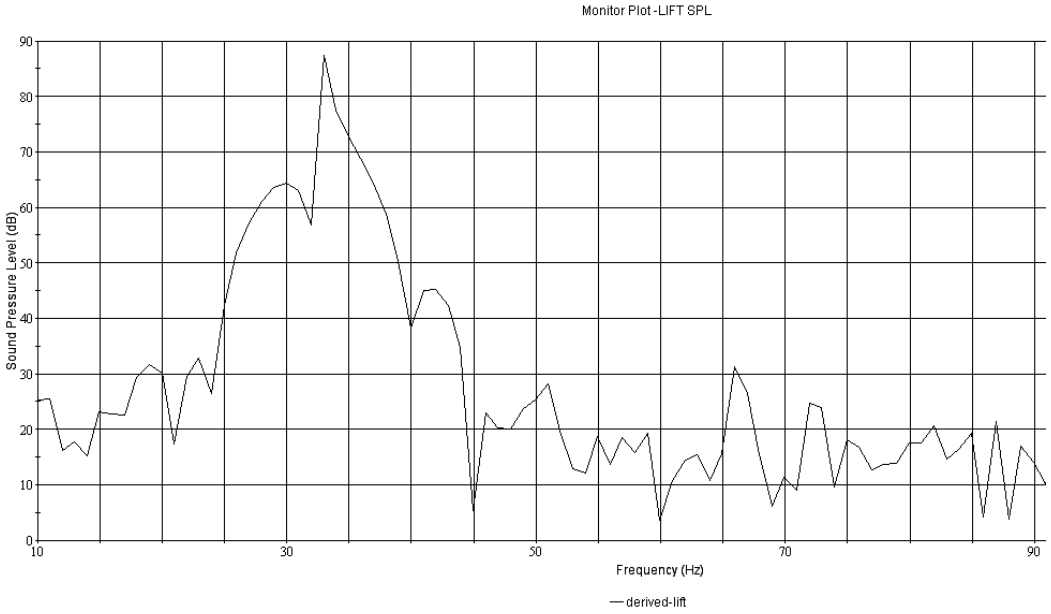

Figure 7-30: Sound Pressure Level vs. Frequency

The frequency of pressure fluctuations was found in the range of 32–40 Hz. The corresponding Strouhal Number was in the range of 0.18–0.20 (Figure 7-31). This

result is reasonable compared to previous studies (Taylor et al. 2003; Krylov and Porteous 2010).

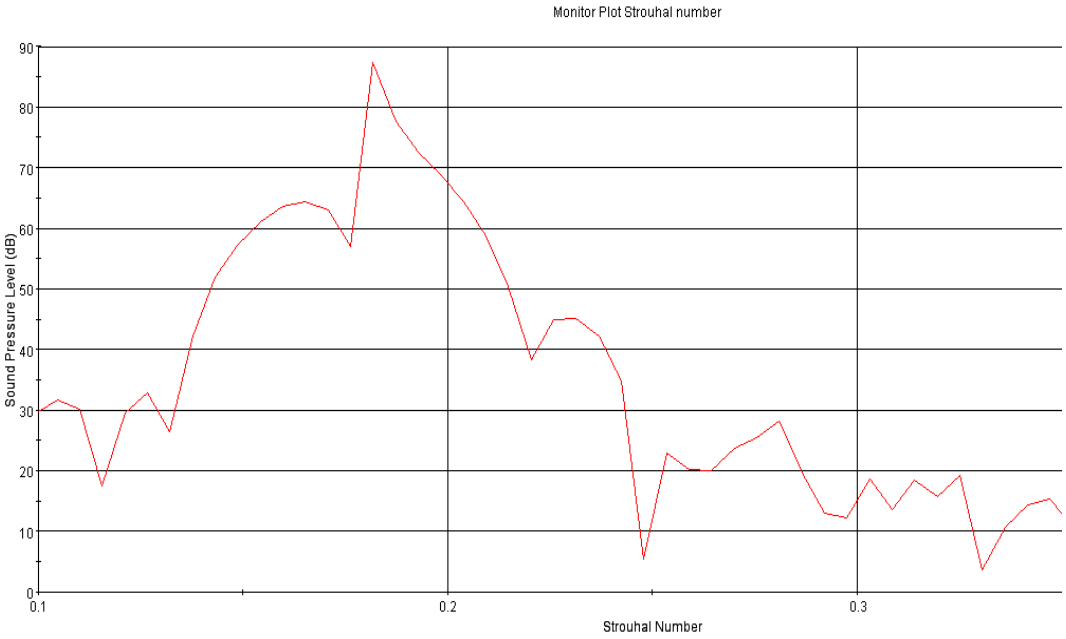

Figure 7-31: Sound Pressure Level vs. Strouhal Number

7.3.2 Flow-Induced Vibration Damping with the Passive Piezoelectric Shunt Circuit

PZT-5H plate elements are bonded on the port side and starboard side surfaces of the fin of the keel. The thickness h is 1mm; the top and the bottom surface dimensions are 20x10mm^2. In Figure 7-32, the piezoelectric plate elements are poled in thickness direction (z or x_{33} axis).

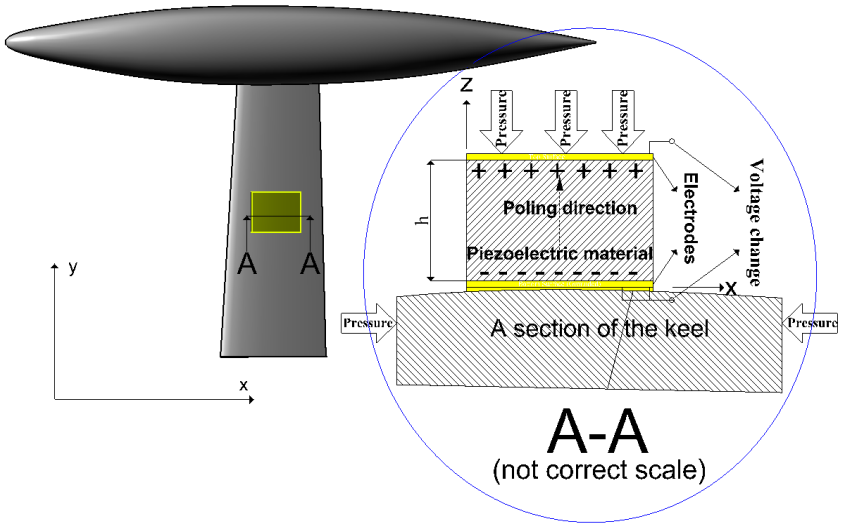

Figure 7-32: Physical model of the keel bulb bonded by the piezoelectric patches

A finite element model of the keel structure attached with piezoelectric material was created for vibration control using shunted piezoelectric circuits. The finite element model is shown in Figure 7-33, illustrating the connection of the electrical circuits at the top and the bottom surfaces.

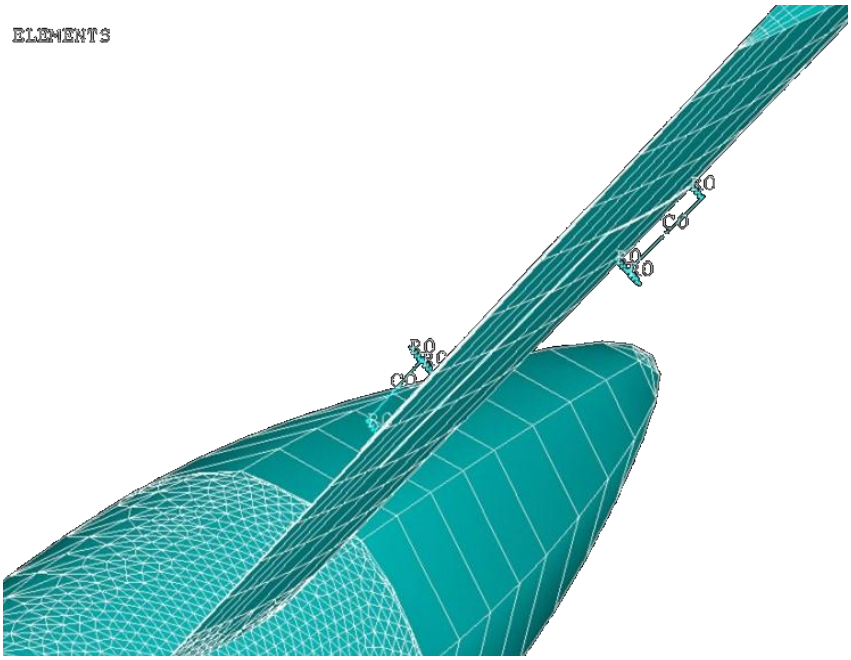

Figure 7-33: The FEM of the structure shunted with R-L parallel electrical circuit

7.3.3 Modal Analysis of the Keel and Results

A modal analysis was carried out to estimate the natural frequencies of the keel with and without piezoelectric patches. Short circuit electrical boundary conditions were applied to piezoelectric bonded structure. In other words, top and bottom surfaces of the piezoelectric materials were grounded (V=0 Volt) not to have any piezoelectric effect. A comparison of natural frequencies with and without piezoelectric patches is given in Table 7-12.

Table 7-12: Natural frequencies of the keel with and without piezoelectric material

Mode No	Frequency without piezoelectric (Hz)	Frequency with piezoelectric (Hz)
1	1.3	1.5
2	2.4	2.7
3	9.3	9.4
4	16.9	16.7
5	36.5	35.7
6	74.0	79.9
7	80.2	82.1

As can be seen in Figure 7-34 the mode shapes provide a preliminary idea about the ideal application location of the piezoelectric materials.

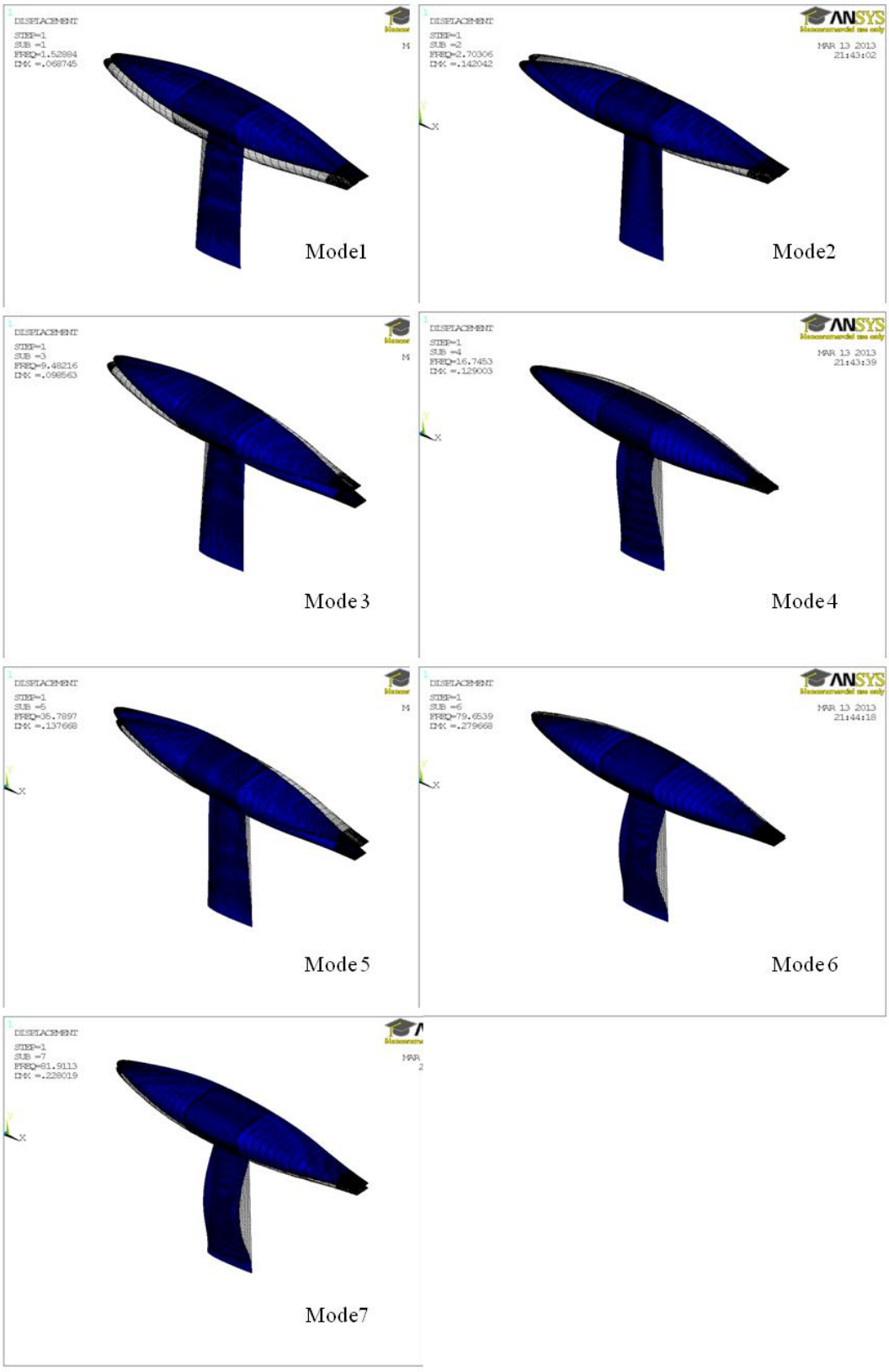

Figure 7-34: Mode Shapes of the keel bulb

7.3.4 Harmonic Analysis of the Keel and Results

A CFD analysis was carried out to find the excitation forces and the predominant frequency caused by vortex shedding around the keel. The vortex shedding produced alternating pressure pulse on the keel surface. The computational fluid dynamic method (Mylonas et al. 2013) used in this simulation calculated the pressure distribution shown Figure 7-35. The pressure distribution was exported into the FEM of the keel (Figure 7-36).

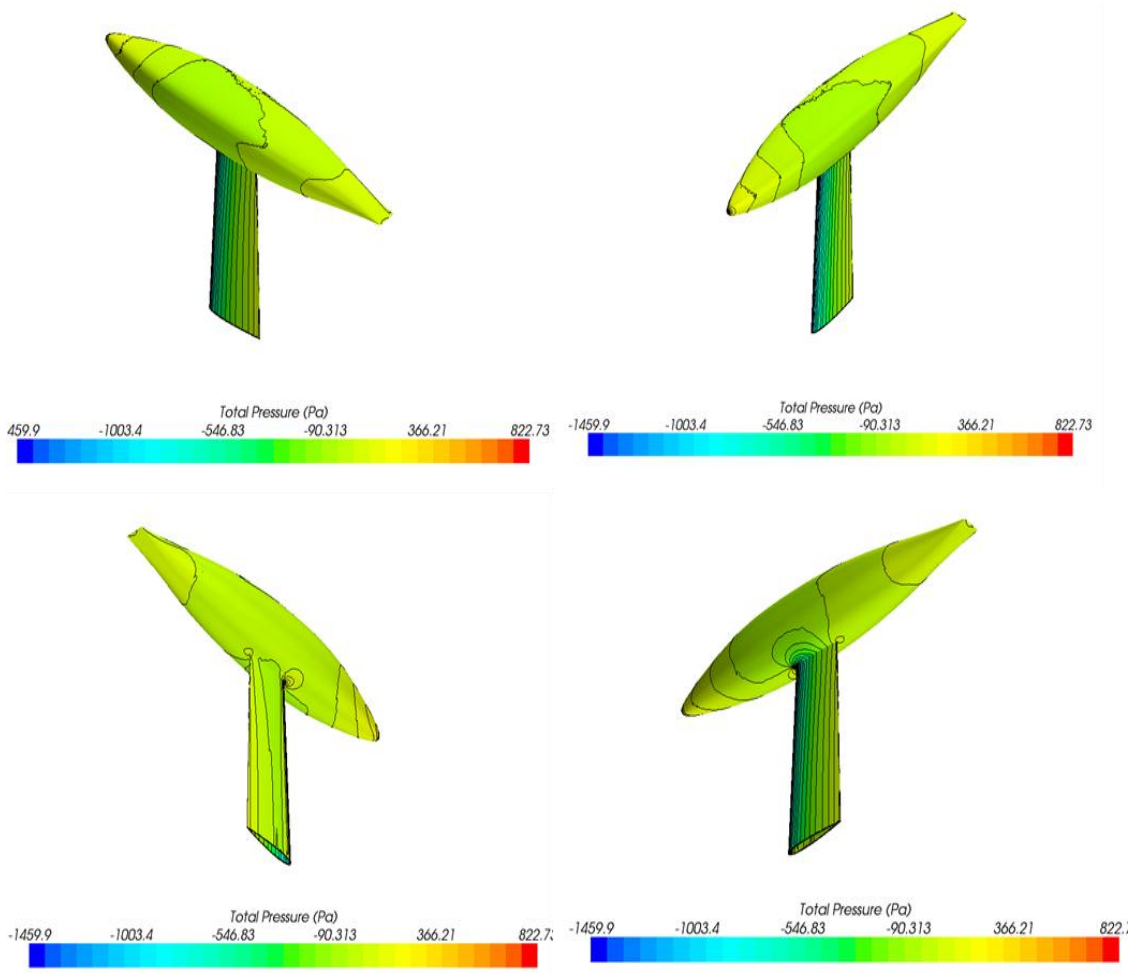

Figure 7-35: Pressure distribution on the keel surface in the CFD

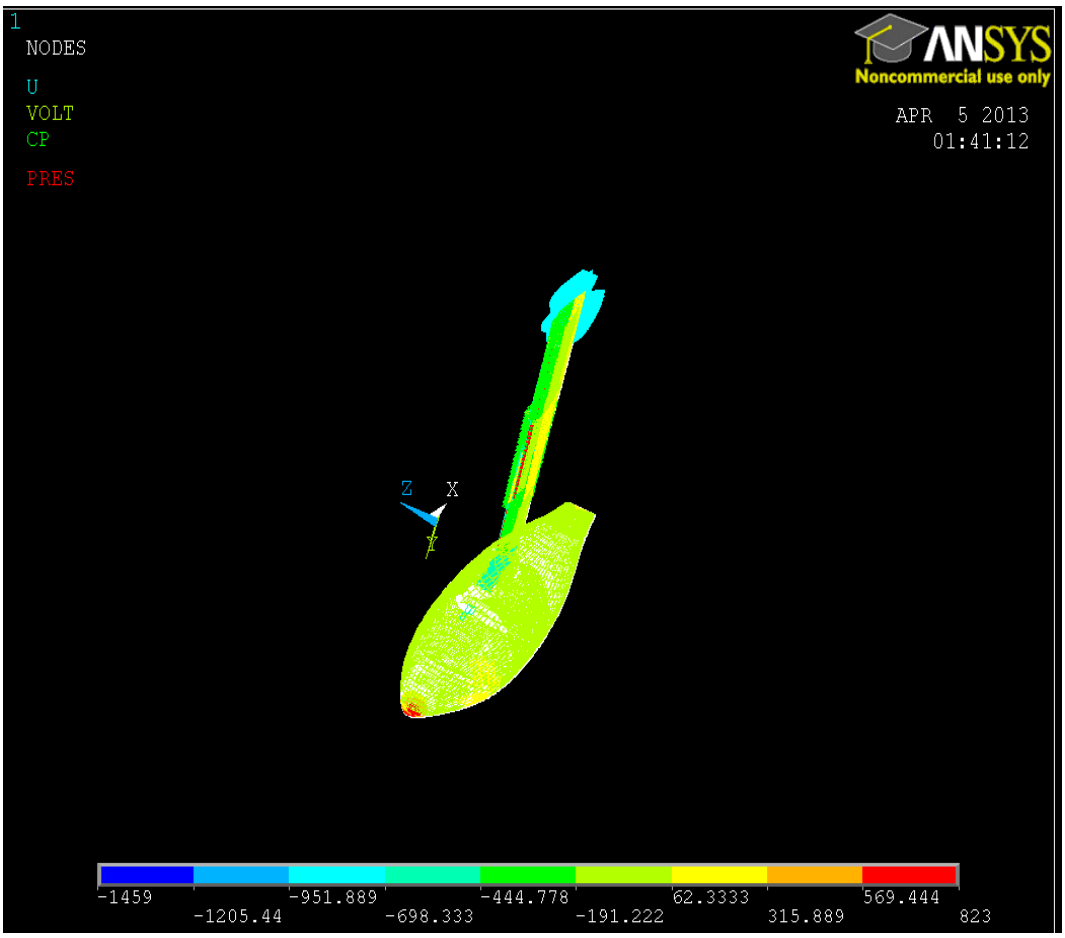

Figure 7-36: The exported pressure distribution on the keel surface in the FEM

For the selection of the correct piezoelectric material type it is crucial to know the mode shape of the structure. There is a strong relation between the mode shape and the corresponding piezoelectric constant d_{ij}. If the dominant forces are imposed in the thickness direction the piezoelectric patch will operate with thickness-stretch mode (d_{33}). Flow pressure generates load in the thickness direction, however, it also causes bending motions on the structure. Consequently, piezoelectric material operates with thickness-shear modes (see Figure 7-37). In this mode shape the parameter d_{31} plays a significant role and must be considered.

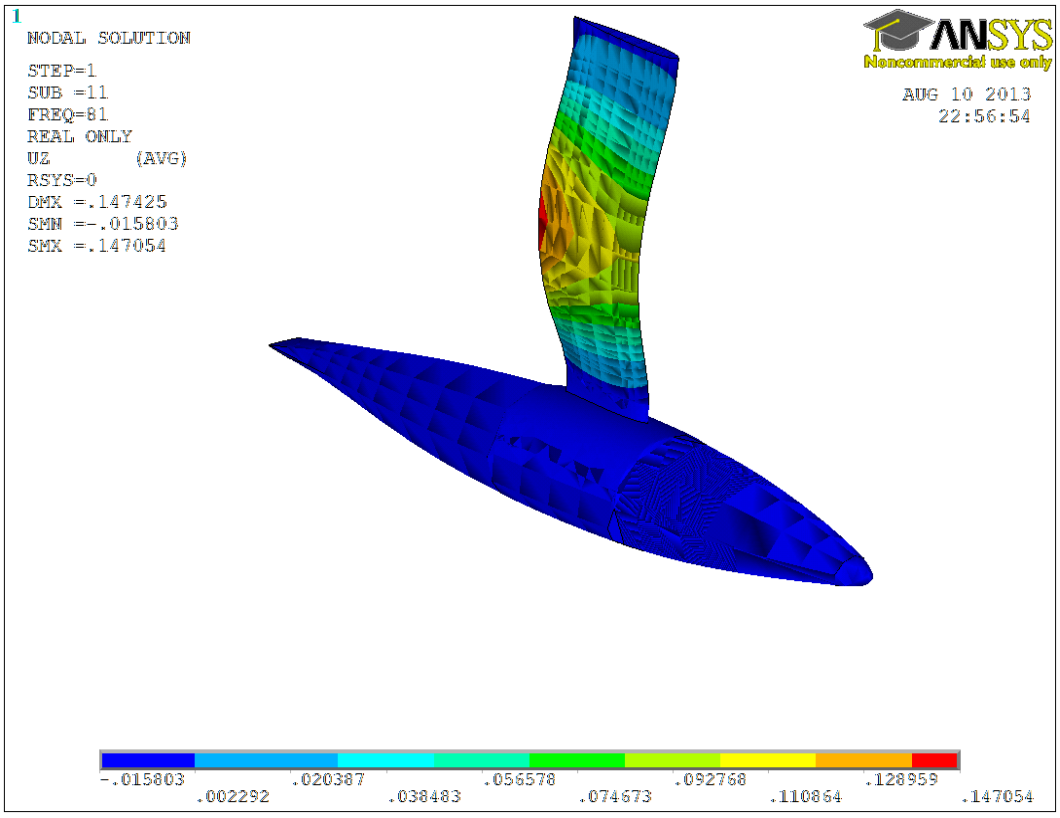

Figure 7-37: The deformation (mm) on the keel bulb due to the pressure on the surface

Harmonic analysis was performed to investigate:

1. The electrical responses of the piezoelectric patches
2. The vibration mitigation performance of the passive piezoelectric shunt damping system

It is expected to find higher electrical output at the natural frequency of the structure. As motion is time-harmonic, output voltage is read from the real part of impedance.

The electrical output result is given in Figure 7-38. Although dominant frequency of vortex shedding is around 35 Hz, the piezoelectric materials develop higher voltage

in the 80–100Hz range. Therefore, this frequency range was chosen for the evaluation of the passive piezoelectric shunt damping.

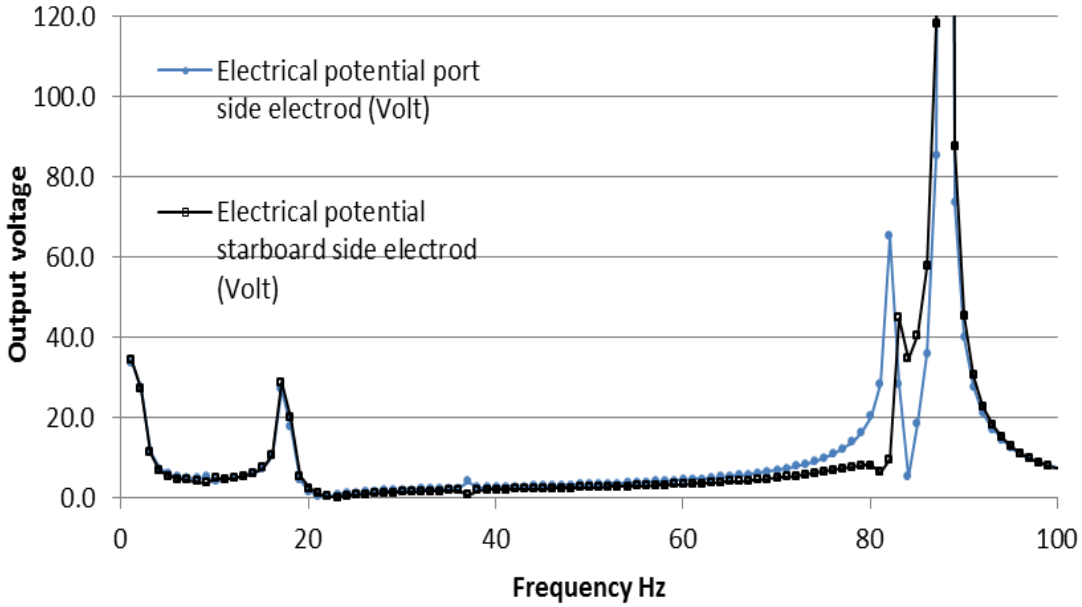

Figure 7-38: Output voltage versus frequency

There is a voltage difference between the two piezoelectric patches. The keel was tested with a three degree inclination angle towards the flow direction. That caused asymmetric flow around the structure and pressure distributions are, as a result, different on the each side of the keel.

The results for the vibration mitigation are presented for the tip node in Figure 7-39 and the middle node in Figure 7-40. The resistor of the circuits was given different values.

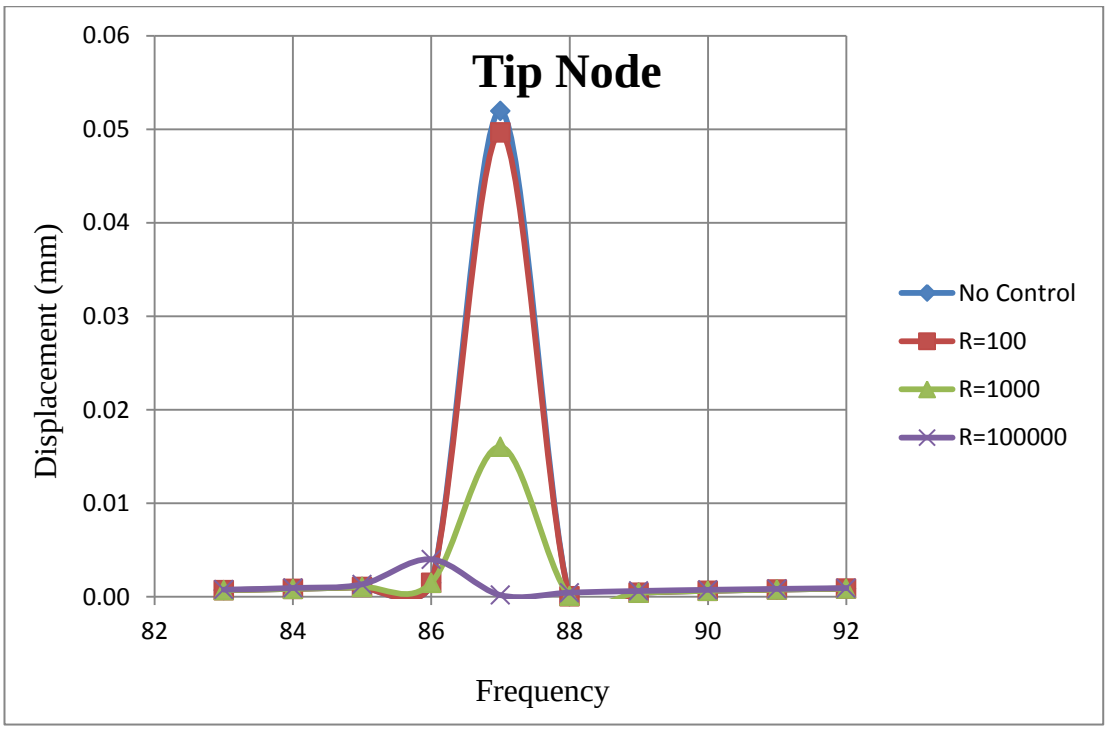

Figure 7-39: The effect of different resistance (ohm) at the tip node of the structure

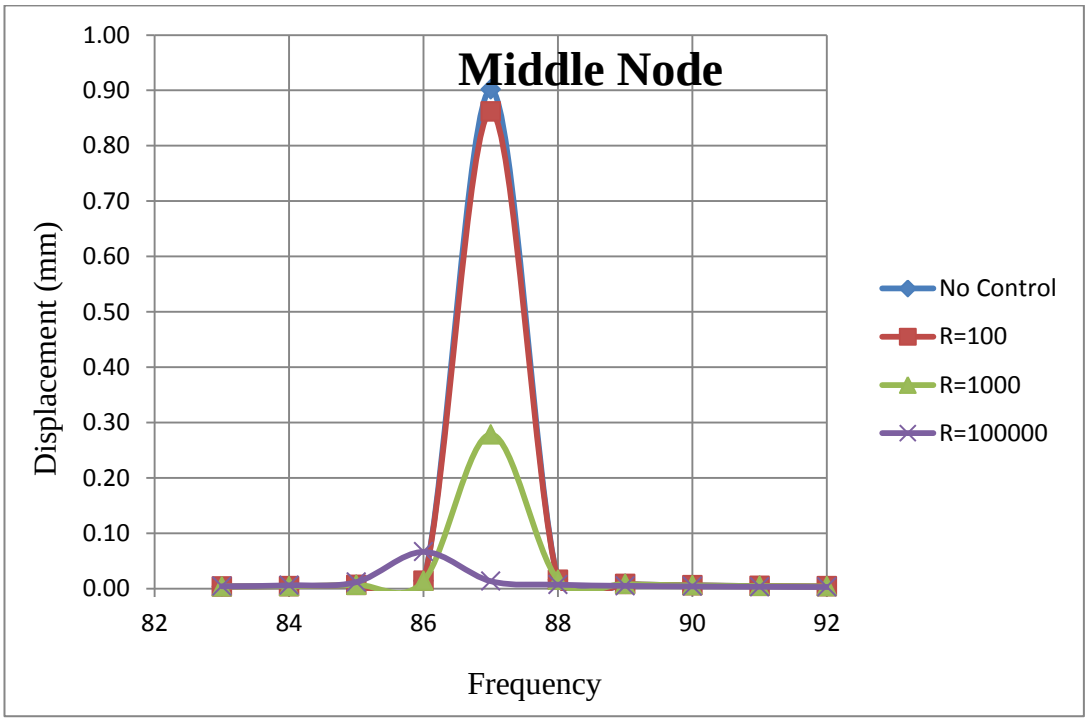

Figure 7-40: The effect of different resistance (ohm) at the middle node of the structure

The passive parallel resonant shunting damper was applied numerically to reduce the seventh mode vibration amplitude of the bulb keel. Vibration reduction of the keel structure was observed when the shunting resistance was increased. The peak point of response became almost a flat plateau when 100,000 ohm shunt resistance value was applied, thus virtually achieving the optimum.

7.4 The Summary of the Chapter

The present study proposes a new vibration damping concept for the marine and sailing industry. The theory of shunted piezoelectric material was used for the study of vibration mitigation on a LNG ship. The study was extended to additionally investigate an underwater ship structure. For that purpose, the bulb keel of a racing boat was selected. CFD was used to identify the dominant excitation frequency and pressure distribution on the shell of the LNG vessel and the keel structure. The Finite element method was chosen to calculate the response of the structure. As a result, CFD output became the input for FEM.

It was observed that the output voltage is dependent on the mechanical resonance frequency of the vibrating structure. It is also important to notice that, in both of the applications presented in this study, the electrical resonance frequency of the shunting circuit had to be tuned to the mechanical resonance frequency. Therefore, a passive piezoelectric shunt damping system is more efficient around these frequencies and the dissipated energy can be maximized.

8.Discussion and Recommendations

8.1 Chapter Introduction

Chapter 8 presents, firstly, an overall recap of the research conducted in this study. Secondly, the main contributions of this thesis are evaluated. The short comings and limitations are presented in the next subchapter followed recommendations for future works are given in subchapter 8.5.

8.2 Recap of the Thesis and Achievements

A literature review was carried out to develop knowledge about smart materials and their applications to mitigate vibration. Main findings of past research on noise and vibration techniques were reviewed in Chapter 3.

The SMs vibration damping system, involving a piezoelectric shunt circuit, was presented. The numerical modelling tool FEM for simulation, used in this study, was also introduced and the theory of numerical modelling of SMs' damping system was given in Chapter 4 and 5.

Chapter 6 presented a numerical study of SM application for beam vibration attenuation. The numerical results were evaluated and compared to experimental results for the purpose of validation.

In Chapter 7 a ship structure vibration was numerically simulated. A SM damping system was applied to reduce the vibration level. This damping system application

was also implemented for a yacht keel vibration simulation. The results were assessed and showed that attenuations of vibration amplitudes were clearly achieved in both applications . A database of numerical results was compiled from the numerical studies, containing curves of structural response frequencies with and without SM damping system.

Therefore the following objectives of the thesis were achieved through numerical studies conducted for the first time for both ship and ship appendage:

- Review of Noise of vibration damping techniques including smart materials and their potential as noise and vibration damping.
- Investigation of working principals of Smart materials and feasibility of smart materials for mitigating the ship noise and vibration
- Development of most suitable mathematical and numerical modelling for Smart materials and their implementation on mitigating the vibration onboard ships.
- Validation of the developed approach for modelling the smart materials
- Application of smart materials on ships through a parametric study to investigate the effectiveness of the smart materials to reduce the vibration on board ships

8.3 Main Contributions of the Thesis

There have been a number of previous studies on vibration reduction employing passive piezoelectric material shunted with electric circuits, as seen in the critical review and theory part of this study. However, there is no specific application, known to the author, regarding ship and ship appendage vibration. This novel study has attempted to fill this gap by developing the theory, numerical model and application to the ship for the first time.

The results, presented in this study have provided an insight for future research of SMs application to reduce structural vibration of ship and ship appendage.

Piezoelectric material, in particular, can be used as a component of a passive damping device, thereby avoiding active controlling, which has feedback systems and amplifiers to drive the piezoelectric actuators.

The Finite Element Method is proposed in this study to create and analyse structural responses of flow induced ship vibration. This study is the first to perform and develop a simulated passive piezoelectric shunt damping system using harmonic analysis in order to achieve optimal vibration reduction. Moreover definition of the tuning inductance at the critical frequency was modified for the LNG vessel and a new formulation was provided.

The choice of the correct calculation tool as well as the competent usage and thorough knowledge of the chosen software have proven to be essential for this study. The commercial ANSYS^{R} software was used to calculate the finite element model.

This study also generated feasibility into the effectiveness of piezoelectricity applied on ships as way of attenuating vibration. Effect of the location and the required area of the smart materials were investigated and presented.

8.4 Short Comings of Piezoelectric Shunt Damping

The potential of piezoelectric shunt damping has been evaluated through running simulation with Finite Element Models. Investigation has been carried out for the frequency range 0–40 Hz which is refers to lower frequency range in a reasonable time. The calculations could be conducted in a couple of hours (with Intel Xeon Quad Processor 3.20 GHz, 24.0 GB RAM). However, the calculation time in the middle frequency range and above was extremely long. It could take more than one day to finish a calculation. In addition, the output file became too large to be stored and further processed. Therefore FEM can be rightfully classified as “limited and impractical” (Lyon and DeJong 1995).

Statistical Energy Analysis (SEA) could have been used for the higher frequency vibration (or noise) simulation. With SEA both the physical and the numerical model of a structure are simpler compared to finite element models. Additionally the calculation time is shorter than for FEM. However the biggest challenges using SEA are estimating the key parameters: the Transmission Loss Coefficient (TL) and the Coupling Loss Factor (CLF). In Appendix A, TL and CLF are described in depth.

In order to reduce vibration with piezoelectric material, a shunt circuit is needed to be bonded to piezoelectric material. Therefore, a good working knowledge of piezoelectricity, electromechanical coupling and shunt damping was absolutely necessary. This proved to be challenging at times for the Author having no previous background in these specific areas of science.

The results of the study show that efficient damping occurs, when the electrical resonant frequency matches the mechanical frequency. Piezoelectric material creates electrical energy, which is dissipated through Joule heating by a resistive shunt. This process occurs, when the electrical natural frequency is tuned by a shunt inductor. Optimum damping, depending on the frequency of vibration, can be challenging to reach (as the Author experienced). The correct estimation of inductor and resistor values will improve the damping.

In the ship application the electric circuit was tuned for 4^{th} harmonic blade passing frequency, which means the damping system was set up for a single mode. The numerical results of the ship vibration simulation showed significant vibration attenuation in the vicinity of that specific resonance frequency. The new damping system was not successful for reducing the response amplitude at the frequencies other than the 4^{th} harmonic frequency.

In this study one type of ship (LNG carrier) was used for the ship application however each ship has different fundamental natural frequencies and complete vibration characteristics. Passive piezoelectric shunt damper may be more or less effective given the range of operations conditions, different type of ships and different type of excitation characteristics.

In the bulb keel application the parallel resonant shunting damper successfully reduced the seventh mode vibration amplitude of the structure. In the simulation almost optimum damping conditions were achieved, when the peak point of response became nearly a flat plateau (the corresponding shunting resistor was 10,000 ohm).

8.5 Recommendations for Future Work

Many topics, including SMs as well as prediction and prevention of noise and vibration, were only briefly introduced in this thesis and could not be investigated in depth. Further recommendations are:

- Investigation of SMs usage for noise reduction and mitigation in the middle and higher frequency range.
- A comparison between classic vibration damping systems and passive piezoelectric shunt damping systems is needed to determine cost efficiency.
- A shunt damping system may perform differently depending on the type of vessel. Therefore, this system should be tested for various types of vessels including container carriers, cruise ships, small crafts etc.
- Experimental studies for ship applications are needed to create a database, which can help the researchers to develop and improve simulation tools and SMs damping systems.
- In the current study a single mode damping system was employed. Vibration mitigation results can be expected for the vicinity of one resonance frequency. The system can be improved for Multi Modes Damping. This new damping system can be functional for a wide frequency range.
- A parallel R-L shunt circuit was used in the passive piezoelectric shunt damping system in this study. This system can be modified for a serial R-L shunt circuit configuration.
- The capacitance value of the piezoelectric material is proportional to the area of the material, inverse of the thickness and dielectric value (when poled in the thickness direction). In case of size limitations of the piezoelectric

material the passive piezoelectric shunt damping system requires a large size inductor to reach the low-frequency electrical resonance. It is important to ensure that inductors for experimental or real application are commercially available. Otherwise a custom made inductor may be required or a synthetic inductor may be applied as it provides various inductance in the shunt circuit.

- Seaway loading causes fatigue and crack propagation from potentially hazardous embedded weld defects. SMs can possibly be employed to overcome the problem.
- Different operating conditions, oscillating stresses and a burst of pressure may cause failure and also affect durability of the piezoelectric shunt damping system. A study of durability in different service environments may be necessary to identify limits and quantitative life of the damping system.
- Energy harvesting by piezoelectric materials can be considered as a possible power supply for ships, rigging of sailing boat and vessels operated in the deep water. The generated energy (voltage) can be stored or used anytime. Two supportive studies of the energy harvesting concept were published during the process of this study (Turkmen et al. 2012; Turkmen et al. 2013).

8.6 The summary of the Chapter

Following the review of the conducted research at the beginning of this chapter, the key objectives of this study were re-examined and presented. It was found, that the objectives 1–5 were successfully met. The main contributions summed up the novelties and benefits of the research, but also listed challenges that were met during the research. Recommendations for future research were presented. Objective 6 was therefore found to be satisfied in subchapter 8.5. This study did not only provide valuable information regarding the successful numerical prediction as well as the mitigation of ship vibration by means of smart material, but further offered innovative ideas and concepts needed for future research employing smart materials.

9.Conclusions

The work presented in this thesis has focused on the application of SMs for reduction of ship vibration. Damping treatments help to mitigate vibration and noise levels in order to comply with national and international regulations. Therefore, to predict and prevent noise and vibration, both conventional and unconventional methods have been reviewed from open literature.

There has been a considerable amount of generic research regarding the reduction of noise and vibration by using piezoelectric materials in either active or passive systems. Even though active damping systems are widely used it is very rare to find passive piezoelectric shunt damping systems for complex structure applications. There are a number of studies about passive piezoelectric shunt damping systems to reduce noise and vibration. However, there has been no study specifically about passive piezoelectric shunt damping systems for ships.

As the electrical properties of piezoelectric materials are strongly coupled with mechanical properties they are more efficient where the strain is bigger. Ships have many structural members. Some members are very stiff such as main and auxiliary engine foundations where structural responses are relatively small. On the other hand, some part of ships has more flexible structure such as decks and cabins. Therefore, it is expected that a passive piezoelectric shunt damping system can be more effective when laminated on a deck structure.

There are two main approaches to modelling the effect of piezoelectric material for investigation of this damping performance: statistical energy analysis (SEA) and finite element method (FEM). In the SEA approach, the input and output data are averaged variables. In FEM, input and output data are local variables. When the frequency is higher, FEM requires longer iteration time than SEA. The size of the output will be also bigger than SEA. SEA can be a strong tool for noise and vibration analysis. However, SEA works best in so-called high frequency range (from 500 Hz on). Additionally, It is difficult to estimate coupling loss factors and transmission loss factors for structures on which piezoelectric materials are applied. Therefore,

this study concentrates on the investigation of ship vibration in a low frequency range through FEM.

The finite element analysis was performed for passive piezoelectric parallel resistive inductive (R-L) circuit damping to calculate beam vibration reduction. The increasing shunting resistor values in shunt circuit improved the damping. A good agreement was found between the presented numerical results and previous experimental test results of Park (2003). The average error percentage obtained 5.4% between experiment and the numerical model. The outcome of the comparison encouraged the Author to apply the same method to numerically investigate reduction of ship vibration. Therefore, a numerical study was performed to develop and demonstrate a piezoelectric vibration damping technique on a LNG vessel. The geometrical and electrical parameters were systematically changed to estimate the performance of this damping system. Further investigation was carried out for a bulb keel, which was vibrated by vortex-induced flow. CFD was used as a tool to calculate the pressure fluctuation on the keel structure. Fast Fourier Transform analysis was carried out to transform time histories of the pressure to the function of frequency, which became the input for FEM simulation of keel structure vibration.

Vibration reduction was up to 25 dB has been calculated through these models. However this has only been achieved at certain frequencies, depending on size of the material, location and how the electrical circuit was tuned.

Some similarity was found between the way piezoelectric damps vibration and viscoelastic materials damps vibration. In this study, however, it has been established that a passive piezoelectric shunt damper can be optimised for a specific frequencies whereas viscoelastic material damps over a broadband frequency range.

10. References

Ansys Fluent User's Guide (2010). "Release 13.0. ANSYS." Inc., Canonsburg, PA.

Anton, S. R., Sodano, H. A. (2007). "A review of power harvesting using piezoelectric materials (2003–2006)." Smart Materials and Structures 16(3): R1.

Asmussen, I., Mumm, H. (2001), Ship Vibration, GL Technology, Germanischer Lloyd.

Badel, A., Benayad, A., Lefeuvre, E., Lebrun, L., Richard, C., Guyomar, D. (2006). "Single crystals and nonlinear process for outstanding vibration-powered electrical generators." IEEE transactions on ultrasonics, ferroelectrics, and frequency control 53(4): 673-684.

Badel, A., Sebald, G., Guyomar, D., Lallart, M., Lefeuvre, E., Richard, C., Qiu, J. (2006). "Piezoelectric vibration control by synchronized switching on adaptive voltage sources: Towards wideband semi-active damping." The Journal of the Acoustical Society of America 119: 2815.

Ballato, A. (1996). Piezoelectricity: history and new thrusts. Ultrasonics Symposium, 1996. Proceedings., 1996 IEEE, IEEE.

Banks, H. T., Smith, R., C., Wang, Y. (1996). Smart material structures: modeling, estimation and control, Wiley, New York

Bertram, V. (2011). Practical ship hydrodynamics, Access Online via Elsevier.

Blevins, R. D. (1990). "Flow-induced vibration." Van Nostrand Reinhold, New York

Burroughs, C. B., Fischer, R., W., Kern, F., R. (1997). "An introduction to statistical energy analysis." Journal of the Acoustical Society of America 101(4): 1779-1789.

Carcaterra, A. (2005). "Ensemble energy average and energy flow relationships for nonstationary vibrating systems." Journal of Sound and Vibration 288(3): 751-790.

Carlton, J. (2007). Marine propellers and propulsion, Elsevier.

Ceccio, S. L. and C. E. Brennen (1991). "Observations of the dynamics and acoustics of travelling bubble cavitation." Journal of Fluid Mechanics 233(1): 633-660.

Chellabi, A., Stepanenko, Y., Dost, S. (2009). "Direct Optimal Vibration Control of a Piezoelastic Plate." Journal of Vibration and Control 15(7): 1093-1118.

Coles, D. and A. J. Wadcock (2012). "Flying-hot-wire study of flow past an NACA 4412 airfoil at maximum lift." AIAA Journal 17(4).

Craik, R. and R. Smith (2000). "Sound transmission through double leaf lightweight partitions part I: airborne sound." Applied Acoustics 61(2): 223-245.

Crocker, M. J. (1998). Handbook of acoustics, Wiley-Interscience.

Crocker, M. J. (2007). Fundamentals of Acoustics, Noise, and Vibration. Handbook of noise and vibration control. M. J. Crocker. Hoboken, N.J., John Wiley: pp. 1-16.

Curie, J. and Curie, P., (1880). "Development by pressure of polar electricity in hemihedral crystals with inclined faces", Bull. Soc. Min. de France, 3, 90-93.

Daniel, J. I. (2001). Engineering vibration, Prentice-Hall, Inc., New Jersey.

De Langhe, K. (1996). High frequency vibrations: contributions to experimental and computational SEA parameter identification techniques. PhD Thesis, Katholieke Universiteit Leuven

Dökmeci, M. C. (1973). "Variational Principles in Piezoelectricity." Lettere Al Nuovo Cimento 7(11): 449-454.

Dökmecí, M. C. (1980). "Vibrations of piezoelectric crystals." International Journal of Engineering Science 18(3): 431-448.

Edition Solas Consolidated (2001). International Maritime Organization, London.

European Commission (2003). "Directive 2003/10/EC of the European Parliament and of the Council of 6 February 2003 on the minimum health and safety requirements regarding the exposure of workers to the risks arising from physical agents (noise)." Official Journal of the European Union 15.

European Commission (2006). "2006/87/EC Directive of the European Parliament

",from http://eurlex.europa.eu/LexUriServ/LexUriServ.do?uri=CELEX:32006L0087:EN:HTML (Last access 17th February 2014)

Fahy, F. (1982). "Statistical Energy Analysis." Noise and Vibration: 165-186. Ellis Horwood Ltd. Chichester

Fahy, F. and J. G. Walker (1998). Fundamentals of noise and vibration. London ; New York, E & FN Spon.

Fein, O. M. (2008). "A model for piezo-resistive damping of two-dimensional structures." Journal of Sound and Vibration 310(4): 865-880.

Fernandes, A. and J. Pouget (2003). "Analytical and numerical approaches to piezoelectric bimorph." International Journal of Solids and Structures 40(17): 4331-4352.

Forward, R. L. (1979). "Electronic damping of vibrations in optical structures." Applied Optics 18(5): 690-697.

Gabbert, U. and H. S. Tzou (2001). IUTAM Symposium on Smart Structures and Structronic Systems: Proceedings of the IUTAM Symposium Held in Magdeburg, Germany, 26-29 September 2000, Springer.

Gandhi, M. V. and B. Thompson (1992). Smart materials and structures,, Chapman and Hall, London

Gardonio, P. (2002). "Review of active techniques for aerospace vibro-acoustic control." Journal of Aircraft 39(2): 206-214.

Genalis, P. (1972). The Application of the Finite Element Method to Multihulled Ship Structural Analysis, DTIC Document.

Gibbs, B. and J. Tattersall (1987). "Vibrational energy transmission and mode conversion at a corner-junction of square section rods." Journal of Vibration Acoustics Stress and Reliability in Design 109: 348.

Hagood, N. W. and A. von Flotow (1991). "Damping of structural vibrations with piezoelectric materials and passive electrical networks." Journal of Sound and

Vibration 146(2): 243-268.

Han, X., Neubauer, M., Wallaschek, J. (2013). "Improved piezoelectric switch shunt damping technique using negative capacitance." Journal of Sound and Vibration 332(1): 7-16.

Harris, C. M. and A. G. Piersol (2002). Harris' shock and vibration handbook, McGraw-Hill, New York

Haun, M., J., Furman, E., Jang, S., J.,Cross, L., E,. (1989). "Thermodynamic theory of the lead zirconate-titanate solid solution system, Part V: Theoretical calculations." Ferroelectrics 99(1): 63-86.

Heckl, M. and M. Lewit (1994). "Statistical Energy Analysis as a Tool for Quantifying Sound and Vibration Transmission Paths." Philosophical Transactions of the Royal Society of London Series a-Mathematical Physical and Engineering Sciences 346(1681): 449-464.

Heywang, W., Lubitz, K.,Wersing, W. (2008). Piezoelectricity: Evolution and Future of a Technology, Springer Verlag, Berlin

Hollkamp, J. J. (1994). "Multimodal Passive Vibration Suppression with Piezoelectric Materials and Resonant Shunts." Journal of Intelligent Material Systems and Structures 5(1): 49-57.

Hrubesh, L. W. (1998). "Aerogel applications." Journal of Non-Crystalline Solids 225(1): 335-342.

Hui, S., Q. Jin-hao, J, Hong-li, Z., Kong-jun (2009). Self-powered structural vibration damping based on the self-sensing semi-passive technique. Piezoelectricity, Acoustic Waves, and Device Applications (SPAWDA) and 2009 China Symposium on Frequency Control Technology, Joint Conference of the 2009 Symposium on.

Hurlebaus, S. (2005). "Smart Structures-Fundamentals and Applications." Lecture Notes, Texas A&M University, Zachry Department of Civil Engineering.

Hurlebaus, S. and L. Gaul (2006). "Smart structure dynamics." Mechanical Systems and Signal Processing 20(2): 255-281.

Hwang, W.-S. and H. C. Park (1993). "Finite element modeling of piezoelectric sensors and actuators." AIAA journal 31(5): 930-937.

Ikeda, T. (1996). Fundamentals of piezoelectricity, Oxford ; New York , Oxford University Press.

International Maritime Organization. (2012), from http://www.imo.org/MediaCentre/pressbriefings/pages/55-msc-91-ends.aspx, (last access 17th February 2014)

International Maritime Organization, A. (1981). Resolutions and Other Decisions (resolutions 463-512): Assembly, Twelfth Session, 9-20 November 1981, IMO.

ISO (2000). ISO 2922:2000. ‗Measurement of airborne sound emitted by vessels on inland waterways and harbours'

ISO (2010). "ISO 3746:2010. ‗Determination of sound power levels of noise sources using sound pressure- Survey method using an enveloping measurement surface over a reflecting plane'. ."

Jaffe, H. and D. Berlincourt (1965). "Piezoelectric transducer materials." Proceedings of the IEEE 53(10): 1372-1386.

Janssen, J. H. and J. Buiten (1973). On acoustical designing in naval architecture. INTER-NOISE and NOISE-CON Congress and Conference Proceedings, Institute of Noise Control Engineering.

Jensen, J. (1976). CALCULATION OF STRUCTUREBORNE NOISE TRANSMISSION IN SHIPS USING THE" STATISTICAL ENERGY ANALYSIS" APPROACH, British Ship Research Association

Ji, H., Qiu, J., Badel, A., Chen, Y., Zhu, K. (2009). "Semi-active vibration control of a composite beam by adaptive synchronized switching on voltage sources based on LMS algorithm." Journal of Intelligent Material Systems and Structures 20(8): 939-947.

Jiashi, Y., Honggang, Z., Yuantai, H, Qing, J. (2005). "Performance of a Piezoelectric Harvester in Thickness--stretch Mode of a Plate." IEEE Transactions on Ultrasonics, Ferroelectrics, and Frequency Control 52(10): 1872-1876.

Johannessen, H. and K. T. Skaar (1980). Guidelines for prevention of excessive ship vibration.

Kawamura, T., Ouchi, K., Nojiri, T. (2012). "Model and full scale CFD analysis of propeller boss cap fins (PBCF)." Journal of Marine Science and Technology: 1-12.

Keane, A. J. and W. G. Price (1997). Statistical energy analysis : an overview, with applications in sturctural dynamics. Cambridge, U.K. ; New York, Cambridge University Press.

Khaligh, A., Zeng, P., Zheng., C. (2010). "Kinetic energy harvesting using piezoelectric and electromagnetic technologies—State of the art." Industrial Electronics, IEEE Transactions on 57(3): 850-860.

Kihlman, T., Plunt, J. (1976). Prediction of noise levels in ships.

Kim, S., Wang, S., Brennan, M., J. (2011). "Dynamic analysis and optimal design of a passive and an active piezo-electrical dynamic vibration absorber." Journal of Sound and Vibration 330(4): 603-614.

Kirkup, S. (1998). The boundary element method in acoustics: a development in Fortran, Stephen Kirkup.

Kong, N., Ha, D., S., Erturk, A., Inman, D.J. (2010). "Resistive impedance matching circuit for piezoelectric energy harvesting." Journal of Intelligent Material Systems and Structures 21(13): 1293-1302.

Kougoulos, E., Jones, A. G.,Wood-Kaczmar, M. (2005). "CFD Modelling of Mixing and Heat Transfer in Batch Cooling Crystallizers: Aiding the Development of a Hybrid Predictive Compartmental Model." Chemical Engineering Research and Design 83(1): 30-39.

Król, R., Brökelmann, M., Wallaschek , J. (2006). "A methodology for automatically deriving simple electromechanical equivalent models from FEM-models." Solid State Phenomena 113: 1-6.

Krylov, V. V., Porteous, E. (2010). "Wave-like aquatic propulsion of mono-hull marine vessels." Ocean Engineering 37(4): 378-386.

Kumar, N. , Singh, P. (2012). "Vibration control of curved panel using smart

damping." Mechanical Systems and Signal Processing 30: 232-247.

Lallart, M., Lefeuvre, É., Richard, C., Guyomar, D. (2008). "Self-powered circuit for broadband, multimodal piezoelectric vibration control." Sensors and Actuators A: Physical 143(2): 377-382.

Langley, R. and K. Heron (1990). "Elastic wave transmission through plate/beam junctions." Journal of Sound and Vibration 143(2): 241-253.

Langley, R., S., Smith, J., R., D. (1997). "Statistical Energy Analysis of Periodically Stiffened Damped Plate Structures." Journal of Sound and Vibration 208(3): 407-426.

Lawson, A. W. (1942). "The Vibration of Piezoelectric Plates." Physical Review 62(1-2): 71-76.

Lesieutre, G. A. (1998). "Vibration damping and control using shunted piezoelectric materials." The Shock and Vibration Digest 30(3): 187-195.

Lindstad, H., Jullumstrø, E., Sandaas, I. (2013). "Reductions in cost and greenhouse gas emissions with new bulk ship designs enabled by the Panama Canal expansion." Energy Policy 59(0): 341-349.

Loeser, H. T. (1999). Fundamentals of Ship Acoustics: Acoustical Phenomena in and Around Ship Hulls.

Lyon, R., H., DeJong, G. (1995). Theory and Appication of Statistical Energy Analysis. Boston, Butterworth-Heinemann.

Manning, J. E. (2007). Statistical Energy Analysis. Handbook of noise and vibration control. M. J. Crocker. Hoboken, N.J., John Wiley: pp. 241-267.

Mason, W. P. (1950). Piezoelectric crystals and their application to ultrasonics, Van Nostrand Reinhold.

Maurini, C., F. dell'Isola, Pouget, J. (2004). "On models of layered piezoelectric beams for passive vibration control." Journal De Physique Iv 115: 307-316.

Meitzler, Tiersten, HF, Warner, A., Berlincourt, D., Couqin, G., Welsh , F. (1988). IEEE standard on piezoelectricity, Society.

Min, J., Duffy, K., P., Provenza, A., J. (2010). Shunted piezoelectric vibration damping analysis including centrifugal loading effects. Proc., 51st AIAA/ASME/ASCE/AHS/ASC Structures, Structural Dynamics and Materials Conf.

Mindlin, R. D. (1972). "Elasticity, piezoelectricity and crystal lattice dynamics." Journal of Elasticity 2(4): 217-282.

Mylonas, D., Sayer, P. (2012). "The hydrodynamic flow around a yacht keel based on LES and DES." Ocean Engineering 46(0): 18-32.

Newnham, R. E. (2004). Properties of Materials: Anisotropy, Symmetry, Structure: Anisotropy, Symmetry, Structure, OUP Oxford.

Nguyen, C. H., Pietrzko, S., J. (2006). "FE analysis of a PZT-actuated adaptive beam with vibration damping using a parallel R–L shunt circuit." Finite Elements in Analysis and Design 42(14–15): 1231-1239.

Nilsson, A.,C. (1977). "Some acoustical properties of floating-floor constructions." The Journal of the Acoustical Society of America 61: 1533.

Nilsson, A. C. (1978). "Noise prediction and prevention in ships." SNAME, Arlington.

Nilsson, S., Tyvand, N., P. (1981). Noise Sources in Ships: I Propellers, II Diesel Engines, Nordic Cooperative Project: Structure Borne Sound in Ships from Propellers and Diesel Engines, Nordforsk, Norway.

Norton, M. P. ,Karczub ,D., G. (2003). Fundamentals of noise and vibration analysis for engineers. Cambridge, UK ; New York, NY, Cambridge University Press.

Ohayon, R., Soize, C. (1998). Structural acoustics and vibration: Mechanical models, variational formulations and discretization, Academic Pr.

Ouchi, K. ,Tamashima, M. (1900). Research and development of PBCF (propeller boss cap fin), new and practical device to enhance propeller efficiency.

Park, C. H. (2003). "Dynamics modelling of beams with shunted piezoelectric elements." Journal of Sound and Vibration 268(1): 115-129.

Park, C. H., Baz, A. (2005). "Vibration control of beams with negative capacitive shunting of interdigital electrode piezoceramics." Journal of Vibration and Control 11(3): 331-346.

Pedersen, O. J. (1973). Inter-noise 73: Proceedings, Inter-noise 73, Technical University.

Piefort, V. (2001). Finite element modelling of piezoelectric active structures, Université Libre de Bruxelles.

Pollard, J. , Dudebout,**A.** (1894). Théorie du navire, Gauthier-Villars.

Priya, S., Inman, D. J. (2008). Energy harvesting technologies, Springer.

Qiu, J., Ji, H., Zhu, K. (2009). "Semi-active vibration control using piezoelectric actuators in smart structures." Frontiers of Mechanical Engineering in China 4(3): 242-251.

Raichel D. (2006). The science and applications of acoustics, Springer.

Rakbamrung, P., M. Lallart, Guyomar, D.,Muensit, N.,Thanachayanont, C., Lucat, C., Guiffard, B., Petit, L.,Sukwisut, P.. (2010). "Performance comparison of PZT and PMN–PT piezoceramics for vibration energy harvesting using standard or nonlinear approach." Sensors and Actuators A: Physical 163(2): 493-500.

Rao, S., S. , Yap, F. F. (1995). Mechanical vibrations, Addison-Wesley New York.

Ross, D. (1976). Mechanics of underwater noise, Pergamon Press, New York, USA.

Ross, D. (1976). Mechanics of underwater noise, DTIC Document.

Sawley, R. (1969). The evaluation of a shipboard noise and vibration problem using statistical energy analysis. ASME, Symp. on Stochastic Processes in Dynamical Problems, Los Angeles.

Schmit, L. A., Farshi ,**B.** (1973). "Optimum laminate design for strength and stiffness." International Journal for Numerical Methods in Engineering 7(4): 519-536.

Schwartz, M. M. (2002). Encyclopedia of smart materials. New York, J. Wiley.

Scowcroft, G., Raposa, K. V., Knowlton, C., Johnen, J. (2006). "Discovery of

Sound in the Sea." University of Rhode Island.

Steffen, V., Inman, D., J. (1999). "Optimal design of piezoelectric materials for vibration damping in mechanical systems." Journal of intelligent material systems and structures 10(12): 945-955.

Koko, T., S., Berry, A., Masson, P.,Besslin, O.,Szabo, J., Sponagle, N. (2002). Vibration Control in Ship Structures. Encyclopedia of Smart Materials. M. M. Schwartz. New York, J. Wiley: 2 v. (xi, 1176 p.).

Taylor, G. K., Nudds, R. L.,Thomas, A., L., R. (2003). "Flying and swimming animals cruise at a Strouhal number tuned for high power efficiency." Nature 425(6959): 707-711.

Tiersten, H. F. (1963). "Thickness vibrations of piezoelectric plates." The Journal of the Acoustical Society of America 35(1): 53-58.

Turkmen, S., D. Mylonas, Khorasanchi, M. (2013). Smart Material Application on High Performance Sailing Tachts for energy Harvesting. Proc. 3rd International Conference on Innovations in High Performance Sailing Yachts, Lorient,France.

Turkmen, S., Turan, O., Zoet,P. (2012). Harvesting Vibration Energy. Glasgow, Scotland: International Conference on Advances and Challeges in Marine Noise and Vibration.

Tzou, H. S. (1993). "Piezoelectric shells- Distributed sensing and control of continua." Dordrecht, Netherlands: Kluwer Academic Publishers(Solid Mechanics and Its Applications. 19.

Vepa, R. (2010). Dynamics of Smart Structures, Wiley.

Vorus, W. S. (2010). Principles of Naval Architecture Vol II: Vibration, SNAME.

Wadhawan, V. K. (2007). Smart structures : blurring the distinction between the living and the nonliving, Oxford ; New York : Oxford University Press.

Wenz, G. (1962). "Acoustic ambient noise in the ocean: spectra and sources." The Journal of the Acoustical Society of America 34: 1936.

Werner, S. (2006). Computational hydrodynamics applied to an America's Cup class

keel-best practice and validation of methods, Chalmers University of Technology.

Werner, S., A. Pistidda, Larsson, L., Regnstrom, B. (2007). "Computational fluid dynamics validation for a fin/bulb/winglet keel configuration." Journal of Ship Research 51(4): 343-356.

Xie, J., Yang, J., Hu, H., Hu, Y., Chen, X. (2012). "A piezoelectric energy harvester based on flow-induced flexural vibration of a circular cylinder." Journal of Intelligent Material Systems and Structures 23(2): 135-139.

Yang, J. (2006). Analysis of piezoelectric devices, World Scientific.

Zienkiewicz, O. C., Taylor, R. L., Zhu, J.Z. (2005). The finite element method: its basis and fundamentals, Butterworth-Heinemann.

Zoet, P., J. Hallander, et al. (2012). DESIGNING SHIPS for LOW VIBRATIONS:A CASE STUDY. Glasgow, Scotland: International Conference on Advances and Challeges in Marine Noise and Vibration.

Zoet, P. (2012) SILENV FP7 - Collaborative Project WP 4: Measurements & Requirements Sub-Task 4.2.2.: Comparison performances versus requirements D 4.7.

Appendix A

A.1 Introduction to Statistical Energy Analysis

Statistical energy analysis (SEA) was developed by Lyon, Smith and Maidinik in 1959 to predict the structure responses (in mean square velocities) of thin space-craft and aircraft, which were excited by sources such as jet noise, turbulent boundary layer, etc.

The complex systems have a number of modes. That causes an increase of the degrees of freedom, which makes calculation using numerical tools (FEM) at middle-frequency and high-frequency range difficult. SEA is a successful tool to predict vibration and sound pressure in complex structures, such as space vehicles, airplanes, buildings, large machines and ships. SEA employs linear energy balance equations to calculate loss factors, coupling loss factors, energy flows and sound power. One main advantage of SEA is that it usually leads to a substantial reduction of the number of degrees of freedom. “The price to pay is that results are only given in terms of average and variance over frequency and space” (Burroughs, Fischer et al. 1997) . Time-average powers are used as inputs rather than external forces or displacements (Keane and Price 1997) .

A.2 Methodology of Statistical Energy Analysis

Lyon et al. (1959) found that if there is an energy difference between the subsystems power will flow from higher to lower modal energy. The power flow is proportional to the difference in the actual kinetic energy, potential energy or total energy (Richard H. Lyon 1995). The function below presents the power balance equation of two coupled subsystems:

$$w\eta_1 E_1 + \sum_1 w\eta_{12}\,\eta_1 \left(\frac{E_1}{n_1} - \frac{E_2}{n_2}\right) = P_{in,1} \qquad \text{A-1}$$

where E_1 and E_2 are time-averaged energy, ω is the harmonic vibration frequency, $P_{in,1}$ is the external power input, η_1 is the subsystem loss factor, n_1 is the modal density (the number of natural frequencies in a frequency band), $\frac{E_1}{n_1}$ is the measure of the energy per mode, η_{12} is the coupling loss factor, which is a very important parameter to define power loss between subsystems (Figure A.1).

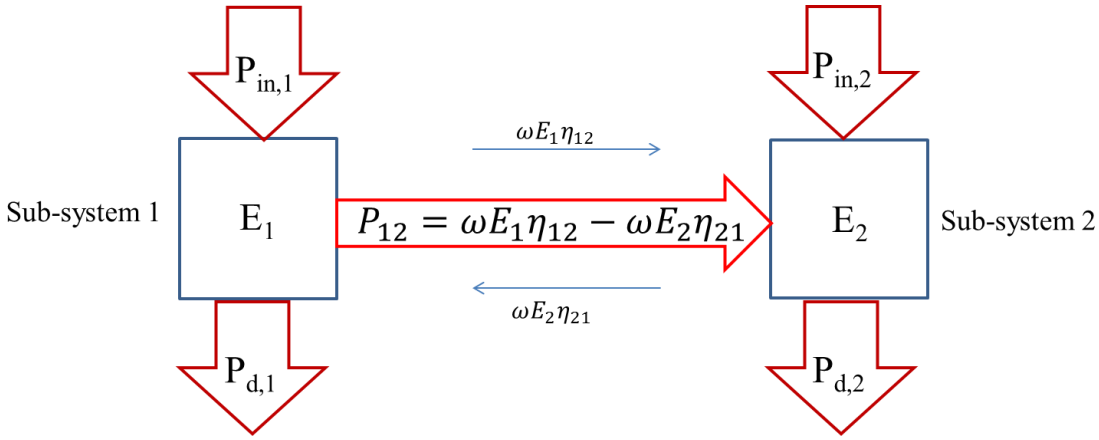

Figure A.1: A Two Subsystem SEA Model

Figure A.2 shows a coupled system with the power flows for each resonance mode. Power flows between a subsystem through dissipation or transmission to another subsystem. A schematic SEA model is shown in Figure A.2.

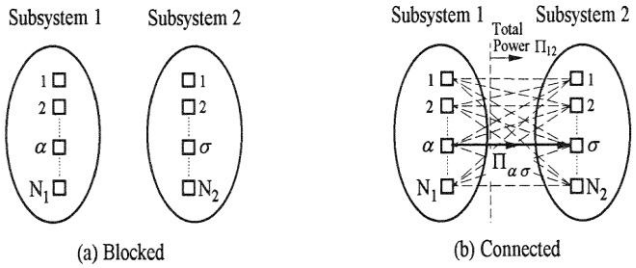

Figure A.2: Illustration of Modal Coupling in Connected Subsystems a) Individual Modal Groups with Subsystems Blocked; b) Interactions of Mode pairs with Subsystems Connected at the Junction (Lyon 1995)

A.3 Sound Measurement

SEA is not able to predict sound level without given parameters such as acoustic power of source sound level, coupling loss factors and transmission coefficients. These parameters should be estimated or measured to complete the power balance equation before any calculation. Estimation of coupling loss factors and transmission coefficients is generally possible by using theoretical approaches given below. However prediction of source power level is not always possible. Therefore measurements are necessary. Pressure measurement can be used to define the source power level as power is function of pressure.

Pressure can be either above atmospheric (ambient) pressure or below it in the domain. Figure A.3 illustrates this fluctuation in a sinusoidal form of time dependence pressure. The atmospheric pressure is denoted as p_o. The increase or decrease in pressure is called acoustic pressure fluctuation p.

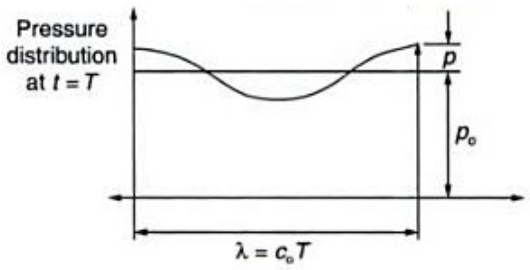

Figure A.3: The acoustic pressure fluctuation

However, most of the system vibrates irregularly, which causes a random displacement from its equilibrium position. For that reason, the magnitude pressure fluctuations are given as mean square value defined by the time average. The averaging time *T* must be large enough to cover a wide frequency band (Fahy and Walker 1998).

$$\overline{p}^2 = \lim_{T\to\infty}\left(\frac{1}{T}\right)\int_{-T/2}^{T/2} p^2(t)dt \qquad \text{A-2}$$

The human sensitivity of noise shows an approximate logarithmic behaviour. Human ears sense the relative loudness of two sounds as roughly the ratio of mean square sound pressures. Thus, the quantity used for the measurement of the sound pressure is the sound pressure level (SPL) defined by

$$Lp = 10\log_{10}\frac{\overline{P^2(t)}}{P_{ref}^2} = 20\log_{10}\frac{P_{rms}}{P_{ref}} \qquad \text{A-3}$$

where P_{rms} *is* the square root of the mean square pressure, P_{ref} is a reference pressure of 20 µPa. P_{ref} corresponds to the root mean square (rms) pressure of a pure tone at 1 kHz, which is just audible to the average young human.

Knowing SPL provides representations of the energy (L_E) in dB. This enables energy calculation of the subsystem:

$$L_E = 10\log_{10}\frac{E}{E_{ref}} \qquad \text{A-4}$$

where E_{ref} is a reference for energy is 10^{-12} joules (or watt-second). The band energy of 0.1 joule, therefore, would correspond to a band energy level of 110dB

$$L_E = 110\ dB$$

The relation between vibratory energy and the space-time mean square velocity of the structure or sound field is

$$E = M < v^2 >= M v_{rms}^2 \qquad \text{A-5}$$

where M is the structural mass in kilograms, v is the speed.

The form of the velocity spectrum also determines the form of the strain and stress spectra. Table A-1 shows the relations between dynamical variables and levels.

Table A-1: Relation between dynamical variables and levels (Richard H. Lyon 1995)

Variable	Relation	Level	Formula	Referance
Energy E	1	$L_E = 10\,log\frac{E}{E_{ref}}$	$L_E = 10\,log\,E + 120$	$E_{ref} = 10^{-12}$
Velocity v	$< v^2 >= \frac{E}{M}$	$L_v = 10\,log\frac{< v^2 >}{v^2{}_{ref}}$	$L_v = L_E - log\,M - 120$	$v_{ref} = 1\frac{m}{sec}$
Displacement d	$< d^2 >= \frac{E}{M}$	$L_d = 10\,log\frac{< d^2 >}{d^2{}_{ref}}$	$L_d = L_v - 20\,log\,f - 16$	$d_{ref} = 1mm$
Acceleration a	$< a^2 >= w^2 < v^2 >$	$L_a = 10\,log\frac{< a^2 >}{a^2{}_{ref}}$	$L_a = L_v - 20\,log\,f - 4$	$a_{ref} = 1\frac{m}{sec^2}$
Strain e	$< e^2 >= \frac{k < v^2 >}{c_l^2}$	$L_e = 10\,log\frac{< e^2 >}{e^2{}_{ref}}$	$L_e = L_v - 20\,log\,c_l - 120$	$e_{ref} = 10^{-12}$
Stress T	$< T^2 >= Y^2 < e^2 >$	$L_T = 10\,log\frac{< T^2 >}{T^2{}_{ref}}$	$L_T = L_v + 20\,log\,\rho c_l$	$T_{ref} = 10^6\frac{N}{m^2}$

where Y is the young's modulus in newton/m^2; c_l is the longitudinal wave speed in m/sec; M is the mass in kg; w is the radian frequency; f is the cyclic frequency in Hz; k is the constant of order unity; ρ is the mass density in kg/m^3. These relations allow generating average (mean space-time square) response of the system if the average energy of vibration or any of the other variables are known.

A.4 Coupling Loss Factor (CLF)

Coupling loss factor (CLF) is one of the key parameters in the SEA modelling. The CLF is used to calculate the sound pressure level or surface velocity of each subsystem in a structure (Craik 1982). The CLF is dependent on geometrical details of the connection of systems and different wave types, which can be generated in structures and at connections.

There are several ways to present the CLF such as numerical, theoretical and experimental. If the systems are connected at one or more points it is easier to calculate the coupling loss factor. Table A-2 shows CLF expressions used for all calculations (Craik and Smith 2000).

Table A-2: Coupling Loss Factor expressions used for all calculations

Description	**CLF**
Plate to room/cavity	$\eta_{1,2} = \frac{\rho_0 c_0 \sigma_1}{2\pi f \rho_{s1}}$
Room to plate	$\eta_{1,2} = \frac{\rho_0 c_0^2 S_2 \sigma_1}{8\pi V_1 \rho_{s1} f^3}$
Cavity to plate	$\eta_{1,2} = \frac{\rho_0 c_0 f_{c2} \sigma_1}{4\pi V_1 \rho_{s2}}$
Room to room/cavity (non-resonant)	$\eta_{1,2} = \frac{c_0 S \tau_{12}}{8\pi V_1 f}$
Cavity to room	$\eta_{1,2} = \frac{\tau_{12}}{4\pi}$
Plate to plate (line)	$\eta_{1,2} = \frac{1}{\pi(\sqrt{3}\pi)^{0.5}} \left(\frac{h_1 c_{L1}}{f}\right)^{0.5} \frac{L_{12}}{S_1} \gamma_{12}$
Structure to structure (point)	$\eta_{1,2} = \frac{Re(Y_2)}{2\pi f \lvert Y_1 + Y_2 \rvert^2}$

In Table A-2 ρ_0 is the density of air, ρ_s is the surface density of a plate, m is the total subsystem mass, c_0 is the wave-speed in air, c_L is the longitudinal wave-speed of a structure, f_c is the critical coincidence frequency of a plate, Y is the structural mobility, h is the thickness, S is the surface area, V is the volume, σ is the radiation efficiency, τ is the non-resonant room to room transmission coefficient, γ is the structure transmission coefficient.

Two systems can be coupled along a line (for two dimensional systems) or along a surface (for three dimensional systems). If the dimensions of the line (or surface) are large compared to the length of a free wave in the system, a set of waves will be incident power called the transmission coefficient τ. The transmission coefficient will depend on the direction of the incident waves travelling with respect to the joining line or surface. A schematic of two subsystems coupled along an edge is shown in Figure A.4.

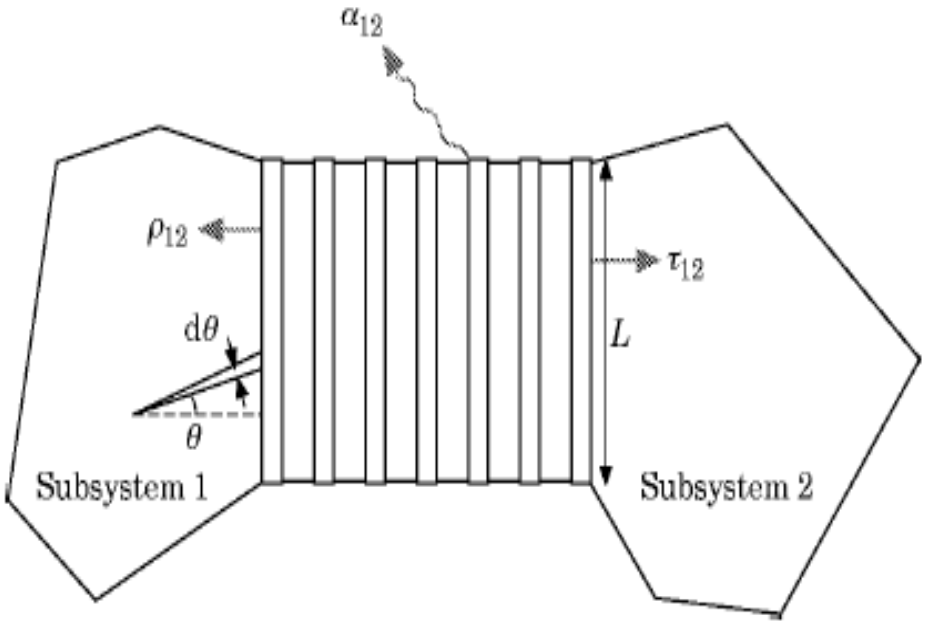

Figure A.4: A schematic of two-subsystems SEA Model (Langley et al. 1997)

A.5 Transmission Coefficients

Sabine (1922) introduced the reverberation time of sound and absorption coefficient (α) namely the ratio between the non-reflected sound intensity and the incident sound intensity with the help of experiments. The reflection coefficient (ρ) is defined as the ratio between the reflected and the incident sound intensity. Their relationship is:

$$\alpha + \rho = 1 \qquad \text{A-6}$$

Part of sound energy is transformed into thermal and heat energy called dissipation. However, sound absorption cannot be explained with only the energy transforming into heat. A large part of the energy may be transmitted through walls or through the boundary of the system and may also radiate to other system. Thus, the absorption coefficient can be given as two components, which are the dissipation coefficient (δ) and transmission coefficient (τ) (Cremer, Müller et al. 1984):

$$\alpha = \delta + \tau \qquad \text{A-7}$$

Noise transmission through a structure occurs generally in the high-frequency range of structural vibration and the characteristic wavelength is small compared to the overall dimension of the structure (Langley and Heron 1990). Conventional methods of structural analysis (FEM) can require high calculation time and computation power because of the large number of degrees of the freedom (Zienkiewicz and Taylor 2006). Relations between transmission coefficients and corresponding coupling loss factors have been derived for some common structural connections such as beam-beam, beam-plate and plate-plate couplings. Many authors have considered the transmission coefficient right angled L, T and X plated junctions (Craven and Gibbs 1981; Gibbs and Craven 1981; Whitney and Ashton 1987; Langley and Heron 1990; Richard H. Lyon 1995).

Langley and Heron (1990) presented an approach that considers the vibrations of the structure in terms of elastic waves, which propagate through the structure and are

partially reflected and transmitted at structural discontinuities. This process of reflection and transmission has been referred to as the attenuation of the structure, such as plate junctions or plate/stiffener connections.

Cremer et al. (1984) explained the power loss and transmission coefficient between coupled systems. In their applications it is assumed that all geometrical sound reflections occur without any loss of energy. But the properties of boundary materials govern energy loss and phase changes upon reflection from the boundaries. Therefore those material properties may have a more profound effect on the Statistical Room Acoustics. Considering acoustic problems would be incomplete without energy loss and phase shifts taken into account.

A.6 Defending Transmission Coefficient

Transmission Coefficient can be found with an approach, which be used to model adjacent plates and their junction (stiffener) as three subsystems. Figure A.5 demonstrates two plates with the junction and the power transmission. In the figure $\tau(\Omega)$ is the transmission coefficient, I_o is the acoustic intensity, $I_o\tau(\Omega)$ is intensity transmitted by plate and Ω is the incident waves direction. That will allow for the three types of wave motion which can occur in a flat plate. With this approach, the stiffener act as coupling elements between the SEA subsystems. The coupling loss factors can be found by considering wave transmission across the stiffener.

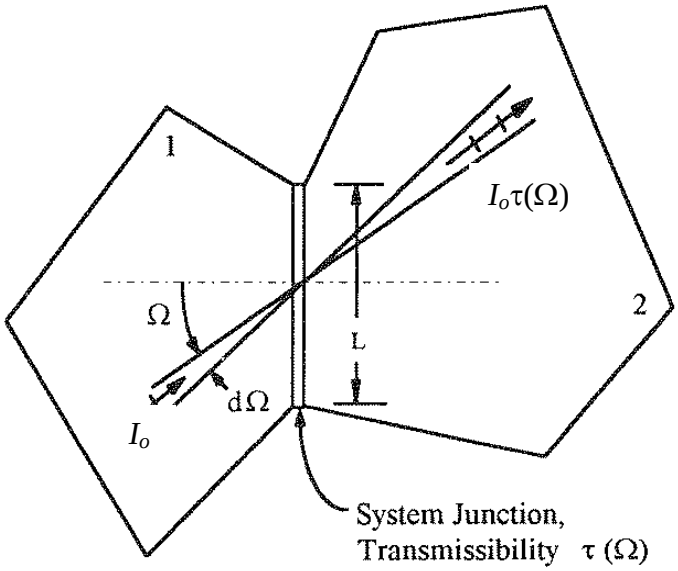

Figure A.5: Sketch showing transmission of power between two systems through a line junction (Lyon 1995)

As it is shown in Figure A.5 the transmission coefficient $\tau(\Omega)$ is presented as a function of the incident waves direction as the coefficient depends on the incident waves, which are moving along the junction.

Langley and Heron (1990) used this approach to calculate transmission coefficient and coupling loss factor. The governor equations and applications are explained next subchapter.

A.7 Plate to Plate High Frequency Wave Energy Transmission

The calculations is based on the wave approach and concern plate to beam junction. The junction behaves as a beam element. Three types of waves (bending,longitudinal,and shear) will be included. Figure A.6 shows displacement and traction coordinates of plate used in mathematical definition.

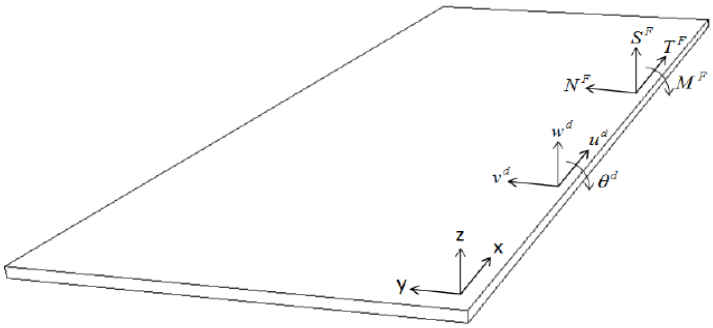

Figure A.6: Displacement and Traction coordinates of plate (Langley et al. 1990)

The incident wave is mathematically defined as $exp^{(-ikx+i\mu y+iwt),}$ which depended on time and space and the wave definition at the junction implies that the response in all the plates must have the dependency $exp^{(-ikx+i\mu y)}$, leaving dependency on y to be determined from the plane equations of motion. x and y are the space coordinates and k and μ are corresponding wave numbers, *w* is angular frequency and t is the time. The wave numbers of the plate J for three different types of waves can be calculated as:

Bending waves $$k_B = \left(\frac{\rho_j w^2}{B_j}\right)^{0.25}$$ A-8

Longitudinal waves $$k_L^2 = \frac{\rho_j w^2(1-v_j^2)}{E_{y,j}h_j}$$ A-9

Shear waves $$k_S^2 = \frac{2\rho_j w^2(1+v_j)}{E_{y,j}h_j}$$ A-8

where ρ_j is the mass per unit area, B_j is the bending stiffness, $E_{y,j}$ is the Young's modulus, h_j is the height of the plate and v_j is Poisson's ratio. The response of the plate is assumed to have a y dependency of $e^{\mu y}$. These implements that μ must satisfy the equations for three types of wave:

Bending waves $$\mu_B^2 = k^2 \pm k_B^2$$ A-9

Longitudinal waves $$\mu_L^2 = k^2 - k_L^2$$ A-10

Shear waves $$\mu_S^2 = k^2 - k_S^2$$ A-13

The relationship between the edge displacement b_j and the tractions F_j can be :

$$F_j = K_j b_j \qquad \text{A-14}$$

Where, K_j is the dynamic stiffness matrix. The matrix of the equation is :

$$\begin{bmatrix} T_j^F \\ N_j^F \\ S_j^F \\ M_j^F \end{bmatrix} = \begin{bmatrix} \alpha_{11} & \alpha_{12} & 0 & 0 \\ \alpha_{21} & \alpha_{22} & 0 & 0 \\ 0 & 0 & \alpha_{33} & \alpha_{34} \\ 0 & 0 & \alpha_{43} & \alpha_{44} \end{bmatrix} * \begin{bmatrix} u_{ej}^d \\ v_{ej}^d \\ w_{ej}^d \\ \theta_{ej}^d \end{bmatrix} \qquad \text{A-15}$$

$T_j^F, N_j^F, S_j^F, M_j^F$ are traction forces coordinates and $u_{ej}^d, v_{ej}^d, w_{ej}^d, \theta_{ej}^d$ are displacement coordinates.

This equation is not valid if the plane wave which is incident on the junction is carried by plane j. In case *Fj* must be replaced by F_j-F'_j and b_j by b_j-b'_j where F'_j and b'_j are the traction caused by the incident wave and the edge displacements.
In case an incident bending wave with an angle ∅ is approaching below is the matrix of the tractions where F'_j and b'_j are given:

$$\boldsymbol{F}'_j = \begin{bmatrix} T_j^{F\prime} \\ N_j^{F\prime} \\ S_j^{F\prime} \\ M_j^{F\prime} \end{bmatrix} = \begin{bmatrix} 0 \\ 0 \\ -\alpha B_j(\mu^3 - (2-\vartheta_j)k^2\mu) \\ \alpha B_j(\mu^2 - \vartheta_j k^2) \end{bmatrix} \qquad \text{A-16}$$

$$\boldsymbol{b}'_j = \begin{bmatrix} u_{ej}^{d\prime} \\ v_{ej}^{d\prime} \\ w_{ej}^{d\prime} \\ \theta_{ej}^{d\prime} \end{bmatrix} = \begin{bmatrix} 0 \\ 0 \\ \alpha \\ \alpha\mu \end{bmatrix} \qquad \text{A-17}$$

where α is the wave amplitude. For a longitudinal wave the corresponding results are:

A-18

$$\boldsymbol{F}_j' = \begin{bmatrix} T_j^{F\prime} \\ N_j^{F\prime} \\ S_j^{F\prime} \\ M_j^{F\prime} \end{bmatrix} = \begin{bmatrix} \alpha E_{y,j} h_j k\mu/(1+\vartheta_j) \\ i\alpha E_{y,j} h_j(\mu^2 - \vartheta_j k^2)/(1-\vartheta_j^2) \\ 0 \\ 0 \end{bmatrix}$$

A-19

$$\boldsymbol{b}_j' = \begin{bmatrix} u_{ej}^{d\prime} \\ v_{ej}^{d\prime} \\ w_{ej}^{d\prime} \\ \theta_{ej}^{d\prime} \end{bmatrix} = \begin{bmatrix} \alpha k \\ i\alpha\mu \\ 0 \\ 0 \end{bmatrix}$$

And for a shear wave the edge displacements and tractions are :

A-20

$$\boldsymbol{F}_j' = \begin{bmatrix} T_j^{F\prime} \\ N_j^{F\prime} \\ S_j^{F\prime} \\ M_j^{F\prime} \end{bmatrix} = \begin{bmatrix} i\alpha E_{y,j} h_j(\mu^2 + k^2)/2(1+\vartheta_j) \\ -\alpha E_{y,j} h_j k\mu/(1+\vartheta_j) \\ 0 \\ 0 \end{bmatrix}$$

A-11

$$\boldsymbol{b}_j' = \begin{bmatrix} u_{ej}^{d\prime} \\ v_{ej}^{d\prime} \\ w_{ej}^{d\prime} \\ \theta_{ej}^{d\prime} \end{bmatrix} = \begin{bmatrix} i\alpha\mu \\ -\alpha k \\ 0 \\ 0 \end{bmatrix}$$

Calculate the wave amplitudes in each plate from the edge displacements of that plate.

A-12

$$\alpha = \frac{k}{b_j'}$$

The corresponding power of the wave amplitude for the different types of waves can be calculated as:

A-23

$$P_B = \frac{\rho_j \omega^3 a^2}{k_B} \sin\phi$$

A-24

$$P_L = \frac{\rho_j \omega^3 a^2 k_L}{2} \sin\phi$$

A-25

$$P_B = \frac{\rho_j \omega^3 a^2 k_S}{2} \sin\phi$$

The transmission coefficient may be calculated by taking the ratio of the transmitted power to the total power which is incident on the junction.

The magnitude of the power transmitted by each propagating wave may be calculated from those equations by using the appropriate amplitude α and the transmitted wave (angle) heading:

$$\phi_r = \frac{k}{k_r} \quad \text{A-26}$$

where k_r is the relevant wave number and k is the wave number of the incident. The transmission coefficient can be calculated by taking the ratio of the transmitted power to the total power.

The transmission coefficients for the junction can be written as the form $\tau_{pr}^{ij}(\omega, \phi)$. Here i, p, ω and ϕ present the carrier plane, wave type, frequency and heading of incident wave, and j and r present the carrier plate and wave type of a generated wave.

The coupling loss factors that are used in SEA can be related to transmission coefficients:

$$\eta_{pr}^{ij} = \frac{c_{pi} L \tau_{pr}^{ij}(\omega)}{\pi \omega A_i} \quad \text{A-27}$$

$$\tau_{pr}^{ij}(\omega) = \frac{1}{2} \int_0^{\pi} \tau_{pr}^{ij}(\omega, \phi) sin\phi d\phi \quad \text{A-28}$$

Appendix B

Thermodynamic Consideration

The first law of thermodynamics (Conservation) is "energy cannot be created or destroyed however energy can be changed type". There exists for every thermodynamic system in equilibrium an extensive scalar property called the entropy (σ), such that in an infinitesimal reversible change of state of the system,

$$\boldsymbol{\sigma = \frac{\partial Q}{\partial \Theta}} \qquad \text{B-1}$$

Where θ is the absolute temperature and Q is the total of heat received by the system. The second law of thermodynamics is "the entropy of a thermally insulated system cannot decrease and is constant if and only if all processes are reversible". Thus, the reversible energy change (dU) in the internal energy U of an elastic dielectric which is affected by a small strain (S), electric displacement (D) (Budimir, Damjanovic et al. 2005).

The energy equations can be derived from Gibbs free energy thermodynamic function G(θ,T,E) per unit volume. This gives:

$$G = U - \Theta\sigma - T_{ij}S_{ij} - E_n D_n \qquad \text{B-2}$$

Here, U is the internal energy per unit volume. The differential form is :

$$dG = -\sigma d\Theta - S_{ij}dT_{ij} - D_n dE_n \qquad \text{B-13}$$

Gibbs potential is found when temperature, stress, and electric field are taken individually. It is obtained by:

$$\sigma = -\left[\frac{\partial G}{\partial \Theta}\right]_{T,E}, S_{ij} = -\left[\frac{\partial G}{\partial T_{ij}}\right]_{\Theta,E}, D_n = -\left[\frac{\partial G}{\partial E_n}\right]_{\Theta,T} \quad \text{B-14}$$

Gibbs free-energy thermodynamic expansion is employed to generate t*he* constitutive linear piezoelectric equations. These equations are used when the function G is differentiated:

$$S_{ij} = {\alpha_{ij}}^{E}\Delta\Theta + {s_{ijkl}}^{E}\Delta T_{kl} + d_{mij}\Delta E_m \quad \text{B-15}$$

$$D_n = {p_n}^{T}\Delta\Theta + d_{nkl}\Delta T_{kl} + {\varepsilon_{mn}}^{T}\Delta E_m \quad \text{B-6}$$

The coupling constants in these equations $\alpha_{ij}{}^{E}$ is the thermal expansion coefficient matrix, ${s_{ijkl}}^{E}$ is elastic compliance matrix at constant electric field, d_{nkl} is piezoelectric constant matrix, ${p_n}^{T}$ is pyroelectric coefficient matrix, and ${\varepsilon_{mn}}^{T}$ is permittivity matrix at constant stress.

Note that the piezoelectric constitutive equations are given in matrix form using Voigt's notation (*i*,*j*,*k*,*l*=1,2,3,4,5,6 and *m*,*n*=1,2,3) and Einstein's summation convention of repeated subscripts.

Appendix C

C.1 ANSYS® APDL CODES

APDL is an abbreviation of ANSYS Parametric Design Language. This is a scripting language to model the engineering problem and the script file is run with ANSYS.

Electromechanical coupling and electrical circuit are numerically modelled partially or fully by utilizing ANSYS APDL CODE. Hereby, the codes are given.

C.2 Piezoelectric material properties

/com PZT-5H Z-polarized
/PREP7
/com Stiffness
TB, ANEL, 8, 1, 0

TBDATA ,1, 1.2720E+11, 8.0212E+10, 8.4670E+10

TBDATA, 7 ,1.2720E+11, 8.4670E+10

TBDATA ,12 ,1.1744E+11

TBDATA, 16, 2.3496E+10

TBDATA ,19 ,2.2989E+10

TBDATA,21 ,2.2989E+10

```
/com Piezo

TB ,PIEZ, 8

TBDATA ,3, -6.6228

TBDATA, 6, -6.6228

TBDATA ,9, 23.2403

TBDATA ,14 ,17.0345

TBDATA ,16, 17.0345

/com Permittivity

EMUNIT,EPZRO,8.85E-12

MP,PERX,8,1704

MP, PERY,8,1704

MP,PERZ,8,1433

/comDensity

MP,DENS,8,7500
```

C.3 Static analysis code for the PZT attached aluminium beam

```
! Piezoelectric Shunt Resistance Inductor Parallel Circuit to

! mitigate Simple Beam Vibration by Serkan Turkmen

/VIEW,1,1,1,1

/VUP,,Z

/PREP7
```

EMUNIT,EPZRO,8.85E-12 !command for information on free-space ! permittivity (F/m)

ET,1,solid5 ! 8-node solid with all DOF, used for

! piezoelectric material

ET,2,solid45 ! 8-node solid with UX,UY,UZ DOF,

! used for aluminum beam

MP,DENS,1,7730 ! Density of piezoelectric material kg/m3

MP,PERX,1,1700 ! Permittivity of piezoelectric material epl

MP,PERY,1,1700

MP,PERZ,1,1470

! Piezoelectric "e" matrix of piezoelectric material (c/m2)

TB,PIEZ,1

TBDATA,3,-6.5 !e31

TBDATA,6,-6.5 !e32

TBDATA,9,23.3 !e33

TBDATA,14,17.0 !e24

TBDATA,16,17.0 !e15

! Stiffness "c" matrix of piezoelectric material

TB,ANEL,1

TBDATA,1,12.6E10,7.95E10,8.41E10

TBDATA,7,12.6E10,8.41E10

TBDATA,12,11.7E10

TBDATA,16,2.3E10

TBDATA,19,2.3E10

TBDATA,21,2.325E10

MP,EX,2,7.1E10 ! Modulus of Elasticity of aluminium

MP,NUXY,2,.33 ! Poisson's ratio of aluminium

MP,DENS,2,2700 ! Density of aluminium

!

BTHK= 0.8E-3 ! Beam thickness

CVTHK= 2.6E-4 ! Piezoelectric material covering thickness

DEPTH= 2.54E-2 ! Depth of assembly

BLNGTH= 20E-2 ! Beam length

CVLNGTH=4.5E-2 ! Length of covering

BLOCK,,CVLNGTH,,DEPTH,,BTHK ! Defines covered beam volume

BLOCK,CVLNGTH,BLNGTH,,DEPTH,,BTHK ! Defines uncovered beam volume

BLOCK,-.1E-2,,,DEPTH,,BTHK

VATT,2,,2 ! Associates material 2 and type 2 with beam volume

BLOCK,,CVLNGTH,,DEPTH,BTHK,BTHK+CVTHK ! Defines piezoelectric material cover

BLOCK,,CVLNGTH,,DEPTH,0,-CVTHK

ESIZE,BLNGTH/30 ! Defines default element size

```
NUMMRG,KP ! Merges duplicate solid model entities

numstr,node,14 ! Set starting node number for the solid model

VMESH,ALL ! Generates nodes and elements within the volumes

!

NSEL,S,LOC,Z, BTHK

NSEL,R,LOC,X,,CVLNGTH

CP,1,VOLT,ALL ! Couples volt DOF at beam interface

CM,INTRFC,NODE ! Creates a component for the interface (Face to beam)

*GET,BOT_ELECTRODE,NODE,,NUM,MIN

NSEL,S,LOC,Z,BTHK+CVTHK

NSEL,R,LOC,X,,CVLNGTH

CP,2,VOLT,ALL ! Couples volt DOF at piezoelectric material outer surface

CM,OUTSIDE,NODE ! Creates a component for the outer surface

*GET,TOP_ELECTRODE,NODE,,NUM,MIN


NSEL,S,LOC,Z, 0

NSEL,R,LOC,X,,CVLNGTH

CP,3,VOLT,ALL ! Couples volt DOF at beam interface

CM,INTRFC2,NODE ! Creates a component for the interface (Face to beam)

*GET,BOT_ELECTRODE2,NODE,,NUM,MIN

NSEL,S,LOC,Z,-CVTHK
```

```
NSEL,R,LOC,X,,CVLNGTH

CP,4,VOLT,ALL ! Couples volt DOF at piezoelectric material outer surface

CM,OUTSIDE2,NODE ! Creates a component for the outer surface

*GET,TOP_ELECTRODE2,NODE,,NUM,MIN


/solu

antype,static          ! Static analysis

F,FORCENODE,FZ,0.1 ! Applying force


D,BOT_ELECTRODE,VOLT,0.0          ! Ground bottom electrodes

D,BOT_ELECTRODE,VOLT,0.0

DDELE,TOP_ELECTRODE,VOLT ! for open circuit condition

DDELE,TOP_ELECTRODE2,VOLT ! for open circuit condition

! Or

!D,TOP_ELECTRODE,VOLT,1.0 ! Apply unit voltage to top electrodes

!D,TOP_ELECTRODE2,VOLT,1.0

solve*get,Cs_PZT,node,TOP_ELECTRODE,rf,amps ! Get electric charge on top
!electrode

*get,Cs_PZT2,node,TOP_ELECTRODE2,rf,amps

Cs_PZT1 = abs(Cs_PZT)! C = Q/V, where V = 1 Volt

Cs_PZT2 = abs(Cs_PZT2) ! C = Q/V, where V = 1 Volt

/com, ------------------------------------------------------------------
```

```
/com,   Equivalent parameters of the piezoelement
/com,
/com, Static capacitance Cs_PZT1 = %Cs_PZT1% F
/com, Static capacitance Cs_PZT2 = %Cs_PZT2% F
Fini
```

C.4 Modal analysis code for the PZT attached aluminium beam

```
/SOLU
ANTYPE,MODAL ! Modal analysis
nmodes = 20
modopt,LANB,nmodes ! Block Lanczos solver
mxpand,nmodes,,,yes ! Calculate element results and
! reaction forces
TOTAL,30,1 ! Requests automatic generation of
! (structural) DOF
D,BOT_ELECTRODE,VOLT,0.0
D,TOP_ELECTRODE,VOLT,0.0 ! Add boundary condition will change
D,BOT_ELECTRODE2,VOLT,0.0
D,TOP_ELECTRODE2,VOLT,0.0 ! Add boundary condition will change
!DDELE,TOP_ELECTRODE,VOLT ! for open circuit condition
```

```
!DDELE,TOP_ELECTRODE2,VOLT ! for open circuit condition
! the modal frequency
TOTAL,30,1 ! Requests automatic generation of
! (structural) DOF
SOLVE
FINISH
!-----------------------------------------
/post1
*dim,C,array,nmodes     ! Define arrays to store equivalent parameters
*dim,L,array,nmodes
PI2 = 2*3.14159
Co = Cs_PZT1
SET,,, ,,, ,7
/com,
*do,i,7,nmodes
*get,Fi,mode,i,freq      ! Get frequency
 *get,Qi,node,TOP_ELECTRODE,rf,amps   ! ! Get electric charge on top electrode
Omi = Pi2*Fi          ! Convert linear frequency to angular
C(i) = (Qi/Omi)**2       ! Calculate equivalent dynamic capacitance
Co = Co - C(i)         ! Adjust static capacitance for dynamic terms
L(i) = 1/(Omi**2*C(i))     ! Calculate equivalent dynamic inductance
```

```
*if,i,eq,7,then        ! Get seventh mode frequency for
! harmonic analysis, Here inductance is also defined.
F7 = Fi $ Om7 = Omi
*endif
/com, Mode %i%
/com, Resonant frequency  F = %Fi% Hz
/com, Dynamic capacitance C = %C(i)% F
/com, Dynamic inductance  L = %L(i)% H
/com,
set,next
*enddo
/com, Adjusted static capacitance Co = %Co% F
/com, ------------------------------------------------------------------
fini
```

C.5 Harmonic analysis code for the PZT attached aluminium beam

```
/PREP7
! The calculation should continue from the previous code
ET,3,CIRCU94,1,0 ! Set up the inductor
R,1,L(i)
RMOD,1,15,0,0 ! Subscript of inductor is 0, i.e. L0
```

```
TYPE,3 $ REAL,1
E,TOP_ELECTRODE,BOT_ELECTRODE ! Parallel the inductor to the
 ! electrodes of PZT
E,TOP_ELECTRODE2,BOT_ELECTRODE2 ! Parallel the inductor to the
 ! electrodes of PZT


ET,4,CIRCU94,0,0 ! Set up the resistor
R,2,R(i)
RMOD,2,15,0,0 ! Subscript of resistor is 0, i.e. R0
TYPE,4 $ REAL,2
E,TOP_ELECTRODE,BOT_ELECTRODE ! Parallel the resistor to the
! electrodes of PZT
E,TOP_ELECTRODE2,BOT_ELECTRODE2 ! Parallel the resistor to the
! electrodes of PZT
NSEL,ALL
FORCENODE = node(0,DEPTH/2,0) ! Node where force applied
DISPNODE = node(BLNGTH,DEPTH/2,BTHK) ! Node where deflection detected
FINISH
/SOLU
ANTYPE,HARM ! Harmonic analysis
HARFRQ,0,1000, ! Frequency range of analysis
```

```
NSUBST,500, ! Number of frequency steps

KBC,0 ! Impulse loads

F,FORCENODE,FZ,0.01 ! Applying force 0.01N

D,BOT_ELECTRODE,VOLT,0.0 ! Assigns zero voltage to bottom electrode

D,BOT_ELECTRODE2,VOLT,0.0 ! Assigns zero voltage to bottom electrode

DDELE,TOP_ELECTRODE,VOLT

DDELE,TOP_ELECTRODE2,VOLT

CNVTOL,F,,,,1E-5 ! Small convergence value for force

CNVTOL,VOLT ! Default convergence value for current flow

!NSEL,S,LOC,X

!D,ALL,UX,,,,,UY,UZ ! Fixes nodes at x=0

!NSEL,ALL

SOLVE

FINISH

/POST26

NSOL,2,DISPNODE,U,Z ! Get z-direction deflection at node DISPNODE


PLVAR,2 ! Plot variable 2 vs. Freq

prvar,2

! and store it into variable 2

/ERASE
```

/axlab,y,Displacement

/YRANGE,0,4

PLVAR,2 ! Plot variable 2 vs. Freq

/window,1,off

/noerase

FINISH

C.6 Harmonic analysis code for the PZT attached aluminium beam with R-L electrical circuit

Modal anaylsis should be calculated before harmonic analysis as the inductor values are defined in modal analysis.

/PREP7

ET,3,CIRCU94,1,0 ! Set up the inductor

R,1,L(i)

RMOD,1,15,0,0 ! Subscript of inductor is 0, i.e. L0

TYPE,3 $ REAL,1

E,TOP_ELECTRODE,BOT_ELECTRODE ! Parallel the inductor to the

! electrodes of PZT

E,TOP_ELECTRODE2,BOT_ELECTRODE2 ! Parallel the inductor to the

```
 ! electrodes of PZT


!E,1,2 ! Parallel the inductor between

 ! node 1 and 2

ET,4,CIRCU94,0,0 ! Set up the resistor

R,2,R(i)

RMOD,2,15,0,0 ! Subscript of resistor is 0, i.e. R0

TYPE,4 $ REAL,2

E,TOP_ELECTRODE,BOT_ELECTRODE ! Parallel the resistor to the

 ! electrodes of PZT

 E,TOP_ELECTRODE2,BOT_ELECTRODE2 ! Parallel the resistor to the

 ! electrodes of PZT

!E,1,2 ! Parallel the resistor between node 1 and 2

NSEL,ALL

FORCENODE = node(0,DEPTH/2,0) ! Node where force applied

DISPNODE = node(BLNGTH,DEPTH/2,BTHK) ! Node where deflection !detected

FINISH

/SOLU

ANTYPE,HARM ! Harmonic analysis

HARFRQ,0,1000, ! Frequency range of analysis

NSUBST,500, ! Number of frequency steps
```

```
KBC,0 ! Impulse loads

F,FORCENODE,FZ,0.01 ! Applying force

D,BOT_ELECTRODE,VOLT,0.0 ! Assigns zero voltage to bottom electrode

D,BOT_ELECTRODE2,VOLT,0.0 ! Assigns zero voltage to bottom electrode

DDELE,TOP_ELECTRODE,VOLT

DDELE,TOP_ELECTRODE2,VOLT

CNVTOL,F,,,,1E-5 ! Small convergence value for force

CNVTOL,VOLT ! Default convergence value for current flow

!NSEL,S,LOC,X

!D,ALL,UX,,,,,UY,UZ ! Fixes nodes at x=0

!NSEL,ALL

SOLVE

FINISH

/POST26

NSOL,2,DISPNODE,U,Z ! Get z-direction deflection at node DISPNODE

NSOL,3,120,U,Z ! Get z-direction deflection at node DISPNODE

PLVAR,2 ! Plot variable 2 vs. Freq

prvar,2

 ! and store it into variable 2

/ERASE

/axlab,y,Displacement
```

```
/YRANGE,0,4

PLVAR,2 ! Plot variable 2 vs. Freq

PLVAR,3 ! Plot variable 2 vs. Freq

/window,1,off

/noerase

FINISH
```

Appendix D

The elements used for FEM in ANSYS^{R}

D.1 SOLID5 Element Description

SOLID5 is tree dimensional element and has a 3-D magnetic, thermal, electric, piezoelectric, and structural field capability with limited coupling between the fields. The element has eight nodes with up to six degrees of freedom at each node which is shown in Figure D.1. Scalar potential formulations (reduced RSP, difference DSP, or general GSP) are available for modeling magnetostatic fields in a static analysis. When used in structural and piezoelectric analyses, SOLID5 has large deflection and stress stiffening capabilities. (AFU Guide 2010)

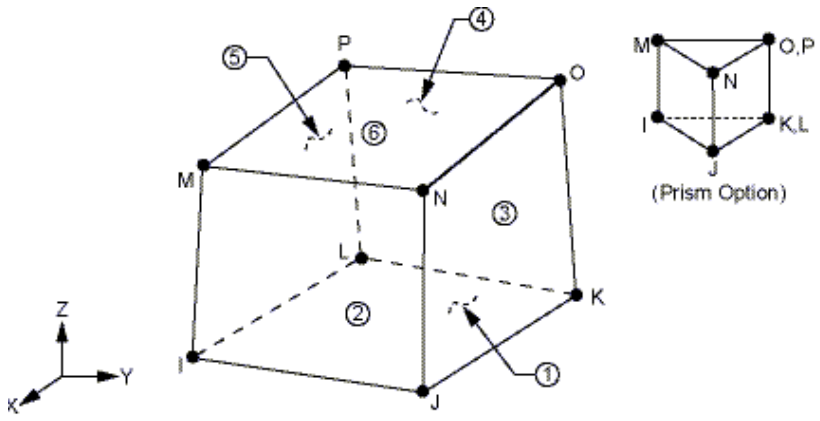

Figure D.1: SOLID5 Geometry (AFU Guide 2010)

D.2 SHELL181 Element Description

SHELL181 is a two dimensional element and suitable for analysing thin to moderately-thick shell structures. It is a 4-node element with six degrees of freedom at each node which is shown in Figure D.2. Translations in the x, y, and z directions, and rotations about the x, y, and z-axes.

SHELL181 is well-suited for linear, large rotation, and/or large strain nonlinear applications. Change in shell thickness is accounted for in nonlinear analyses. In the element domain, both full and reduced integration schemes are supported.

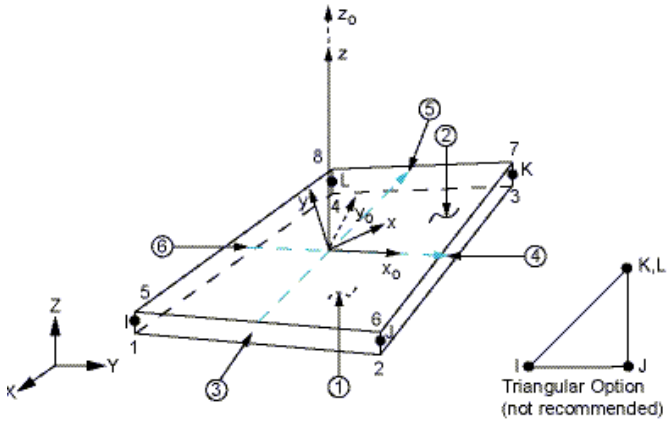

Figure D.2: SHELL181 Geometry (AFU Guide 2010)

x_o = Element x-axis if ESYS is not provided.

x = Element x-axis if ESYS is provided.

D.3 BEAM188 Element Description :

BEAM188 is one dimensional element and suitable for analysing slender to moderately stubby/thick beam structures. The element is based on Timoshenko beam theory which includes shear-deformation effects. The element provides options for unrestrained warping and restrained warping of cross-sections.

The element, shown in Figure D.3, is a linear, quadratic, or cubic two-node beam element in 3-D. BEAM188 has six or seven degrees of freedom at each node. These include translations in the x, y, and z directions and rotations about the x, y, and z directions. A seventh degree of freedom (warping magnitude) is optional. This element is well-suited for linear, large rotation, and/or large strain nonlinear applications.

The element includes stress stiffness terms, by default, in any analysis with large deflection. The provided stress-stiffness terms enable the elements to analyze flexural, lateral, and torsional stability problems (using eigenvalue buckling, or collapse studies with arc length methods or nonlinear stabilization).

Elasticity, plasticity, creep and other nonlinear material models are supported. A cross-section associated with this element type can be a built-up section referencing more than one material.

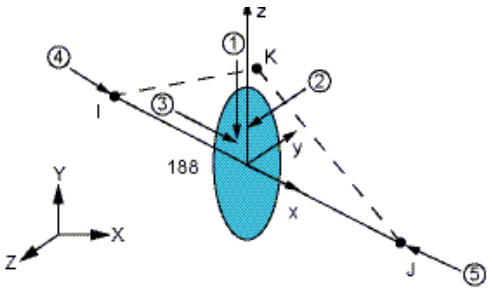

Figure D.3: BEAM188 Geometry (AFU Guide 2010)

BEAM188 Element Technology and Usage Recommendations

BEAM188 is based on Timoshenko beam theory, which is a first-order shear-deformation theory: transverse-shear strain is constant through the cross-section (that is, cross-sections remain plane and undistorted after deformation).

The element can be used for slender or stout beams. Due to the limitations of first-order shear-deformation theory, slender to moderately thick beams can be analyzed. Use the slenderness ratio of a beam structure (GAL^2 / (EI)) to judge the applicability of the element, where:

G = Shear modulus

A = Area of the cross-section

L = Length of the member (not the element length)

EI = Flexural rigidity

Calculate the ratio using some global distance measures, rather than basing it upon individual element dimensions. The following illustration shows an estimate of transverse-shear deformation in a cantilever beam subjected to a tip load. Although the results cannot be extrapolated to any other application, the example serves well as a general guideline. A slenderness ratio greater than 30 is recommended.

D.4 CIRCU94 Element Description

CIRCU94 is one dimensional element. a circuit element for use in piezoelectric-circuit analyses. The big difference of this element from the other one dimensional elements is that CIRCU94 element has two or three nodes to define the circuit component and one or two degrees of freedom to model the circuit response. The element may interface with the following piezoelectric elements:

PLANE13, KEYOPT(1) = 7 coupled-field quadrilateral solid

SOLID5, KEYOPT(1) = 0 or 3 coupled-field brick

SOLID98, KEYOPT(1) = 0 or 3 coupled-field tetrahedron

PLANE223, KEYOPT(1) = 1001, coupled-field 8-node quadrilateral

SOLID226, KEYOPT(1) = 1001, coupled-field 20-node brick

SOLID227, KEYOPT(1) = 1001, coupled-field 10-node tetrahedron

CIRCU94 is applicable to full harmonic and transient analyses. For these types of analyses, you can also use CIRCU94 as a general circuit element.

The geometry, node definition, and degree of freedom options are shown in Figure D.4Active nodes I and J define the resistor, inductor, capacitor and independent current source. They are connected to the electric circuit. Active nodes I and J and a passive node K define the independent voltage source. The passive node is not connected to the electric circuit. It is associated with the CURR (current) degree of freedom (which represents electric charge for this element).

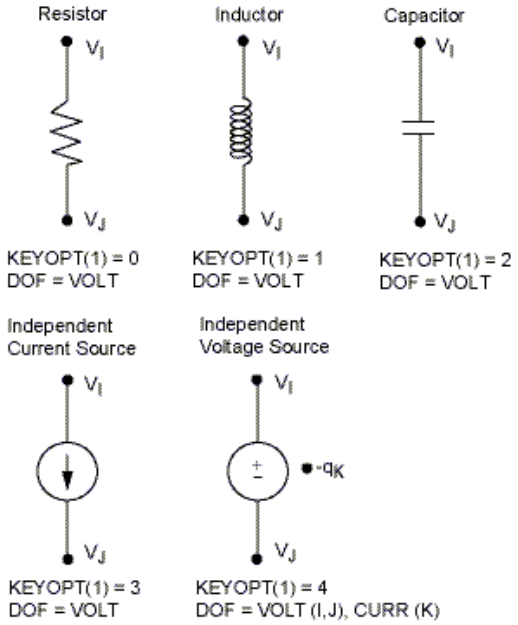

Figure D.4: CIRCU94 Circuit Options (AFU Guide 2010)

CIRCU94 is only compatible with elements having a VOLT DOF and an electric charge reaction solution. Electric charge reactions must all be positive or negative. KEYOPT(6) sets the electric charge reaction sign. In the study, a resistor KEYOPT(0) and a inductor KEYOPT (1) are used. (Guide 2010)

Appendix E

E.1 Piezoelectric material constants in ANSYS

Manufacturer of the material data and ANSYS^{R} notation can be different. In that case, it is necessary to convert the manufacturer's data in the form of constitutive equations of piezoelectric material (presented in Chapter 3) to ANSYS^{R} notation. In the appendix, all the parameters are presented in the form that ANSYS^{R} uses. Here is the ANSYS^{R} required values for stiffness matrix at the constant electric field (ie short circuit), dielectric matrix evaluated at constant strains (i.e. mechanically clamped) and piezoelectric matrix relating stress/electric field are given respectively:

$$[c] = [s^E] \quad \text{E-1}$$

$$[\varepsilon^S]=[\varepsilon^T] - [d]^t[s^E]^{-1}[d] \quad \text{E-2}$$

$$[c] = [s^E]^{-1}[d] \quad \text{E-3}$$

Stress is used rather than strain:

$$\{\sigma\} = [s^E]^{-1}\{S\} - [s^E]^{-1}[d]\{E\} \quad \text{E-4}$$

In electric displacement equation, strain is used rather than stress:

$$\{D\} = [d]^t[s^E]^{-1}\{S\} + [\varepsilon^T]\{E\} - [d]^t[s^E]^{-1}[d]\{E\} \quad \text{E-5}$$

Appendix F

F.1 Definition of Root Mean Square

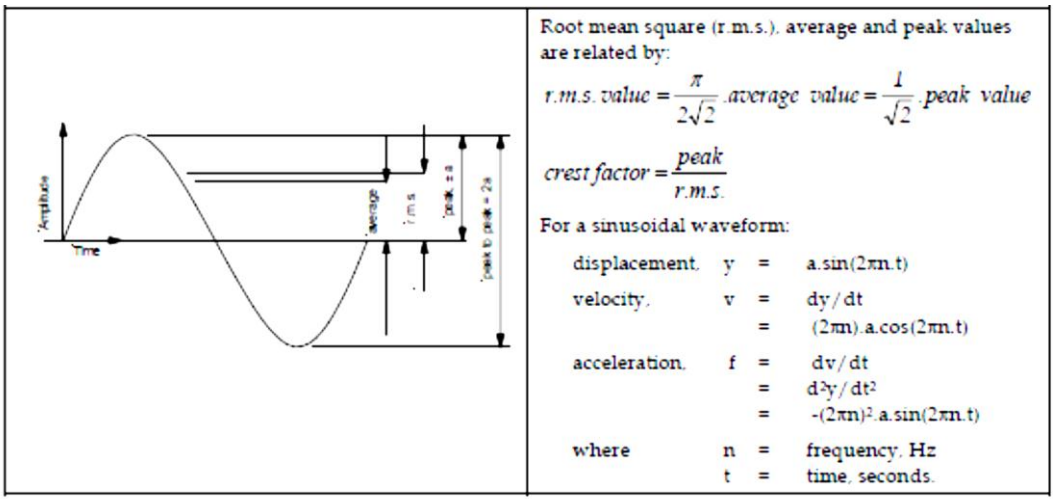

Figure F.1: Definition of Root Mean Square(Lyon 1995)

Appendix G

Piezoelectric coupling constant

G.1 The crystallographic point groups

The piezoelectric effect depends upon the crystallographic symmetry. In the other word, the arrangement of atoms in a different type piezoelectric material has different the point groups. In total, there are thirty-two point groups which is shown in Figure G.1.

CRYSTAL SYSTEM	CENTRIC POINT GROUPS		ACENTRIC POINT GROUPS					OPTIC AXES
			POLAR		NONPOLAR			
TRICLINIC	$\bar{1}$		1		NONE			BIAXIAL
MONOCLINIC	2/m		2	m	NONE			
ORTHORHOMBIC	mmm		mm2		222			
TETRAGONAL	4/m	4/mmm	4	4mm	$\bar{4}$	$\bar{4}$2m	422	UNIAXIAL
TRIGONAL	$\bar{3}$	$\bar{3}$m	3	3m	32			
HEXAGONAL	6/m	6/mmm	6	6mm	$\bar{6}$	$\bar{6}$m2	622	
CUBIC	m3	m3m	NONE		23	$\bar{4}$3m	432	ISOTROPIC
	11 GROUPS		10 GROUPS		11 GROUPS			

Figure G.1: The crystallographic point groups (Ballato 1996)

Piezoelectric material's mechanic and electric properties are determined by the crystallographic point groups. One of these properties piezoelectric coupling constant (K_{ij}) represents the efficiency of piezoelectric effect. Figure G.2 shows the values for the piezoelectric coupling constant of piezoelectric materials.

MATERIAL, CUT	CLASS	COUPLING FACTOR
Lithium niobate crystal X-cut 36° rotated-Y-cut	**3m**	$k_{15} = 68.9\%$ $k_{22} = 48.7\%$
Quartz crystal AT-cut BT-cut	**32**	$k'_{26} = 8.8\%$ $k'_{26} = 5.0\%$
PZT ceramic solid solutions Z-cut	**∞mm**	$k_{33} = 30$ to 60%
Polyvinylidene fluoride, PVDF Z-normal sheet	**mm2**	$k_{31} = 16\%$
Gallium Arsenide (110)-cut (111)-cut	**$\bar{4}$3m**	$k'_{26} = 6.1\%$ $k'_{11} = 4.3\%$
Silicon Carbide, α-SiC X- or Y-cut Z-cut	**6mm**	$k_{15} = 2.5\%$ $k_{33} = 3.5\%$
Zinc Oxide Z-normal, thin film	**6mm**	$k_{15} = 26\%$ $k_{33} = 29\%$
Aluminum Nitride Z-normal, thin film	**6mm**	$k_{15} = 15.5\%$ $k_{33} = 24.2\%$

Figure G.2: Piezoelectric coupling constant of representative materials(Ballato 1996)

Appendix H

Detailed Results

H.1 The Attenuation (dB) Vibration

Table H-1: The effect of different resistance on attenuation (dB) vibration at Node 22

Frequency (Hz)	R=10,000,000 Ω	R=1,000,000 Ω
19.038	-2.80	-2.68
20.5	-0.25	-0.24
26.838	-2.31	-2.29

Table H-2: The effect of different resistance on attenuation (dB) vibration at Node 23

Frequency (Hz)	R=10,000,000 Ω	R=1,000,000 Ω
19.038	-1.77	-1.66
20.5	-1.76	-1.73
23.425	-0.08	-0.11
26.838	-2.22	-2.20

Table H-3: The effect of different resistance on attenuation (dB) vibration at Node 29

Frequency (Hz)	R=10,000,000 Ω	R=1,000,000 Ω
19.038	-3.21	-3.09
20.5	-0.38	-0.38
23.913	-0.01	-0.02
26.838	-2.22	-2.20

Table H-4: The effect of different resistance on attenuation (dB) vibration at Node 30

Frequency (Hz)	R=10,000,000 Ω	R=1,000,000 Ω
19.038	-2.19	-2.07
26.838	-1.98	-1.96
28.788	-1.70	-1.69

Table H-5: The effect of different resistance on attenuation (dB) vibration at Node 36

Frequency (Hz)	R=10,000,000 Ω	R=1,000,000 Ω
20.5	-0.17	-0.16
23.913	-0.82	-0.80

Table H-6: The effect of different resistance on attenuation (dB) vibration at Node 37

Frequency (Hz)	R=10,000,000 Ω	R=1,000,000 Ω
19.038	-2.7	-2.5
23.913	-0.2	-0.2
26.838	-1.9	-1.9

Table H-7: The effect of different resistance on attenuation (dB) vibration at Node 38

Frequency (Hz)	R=10,000,000 Ω	R=1,000,000 Ω
19.038	-1.7	-1.6
26.838	-0.5	-0.5

Table H-8: The effect of different resistance on attenuation (dB) vibration at Node 39

Frequency (Hz)	R=10,000,000 Ω	R=1,000,000 Ω
26.838	-0.8	-0.8

H.2 Structural displacement

Results are given as amplitude of the structural response in the thickness axis for a range of frequency values. The frequency values varied from 1 Hz to 40 Hz.

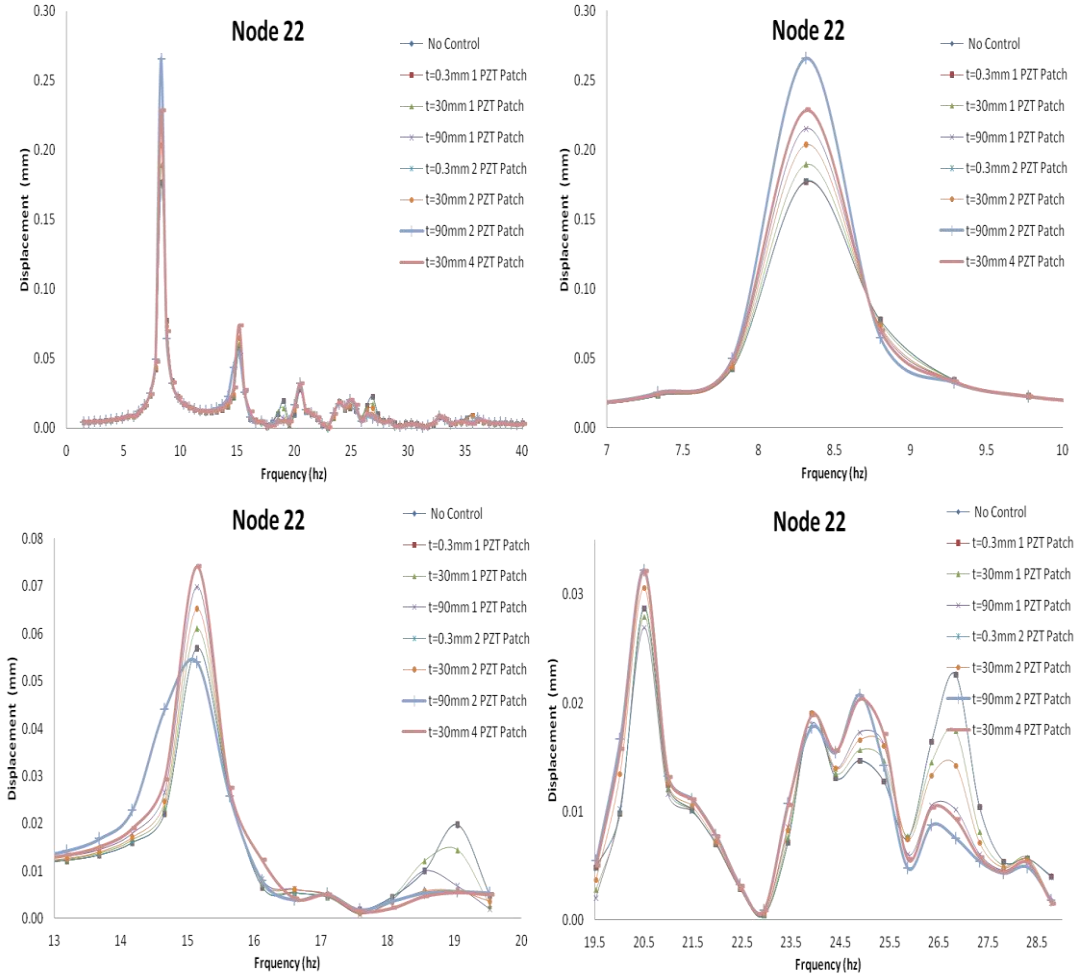

Figure H.1: The response of the structure at Node 22 without control, with piezoelectric shunted RL circuit

Node 22 is relatively far point from the piezoelectric patch. 11dB reduction is produced at 19 Hz for t=90mm 2 PZT Patch.

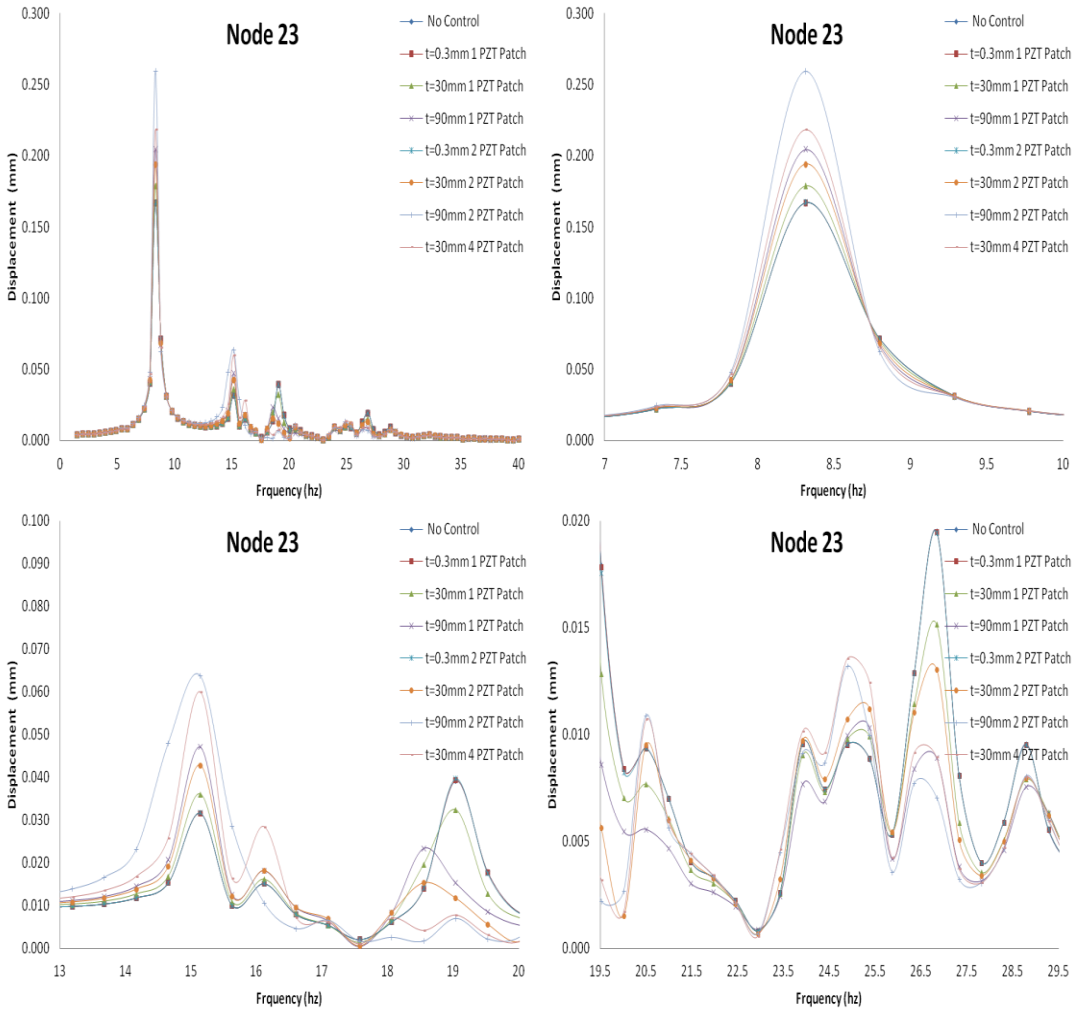

Figure H.2: The response of the structure at Node 23 without control, with piezoelectric shunted RL circuit

10dB reduction is produced at 15 Hz for t=90mm 2 PZT Patch.

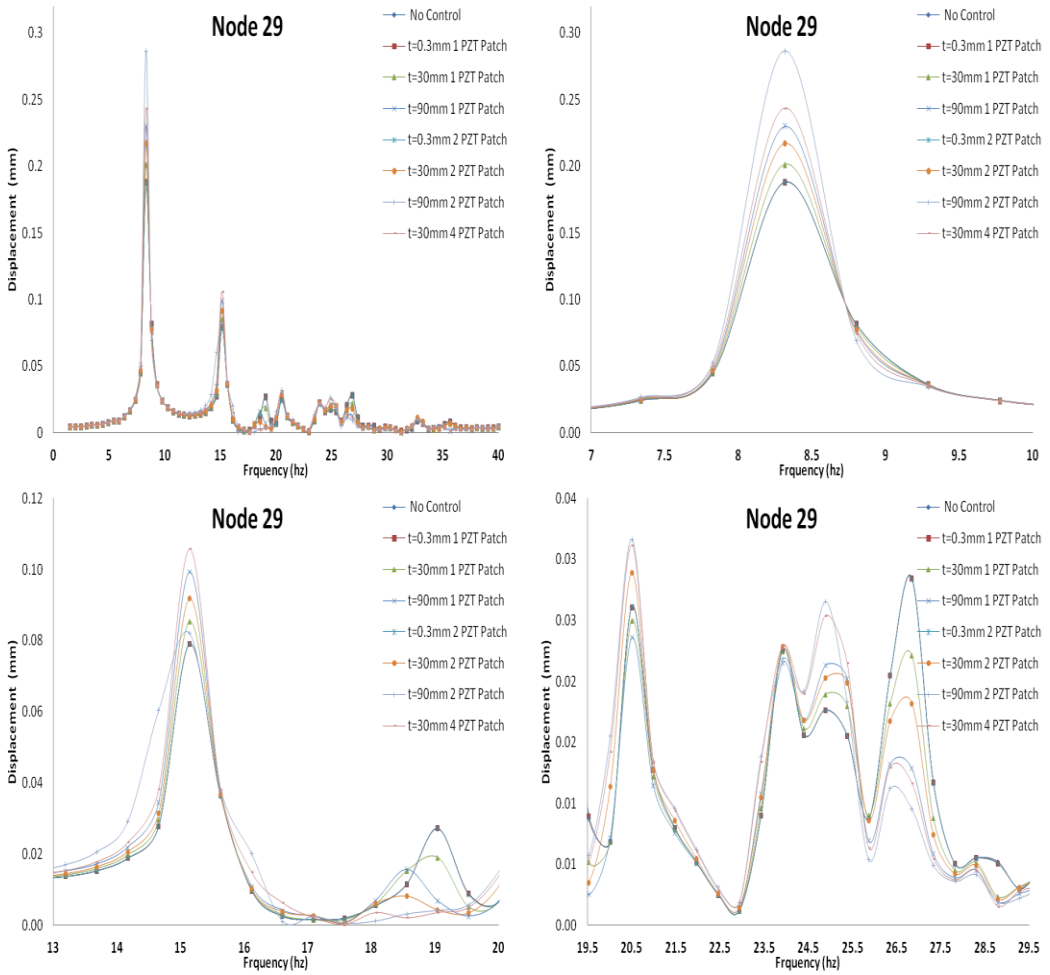

Figure H.3: The response of the structure at Node 29 without control, with piezoelectric shunted RL circuit

7dB reduction is produced at 16 Hz for t=30mm 4 PZT Patch.

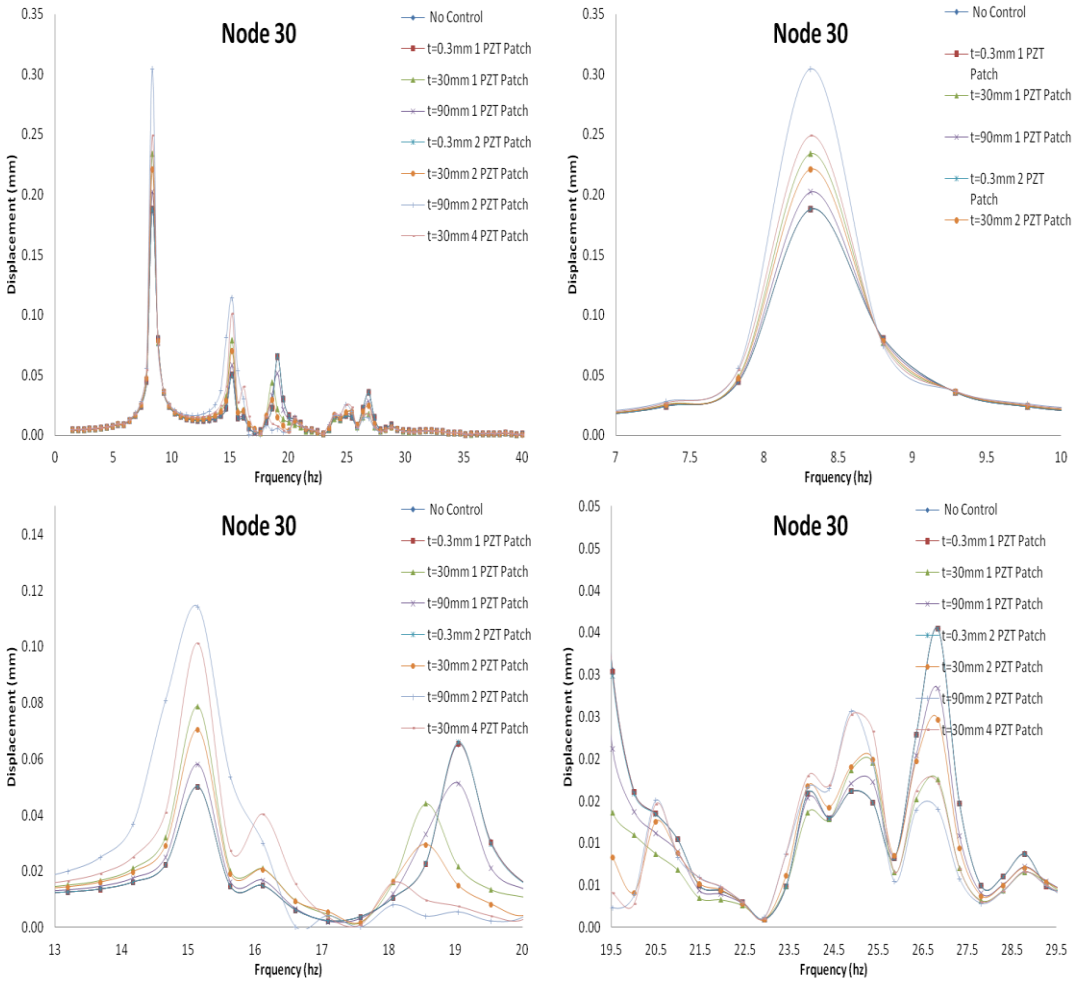

Figure H.4: The response of the structure at Node 30 without control, with piezoelectric shunted RL circuit

11 dB reduction is produced at 15 Hz for t=90mm 2 PZT Patch.

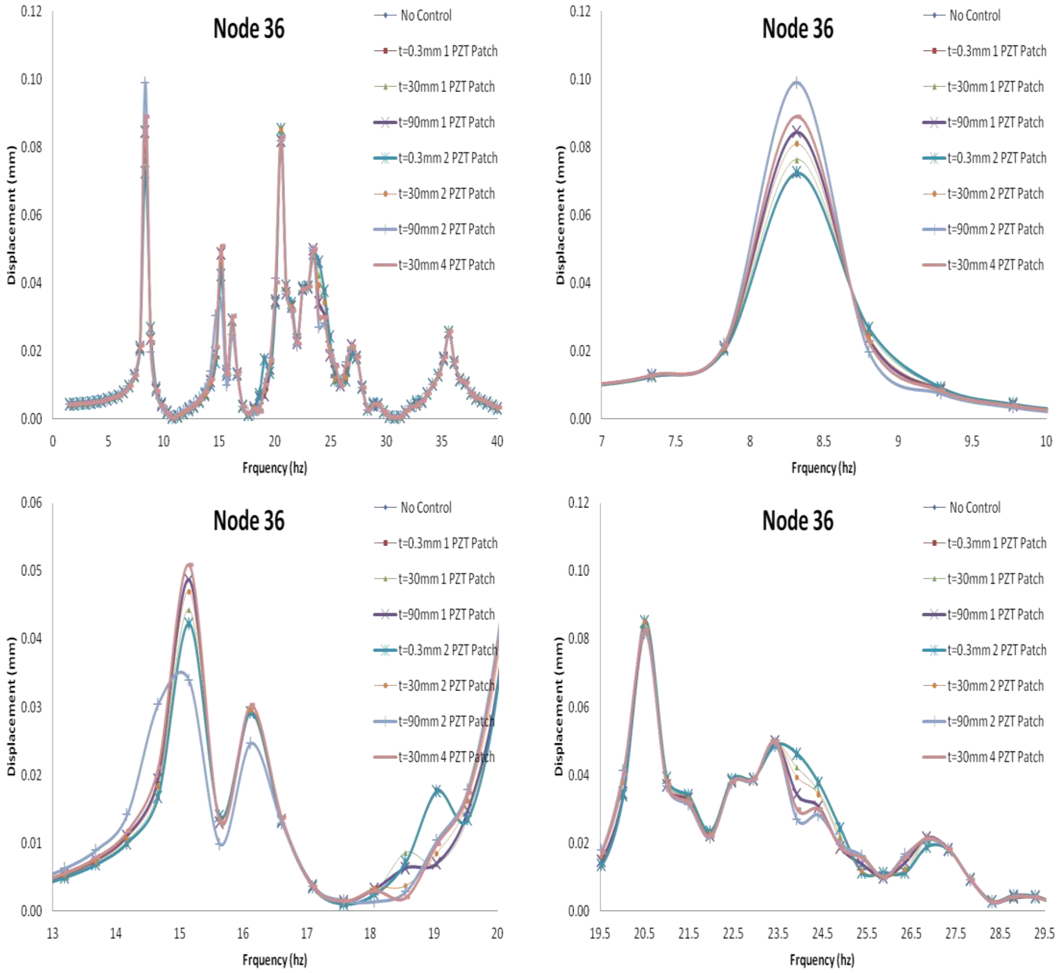

Figure H.5: The response of the structure at Node 36 without control, with piezoelectric shunted RL circuit

6 dB reduction is produced at 11 Hz for t=90mm 2 PZT Patch.

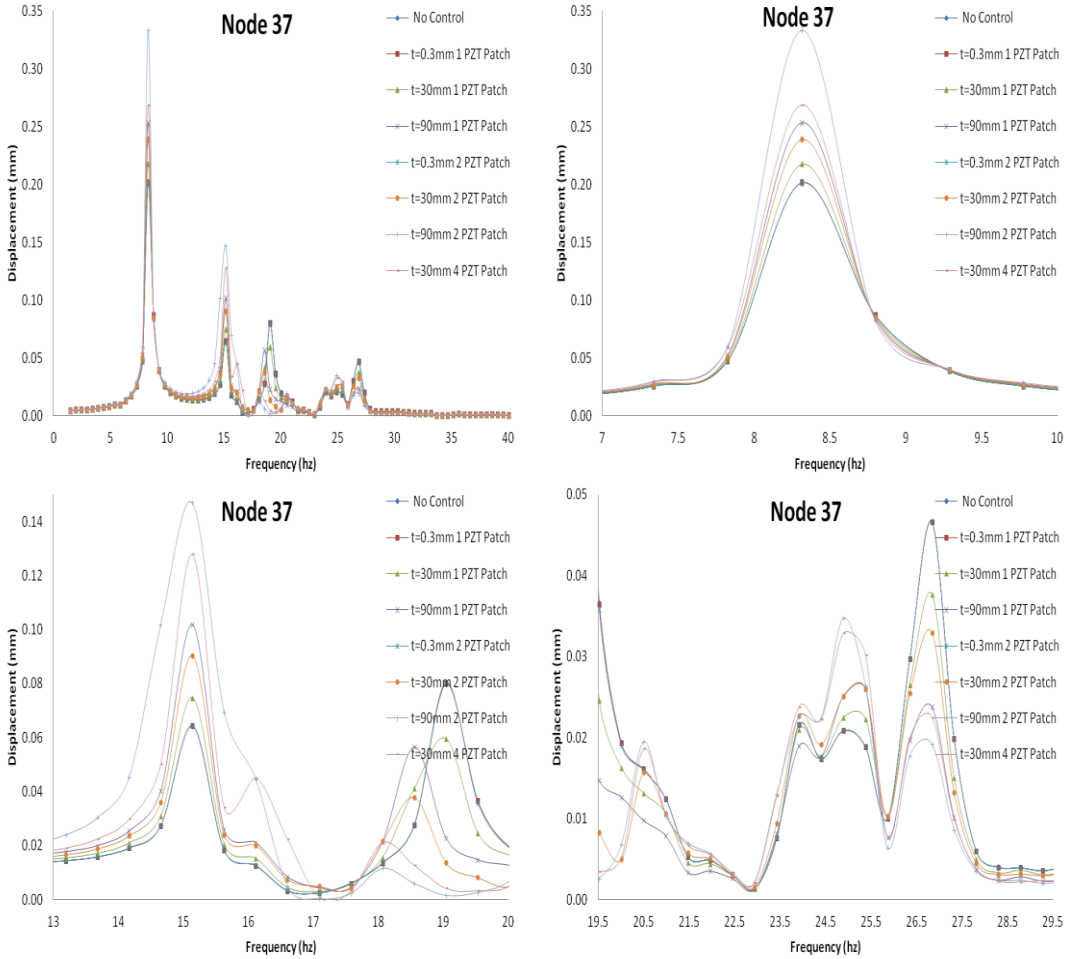

Figure H.6: The response of the structure at Node 37 without control, with piezoelectric shunted RL circuit

17 dB reduction is produced at 16 Hz for t=30mm 4 PZT Patch.

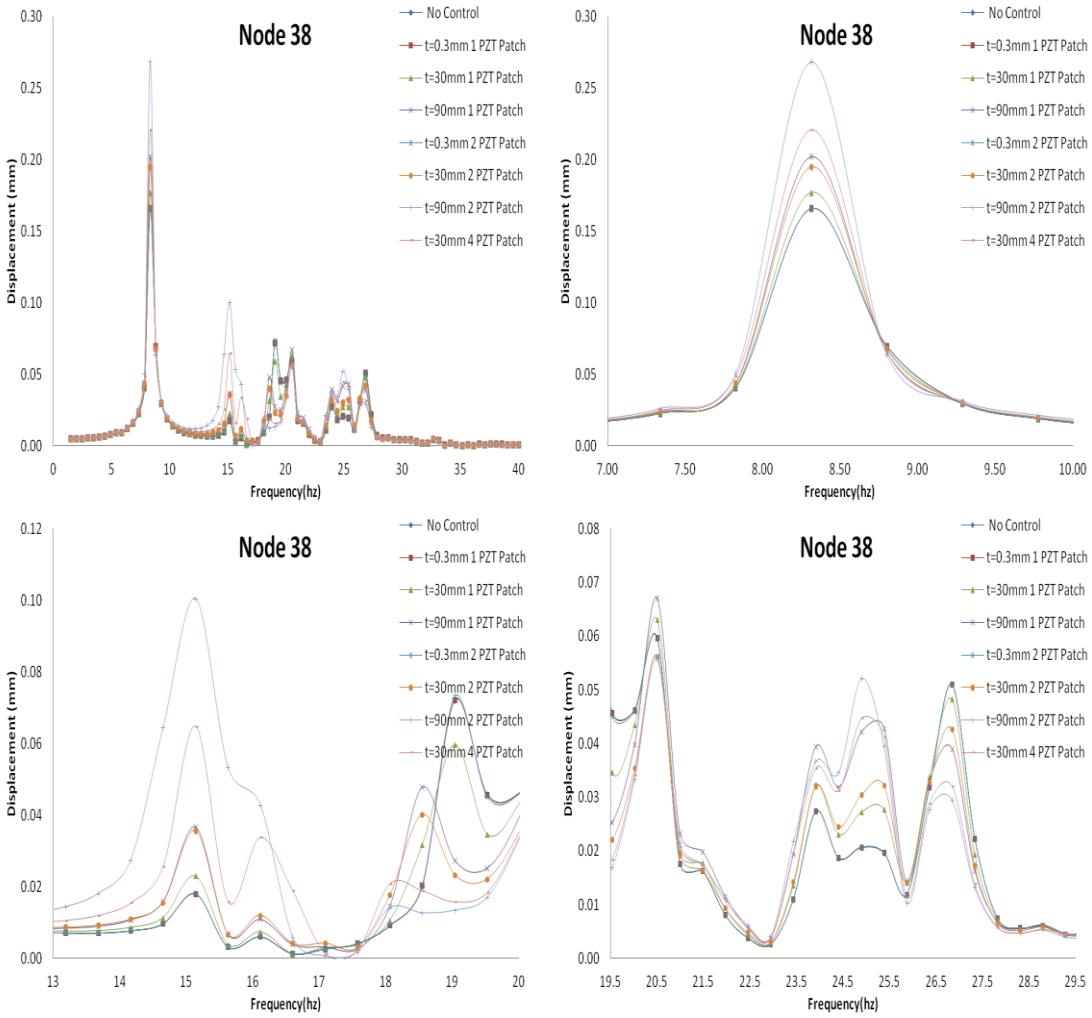

Figure H.7: The response of the structure at Node 38 without control, with piezoelectric shunted RL circuit

24 dB reduction is produced at 15 Hz for t=90mm 2 PZT Patch.

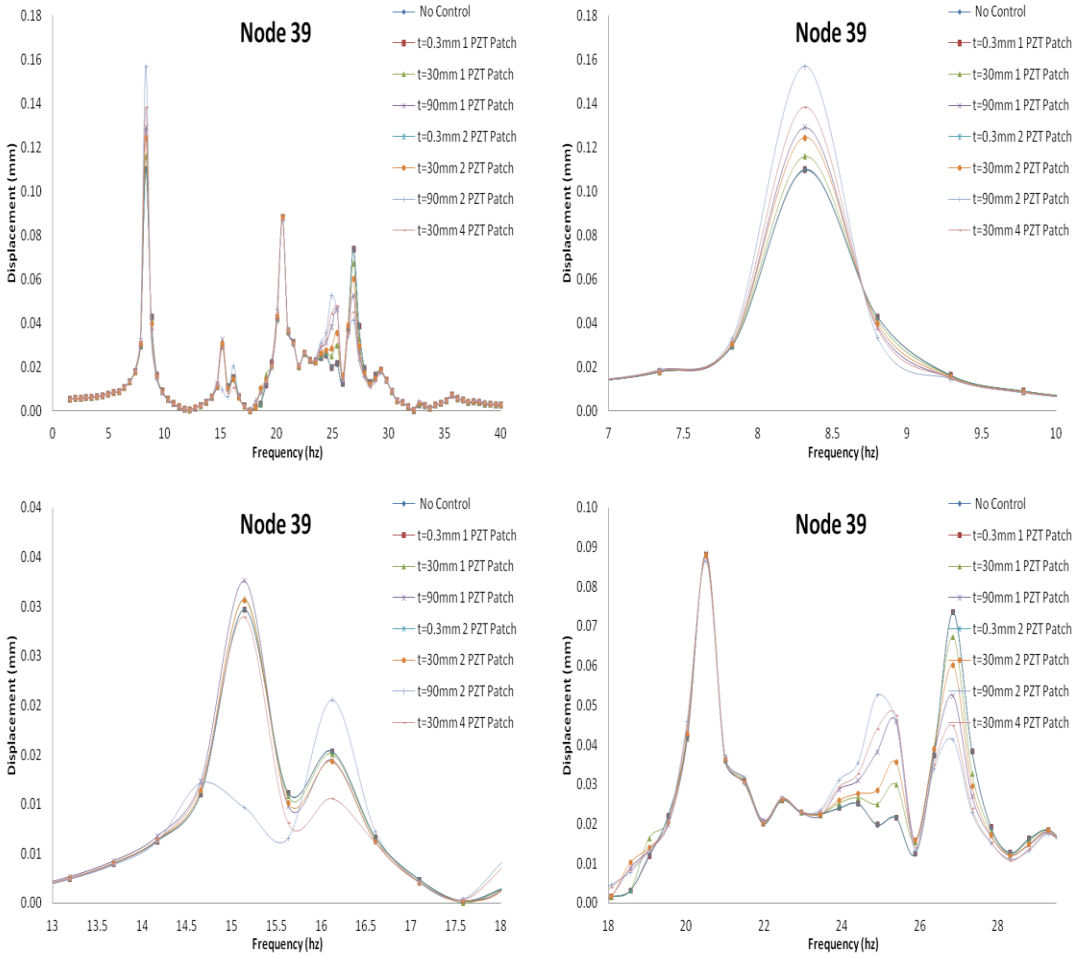

Figure H.8: The response of the structure at Node 38 without control, with piezoelectric shunted RL circuit

11 dB reduction is produced at 32 Hz for t=30mm 4 PZT Patch.

H.3 Attenuation (dB) of responce vs. Thickness

Thickness effect is presented in the following figures.

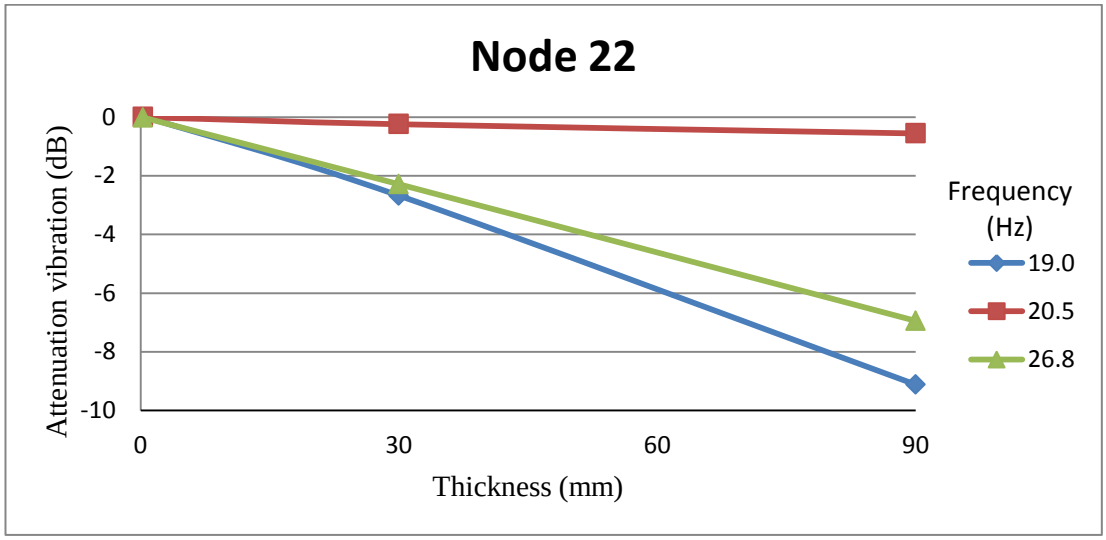

Figure H.9: Thickness effect at Node 22

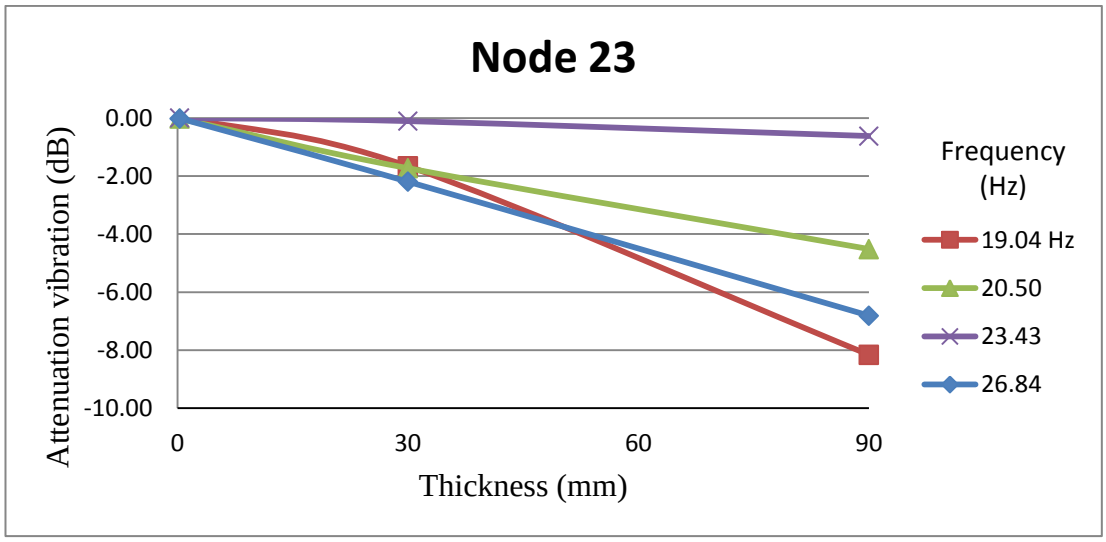

Figure H.10: Thickness effect at Node 23

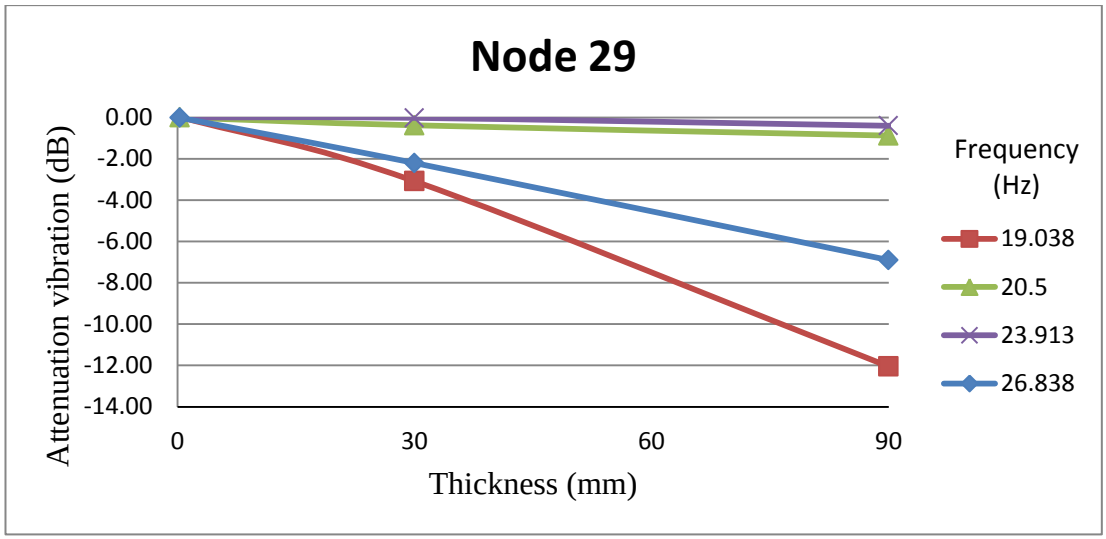

Figure H.11: Thickness effect at Node 29

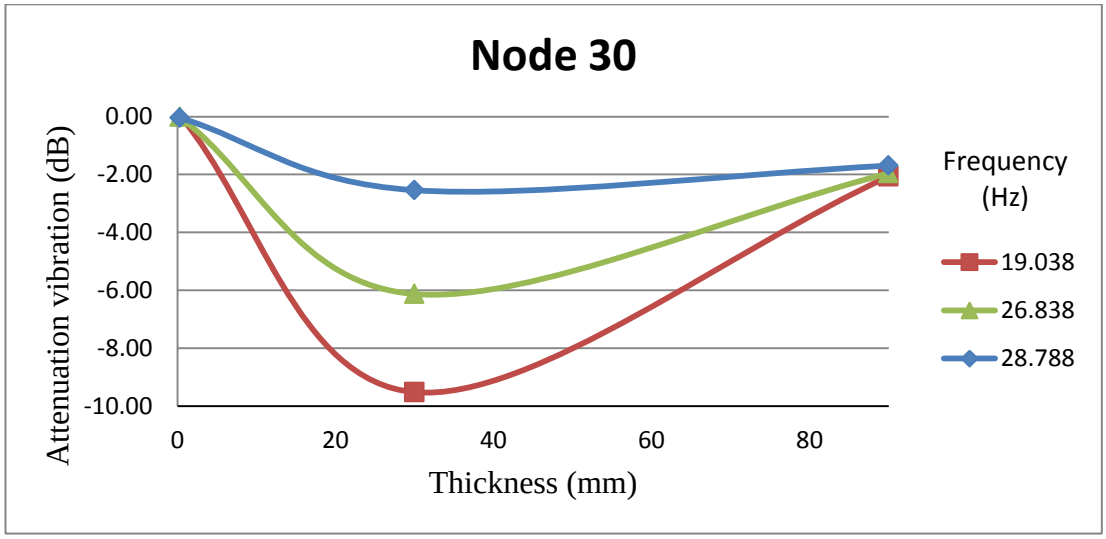

Figure H.12: Thickness effect at Node 30

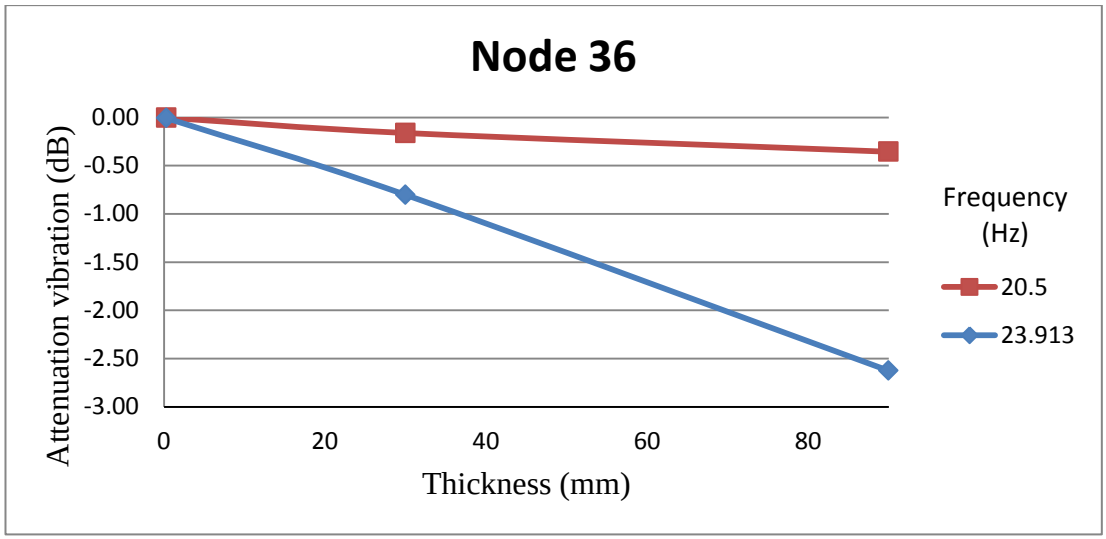

Figure H.13: Thickness effect at Node 36

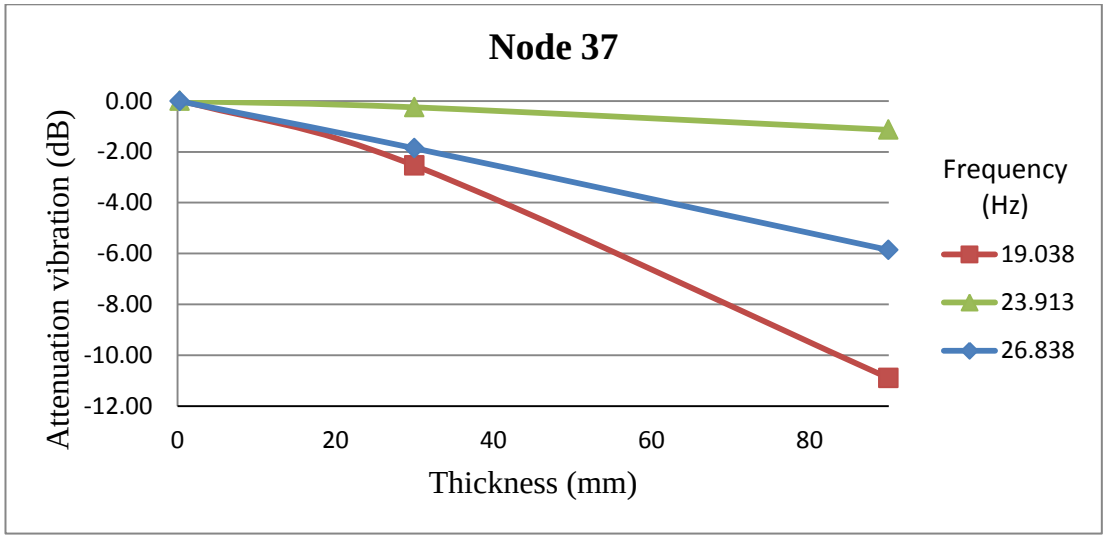

Figure H.14: Thickness effect at Node 37

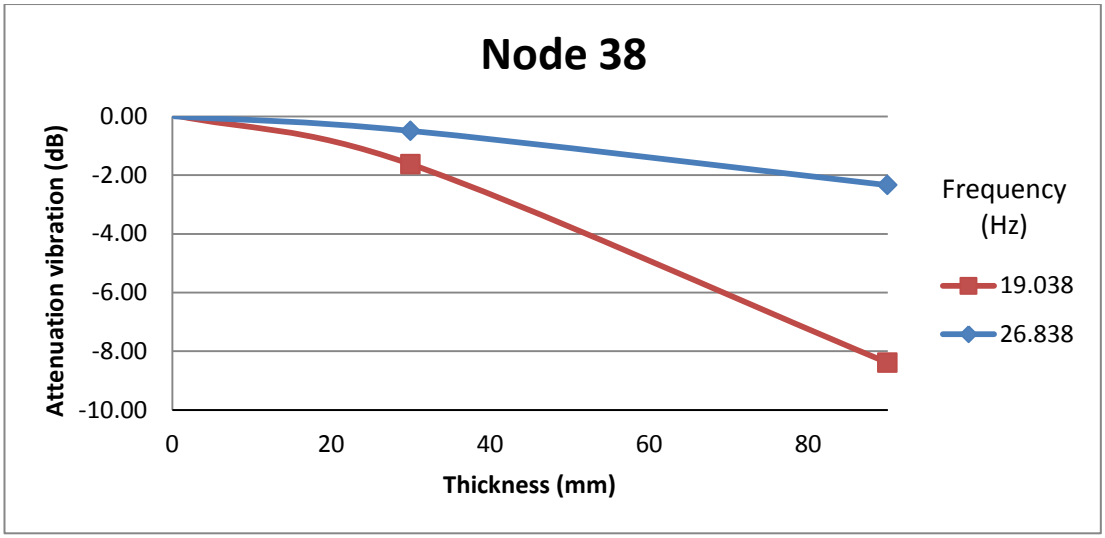

Figure H.15: Thickness effect at Node 38

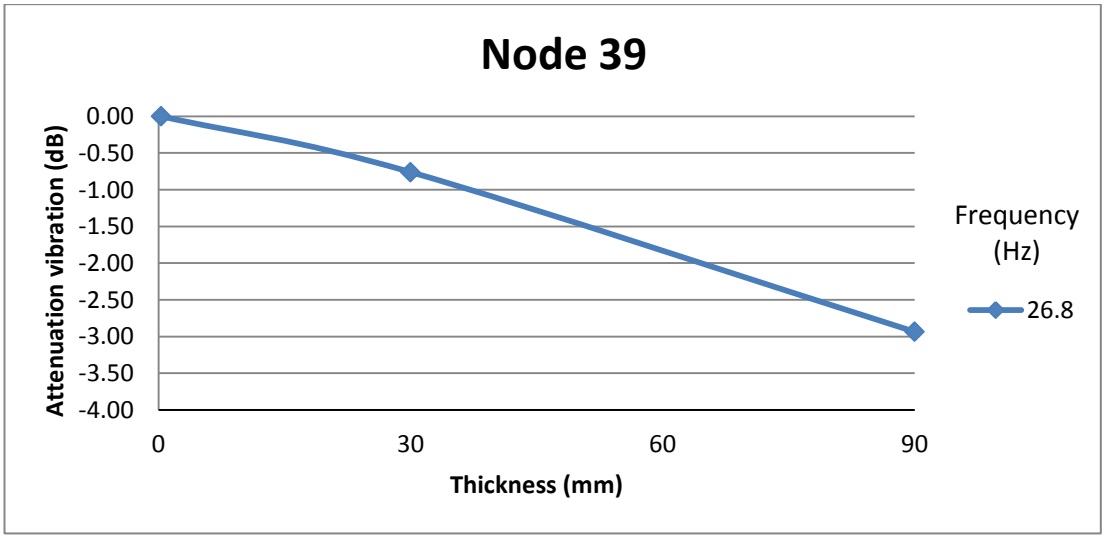

Figure H.16:Thickness effect at Node 39

H.4 Attenuation (dB) of responses vs. The Piezoelectric Patch Number

The vibration reduction is shown when the number of the piezoelectric patches is changed. The thickness and electric circuit components are kept constant.

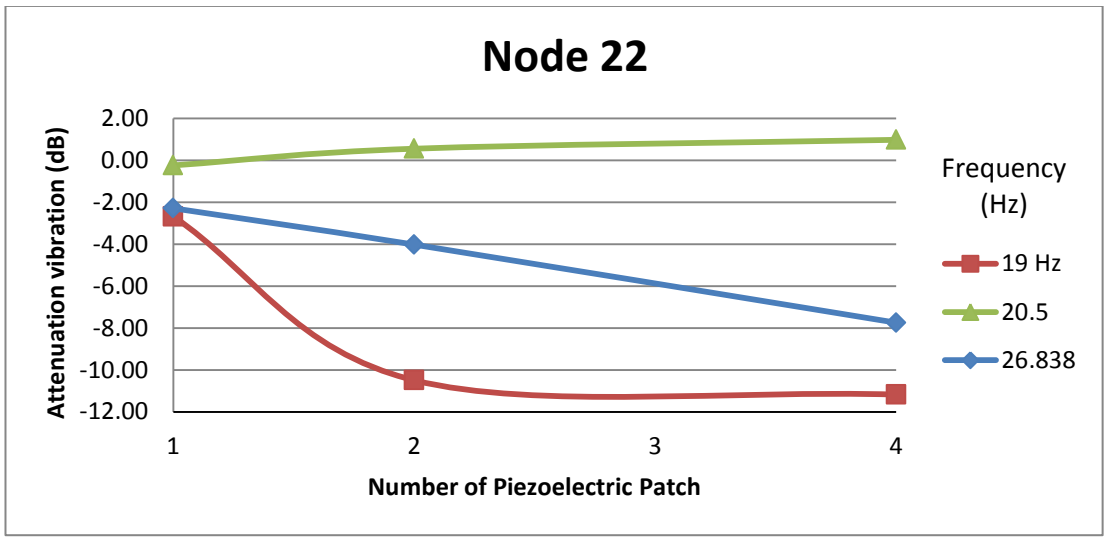

Figure H.17: Attenuation vs. the piezoelectric patches at node 22

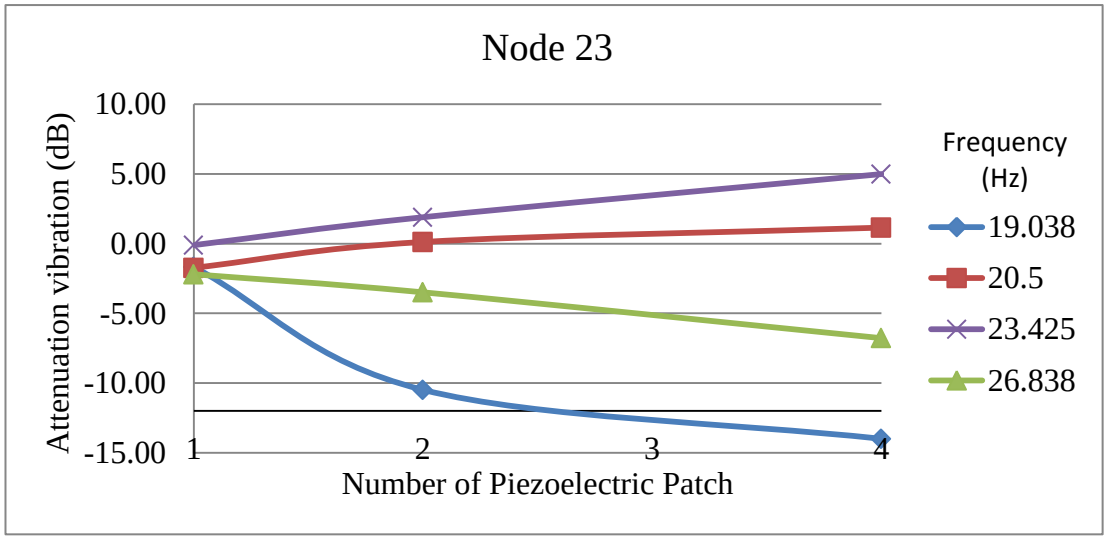

Figure H.18: Attenuation vs. the piezoelectric patches at node 23

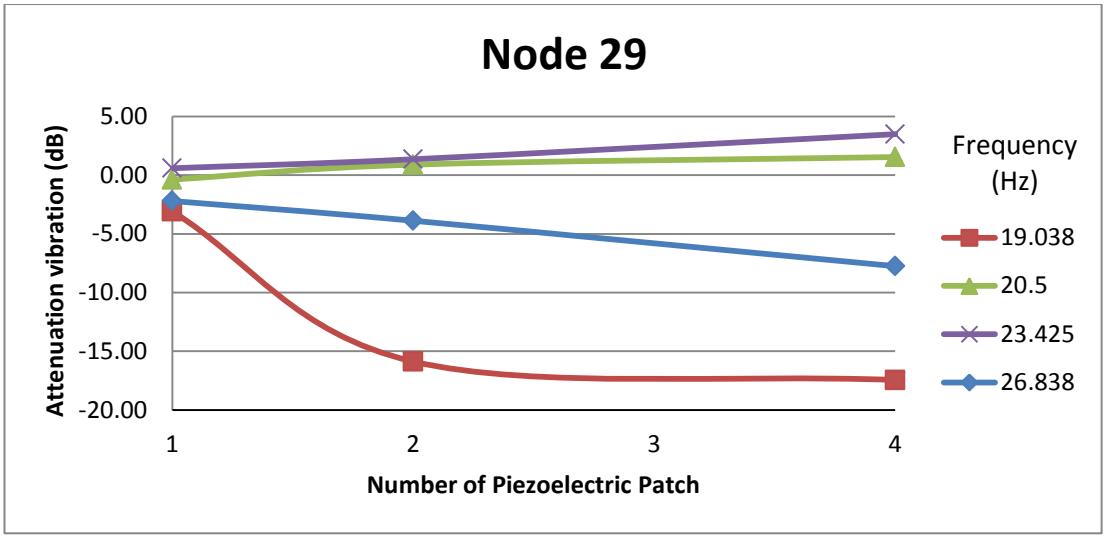

Figure H.19: Attenuation vs. the piezoelectric patches at node 29

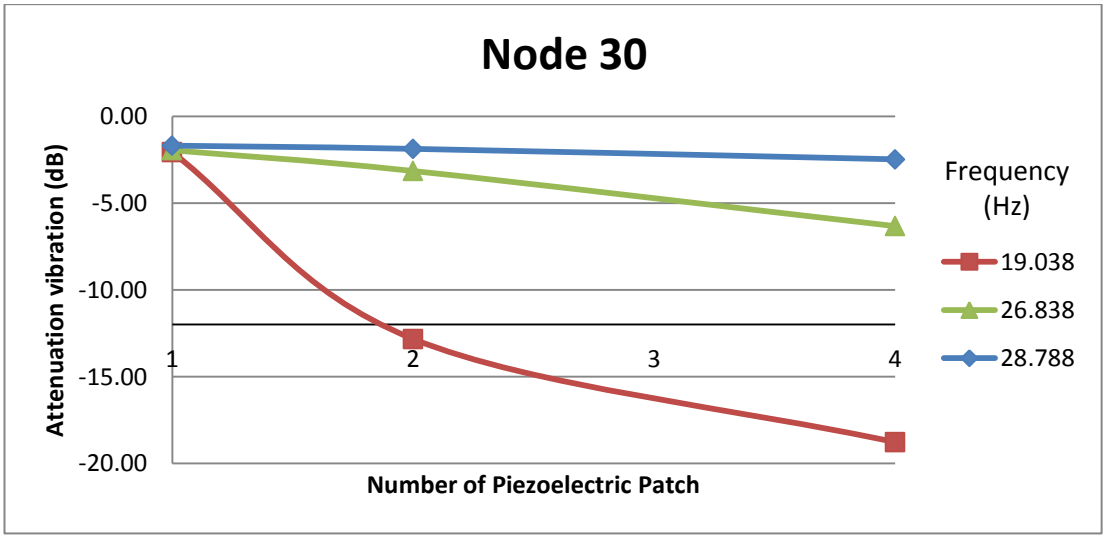

Figure H.20: Attenuation vs. the piezoelectric patches at node 30

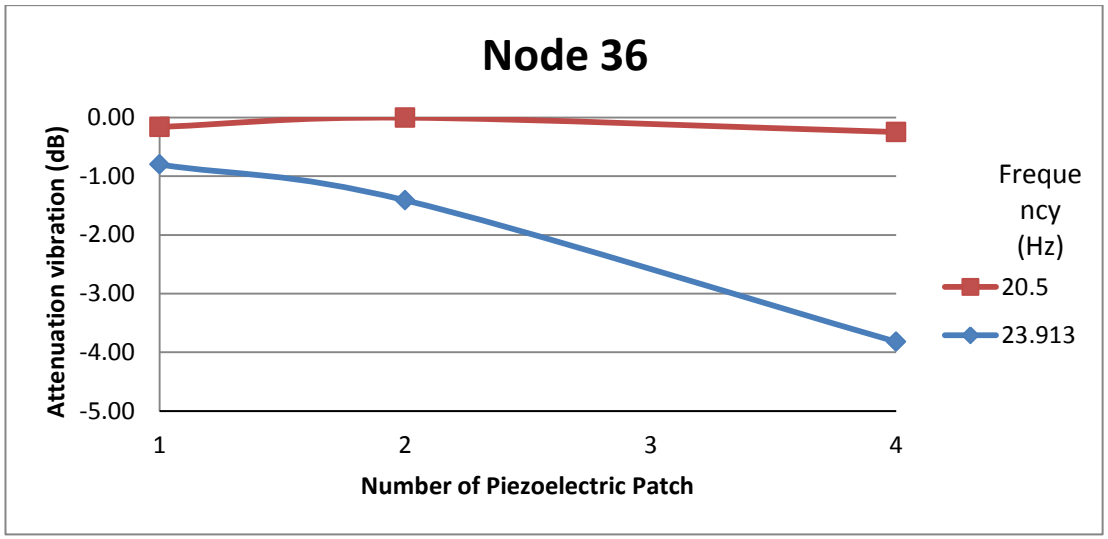

Figure H.21: Attenuation vs. the piezoelectric patches at node 36

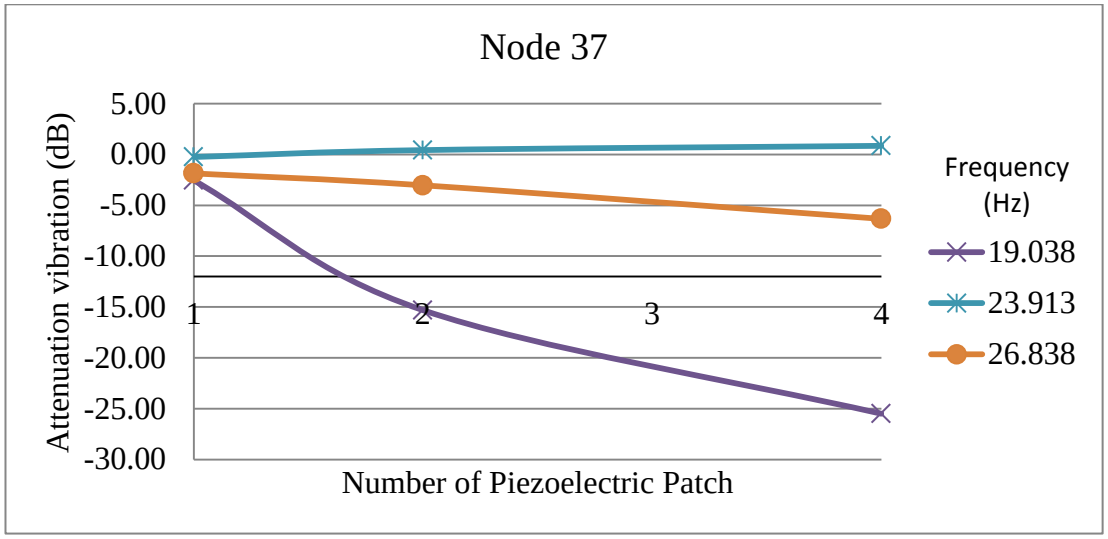

Figure H.22: Attenuation vs. the piezoelectric patches at node 37

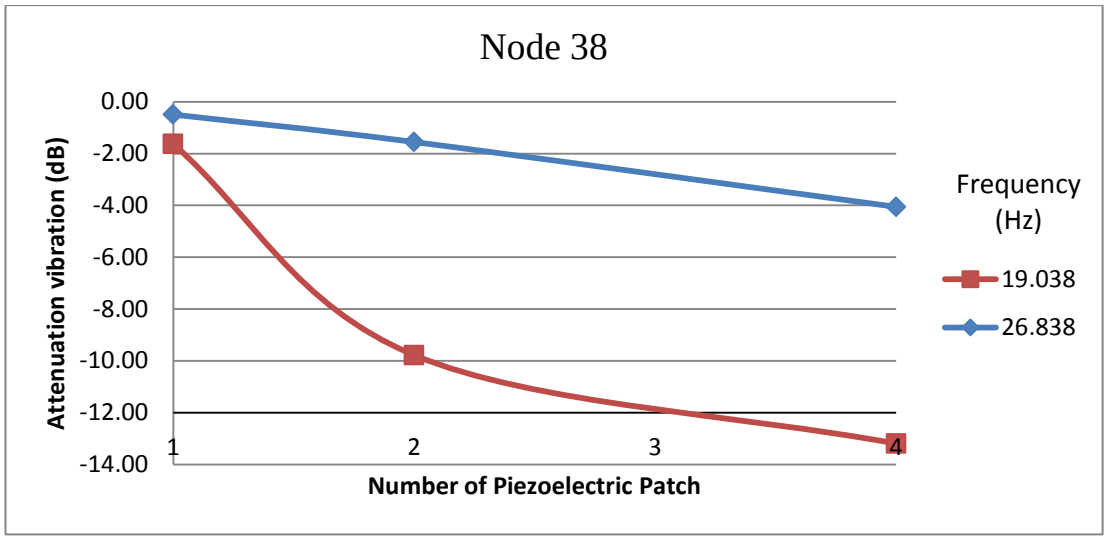

Figure H.23: Attenuation vs. the piezoelectric patches at node 38

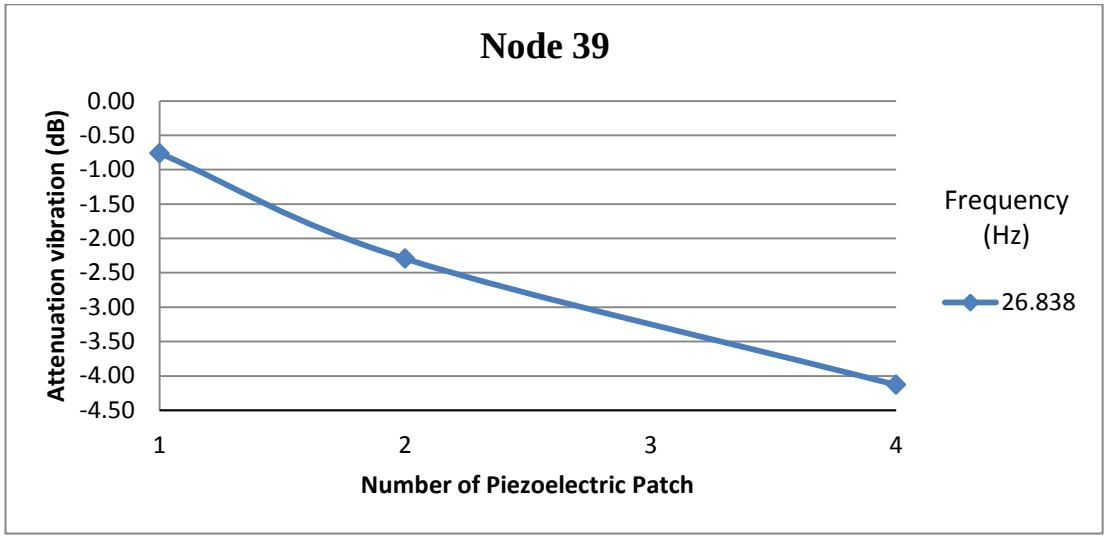

Figure.H.24: Attenuation vs. the piezoelectric patches at node 39

Appendix I

The Finite element Analysis

I.1 Introduction

In this appendix, the finite element analysis is explained. This method is used as the numerical simulation tool in this study.

I.2 The Finite Element Analysis

Finite element analysis is the most known numerical tool which has been used since the late 1960's. For three dimensional structure, the displacement within a typical element is *u(x,y,z,t)* which can be expressed in terms of unknown nodal displacements $u_i(t)$ in the form :

$$u(x,y,z,t) = \sum_{i=1}^{n} N_i(x,y,z)u_i(t) \qquad \text{I-1}$$

where, N_i is called the shape function corresponding to the nodal displacement $u_i(t)$; n is the number of unknown nodal displacement; x,y,z are coordinates. A finite element model of a bar in a cantilevered configuration which has n=2 nodes is illustrated in Figure I.25.

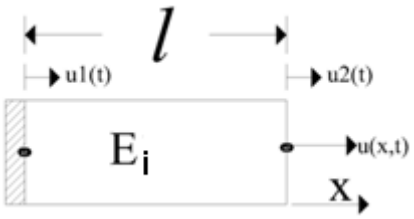

Figure I.25: One-element, six-node mesh

In the figure, *l* is the length of the bar; E_i (i=1to 6) means element; $u_i(t)$ are the static time dependent displacements and they must satisfy the equation for each x value from 0 to *l* :

$$EA\frac{d^2u(x)}{dx^2} \qquad \text{I-2}$$

Here, E is the elastic modulus and A is the cross sectional area of the beam element. A displacements function can be integrated from equation I-2 which is:

$$u(x) = c_1x + c_2 \qquad \text{I-3}$$

Where, c_1 and c_2 are constants of integration with respect to x and they are time-dependent. At each node, the value of u is allowed to be time dependent, hence the use of labels $u_1(t)$ and $u_2(t)$ in Figure I.25. The time-variable functions labels $u_1(t)$ and $u_2(t)$ are called nodal displacements of the model and will eventually be solved for and used to describe the longitudinal vibration of the bar. The spatial function u(x) and the temporal functions labels $u_1(t)$ and $u_2(t)$ are related through using the nodes as boundaries to estimate the spatial constants in equation. Equation I-3 becomes at *x*=0:

$$u(0) = u_1(t) = c_10 + c_2\,, t \geq 0 \qquad \text{I-4}$$

The displacement at this point must be zero as this end is fixed. So that makes:

$$c_2 = u_1(t) \qquad \text{I-5}$$

The other boundary is defined at x=*l* and the equation yields:

$$u(l) = u_1(t) = c_1L + c_2 \qquad \text{I-6}$$

This equation yields $c_1 = \frac{[u_2(t)-u_1(t)]}{l}$. When c_1 and c2 are substituted into equation I-3 that will give the approximation of the displacement u(x,t) :

$$u(x,t) = (1 - \frac{x}{l})u_1(t) + (\frac{x}{l})u_2(t) \quad \text{I-7}$$

or

$$u(x,t) = N_1(x)u_1(t) + N_2(x)u_2(t) \quad \text{I-8}$$

where,

$$N_1(x) = \left(1 - \frac{x}{l}\right), N_2(x) = \frac{x}{l}$$

The coefficient functions N1 and N2 are called shape functions because they determinate the spatial distribution or shape of the solution u(x,t) (Rao and Yap 1995; Daniel 2001).

Next is determination equation of motion by using total energy. In this study the governing equations of motion of the smart material is derived by using Hamilton's variational principle, which can be written as :

$$\delta \int_{t_1}^{t_2} (K - U + W)dt = 0 \quad \text{I-9}$$

where K is the kinetic energy; U is the total potential energy; W is the virtual; δ denotes the variation; t_2 and t_1 are starting and finishing time, respectively. The first variation of total energy leads directly to the classical form of equation of motion. The governing equations of motion in variational form which can be written as(Rao and Yap 1995) :

$$[M]\{\ddot{u}\} + [C]\{\dot{u}\} + [K]\{u\} = \{F\} \quad \text{I-10}$$

where M is the mass matrix, C is the damping matrix, K is the stiffness matrix, and F is the external force matric.

Appendix J

The Finite element Analysis with ANSYS^{R}

J.1Finite Element Modelling Passive Piezoelectric Shunt Damping System in ANSYS^{R}

Analytical solutions for simple structures are available. For the complex structure, numerical modelling is the most known solution. Finite element method is chosen to achieve the aim of the thesis and ANSYS^{R} commercial software package is used for solid modelling and analysing due to the powerful numerical modelling, analysing and post-processing capabilities of the software. The software is a tool to overcome a number of engineering problems like mechanical, electrical, electromagnetic, electronic, thermal, fluid, coupled-field and so on. (Guide 2010)

J.2Setting up the solid model

There is several type of analysis which can be chosen in ANSYS^{R} such as static, modal, transient, harmonic, fluid dynamic, buckling are most commons. There is a hierarchy for any analysing type to solve the problem. The calculation hierarchy has three main processes as:

1. Pre-processing
2. Solution processor
3. Post-processing

Popular usage of ANSYS is graphical interface which means user can access processors from the software menu. There is another way to set up and solve the

problem that is text interface. That allows mode flexibility to change the variables and overview the processers. Beam application is done by using text interface. The other applications partly are more complicated to use only text interface so biggest part of the calculation is set with graphical interface.

J.3Pre-processing

In Pre-processing, a solid model is prepared to analysis which requires more time than the other processors in analysis. This process starts with PREP7 command.

Modelling, material type definition and meshing are main parts. Solid model can import from other modelling software as IGES or SAT formats. The model can be also created in this module.

J.4Solution processor

Solver process is to define the type of analysis and boundary conditions such as mechanical and/or electrical. Process starts SOLUTION command. In this processor, boundary conditions and solution method can be defined.

J.5Post-processing

Post-processing is to review the results. This process depends on the analysing type. Results of static and modal analyses are given in general post-process (POST1) and time depended solutions (harmonic, transient etc) are given in time history post-process (POST26).

Appendix K

The piezoelectric constitutive equations

*S,D	$T_{ij} = c_{ijkl}{}^{D} S_{kl} + h_{mij} D_m$	K.11
*S,D	$E_n = -h_{nkl} S_{kl} + \beta_{nm}{}^{S} D_m$	K.12
*T,D	$S_{ij} = s_{ijkl}{}^{D} T_{kl} + g_{nij} D_n$	K.13
*T,D	$E_n = -g_{nkl} T_{kl} + \beta_{nm}{}^{T} D_m$	K.14
*S,E	$T_{ij} = c_{ijkl}{}^{E} S_{kl} - e_{nij} E_m$	K.15
*S,E	$D_n = d_{nkl} S_{kl} + \varepsilon_{mn}{}^{S} E_m$	K.16
*T,E	$S_{ij} = s_{ijkl}{}^{E} T_{kl} + d_{mij} E_m$	K.17
*T,E	$D_n = d_{nkl} T_{kl} + \varepsilon_{mn}{}^{T} E_m$	K.18

* Independent variable

The superscripts explain the boundary conditions. The superscripts T, D, E stand for constant stress, constant dielectric displacement, and electrical field respectively. c^E is the short-circuit (constant E) and c^D is the open-circuit (constant D) elastic stiffness. s^E is the short-circuit (constant E) and s^D is the open-circuit (constant D) elastic compliances.ε^T and ε^E are the free (constant stress) and clamped (constant electrical field) permittivities, β^T and β^S are the free (constant stress) and clamped (constant strain) impermeability. The piezoelectric compliances are d (strain coefficients), e (stress coefficients), h (h coefficients), and g (voltage coefficients). t denotes transposed matrices.